Identification of galectin-1 as a marker for claudin-low breast cancer and implications for tumor progression

by

Kassondra Balestrieri

December, 2023

Director of Dissertation: Kathryn Verbanac

Major Department: Interdisciplinary Biological Sciences, Surgery

Triple-negative breast cancer (TNBC) is an aggressive subtype of breast cancer. Patients with TNBC have a high rate of metastasis and mortality due to the lack of targeted therapies and resistance to chemotherapy. The aim of this research was to develop reliable models of metastatic TNBC to investigate targetable proteins and pathways. The 2225L and T11 murine tumor lines, which are highly analogous to human basal-like and claudin-low TNBC subtypes, were serial passaged heterotopically and orthotopically in syngeneic mice to generate lines that would consistently metastasize to the lung. Immunochemical and transcriptomic methods were used to define the immune microenvironment of the primary and metastatic tumors and to compare tumors with variable metastatic potential. Both resulting 2225LM and T11 tumor lines displayed an immunosuppressive tumor microenvironment characterized by high myeloid-to-lymphocyte ratio ($CD11b^{+}$:$CD3^{+}$) and elevated expression of protumor cytokines compared to control tissues. Subsequent analysis of T11 primary and metastatic claudin-low breast tumors employed a discovery-based proteomic approach that detected significant differential galectin-1 expression compared to normal control tissues. Label-free quantitation, Western immunoblot, and ELISA confirmed galectin-1 identity and elevated expression in primary and metastatic tumors compared to normal control tissues. Mass spectrometry spatial mapping and immunohistochemistry revealed high localization of galectin-1 in T11 metastatic lung foci. Transcriptomic analysis of mouse and human breast cancer subtypes showed significant and differential galectin-1 expression in claudin-

low primary tumors compared to other breast cancer subtypes. Galectin-1 is an N-acetyllactosamine (LacNAc)-binding protein that promotes anti-inflammatory actions and has a wide range of reported intracellular and extracellular activities, but its role in breast cancer has not been well studied. We next evaluated galectin-1 effects on $CD11b^+$ myeloid cells, based on their high proportion in T11 tumors, using *in vitro*, *ex vivo*, and *in vivo* models. The $CD11b^+$ murine macrophage cell line RAW 264.7 was susceptible to galectin-1-induced apoptosis *in vitro* in a dose-dependent, carbohydrate-specific manner. However, *ex vivo* assays with murine $CD11b^+$ peritoneal exudate cells showed no effect on apoptosis. *In vivo* systemic administration of galectin-1 allosteric inhibitor OTX008 in T11-tumor-bearing mice slowed tumor growth but did not affect the percentage of infiltrating myeloid populations. Fluorescence microscopy evaluation of overall tumor apoptosis and $CD3^+$ and $CD11b^+$ cell apoptosis in primary tumors at sacrifice showed no statistical difference between the OTX008 treatment and the vehicle control groups. These findings suggest that galectin-1 does not affect $CD3^+$ or $CD11b^+$ immune cell infiltration or apoptosis in claudin-low primary tumors. Larger *in vivo* studies and analysis of different drug regimens, smaller tumors and metastatic models are indicated. Future studies focusing on alternative actions of galectin-1 in claudin-low breast cancer, including its potential effects on tumor proliferation and angiogenesis, should be conducted to explore its viability as a therapeutic target.

Identification of galectin-1 as a marker for claudin-low breast cancer and implications for tumor progression

A Dissertation

Presented to the Faculty of the Department of Interdisciplinary Biomedical Sciences

East Carolina University

In Partial Fulfillment of the Requirements for the Degree

Doctor of Philosophy Interdisciplinary Biomedical Sciences

By

Kassondra Wright Balestrieri

December 2023

Director of Dissertation: Kathryn Verbanac, PhD
Dissertation Committee Members:
Nasreen Vohra, MD
Kimberly Kew, PhD
Mark Mannie, PhD
Mary Jane Thomassen, PhD

DEDICATION

This work is dedicated to:

My dearest friend, Keith Pittman, for demonstrating gracious patience while teaching me and always being there to help me solve problems in both lab and life. I miss you every day.

My aunt, Tara Richmond, for inspiring me to take this journey. I strive every day to live my life to bring honor to your memory.

Thank you both for believing in me, in life and after.

ACKNOWLEDGEMENTS

I want to offer thanks to my advisor, Kathryn Verbanac, for the constant encouragement and faith in my ability to do well amid adversity. I would also like to offer a special thanks to Dr. Nasreen Vohra and Dr. Kimberly Kew for their advice, encouragement, and understanding, which has helped me grow personally and professionally. Special thanks to Cindy Kukoly, Dr. Tonya Zeczycki, Dr. Elizabeth Ables, Dr. Gina Murray, Dr. Amanda Petritsch, and Dr. Mona Marie for their help in troubleshooting methods and collecting data. I owe my deepest gratitude to my committee members, Dr. Nasreen Vohra, Dr. Kimberly Kew, Dr. Mark Mannie, and Dr. Mary-Jane Thomassen, for their suggestions and patience.

I want to thank past and current members of the Verbanac and Vohra labs: Keith Pittman, Moses McDaniel, Dr. Mohamed Ramez, Dr. Matthew Britt, Christiana Shoopman, and Robin Alligood for their assistance in the lab and their friendship. Each one made every day of my time at ECU a little better and brighter.

Thank you to my family, especially my parents, Laurie and Tom Wright, and my dearest friends, for always supporting me, believing in me when I had lost faith in myself, and picking up the phone at all hours of the day and night to talk me through the most challenging times. Their love, support, and guidance have made me into the person I am today.

Last, thanks to my husband, Nicholas Balestrieri, for supporting me, pushing me when I lacked motivation, and carrying me when it all seemed too much. I wouldn’t choose to share this life with anyone else.

TABLE OF CONTENTS

LIST OF TABLES

LIST OF FIGURES

List of Abbreviations

CHAPTER 1: INTRODUCTION

1.1 Triple Negative Breast Cancer

1.1.1 Clinical and Pathological Characteristics

A hallmark of triple-negative breast cancer (TNBC) is the absence or reduced expression of the commonly targeted estrogen receptor (ER), progesterone receptor (PR), and human epidermal growth factor receptor 2 (HER2), which limits therapeutic options. TNBC patients have a shorter overall survival (OS) and are at a higher risk of recurrence within five years of diagnosis,[1-3], with metastases 2–3 times more often in the lung and brain[2, 4] compared to non-TNBC subtypes. TNBC accounts for 10-20% of invasive breast cancers and is more commonly diagnosed in young, premenopausal African American and Hispanic women compared to Caucasian women.[2, 3] High histological grade, high mitotic index, low differentiation, and high neovascularization caused by overexpression of vascular endothelial growth factor (VEGF) are primary pathological TNBC characteristics.[5]

1.1.2 Diagnosis and Standard of Care

Breast cancer subtypes (**Table 1**) are determined by immunohistochemical (IHC) staining for ER, PR, and HER2 or gene amplification by fluorescence *in situ* hybridization.[6] The majority of patients with TNBC present with high-grade disease. Medical guidelines (e.g., American Society of Clinical Oncology or National Comprehensive Cancer Network) recommend neoadjuvant therapy for those with locoregional disease to reduce tumor size and prevent tumor spread. Chemotherapy drugs such as anthracycline, alkylators, and taxanes are commonly used. However, they are highly toxic and act non-specifically by preventing deoxyribonucleic acid (DNA) and ribonucleic acid (RNA) synthesis, crosslinking DNA to promote strand breaks or inhibiting cell division.[7] Unfortunately, TNBC can still reoccur even with radiation and

chemotherapy, resulting in a lower 5-year survival rate compared to hormone receptor-positive breast cancers (75% vs. 90%, respectively).[8] Therefore, there is an urgent need for more specific and less toxic therapies.

Table 1: Intrinsic Subtypes of Human Breast Cancer

Subtype	Estrogen receptor	Progesterone receptor	Human epidermal growth factor 2	3-Year Survival Rate[1]
Luminal A	+	+	−	96%
Luminal B	+	+	+	93%
HER2	−	−	+	90%
Triple-negative	−	−	−	83%

1.1.3 Molecular Subtypes of Triple Negative Breast Cancer

In recent years, utilizing transcriptional profiles to categorize breast cancer subtypes has become widely accepted for determining a patient's prognosis and potential benefit from therapy. These methods offer more comprehensive and reliable strategies for evaluating patient prognosis and developing therapies than standard pathology-based assessments. OncotypeDx is among the earliest and most commonly adopted approaches, used to accurately predict the likelihood of early-stage breast cancer recurrence which incorporates a panel of 21 genes and a risk reoccurrence algorithm.[9] However, early transcriptional profiling methods, like OncotypeDx, only focused on ER-positive breast cancers.[10] In the early 2000s, Perou and his team developed an alternative method using a 550-gene signature to predict prognosis and optimize treatment, which classified breast tumors into five intrinsic subtypes (**Table 1**). This method was later refined to only 50 genes, was approved by the FDA in 2013, and is commercially marketed as Prosigna known as PAM50.[10]

Transcriptional profiling has further emphasized that TNBC encompasses a minority of breast cancers but is vastly heterogeneous on a molecular and biological level.[11-14] Transcriptomics of human breast cancers has identified several subtypes of TNBC: basal-like type I and II, immunomodulatory, luminal androgen receptor, mesenchymal, and mesenchymal stem-

cell-like.[15] Approximately 75-80% of Basal-like type I and II tumors are triple negative for ER, PR, and HER2, while 50% of TNBC tumors are subtyped basal-like. Therefore, these terms have historically been used interchangeably.[16] The characteristics of these six TNBC subtypes described by Lehmann *et al.* are consistent with data published by other groups.[11-14] The biological diversity within TNBC highlights the complexity of the disease.

1.1.4 Introduction to Claudin-low Breast Cancer

Claudin-low breast cancer (CLBC) was first described by Perou *et al*. in 2007. It was characterized by low expression of tight-junction proteins, claudin-3, -4, and -7, and cell-cell adhesion protein, E-cadherin.[17] CLBC is frequently referred to as a sixth intrinsic subtype; however, tumors must first be classified as one of the other five intrinsic subtypes (basal-like, HER2-enriched, luminal A, luminal B, and normal-like) by PAM50.[10] Following, the genetic expression values from the tumor are correlated to two centroids, one for tumors with the claudin-low gene expression features and the other for all other breast cancers, to determine if the tumor is CLBC. Tumors with a stronger correlation to the claudin-low centroid are deemed claudin-low, overwriting the PAM50 subtype. Thus, CLBC is classified as independent of the underlying intrinsic subtype.[18-20] Most CLBC are reported as basal-like or normal-like and are commonly histologically triple negative. Therefore, these patients receive the same non-specific standard of care radiation and chemotherapy as other TNBC patients.

Due to their mesenchymal features, CLBC profoundly overlaps with the TNBC mesenchymal and mesenchymal-like subtypes characterized by Lehmann et al.[15] Furthermore, they are enriched in immune response genes (e.g., CD79b, CD14, and VAV1), and have primitive cancer stem cell-like properties designated by expression of cell-cell adhesion glycoproteins, $CD44^{+}CD24^{-/low}$.[15, 17] The subtype also has low genomic instability, mutational burden, and

proliferation levels, with a high degree of immune and stromal cell infiltration, contributing to the diverse intratumoral heterogeneity and complex microenvironment.

Approximately 7-14% of breast cancer patients have the claudin-low phenotype.[3, 16, 18, 20, 21] Moreover, about 25-39% of TNBC are claudin-low.[16, 22] Both human and animal studies have demonstrated that CLBC is more resistant to chemotherapy and has a worse prognosis compared to other TNBC subtypes.[20, 23, 24] Similar to TNBC, most CLBC recurrences happen within five years of the initial diagnosis.[20]

CLBC has been studied in various transcriptomic studies but remains the least understood subtype in literature. This lack of knowledge creates significant gaps in understanding tumor biology.[25-27] To classify CLBC, tumor samples undergo RNA isolation and transcriptional analysis which presents significant challenges in clinical sample collection. Ideally, patient samples would be immediately frozen or stored in an RNA stabilization reagent. However, clinical samples are not always handled this way, which may result in low-quality RNA for downstream analysis. Additionally, the claudin-low classifier algorithm requires comparing the tumor sample to other breast cancer samples, which limits sample availability for processing.[18, 22] Furthermore, CLBC patient samples for research are scarce. Thus, alternative models are vital for investigating how the unique features of CLBC may be targeted therapeutically.

1.1.5 Mouse Models of Claudin-low Breast Cancer

Studying claudin-low cell lines *in vitro* can provide insights for understanding specific properties of tumor cells. However, it is limited in understanding the biological intricacies of a tumor microenvironment due to its homogeneous nature. The tumor microenvironment consists of various components such as extracellular matrix, endothelial cells, and immune cells, which add cellular heterogeneity that is not accurately reflected *in vitro*. *In vivo* studies using mouse

models are preferred to investigate mechanisms within a complex system. Unfortunately, there are limited *in vivo* mouse models for CLBC, but the ones available provide a powerful alternative for studying complex claudin-low tumor biology.

Patient-derived xenograft (PDX) models are translational tools that effectively bypass many *in vitro* model limitations by engrafting human tumors into immunocompromised mice to investigate tumors' genomic and biological diversity.[28] However, mouse cells and other extracellular matrix (ECM) components may invade the patient's tumor over time, leading to the loss of the original human features. PDX models help examine tumor mutations or response to therapy,[22] but this model has a considerable disadvantage in studying the immune response to CLBC. To overcome this limitation, humanized PDX models have been developed in recent years. These models are created by irradiating immunocompromised mice and injecting them with human $CD34^+$ hematopoietic stem cells (HSC). Over several months, HSCs differentiate into a competent human immune system, which allows for the grafting of patient-derived tumors into the mice. Humanized PDX models are primarily used to investigate the efficacy of immunotherapies and mechanisms of drug resistance.[29] However, there is currently no established humanized PDX model for CLBC. This may be because PDX models take several months to develop and require specific claudin-low patient samples, which are limited.

Under certain conditions, such as when mice are exposed to chemicals or radiation, normal mice may spontaneously develop breast tumors with diverse molecular subtypes.[28] Spontaneous breast cancer of various molecular subtypes, including claudin-low, can also happen in transgenic mouse models that overexpress Myc, Akt, COX2, or T-antigen or lack the tumor suppressor protein, p53.[16] Although it’s difficult to predict which tumor phenotype will develop. To overcome this, claudin-low mouse tumors can be transplanted into mice with a matching genetic

background.[16, 28] This syngeneic model simulates the biology of human claudin-low breast cancer within a competent immune system.

Our lab acquired a transplantable, claudin-low tumor line from North Carolina University at Chapel Hill and Baylor Medical College, known as T11. This tumor line was derived from a transgenic model optimized to develop TNBC at a high frequency with a short latency period. To establish this model, a p53 null mouse was backcrossed onto the mammary tumor-prone BALB/c background. Then, mammary glands from 6-week-old p53 null mice were transplanted into 3-week-old normal BALB/c mice to produce only breast tumors.[16, 30] Herschkowitz *et al.* conducted microarray analysis on mammary tumors isolated from this model and showed that the transcriptional profiles mimicked human breast tumors. The T11 tumor line was identified as a murine equivalent to human claudin-low breast cancer,[16, 31] which has primitive cancer stem cell-like properties, high immune infiltration, and low expression of claudin-3, -4, and -7 and E-cadherin.[32] The T11 tumor line has an aggressive phenotype and responds to combinatorial therapies in a similar manner as human CLBC.[24, 31] Although there is no single murine model that can mimic all features of human breast cancer, the transplantable T11 model is a highly analogous model for studying the biology of CLBC within an immunocompetent environment.

1.2 Immunology in the Tumor Microenvironment

1.2.1 Role of the Microenvironment in Tumor Progression

The tumor microenvironment (TME) influences many aspects of tumor progression, such as proliferation, angiogenesis, tumor cell apoptosis inhibition, and host immune function dysregulation.[33] It is a dynamic environment that unfolds over time, the progression of the tumor, and appears to vary among cancer types. Immune cells within the TME play a crucial role in

promoting or inhibiting tumor growth. These cells are of particular interest in TNBC and CLBC due to their impact on prognosis and chemotherapy response.[34, 35]

An immunosuppressive TME is conducive to tumor cell growth and metastasis, the process by which cancer cells can colonize distant organs, such as the brain, liver, bone, or lungs, through intravasation into circulation or lymphatics. The highly complex TME contributes significantly to developing highly metastatic tumor cells.[36] For successful metastatic dissemination, cancer cells must home to secondary sites primed by primary tumor signals. These sites are known as the pre-metastatic or metastatic niches.[37] The metastatic microenvironment varies across tissues. Therefore, the interactions between tumor cells and the metastatic niche are critical for tumor cells to survive and grow. Unfortunately, metastatic tumor cells are often resist to treatment, which leads to metastasis, causing approximately 90% of cancer-related deaths.[38] Research has invested a great deal of effort and resources into discovering how the TME works to protect and spread cancer cells, but it remains a complex and elusive subject. To better understand these complex mechanisms, we must first understand the different types of cells present within the TME and their roles.

1.2.2 Infiltrating Immune Cells in Breast Cancer

In breast cancer, tumor-infiltrating lymphocytes (TILs) are a type of mononuclear immune cell that mainly consists of T cells..[39, 40] TILs include $CD4^+$ T helper cells, T regulatory cells (Treg) commonly defined as $CD4^+CD25^+FoxP3^+$, and effector cells like natural killer cells (NKC) and CD8+ T cells.[41] TIL levels tend to be higher in highly proliferating tumors, such as TNBC and CLBC.[42, 43] A higher number of $CD8^+$ effector TILs are correlated with better clinical outcomes and a better response to treatments, especially in patients with TNBC. Conversely, patients with a high infiltration Treg have significantly worse outcomes.[44-46] CLBCs are enriched

with Treg compared to other breast cancer subtypes, contributing to the poor prognosis of these patients and their unresponsiveness to therapies.[47] Depletion of Treg has shown significant reductions in primary and metastatic tumor growth in murine breast cancer models. Treg can suppress many immune cells as key mediators of peripheral tolerance, preventing undesirable immune responses.[48] Elevated Treg levels in breast cancer patients are linked with an invasive phenotype, diminished disease-free (DFS), and OS.[49-54] Thus, TILs have been suggested as a useful prognostic marker for determining patient outcomes and response to therapy.

TIL regulation is maintained by a balance between co-stimulatory and co-inhibitory signals called immune checkpoints that control immune reactions and restrict the intensity of the immune response.[55] One of the most extensively studied immune checkpoint inhibitors is programmed death-1 (PD1), which binds to its ligands PD-L1 and PDL2 to impede T-cell function.[55-57] Unfortunately, tumor cells, including those found in CLBC, hijack this pathway by expressing PD-L1 on their surface to suppress the effector T cell response. This leads to an immunosuppressive TME and is associated with a worse prognosis.[55, 58-63] Since 2001, several immunotherapies, such as Pembrolizumab (anti-PD1) and atezolizumab (anti-PD-L1), have been developed to target this pathway.[64] However, aggressive breast cancers with high Treg infiltration and an immunosuppressive TME, such as CLBC, are particularly resistant to these therapies.[47, 65-67] One possible explanation for the phenomenon is that PD-L1 in CLBC is hyper-glycosylated, which may prevent targeted anti-PD1 antibodies from being effective.[68-70] In such cases, a strategic therapeutic option for anti-PD-1/PD-L1 resistant tumors may be a combination therapy targeting PD-L1 glycosylation.

While there is abundant evidence for the role of T cells in tumor immunity and cancer progression, the exact role of B cells is not well-defined. B cells are primarily responsible for

internalizing foreign antigens through receptor-mediated endocytosis. They then load them onto major histocompatibility complex class II (MHCII) cell surface molecules presented to $CD4^+$ T cells. MHCII engagement with T cell receptors typically occurs in the spleen or lymph nodes, and this interaction stimulates B cells to differentiate into memory B cells or plasma cells. In the TME, B cells can act directly on tumor cells to induce cell death or regulate the effects of T cell responses through antigen presentation. Despite evidence that suggests B cells represent an important fraction of infiltrating immune cells,[71, 72] the data is inconclusive on whether these cells have any prognostic value in breast cancer.[40, 73-76]

Along with lymphocytes, myeloid cells play a pivotal role in the TME and breast cancer progression. Myeloid cells are the most prevalent immune cells that infiltrate tumors and are highly adaptable hematopoietic cells with diverse gene expression profiles and functions.[77-79] Although they are classified by lineage, phenotype, and location, myeloid cells have a high degree of plasticity, allowing them to respond rapidly to environmental signals. Tumor cells can thwart anti-tumor activities by releasing systemic, soluble factors that increase myelopoiesis and reprogram myeloid cells to become immunosuppressive and pro-tumorigenic.[80] Pro-tumor myeloid cells have a significant role in the initiation, progression, and metastasis of tumors and are associated with worse DFS and OS of breast cancer patients.[81-84]

1.2.3 Types of Tumor-Infiltrating Myeloid Cells

Dendritic cells (DCs) are specialized myeloid-derived cells that activate the adaptive immune response by presenting antigens to T cells. They are a target for immunotherapies because they are a significant source of anti-inflammatory cytokines and immune checkpoint molecules.[85] Like other immune cells, DCs can be useful prognostic indicators. The different subtypes of breast cancer have varying genetic signatures of DCs, with luminal breast cancer enriched with DC pathways in wound healing and ECM pathways. In contrast, DCs in TNBC have a high expression for interferon pathways. The differences between the DC profiles of these two breast cancer subtypes may be linked to patient outcomes.[85] Likewise, immature DCs infiltrating tumors are linked to poor prognosis in early-stage breast cancer, while conventional dendritic cells can predict TNBC survival. [85, 86]

Cancer growth leads to the expansion of a diverse group of myeloid cells, including tumor-associated macrophages and neutrophils, which exhibit a high degree of plasticity and are located within the primary tumor. While immature myeloid cells called myeloid-derived suppressor cells (MDSCs) are found primarily in tumor-bearing mice and cancer patients' circulation and secondary lymphoid organs.

There are two types of tumor-associated macrophages or neutrophils (TAMs or TANs): M/N1-like and M/N2-like. M/N1-like cells are considered classically activated and express many pro-inflammatory genes. They are efficient antigen-presenting cells that display anti-tumor functions. On the other hand, M/N2-like cells are alternatively activated through type 2 cytokines and express high levels of anti-inflammatory genes. Their function is to promote tumor growth. Although the primary function of TAN is not fully understood, TANs and TAMs likely work together within the TME to suppress and promote tumor progression.

Like TAMs and TANs, there are two groups of MDSCs: monocytic and polymorphonuclear (M-MDSC and PMN-MDSC/G-MDSC, respectively). Phenotypically and morphologically, M-MDSC are most like monocytes, while PMN-MDSC are comparable to neutrophils.[87] Although PMN-MDSC and TAN are considered separate cell types, they express the same markers (**Table 2**), making it difficult to differentiate between them.[80] Most researchers refer to TANs when discussing both MDSC and M2-like TAM/TAN aid in tumor growth and progression (pro-tumor) and share commonalities in secretion of immunoregulatory mediators, which are like those involved in wound repair, such as arginase, interleukin 10 (IL-10), granulocyte colony-stimulating factor (G-CSF), monocyte chemoattractant protein-1 (MCP-1), keratinocyte chemoattractant (KC), and VEGF.[88-90] Additionally, all subsets have been shown to play critical roles in sustaining cancer progression through increased angiogenesis, stroma disposition, tumor cell intravasation, extravasation, upregulation of factors involved in tissue remodeling, and suppression of the tumoricidal immune response.[80, 91, 92] When MDSC localize to primary tumors, they can differentiate into either pro- or anti-tumor TAM/TAN and are known to have more potent immunosuppressive activity compared to circulating MDSC. Both TAM/TAN and MDSC are observed within metastatic tissues.[93]

Table 2: Flow Cytometric Panel for Murine Myeloid Cells in Cancer

	CD45	IA/IE[d]	CD68	CD11b	CD11c	F4/80	Ly6C	Ly6G	CD206
G-MDSC*	+	-	-	+	-	Lo/-	+	+	-
M-MDSC	+	-	-	+	-	Lo/-	+	-	-
M1-like TAM	+	+	+	Lo/+	-	+	-	-	-
M2-like TAM	+	+	+	Lo/+	-	+	-	-	+
TAN*	+	-	-	+	-	Lo/-	+	+	-
CD11b$^+$ Dendritic Cell	+	+	++	+	+	+	-	-	-/+
Ly6C- Monocytes	+	-	+	+	-	+	-	-	-
Ly6C+ Monocytes	+	-	-	++	-	++	+	-	-
Alveolar Macrophage	+	+	-/+	+	+	++	+	-	++
Table References[80, 94-96]									

*G-MDSC, N1-like, and N2-like TAN cannot be differentiated by markers alone. Differences are determined by morphology, inflammatory, and immunosuppressive properties.[95]

1.2.4 Role of Myeloid Cells in Tumor Progression

A high frequency of circulating or infiltrating myeloid cells in TNBC is associated with poor prognosis.[97-101] Myeloid cells are also associated with increased angiogenesis and higher histopathological grade in cancer patients.[102-104] Using murine breast cancer models, studies demonstrate that myeloid cells aid in tumor cell seeding and growth at metastatic sites.[105] Moreover, inhibition of myeloid cells improves responses to radiation therapy in murine tumor models.[106]

In murine breast cancer models, tumor-infiltrating MDSC are responsible for colonizing breast cancer cells in the lung. MDSC appear to be located in hypoxic areas preferentially, producing higher levels of pro-inflammatory molecules and reduced expression of anti-inflammatory factors.[107] MDSC have also been shown to suppress T-cell function through STAT3-dependent induction of indoleamine 2,3-dioxygenase (IDO), a tryptophan-metabolizing enzyme involved in tumor immune tolerance.[108] It is apparent from these studies that MDSC prevent anti-tumor immunity in breast cancer and, therefore, play a significant role in its advancement.

In human breast cancer patients, circulating MDSC levels correlate strongly with clinical stage, metastatic burden, pathologic complete response (pCR) to therapy, and OS.[109] Specifically, high frequencies of M-MDSC are associated with an increased rate of recurrence and metastasis and lower OS. In metastatic breast cancer patients, levels of circulating MDSC increase following chemotherapy likely due to the bone marrow recovering following depletion from chemotherapy.[110, 111] It is widely accepted that higher levels of MDSC are associated with worse outcomes; however, the subclassification and percent of MDSC varies greatly among breast cancer

subtypes. This is most likely due to several influential factors in the TME and the heterogeneity among breast cancer subtypes.[112]

Similarly, the phenotype of TAM present in TME may determine the activity of breast cancer cells. For example, M2-like TAM signal tumor progression, whereas M1-like promote dormancy of metastatic breast cancer cells.[113] In humans, TAM accumulate in normal tissue surrounding breast cancer mesenchymal stem cells and interact with the TME by secreting interleukin-6 (IL-6), a pro-inflammatory cytokine that promotes tumor stroma inflammation and is associated with poor prognosis and lower OS.[114, 115] Additionally, TAM have been shown to produce matrix-degrading enzymes, such as matrix metalloproteinase-2 (MMP-2), potentially facilitating tumor cell dissemination and spread.[116] TAM cytokines play a critical role in mediating angiogenesis and invasion of cancer cells.[117] M2-like TAM that secrete Chitinase-3-like protein 1 have been shown to promote metastasis of breast cancer cells both *in vitro* and *in vivo*.[118] High expression of MCP-1 on both macrophages and tumor cells in primary breast cancer has been shown to correlate significantly with intensive TAM accumulation, high expression of VEGF, and early relapse.[119] Annexin 1 has been shown to regulate the polarization of TAM and interactions with other cell types. In annexin-deficient mice, M1-like TAM are elevated in TME, and there is reduced tumor growth and enhanced survival.[120] Several studies have reported a correlation between TAM phenotype, location, and density in determining the survival of breast cancer patients, particularly in TNBC. [101, 121] In breast cancer patients, higher TAM density in primary tumors and TAM expression of macrophage colony-stimulating factor (M-CSF or CSF1) and its receptor (CSF1R) correlate to poor prognosis.[122-127]

G-MDSC and TAN have the same morphology and phenotype as bone-marrow-derived neutrophils. In a healthy immune system, neutrophils are the most abundant leukocyte in the

blood. As part of the innate immune system, they aim to eliminate foreign microorganisms through phagocytosis. However, in tumorigenesis, they appear to serve a dual role in that they can either promote or inhibit tumor progression, depending on TME signals. TAN have been found to polarize in response to stimulatory or inhibitory factors, rendering them pro-tumorigenic or anti-metastatic.[128, 129] TAN can promote tumor growth by producing elements that stimulate vasculature, enabling angiogenesis.[130] Alternately, in a murine breast cancer model, the primary tumor is shown to activate neutrophils and prevent metastatic seeding in the lung.[129] In patients, the neutrophil-to-lymphocyte is a good indicator of tumor-related inflammation. Studies from human breast patients demonstrate that a higher NLR is associated with a reduced DFS and OS, a particularly prognostic finding.[131-134]

1.2.5 Current Myeloid-Targeted Therapies for the Treatment of Breast Cancer

Immunotherapies have shown remarkable therapeutic outcomes; however, responses vary significantly due to immunosuppressive tumor microenvironments. The leading theory of immunotherapy is dependent on immune system plasticity and the ability of immune cells to be stimulated toward a potent anti-tumorigenic response. As described in the previous section, myeloid cells have effective immunosuppressive mechanisms that promote tumor growth, establish niches at distant sites, and contribute to therapeutic resistance. Thus, myeloid cells have become a primary target for cancer therapy, and in the last few years, multiple therapeutic strategies targeting these cells have been developed.

Myeloid cells are targeted by several mechanisms, such as depletion, blocking recruitment and trafficking, or inhibiting immunosuppressive pathways. Depletion of myeloid cells has conflicting results in tumor-bearing mouse studies, is systemic and not selective, and alters patients' ability to fight foreign pathogens.[135] A more strategic approach to myeloid cell reduction

is to target abundant chemokine receptors, such as CXCR2, which promotes macrophage migration and causes T-cell anergy through ligand binding.[136-141] The downside to this approach is that chemokine receptors are not present on all myeloid cells, nor is their expression limited to only myeloid cells. Reparixin, a non-competitive allosteric inhibitor of CXCR2, is currently in Phase 2 clinical trials as a combination therapy for metastatic breast cancer (NCT02370238).[142] A third approach is to temper MDSC immunosuppression, allowing T-cell activity to be re-established. This method involves targeting inflammatory mediators, such as Prostaglandin E2 (PGE2), cyclooxygenase 2 (COX2), or arginase I.[143-145] Since COX2 is upstream of PGE2, COX2 inhibitors, such as celecoxib, have been shown to reduce MDSC recruitment and improve cytotoxic T cell frequency in the TME and at metastatic sites in breast cancer models.[124, 146] Additionally, sildenafil or tadalafil, phosphodiesterase-5 (PDE-5) inhibitors that directly target ARG1 function, have been shown to thwart MDSC immunosuppressive mechanisms.[147-149] The most novel approach for targeting MDSC pro-tumorigenic activities is epigenetic reprogramming. Histone deacetylases (HDAC) remove acetyl groups from histones to regulate gene expression.[150] In mouse models of breast cancer, Entinostat, a class I histone deacetylase inhibitor (HDAC), neutralizes MDSC function. It is currently used in a clinical trial for TNBC (NCT02708680) and metastatic breast cancer (NCT02115282 and NCT02453620).[151-153] The most potent myeloid-targeting anti-tumor strategy is reprogramming tumor-promoting myeloid cells to tumor suppressing, enhancing therapeutic efficacy, and alleviating therapeutic resistance.[154] Class I phosphoinositide 3-kinases (PI3K) drive metabolic and transcriptional pathways in inflammation and cancer and are primarily expressed by myeloid cells.[155, 156] IPI-549 (MARIO-3), a PI3K inhibitor in a phase 2 clinical trial as a combinational therapy for patients with TNBC

(NCT03961698), has been shown to reduce immune suppression and restore T cell cytotoxicity.[157-159]

New evidence is emerging about the importance of extracellular glycosylation on cancer-associated myeloid cells. In the TME, UDP-GlcNAc is elevated and serves as a donor for classical GlcNAc transferases to build extracellular glycoproteins. Adding a ß-GlcNAc to asparagine residues on the cell surface or secreted proteins initiates *N*-glycosylation. N-linked glycans are composed of a conserved pentasaccharide core (Manα1-6(Manα1-3)Manβ1-4GlcNAcβ1-4GlcNAcβ1-Asn) decorated with different carbohydrate motifs.[160] Most growth factor receptors and molecules expressed on the cell surface that are important for macrophage function are *N*-glycosylated, including integrins (e.g., CD11b, CD18)[161], TNFα receptor (TNFR)[162], and CD206.[163] In a study to investigate the role of glycosylation in macrophage polarization, bone marrow-derived macrophages were treated with Tunicamycin, an inhibitor of GlcNAc phospho-transferase that catalyzes the transfer of *N*-acetylglucosamine-1-phosphate from UDP-*N*-acetylglucosamine to dolichol phosphate in the first step of N-linked glycosylation, then stimulated for polarization to an M1 or M2 phenotype. Results showed that expression of M2 activation markers, such as CD206, an endocytic receptor that recognizes ligands with high-mannose expression, are suppressed by *N*-glycosylation inhibition but have minimal effect on M1 polarization.[163, 164] Thus, protein glycosylation on myeloid cells could potentially provide an alternate pathway for re-programming myeloid cells to an anti-tumor phenotype.

Many drugs impact the quantity, function, and differentiation of myeloid cells and have shown improved outcomes in mice and humans. Targeting myeloid cells in cancer patients can enhance the efficacy of current therapies and may establish a novel approach to improve the long-

term survival of cancer patients. Additionally, the role of glycosylation on macrophage functions during tumorigenesis may be a new field that could provide novel targets for cancer therapies.

1.3 Galectin-1

1.3.1 Galectin Family

Galectins (formerly S-type lectins) are a family of fifteen glycan-binding proteins. They are found throughout eukaryotes, and galectin homologs are phylogenetically preserved in nematodes, sponges, and fungi.[165] This family of lectins shares carbohydrate binding specificity for β-galactosides, molecules in which galactose is covalently bonded to another carbohydrate functional group.[166] Beta (ß) indicates the relative stereochemistry of the anomeric stereocenter furthest from the first carbon in the cyclic saccharide, which occurs when the two carbons have different stereochemistry. Lactose, a disaccharide composed of galactose and glucose, is a common and recognizable example of a β-galactoside.

Galectins are expressed in the cytosol or nucleus of a cell or can be secreted into the ECM or circulation.[167-169] The mechanism for galectin secretion is unknown because it lacks a classical secretion sequence[170], however, this process is thought to occur by exosomes fusing with the cell membrane where galectins accumulate.[171, 172] The key carbohydrate-binding role for Gal-1 occurs extracellularly. Glycoproteins and glycolipids on the extracellular membrane often contain β-galactosides.[166] Therefore, even though galectins are not synthesized as membrane-bound proteins, they can associate with membranes by binding to glycoproteins or glycolipids on the cell surface and regulate signaling pathways.

Galectins are categorized into three subgroups based on their structure: prototype (galectin-1, -2, -5, -7, -10, -11, -13-, -14, and -15), tandem-repeat (galectin-4, -6, -8, -9 and -12) and chimeric (galectin-3).[173] All galectins have a conserved carbohydrate-recognition domain (CRD) where

glycoconjugates bind, and some are capable of lectin-protein interactions. Galectins have the capacity to bind various ligands, specifically recognizing diverse carbohydrate motifs presents on glycoproteins. The inherent multivalence enables galectins to facilitate the clustering of cell surface glycoproteins, cross-link receptors, and influence downstream processes such as cell signaling, cell cycle proliferation, apoptosis, and pre-mRNA splicing. However, the galectin-binding partner determines the binding interaction's specific downstream effect.[174] Galectins have been extensively characterized functionally and have been reported to play a role in various diseases, including cancer. Seven galectins reportedly play a role in murine and human cancers, galectin-1, -2, -3, -4, -7, -8, and -9. A few studies have reported, poorer outcomes associated with breast primary tumors that overexpress Galectin-1 and -7; additionally, in one study, serum from breast cancer patients contained higher levels of Galectin -2, -3, -4, and -8 compared to healthy controls.[175-177] Galectins have many functions in tumor development and progression, such as apoptosis, metastasis, and angiogenesis. In addition, the role of galectins in immune regulation is another reason to focus on galectin biology. Galectin-3 is the most studied member of the galectin family involved in cancer. There are several ongoing Phase 1-2 clinical trials targeting galectin-3 in cancer. Due to their multivalence, galectin inhibition is potentially a therapeutic target for breast cancer.[178] The proposed roles of galectin-1 in cancer are summarized in **Table 3**. Most reports are from *in vitro* human or mouse cell lines or *in vivo* data using mouse models. There are few investigations in breast cancer and none that have specifically examined the claudin-low subtype.

Table 3: Galectin-1 Proposed Roles in Cancer

Cancer Type	Proposed Gal-1 Role	Experimental Models	Reported Gal-1 Activity
Breast cancer	• Promotes tumor inflammation and avoids immune destruction • Induces angiogenesis	• *In vitro* assays with human peripheral $CD14^+$ and $CD4^+$ cells from healthy donors[179]	• Increases frequency of $CD14^+CD16^+$ cells with increased expression of CD163, CD209, and MHC class II and lower CD1a expression[179] • Increases cytokine expression of IL-10, G-CSF, and IL-6 and decreases IL-8 in dendritic cells[179] • Enhances ability of $CD14^+CD16^+$ cells to increase regulatory T cells and induce IL-6 and IL-10 secretion in T cells[179] • IL-10 expression in $CD11c^+$ cells[179] • Directly binds to myosin IIa and increases activation in tolerogenic dendritic cells[179]
		• *In vitro* proliferation assay using T cells isolated from mouse draining lymph nodes[180] • *In vivo* Gal-1 knockdown in 4T1 basal-like syngeneic murine mouse model[180]	• Increases suppressive activity of $CD4^+CD25^-$ cells[180] • Increases $CD4^+CD25^+Foxp3^+$ T cells in spleen, tumor-draining lymph nodes, primary tumors, and lungs[180] • Increases production of IL-5, IL-10, and IL-10/IFN-g ratio in spleens and tumor-draining lymph nodes[180]
		• *In vivo* Gal-1 knockdown or inhibition with thiodigalactoside (TDG) in 4T1 basal-like syngeneic murine mouse model[181]	• Promotes tumor growth[181] • Reduces the number of tumor infiltrating $CD4^+$ and $CD8^+$ T cells in primary tumors[181] • Promotes angiogenesis[181]
		• *In vivo* Gal-1 knockdown or inhibition with TDG in 4T1 basal-like syngeneic murine mouse model[182]	• Reduces the number of metastases in the lung[182] • Reduces the frequency of $CD4^+$ and $CD8^+$ T cells in lung metastases[182] • Co-localizes with $CD44^+CD326^+$ cells in immunofluorescence assay and binds to both CD44 and CD326 in immunoprecipitation[182]
Prostate cancer	• Inhibits T-cell transendothelial migration	• *In vitro* migration and adhesion assays using immortal human T cell lines[183]	• Increases cell surface expression and extracellular matrix deposition of Gal-1[183] • Decreases the number of T cells that migrate across an endothelial cell barrier or through extracellular matrix[183] • Increases cell death in T cells[183] • Causes CD43 clustering on the surface of T cells[183]

Cancer Type	Proposed Gal-1 Role	Experimental Models	Reported Gal-1 Activity
Pancreatic cancer	• Induces angiogenesis • Promotes tumor inflammation and avoids immune destruction • Enabling replicative immortality	• *In vitro* assays with human pancreatic stellate cells (knockout) and human pancreatic cancer cell line (knockdown)[184] • *In vivo* Gal-1 knockout in tumor cells in syngeneic and xenograft transplant mouse models or genetically engineered mouse model[185-187]	• Decreases $CD4^+$ and $CD8^+$ T cells in primary tumor[185] • Increases $CD11b^+Gr1^+$ cell in primary tumor[185] • Increases NFkB/p65 nuclei translocation[184] • Gal-1 expression correlates with SDF-1 expression in tumor cells[184] • Increases angiogenesis[187] • Decreases T cell and neutrophil infiltration in spontaneously developing ductal tumors[187] • Loss of Gal-1 decreased occurrence of spontaneously developing ductal tumors[187] • Low Gal-1 expression correlates with high MMP7 and low EGFR and Pdx1[186]
Neuroblastoma	• Promotes tumor inflammation and avoids immune destruction • Induces angiogenesis	• *In vitro* assays with murine neuroblastic cell line[188] • *In vivo* Gal-1 knockout in spontaneous neuroblastic mouse model[188]	• Decreases splenic and intratumoral $CD4^+$ T cells[188] • Increases $CD4^+$ T cell expression of CD62L and reduced CD43 and INFγ[188] • Increases angiogenesis[188] • Reduces migration of $CD4^+$ cells[188]
Melanoma	• Avoids immune destruction	• *In vitro* knockdown in mouse melanoma cell line[189]	• Induces apoptosis of splenic T cells from mice and peripheral phytohemagglutinin activated T cells from healthy patients[189]
Lymphoma	• Promotes tumor inflammation and avoids immune destruction	• *In vitro* RNAi-mediated inhibition of Gal-1 and co-culture of activated T cells with human lymphoma cells[190]	• Decreases T cell viability, the secretion of Th2 cytokines, and the expansion of $CD4^+CD25^{high}$ $FOXP3^+$ Treg cells in primary tumor[190] • Gal-1 overexpression controlled through AP-1-dependent enhancer[190]
Lung cancer	• Promotes tumor inflammation and avoids immune destruction • Sustains proliferative signaling	• *In vitro* co-culture human normal lung fibroblasts with lung cancer[191] • *In vivo* Gal-1 knockdown in tumor cells in syngeneic transplant mouse model[191, 192]	• Alters monocyte-derived dendritic cell phenotypic expression of surface markers[191, 193] • Reduces production of anti-tumor cytokines and increased pro-tumor cytokines[191] • Reduces naïve $CD4^+$ T cell proliferation[193] • Increases production of IL-10 in $CD11c^+$ dendritic cells[191] • Increases tumor migration (*in vitro*) and growth rate (*in vivo*)[194] • High Gal-1 expression correlates with components of the arachidonic acid pathway in inflammation, COX-2 and PGE2[194]

Cancer Type	Proposed Gal-1 Role	Experimental Models	Reported Gal-1 Activity
			• TGFβ1-induced COX-2 expression is Gal-1-depenedent[194] • Gal-1 directly binds to Ras[194] • Increases apoptosis of $CD4^+$ and $CD8^+$ T cells[192] • Increases angiogenesis[192]
Head and neck cancer	• Promotes tumor inflammation and avoids immune destruction	• *In vitro* transendothelial migration assay[195] • *In vivo* Gal-1 knockout in murine tumor cells in immunocompetent mouse[195]	• Decreases $CD4^+$ and $CD8^+$ T cells in primary tumor[195] • Activates endothelial cells to suppress T cell migration[195] • Positive correlation between Activates JAK/STAT pathway[195] • Gal-1 expression in tumors correlates with PD-1 and Tim-3 expression on T cells[195]
Glioma	• Promotes tumor inflammation and avoids immune destruction	• *In vitro* Gal-1 knockdown in mouse glioma cell line[196] • *In vivo* Gal-1 knockout in tumor cells in syngeneic and xenograft transplant mouse models[196, 197]	• Reduces NK cell mediated apoptosis of tumor cells[196] • Reduces infiltration of granzyme B^+ NK cells[196] • Increases infiltration of $CD11b^{High}F4/80^+$, $CD11b^{High}Ly6C^{High}$, and $CD11b^{High}Ly6G^{High}$ cells in primary tumors[197] • Increases INFγ production from $CD8^+$ T cells[197] • High Gal-1 expression correlates with expression levels of CCL2 and VEGF[197] • Gal-1 knockout improves outcomes after dendritic cell vaccination[197]
Colorectal cancer	• Enabling replicative immortality	• *In vitro* Gal-1 knockdown in tumor cell lines, scratch, and transwell invasion assays[198]	• HIF-1α significantly increases galectin-1 mRNA and protein expression[198] • Mediates migration in hypoxic conditions[198]

1.3.2 Galectin-1 Structure and Functions

Human *LGALS1*, located on chromosome 22q12-q13.1 or mouse *Lgals1* on chromosome 15 in the E-region, encodes for a 14.5 kDa prototype member of the galectin family of ß-galactoside binding proteins, galectin-1 (Gal-1). *LGALS1* is highly conserved between mice and humans, with 58% homology and 88% shared protein sequence.[199, 200] The tertiary structure of Gal-1 protein consists of 135 amino acids arranged into two anti-parallel beta sheets, one five-stranded (F1-F5) and the other six-stranded (S1-S6). It contains one CRD comprising eight highly conserved amino acids (His44, Asn46, Arg48, Val59, Asn61, Trp68, Glu71, and Arg73) located on S3-S6. The CRD forms a negatively charged channel with high affinity for repeating *N*-acetyllactosamine (LacNAc) residues composed of either ß-1, 3- or ß-1, 4-linkages between galactose and *N*-acetylglucosamine (Galβ1-3-NAcGlc or Galβ1-4-NAcGlc).[201-203] The addition of LacNAc residues to proteins and lipids involves a series of enzymatic steps primarily taking place in the Golgi apparatus. The majority of mammalian poly-LacNAc is synthesized by the alternating action of β-1,3-N-acetylglucosaminyltransferase 2 and β-1,4-galactosyltransferases. The process is initiated by β-1,4-N-acetylgalactosaminyltransferase, which conjugates activated galactose in a β-1,4 bond to the outer arm of N-acetylglucosamine in type 2 N-glycans and forms the LacNAc unit. Subsequently, other glycosyltransferases catalyze the addition of galactose, N-acetylglucosamine, and other sugar residues to elongate the glycan chain. Additionally, the backbone can be branched by an N-acetylglucosamine at the 6-position of the galactose units by the enzyme β-1,6-N-acetylglucosaminiltransferase; thereby increasing the affinity of Gal-1 for its ligand[204] Gal-1 can non-covalently dimerize with each monomer's N- and C-termini at the connection site and the CRD on opposing sides. This arrangement reduces steric hindrance at the lectin binding site and is necessary to enhance galectin-1-LacNAc complexes.[201-203] Gal-1 cross-

linking capability contributes to the organization of cell surface receptors and can control their segregation, internalization, and signaling.[205]

The Gal-1 monomer to dimer ratio reaches equilibrium at 7 μM; therefore, at low concentrations, dimers will dissociate.[206-209] The monomeric and dimeric conformations can bind to LacNAc; however, the avidity between LacNAc and Gal-1 increases when Gal-1 is dimerized and poly-LacNAc residues are branched.[207, 210] For example, the dissociation constant (Kd) of monomeric Gal-1 with a single LacNAc motif is approximately 81±12 μM as determined by isothermal titration calorimetry (ITC), but dimerized Gal-1 binds to CD45, a glycoprotein with poly-branched LacNAc residues, with a Kd of 2.3 nM.[211, 212] Modifications to LacNAc residues such as sialylation, fucosylation, and sulfation also affect the binding affinity of Gal-1. For example, α-2,6-sialation on terminal galactose residues prevents Gal-1 binding, while 3-*O*-sulfation enhances LacNAc recognition.[173, 213] Gal-1 is susceptible to post-translational modifications as well. Once Gal-1 is synthesized it may remain inside the cell to control intracellular processes, or it can be released to the extracellular space through a nonconventional pathway that is unknown.[205] Post-translational modifications to Gal-1, such as, phosphorylation, acetylation, or sumoylation, influence the intracellular location of Gal-1.[214] Since Gal-1 lacks a traditional secretion sequence and does not pass through the standard ER/Golgi pathway, it is not susceptible to N-glycosylation. Also, Gal-1 has six cysteine residues that can be oxidized. Intramolecular disulfide linkages (Cys2-Cys130, Cys16-Cys88, and Cys42-Cys60) change the protein conformation significantly, preventing Gal-1 homodimer formation and inhibiting lectin binding.[215, 216] This modification may control the ability of Gal-1 to have lectin-protein interactions. Intracellular activity of Gal-1 is independent of its lectin-binding activity, while its extracellular activity is lectin-dependent.[217]

1.3.3 Galectin-1 in Immune Regulation

One of the significant roles of Gal-1 is to regulate the differentiation, activation, and function of immune cells in both the innate and adaptive immune systems. Gal-1 promotes anti-inflammatory pathways and contributes to resolving acute inflammation. With the ability to associate with many different cell surface proteins, Gal-1 can control innate and adaptive immune responses through macrophage polarization, neutrophil migration, alteration of the dendritic cell profile, and T cell viability and function.[205, 218]

The effect of Gal-1 on T cells has been extensively studied. It was first reported in 1995 that Gal-1 induces apoptosis in activated T cells.[219] Later research determined that Gal-1 binding to several different surface glycoproteins, such as CD7, CD43, and CD45, causes receptor clustering and cross-linking followed by apoptotic signaling through an undefined pathway.[189, 220-222] Alternate apoptotic pathways have also been proposed, such as induction of the transcription factor, activation protein-1 (AP-1)[223], phosphorylation of T cell receptor ζ chain[224, 225], or CD95 and caspase-mediated cell death signaling.[226] In primary tumors and at metastatic sites, there is a strong correlation between elevated Gal-1 expression and reduced infiltrating T cells.[180, 182, 183, 187, 189, 192, 197] In TNBC, two studies describe this observation using the basal-like 4T1 murine model. Ito and Ralph reported 4T1 cells containing a Gal-1 shRNA lentivirus (4T1-G1KD) injected intravenously into syngeneic Balb/c mice through the tail vein (non-spontaneous metastasis) resulted in augmented tumoricidal T cell populations ($CD3^+CD4^+$ and $CD3^+CD8^+$) in peripheral blood, reduction in the overall number of tumor cells and increased the percentage of $TUNEL^+$ apoptotic tumor cells in the lungs compared to controls. This observation was confirmed by inhibiting Gal-1 in 4T1 wild-type tumors with thiodigalactoside (TDG), a competitive inhibitor of

galectin-1, -3, -8, -9, suggesting that Gal-1 regulates metastasis by reducing tumoricidal T cell populations at metastatic sites.[182]

Though the exact signaling pathway remains undefined, it is evident that Gal-1 induced T cell apoptosis depends on the specific glycosylation patterns on the T cell surface. Researchers have inhibited Gal-1 binding to T-cell glycoproteins using enzymes that modify glycan structure.[227, 228] Interestingly, one study showed that Th2 cells are resistant to Gal-1 binding, although they show similar expression of known Gal-1 binding proteins, such as CD7, CD43 and CD45. Researchers found this was most likely due to sialic acid capping on the LacNAc residue, as demonstrated by high expression of the sialyltransferase enzyme, ST6Gal-1.[229] Thus, Gal-1 may be important for regulating T cell subsets by differential expression of glycoproteins on the cell surface.

Treg have been shown to differentiate in the presence of Gal-1. In one study, when activated T cells were cultured in the presence of Gal-1, the percentage of Treg, defined by $CD4^+CD25^+FoxP3^+$ expression, increased and produced higher amounts of Th2 cytokines, such as IL-4, IL-5, IL-10, and IL-13.[190] This is consistent with studies showing that *Lgals1*$^{-/-}$ mice produce higher quantities of INF-γ and IL-17 compared to wild-type mice.[229] In the orthotopic 4T1 transplantable model, Gal-1 knockdown results in decreased tumor growth, metastasis, and frequency of Treg cells ($CD4^+CD25^+FoxP3^+$) in the spleen, draining lymph nodes, primary tumor, and lungs, as well as reduced Treg immunosuppression against tumoricidal $CD4^+CD25^-$ cells.[180]

Although several studies report the effect of Gal-1 on T cells, less is known about its effect on B cells. In one study, secreted Gal-1 in bone marrow stromal cells increased B cell differentiation and proliferation, suggesting it is required for B cell development.[230] Stromal cells surrounding pre-B cells were shown to secrete Gal-1, which is bound to the B cell receptor (BCR)

to influence the activation state.[231] In a study using *Lgals*$^{-/-}$ mice, IL-10 and Tim-1 glycoprotein expression were reduced on Gal-1- depleted B cells compared to wild-type, suggesting Gal-1 is responsible for B cell regulatory function.[232] Besides binding glycans, Gal-1 is a pre-B cell receptor (pre-BCR) ligand that induces clustering, the first step of B cell differentiation.[233] In the TME, this may lead to more robust antigen presentation by lowering the B cell activation threshold. Evidence suggests that exogenous Gal-1 binds tightly to mature B cells, increasing overall immunoglobulin production.[234] The transition of activated B cells toward memory B cells or plasma cells is also controlled by Gal-1, possibly contributing to poorer outcomes in patients with high plasma cell tumor infiltration.[235, 236]

In DC, exogenous Gal-1 regulates migration and tolerance. Bone marrow mesenchymal stem cells produce Gal-1, which upregulates the expression of costimulatory molecules on the surface of DC, such as CD80, CD83, CD86, and MHCII, thereby preventing antigen presentation and promoting immune tolerance.[237] *In vitro*, Gal-1 is produced by spermatozoic nurse cells that promote the differentiation of tolerogenic DC.[238] Accordingly, Gal-1-deficient DC are more immunogenic than normal DC in mice and favor polarization toward pro-inflammatory T cell profiles thwarting Treg responses.[239, 240] In other studies, Gal-1 has been shown to promote DC maturation and migration and inhibit tissue infiltration of immunogenic DC while allowing in tolerogenic DC.[209, 241, 242] Combined these effects provide evidence of a suppressive, anti-inflammatory function of Gal-1 on DC.

Exogenous Gal-1 induces inflammatory stimuli to inhibit activation, chemotaxis, and extravasation of neutrophils.[243, 244] Gal-1 has a dual capacity to both attract or prevent the trafficking of neutrophils to sites of inflammation, such as the TME.[245] In Gal-1 knockout mice, neutrophil trafficking is significantly enhanced.[243] Likewise, in the presence of exogenous Gal-1,

neutrophil recruitment is inhibited.[244] However, *in vitro*, Gal-1 has been shown to promote the directional migration of human peripheral blood neutrophils at low concentrations, while at high concentrations, it causes random chemokinetic movement. Though, this phenomenon was only observed in the absence of additional inflammatory signals.[245-247] Moreover, Gal-1 promotes cell surface phosphatidylserine exposure on activated neutrophils, favoring phagocytic removal of viable neutrophils.[248, 249] This data is further supported by recent findings, which showed that following peak inflammation, Gal-1 administration induced neutrophil apoptosis and clearance, thereby resolving inflammation.[250] *In vitro*, under acute experimental inflammation, Gal-1 can exert anti-inflammatory activity through inhibition of IL-8 or TNFα-induced chemotaxis.[243, 246] Similarly, *Lgals*$^{-/-}$ mice display significant increases in the pro-inflammatory cytokine, IL-6, and VEGF, with a trend toward elevated anti-inflammatory chemokines, CCL2, CCL3, and CXCL1 and the pro-inflammatory cytokine TNF-α.[250] These cytokines and chemokines are expressed by immune cells, suggesting that Gal-1 may regulate the production of inflammatory molecules or differentiation into pro-inflammatory or anti-inflammatory cells. Additionally, the stage of activation may affect neutrophil response to exogenous Gal-1. In a recent study, naïve, primed, and activated neutrophils were treated with Gal-1 to determine the effect on ROS production. Gal-1 did not induce ROS production in naïve or primed neutrophils; however, it did elicit concentration-dependent ROS in activated neutrophils. Interestingly, exogenous Gal-1 induced ROS production in *Lgals1*$^{-/-}$ neutrophils more effectively than in normal, wild-type neutrophils, suggesting that endogenous Gal-1 may control the effects of exogenous lectin exposure.[251] ROS is known to cause chronic inflammation and DNA damage that can result in carcinogenesis and tumor progression. Based on this data, Gal-1 in the TME may limit neutrophil recruitment, induce neutrophil apoptosis and phagocytosis, and increase ROS to aid in tumor progression.

In monocytes and macrophages, Gal-1 promotes an anti-inflammatory phenotype. Exogenous Gal-1 reduces pro-inflammatory cytokine production from murine macrophages and shifts macrophages toward an M2-like profile by inhibiting IFNγ-induced MHCII expression and MHCII-dependent antigen presentation.[252, 253] Additionally, macrophages treated with Gal-1 have been shown to induce 12/15-lipoxygenase expression, an enzyme involved in the metabolism of polyunsaturated fatty acids during the resolution of inflammation.[254] Macrophages increase secretion of TNFα in the presence of Gal-1. Moreover, iNOS, an enzyme responsible for catalyzing the production of nitric oxide (NO) from L-arginine, is elevated in macrophages in response to Gal-1 binding following nerve injury.[255-257] By controlling L-arginine metabolism, either by reducing NO levels or favoring the arginase pathway, Gal-1 promotes the differentiation of macrophages into an M2-like phenotype.[258]

Furthermore, Gal-1 was found to stimulate the chemotaxis of cultured monocytes via the p44/42 MAP kinase pathway.[259] However, in an alternate *in vitro* study, Gal-1 inhibited monocyte migration and induced apoptosis but did not affect macrophages.[260] There were two confounding factors in these studies: the concentration of Gal-1 used to induce cell migration and the source of monocytes. The combined data suggests that lower concentrations of Gal-1 may induce cell migration, while higher doses induce apoptosis. This is consistent with neutrophil experiments that show the effects of Gal-1 are concentration-dependent. In addition, the study that observed the migration of monocytes used cells isolated from healthy patients, whereas the other study used monocytes isolated from patients with inflammatory bowel disease. It is well-known that Gal-1 is elevated in inflammatory conditions; therefore, these monocytes may have been desensitized to Gal-1 stimulation. Altogether, the data suggests Gal-1 contributes to an M2-like and promigratory macrophage or monocyte phenotype in a protein-glycan-dependent manner.

Oxidized Gal-1 also impacts monocyte and macrophage function. Using cultured activated rat peritoneal macrophages, oxidized Gal-1-induced macrophages were shown to stimulate axonal growth and repair.[217] In a follow-up study, oxidized Gal-1 inhibited IFNγ-induced NO and iNOS expression in RAW 264.7 macrophages.[261] Similarly, incubating lipopolysaccharides (LPS)-activated rat peritoneal macrophages with oxidized Gal-1 reduced RNA expression of pro-inflammatory markers, including IL-1β, IL-6, and iNOS, compared to activated macrophages not treated with oxidized Gal-1.[262] Therefore, when macrophages are in an activated state the configuration of Gal-1 may have opposing effects on their production of pro-inflammatory markers.

The mechanisms underlying the role of Gal-1 in the immune system remain poorly understood. This is partly due to the vast number of molecules on cell surfaces that express ß-galactosides and LacNAc residues. Known Gal-1-binding partners on the surface of leukocytes include CD45, CD7, CD43, CD2, CD3, CD4, CD107, glycosaminoglycans, integrins, GM1 ganglioside, glycoprotein 90K/MAC-2BP, BCR, and complement receptor 3 (CD11b and CD18).[210, 263] CD45 is highly glycosylated with complex sugars and has ubiquitous expression across all immune cells. CD7, CD3, and CD4 on T cells have been shown to bind to Gal-1 and induce T cell apoptosis. CD43 is also present on neutrophils and is a likely Gal-1 binding partner for the regulation of neutrophil function. Gal-1-BCR pairing activates B cells. Gal-1 has been shown to co-precipitate with complement receptor 3 on monocytes and macrophages, though the downstream effects of this interaction are unknown.

Gal-1-regulated functions on immune cells are dependent on the glycosylation status of key cell surface receptors. Glycosylation patterns modulate cellular responses by generating or masking ligands for lectins to control intermolecular interactions and intracellular signaling

pathways.[227, 264] Furthermore, glycosylation patterns are known to differ widely between cell lineages and differentiation stages.[265, 266] To add to the complexity of these systems, Gal-1 concentrations and the relative distribution of oxidized, monomeric, or dimeric forms may significantly affect how the lectin interacts with different cell surface glycol-proteins or lipids.[267] Likewise, other galectins or immune regulatory signals may work in concert to balance and regulate the inflammatory response. Also, it should not be overlooked that all immune cells are capable of synthesizing and secreting Gal-1, especially in an activated state, which may contribute to the regulation of cellular function both through protein-glycan or protein-protein interactions.[205] However, evidence suggests that protein-carbohydrate interactions may serve a critical function in immune system management, and Gal-1 may have a dual role in tolerance and immunogenicity, depending on its source (i.e., endogenous, or exogenous), relative concentration, or the prevalence of immunosuppressive versus inflammatory signals in the local microenvironment.

1.3.4 Functions of Galectin-1 in the Tumor Microenvironment

In the TME, Gal-1 uses many mechanisms to promote pro-tumor activity. One prominent feature of Gal-1 is its ability to promote cancer growth through angiogenic activity. Tumor angiogenesis is the formation of new blood vessels caused by tumor cell-secreted factors, such as VEGF. New blood vessels are required to provide and supply oxygen and nutrients to sustain continued tumor growth. In the TME, blood vessels are relatively immature and express low levels of adhesion molecules (e.g., ICAM-1, VCAM-1, and E-selectin), preventing the recruitment and activation of effector cells. The structural abnormality of the blood vessels causes atypical blood flow and high vascular permeability, increasing the probability of metastatic dissemination.[268, 269]

In the TME, Gal-1 is expressed by endothelial cells, stromal cells, immune cells, and tumor cells.[270] Gal-1 can bind endothelial cells or the cell matrix using its cross-linking capabilities to

form cell-cell or cell-ECM interactions and aid in creating new blood vessels. Through Gal-1 cross-linking capabilities, it interacts with vascular endothelial cells highly decorated with *N*-glycans. Likewise, the ECM in tumor stroma contains high levels of fibrous glycoproteins (e.g., laminin and fibronectin) that are well-known for Gal-1 binding.[182, 271-273] Gal-1 can also bind neuropilin, which is a highly glycosylated transmembrane co-receptor for VEGFR.[274, 275] The Gal-1-neuropilin-1 interaction on vascular endothelial cells promotes VEGFR2 phosphorylation and endothelial cell migration and adhesion.[275]

One study has shown that hypoxia-induced colorectal cancer cells produce high levels of Gal-1, which correlates with hypoxia-inducible factor 1-alpha (HIF-1α) expression. Under hypoxic conditions, reactive oxygen species (ROS) and HIF-1α are upregulated. ROS causes stabilization of the HIF-1 complex, which binds to hypoxia-response elements of the gene promoter for transactivation and promotes the expression of other pro-tumorigenic proteins, such as glucose transporter-1 (GLUT-1) and VEGF.[276, 277] Hypoxia responsive elements are located upstream of the transcriptional start site of *LGALS1* and are essential for HIF-1α controlled Gal-1 expression.[198] This pathway plays a vital role in tumor progression, metastasis, angiogenesis, metabolic switching to aerobic glycolysis (i.e., Warburg effect), and therapy resistance.[278-280] Additionally, knocking down Gal-1 expression reduces hypoxia and migration of cancer cells *in vitro*.[198, 281]

Gal-1 may also regulate effects in the TME through carbohydrate-independent mechanisms. Gal-1 improved DNA repair and proliferation in cervical cancer when interacting with H-Ras (p21), a small G protein that regulates cell division. Before activation, H-Ras is equally distributed between lipid raft and non-raft domains in the plasma membrane, where it initiates intracellular signaling.[282] Gal-1 appears to form a lattice network, resulting in a non-raft

microdomain necessary for H-Ras-induced activation of the Phosphoinositide-3-kinase (PI3K) cell growth pathway.[283] Evidence suggests that the Gal-1-H-Ras interaction occurs within the hydrophobic pocket of Gal-1, independent of the CRD. This domain can bind the farnesyl group on H-Ras and stabilize the translocation of the H-Ras-GTP complex onto the Gal-1 microdomains.[284-286] Intracellular binding of reduced galectin-1 to H-Ras promotes Ras membrane anchorage, requiring Ras signal transduction to occur and regulate cell growth and transformation.[284, 286, 287] Since hypoxia induces radioresistance and increases Gal-1 expression, the interaction between Gal-1 and H-Ras may play a significant role in tumor hypoxia-facilitated radiotherapy resistance by stimulating H-Ras signaling and DNA repair.

1.3.5 Summary of Galectin-1 in Breast Cancer Progression and Metastasis

As described in previous sections, Gal-1 has been shown to have many roles in cancer progression, such as tumor proliferation, transformation, invasion, metastasis, and angiogenesis.[274] Gal-1 is overexpressed in breast cancer, and even more specifically TNBC,[180, 182, 288, 289] and expression may be further increased under hypoxic conditions and after radiotherapy.[290-292] In breast cancer specimens stained for Gal-1 by IHC, there is a significant correlation between Gal-1 expression in cancer-associated stromal cells and tumor invasiveness, T stage, TNM stage, and axillary lymph node metastasis.[180]

Circulating Gal-1 levels are reportedly higher in breast cancer patients than healthy controls.[169] Patient serum samples have shown contradictory results demonstrating that circulating Gal-1 concentrations were lower in breast cancer patients than in healthy individuals.[175] However, Gal-1 is known to activate platelets to induce P-selectin and membrane glycoprotein complexes, leading to platelet aggregation.[169, 293] Gal-1 on circulating cancer cells may bind to these molecules and form platelet-cancer complexes. The aggregated cell clusters can arrest within capillaries in

secondary organs and then develop into macrometastases. Additionally, this may explain why Gal-1 is found in high concentrations in plasma but not serum; plasma samples would contain Gal-1-bound platelet aggregates while these compounds are absent from sera.

Specific mechanisms for how overexpressed Gal-1 may regulate breast cancer progression are lacking. Murine studies have shown that the knockdown of Gal-1 in breast cancer significantly reduces the potential of tumor cells to metastasize to the lung. Additionally, this study showed a decreased frequency and low immunosuppressive function in Treg cells compared to wild-type tumor cells.[180] Other murine studies have suggested that Gal-1 promotes tumor growth through its effect on effector T cell apoptosis.[182, 192] Another study showed tolerogenic DC populations were higher in breast cancer patients compared to healthy donors, and conditioned medium containing recombinant Gal-1 (rGal-1) or Gal-1 secreted from cultured MDA-MB-231 claudin-low cell line induced tolerogenic DC differentiation. Furthermore, the murine 4T1 breast cancer cell line enhanced IL-10 expression in DC compared to the 4T1 Gal-1 knockdown cell line. Myosin IIa, a motor protein involved in cytokinesis, cell migration, and adhesion, was identified as the primary binding partner for Gal-1 after caveolin-dependent endocytosis.[294] These studies are consistent with studies investigating the effects of Gal-1 on immune cell function. Gal-1 promotes an immunosuppressive TME that facilitates breast cancer cell immune escape and metastasis.

Alternatively, Gal-1 may promote breast cancer metastasis by stimulating the upregulation and secretion of enzymes that degrade the ECM.[295] Gal-1 binding to glycosylated breast cancer markers, such as CD44 and CD326, promotes the attachment of tumor cells to the ECM and endothelial cells.[182] This is consistent with previous studies showing that Gal-1 promotes the adhesion of cancer cells to the ECM.[219, 273, 296] Altogether, Gal-1 may promote attachment of breast

cancer cells to the ECM, then upregulate ECM degradation enzymes to facilitate metastatic dissemination.

Gal-1 binds to the α5ß1 fibronectin receptor on the surface of T-47D breast cancer cells to stop cell proliferation through inhibition of the Ras-MEK-ERK signaling cascade, which ultimately prevents cell cycle progression and growth.[297] Nevertheless, knockdown of galectin-1 expression in TNBC cell lines, MDA-MB-231 and Hs578T, reduced cell proliferation, migration, invasion, and chemotherapy resistance by reducing Gal-1-integrin ß1 interactions. Furthermore, Gal-1 ablation inhibited ERK/signal transducer/STAT3 signaling and suppressed survivin expression, a protein inhibiting apoptosis and regulating the cell cycle.[298] Integrins are heterodimeric transmembrane receptors that are essential for epithelial cell proliferation. Additionally, integrins regulate growth in immune cells and initiate signal transduction cascades that modulate cell growth.[297, 298] These studies indicate that Gal-1 modulates cell cycle proliferation through integrin interactions. However, the downstream effects of these interactions may be controlled by the specific breast cancer subtype being studied. T-47D breast cancer cells are hormone receptors positive, while MDA-MB-231 and Hs578T are triple negative, and even more specifically, claudin-low. From these studies, Gal-1 appears to halt cell proliferation in hormone receptor-positive breast cancer; however, in claudin-low TNBC breast cancer cell lines, Gal-1 promotes cell proliferation, cancer progression, and chemotherapy resistance, possibly contributing to worse OS in patients with this breast cancer subtype.

Other proteins that have been identified in breast cancer as Gal-1 binding partners are: Sushi domain containing 2 (SUSD2)[299], Galectin-3 binding protein (Gal-3BP)[300], and forkhead box P3 (FOXP3).[301] SUSD2, a transmembrane protein on breast cancer cells involved in angiogenesis, was identified with high confidence by mass spectrometry and co-

immunoprecipitation to have protein-protein interactions with Gal-1.[299, 302] Localization of Gal-1 on the surface of SK-BR-3 (HER2 subtype) and MDA-MB-231 (claudin-low subtype) breast cancer cells were dependent on the presence of SUSD2. When Susd2 was knocked down by RNA interference in TNBC syngeneic mouse models (4T1 and 66CL4), tumor growth slowed, and survival increased compared to wild-type Susd2-expressing tumors. Additionally, TIL were higher in Susd2-expressing mice.[299] Gal-1 was identified as a binding partner for SUSD2, but the specific pathway regulating Gal-1-SUSD2 function in breast cancer progression was never addressed. However, more recent studies have suggested that SUSD2 is cleaved in the endoplasmic reticulum by an unidentified serine protease at the glycine-aspartic acid-proline-histidine amino acid sequence. Generation of a non-cleavable SUSD2-mutant demonstrated that SUSD2 cleavage with both the N- and C-terminus intact were required for SUSD2 and Gal-1 plasma membrane localization.[303] Additionally, SUSD2 has been shown to promote TAM recruitment by increasing levels of CCL2/MCP-1 in TNBC breast cancer cell lines.[302] Thus, SUSD2-promoted surface presentation of Gal-1 may contribute to many Gal-1-controlled tumor immune evasion, progression, and metastasis mechanisms.

Gal-3BP is a large hyperglycosylated protein that acts as a ligand for several galectins through carbohydrate-dependent binding. Using liquid chromatography-mass spectrometry, the human claudin-low cell line, MDA-MB-231, showed no surface galectin-3, but surface expression of Gal-1 was shown to interact with Gal-3BP to form large oligomers and cell aggregates. Whereas hormone-receptor-positive MCF breast cancer cells had a lower level of homotypic cell aggregation, most likely due to reduced levels of LacNAc expression, which would cause lower Gal-1 affinity at the cell surface.[300] This study demonstrates the importance of glycolytic structures in the role of breast cancer metastasis. Galectins bind specifically to unique

carbohydrate structures, whereby they can generate downstream signaling pathways to control tumor progression. This study shows that claudin-low tumors may have a more aggressive cancer phenotype due to specific terminal LacNAc structures that bind Gal-1 with high affinity.

Gal-1 has been shown to bind to FOXP3 intracellularly. Previous studies showed that reduced nuclear FOXP3 protein expression was significantly associated with tumor progression in breast cancer patients. In this study, breast tissues expressed higher levels of nuclear Gal-1 than adjacent normal mammary tissue. Additionally, there was no statistical significance between the expression of nuclear Gal-1 and breast carcinoma characteristics, such as age, clinical stage, or hormone receptor status. For Gal-1 to bind to FOXP3, it must contain the carboxyl-terminal forkhead (FKH) domain required for FOXP3 nuclear localization and DNA binding, which results in the dysregulation of several oncogenes.[301] This data may be consistent with the previous study, which showed reduced FOXP3 expression in breast cancer, as it may be more challenging to detect the protein by standard biochemical methods when bound to Gal-1. The Gal-1-FOXP3 interaction may also shuttle Gal-1 to the nucleus, acting on other nuclear factors to regulate gene expression and pre-mRNA splicing.

1.3.6 Inhibitors of Galectin-1 Function

Methods for targeting Gal-1 include neutralizing monoclonal antibodies, glycoamine, and synthetic peptides. Many of these approaches have been tested in pre-clinical models, and few are used in clinical trials. Currently, there are no FDA-approved Gal-1-targeted therapies.

Most drug discovery efforts to date focus on preventing Gal-1 from binding galactosides. Many of these inhibitors are synthetically modified mono- or di-saccharides containing galactose, such as galactosides, lactosides, or similar molecules, such as TDG. Each saccharide is unique in its affinity, stability, or selectivity. For example, the monosaccharide galactose has a weaker

affinity for Gal-1 (Kd 10 mM) compared to the disaccharide, lactose (Kd 190 μM) or the oligosaccharide, TDG (Kd 24 μM).[304, 305] Monosaccharide inhibitors have better bioavailability and uptake but have a lower Gal-1 selectivity and affinity. When the C1 hydroxyl of galactose is modified with an aromatic moiety, the affinity towards Gal-1 increases by up to 10-40-fold,[305-307] however, this increase still does not reach the same affinity as a disaccharide, such as lactose. Even though lactose has a higher affinity over monosaccharides, it is efficiently catalyzed *in vivo* into its monosaccharides by the enzyme α-galactosidase and requires at least 10 mM concentrations before it can effectively inhibit Gal-1.[304]

Perhaps the most successful saccharide-based Gal-1 inhibitors are based on the molecular structure of TDG.[308] TDG has approximately an 8-fold higher affinity to Gal-1 compared to lactose.[309] *In vitro* and *in vivo,* TDG has been shown to positively affect the pro-inflammatory TME through Gal-1 inhibition by regulating immunosuppression and angiogenesis.[182] However, it is not selective towards a specific galectin; therefore, the effects cannot be exclusively attributed to the inhibition of Gal-1.[309, 310] To increase the affinity between TGD and Gal-1, derivatives with two aromatic amide substitutes have been developed.[308, 309] Like the parental TDG, Gal-1 is not the primary intended target of these derivatives; however, galectin-1 inhibition has been reported.[305, 309, 311]

Currently, the only non-carbohydrate inhibitors for Gal-1 are peptides and peptide mimics. The most well-known Gal-1 peptide inhibitor is Anginex, a small 33-amino acid ß-peptide that affects angiogenesis by diminishing the affinity of Gal-1 towards glycoproteins.[312, 313] One cellular target of Anginex is Gal-1, which is known to induce cell-cell attachment in endothelial cells.[314] Anginex has been shown to block micro-vessel formation *in vivo* without affecting major blood vessels.[315] Additionally, one study suggested that Anginex was able to decrease membrane-bound

H-Ras and downstream pathways significantly (Raf/MEK/ERK) in vascular endothelial cells.[316] However, Anginex is not selective for Gal-1 and reportedly binds to Gal-2, -7, -8, and -9.

After the success of Anginex, peptide topomimetics were developed based on the calix[4]arene-based backbone, which contains hydrophobic and hydrophilic faces similar to those found in the ß-sheet of Anginex. One of the most effective Gal-1 inhibitors, OTX008 (also known as PTX008, 0118, PTX009, and compound 1097), works as an allosteric inhibitor by binding the beta-sheet on the opposite side of the CRD.[317] This changes the conformation of Gal-1 and prevents it from binding to carbohydrate ligands.[318] The affinity of OTX-008 affinity for Gal-1 is approximately 50 μM, and it has been shown to be a potent angiogenesis inhibitor in ovarian and melanoma mouse models when used as a monotherapy.[314] When combined with chemotherapeutics *in vitro* and *in vivo*, OTX008 has demonstrated synergistic anti-angiogenic effects.[318, 319] It has been registered in a phase I clinical trial for solid tumors (NCT01724320).[320]

However, before Gal–1–based therapeutics can be effective, we must better understand the mechanisms of Gal-1 function in TME and metastasis. Other galectin functions and signaling pathways may also complicate Gal-1 signaling pathways, and understanding galectin-specificity for ligands under varying degrees of microenvironmental influence is imperative for determining the best approach for targeting galectin-glycan. Protein-protein interactions of Gal-1 may play a role in ligand association and maybe another pathway for therapeutic intervention. While there are multiple regulatory functions of Gal-1, more research is needed to determine how to best utilize its broad therapeutic potential.

1.4 Dissertation Synopsis

1.4.1 Research Hypothesis and Synopsis of Experiments

This research aimed to identify differentially expressed proteins in claudin-low breast cancer to gain insight into pathways and mechanisms that could lead to biomarkers or targets for intervention. Two murine transplantable triple-negative breast cancer (TNBC) tumors, denoted as 2225L and T11, were obtained for experimentation due to their analogous gene expression profiles mirroring those observed in human TNBC subtypes. Both tumor types were serial passaged heterotopically and orthotopically in syngeneic mice to generate lines that would consistently metastasize to the lung. The reliably metastatic variant of 2225L was termed 2225LM. In initial studies described in Chapter 3, biochemical, immunophenotyping, and RNA sequencing were used to characterize 2225LM and T11 reliably metastatic tumors and to compare tumors with variable metastatic potential. Both resulting 2225LM and T11 tumor lines displayed an immunosuppressive tumor microenvironment characterized by high myeloid-to-lymphocyte ratio ($CD11b^+$:$CD3^+$) and elevated expression of protumor cytokines compared to control tissues. The purpose of characterizing these tumors was to create reliable metastatic TNBC models in immunocompetent mice that could be utilized for translational research.

After initial characterization studies, proteomic analyses focusing on claudin-low T11 primary and metastatic tumors were conducted.. A pioneering discovery-based proteomic approach employing nano-liquid chromatography-tandem mass spectrometry (Nano-LC-MS/MS) and matrix-assisted laser desorption ionization imaging mass spectrometry (MALDI/IMS) was implemented to identify differentially expressed proteins in claudin-low breast cancer (CLBC). LC-MS/MS revealed galectin-1 (Gal-1) as a differentially overexpressed protein in claudin-low breast cancer compared to normal tissue. Label-free quantitation, Western immunoblot, and

ELISA techniques were used on T11 primary and metastatic tumors to validate this finding. Spatial distribution analyses utilizing MALDI/IMS and immunohistochemistry were performed on T11 metastatic tumors in the lungs. Additionally, immunohistochemistry of human breast cancer intrinsic subtypes showed intermediate to high-intensity Gal-1 staining in claudin-low primary tumors. *In silico* gene expression analysis using previously published microarray data and RNA sequencing analysis conducted by our lab on mouse and human breast cancer subtypes showed that Gal-1 levels were highest in the claudin-low subtype. Our lab was the first to demonstrate and subsequently validate that the carbohydrate-binding protein, Gal-1, was differentially expressed in mouse T11 claudin-low tumors compared to normal tissue, and in mouse and human claudin-low tumors compared to other breast cancer subtypes. . This work was presented at multiple extramural meetings and resulted in a publication by K. Balestrieri *et al.* in *Biochim. Biophys. Acta*, 2020.[321]

Galectin-1 is an N-acetyllactosamine (LacNAc)-binding protein that promotes anti-inflammatory actions and has a wide range of reported intracellular and extracellular activities, but its role in breast cancer has not been well studied. Inhibiting Gal-1 may target multiple pathways that aid in tumor progression, which could lead to improved strategies for cancer therapy. Previous studies in other labs have shown that exogenous Gal-1 can induce an M2-like cytokine profile in murine $CD11b^+$ macrophages and cause apoptosis in $CD11b^+$ monocytes. We conducted *in vitro*, *ex vivo*, and *in vivo* aimed to unravel Gal-1's impact on tumor-infiltrating immune cells, particularly $CD11b^+$ myeloid lineage cells.

Initial *in vitro* experiments using RAW 264.7 macrophages demonstrated that Gal-1 induced apoptosis in a dose-dependent, carbohydrate-specific manner. However, *ex vivo* experiments using thioglycolate-induced peritoneal exudate cells yielded discrepant results. To

reconcile these findings and garner a more physiologically relevant understanding, we transitioned to an *in vivo* orthotopic T11 CLBC model.

To resolve the discrepant *in vitro* and *ex vivo* apoptosis findings and to further investigate the effects of Gal-1 on $CD11b^+$ myeloid lineage cells and claudin low breast cancer (CLBC), we moved to an *in vivo* orthotopic T11 CLBC model. The transition to *in vivo* experiments was guided by the need for more physiologically relevant conditions to comprehensively evaluate the apoptotic effects of Gal-1 on $CD11b^+$ myeloid cells in the tumor microenvironment. *In vivo* systemic administration of galectin-1 allosteric inhibitor OTX008 in T11-tumor-bearing mice slowed tumor growth but did not affect the percentage of infiltrating myeloid populations. Fluorescence microscopy evaluation of overall tumor apoptosis and $CD3^+$ and $CD11b^+$ cell apoptosis in primary tumors at sacrifice showed no statistical difference between the OTX008 treatment and the vehicle control groups. These findings suggest that galectin-1 does not affect $CD3^+$ or $CD11b^+$ immune cell infiltration or apoptosis in claudin-low primary tumors. Larger *in vivo* studies and analysis of different drug regimens, smaller tumors and metastatic models are indicated.

Our research was not only the first to demonstrate the identification of Gal-1 as a highly differential protein in claudin-low breast cancer compared to normal tissue and other breast cancer subtypes but also laid the groundwork for future studies investigating actions of Gal-1 in this subtype. Future experiments should focus on exploring its potential effects on tumor proliferation and angiogenesis, positioning Gal-1 as a promising candidate for therapeutic targeting in claudin-low breast cancer.

1.4.2 Significance

Claudin-low breast cancer is an aggressive breast cancer subtype that does not have targetable markers for treatment. The primary course of treatment is chemotherapy, which is non-specific and highly toxic. Developing new therapies that can improve patient outcomes is imperative. We were the first to demonstrate that the carbohydrate-binding protein, Gal-1, was differentially expressed in mouse T11 claudin-low tumors compared to normal tissue, and in mouse and human claudin-low tumors compared to other breast cancer subtypes. Gal-1 is a multifunctional protein with many roles in the progression of cancer. Understanding how Gal-1 regulates claudin-low breast cancer progression could elucidate novel mechanisms or pathways that could be used as a claudin-low-specific therapy.

CHAPTER 2: MATERIALS AND METHODS

2.1 Contribution Acknowledgments

Dr. Kathryn Verbanac, Dr. Karen Oppelt, Keith Pittman, and Matthew Britt designed and executed experiments to eliminate LDEV from T11 primary tumors. Keith Pittman and Moses McDaniel provided hands on assistance when conducting *in vitro* and *in vivo* assays. Mohamed Ramez conducted flow cytometry data acquisition on infiltrating immune cells in primary 2225LM and T11 tumors presented in Chapter 3. Dr. Kim Kew advised on the design and analysis of proteomic experiments and helped with the execution of data acquisition for both the nano-liquid chromatography tandem mass spectrometry (nano-LC-MS/MS) and matrix-assisted desorption ionization imaging (MALDI-IMS) presented in Chapter 4. Dr. Kathryn Verbanac and Moses McDaniel conducted drug administration and blinded tumor volume assessments for the *in vivo* experiment presented in Chapter 5. For florescent microscopy experiments presented in Chapter 5, Dr. Elizabath Ables advised on the overall approach for collecting immunofluorescence and TUNEL data, and she helped acquire images and data using the confocal microscope. Additionally, Cindy Kukoly and Amanda Petritsch acquired the florescent images and data on the Cell Discoverer 7 and advised on the data acquisition and analysis. This work was supported by awards from the Leo W. Jenkins Cancer Center Oncology Research and Education Fund (KV and NV). We acknowledge the support of the Brody School of Medicine Mass Spectrometry Core at East Carolina University and the instrument that was sponsored by the Golden Leaf Foundation. This project used the North Carolina Tissue Consortium (NCTC) shared resource which is supported in part by the University Cancer Research Fund (UCRF) to the UNC Lineberger Cancer Center.

2.2 Animal Care

2.2.1 Generation of an LDEV-free T11 Murine Claudin-low Tumor

The original T11 tumor was received from two sources: Dr. Jason Herschkowitz and Dr. Jeffrey Rosen (Baylor College of Medicine) and David Darr and Dr. Charles Perou (University of North Carolina at Chapel Hill). When tested for mouse pathogens by PCR (Charles River). Tumors from both sources were found to be infected with murine Lactate Dehydrogenase Elevating Virus (LDEV). To generate T11 tumors free of LDEV, virally infected mouse tumors were serially passaged in nude rats using a protocol adapted from several publications.[322, 323] Female RNU nude rats (Charles River, strain #316) were housed in isolator cages in a specific pathogen-free room. Tumors [2x2 mm fragments] were implanted into the subcutaneous flank of 6–14-week-old rats within a biosafety cabinet. Tumors were resected between 13-26 days post-implant when they reached approximately 4 cm in diameter. A 10 mm^3 fragment of the resected tumor was subsequently passage into naïve nude rats for an additional two passages. Residual tumor tissue from each source and at each passage was placed in 50% freezing media (Dulbecco's Modified Eagle Medium (DMEM), 30% Fetal Bovine Serum (FBS), 20% dimethylsulfoxide (DMSO)) and frozen in liquid nitrogen for long-term storage. Tumors were analyzed for the single-strand LDEV RNA by PCR at Charles River Labs. LDEV-free T11 tumors were passaged into the subcutaneous (sc) flank or mammary fat pad of female, syngeneic, Balb/c mice. This work was carried out by Matt Britt, Keith Pittman, and Dr. Kathryn Verbanac. All procedures involving animals were performed using ECU IACUC-approved protocols.

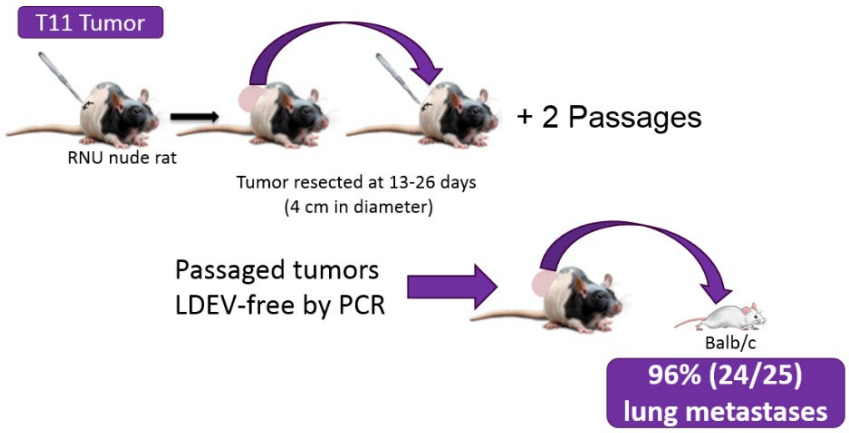

Figure 1 Removal of Lactate dehydrogenase elevating virus (LDEV) from murine T11 transplantable tumor model by serial passaging into athymic nude rats

The murine T11 transplantable tumor model is representative of claudin-low breast cancer. When tested for mouse pathogens before implantation, T11 was positive for LDEV, a murine virus that infects macrophages. To eliminate LDEV, T11 tumors were serially passaged twice into athymic nude rats. The resulting LDEV-free T11 tumors were tested for LDEV by PCR and were virus-free. The LDEV-free T11 tumor was passaged into syngeneic Balb/c mice for *in vivo* studies. In initial studies (passages 1-5), mice developed metastatic lung lesions 96% (24/25) of the time after serial resection of the subcutaneous primary tumors. Dr. Kathyrn Verbanac, Dr. Karen Oppelt, Keith Pittman, and Matthew Britt designed and executed these experiments.

2.2.2 *In vivo* Studies with T11 Claudin-low Tumor Model

T11 dissociated tumor cells ($5x10^5$ cells/mouse), or 2x2 mm^3 tumor fragments were implanted into a mammary fat pad (mfp) of female (6-8-week-old) Balb/c mice (Charles River, strain #028) through a midline abdominal incision. When tumors became palpable (5-9 days post-implant), tumor growth was measured using digital calipers, and the volume was calculated as (width x width x length)/2. Primary tumors were surgically resected when they reached a volume of approximately 500 mm3 to promote the growth of seeded metastases. Before surgery, mice were anesthetized with 1-4 % isoflurane in oxygen and were administered buprenorphine (0.1 mg/kg via subcutaneous injection) before and after surgery to minimize pain. After tumor inoculation and subsequent tumor removal until euthanasia, mice were monitored daily for clinical signs of discomfort, including body weight loss and lethargy. Mice were sacrificed approximately

30 days post-tumor resection by isoflurane asphyxiation. All procedures involving animals were performed using ECU IACUC-approved protocols.

2.2.3 Intraperitoneal Treatment with Allosteric Galectin-1 Inhibitor OTX008

T11 cells ($5x10^5$ cells/mouse in 100 µL 1:1 DMEM: Matrigel; Corning, 354234) were injected into the mammary fat pad of 8 weeks old, female Balb/c mice through a small midline incision using a 25-gauge sterile syringe. After tumors were palpable, volumes were measured with calipers daily. On day 7, when the average tumor size had reached approximately 100 mm3, OTX008 (Caymen Chem, 23130, 10 mg/kg) or sterile PBS was intraperitoneally injected using a 22-gauge sterile syringe. Mouse body weight was monitored, and injections were repeated every three days until day 14 and 15 post-tumor injections when the average tumor size reached approximately 1000 mm^3. Harvested tumors were cut into three pieces for subsequent flow cytometry and fluorescent microscopy analysis. Tumor growth curves were analyzed using a two-way ANOVA with post-hoc Sidak's test and linear regression to compare the slope of two lines. Potential outliers were determined using three methods, interquartile range, ROUT, and Grubbs' outlier analysis.

2.2.4 Peritoneal Macrophage Isolation by Thioglycolate-injection

Male or female 5–36-week-old mice (Balb/c, CD-1, or C57BL/6) were injected intraperitoneally with 0.5 mL of warmed, sterile 4% thioglycolate medium (Sigma) as described.[324-327] Mice were euthanized four days post-injection by isoflurane overdose and cervical dislocation. Peritoneal exudate cells (PEC) were collected by injecting 5 mL cold PBS into the abdomen, massaging the abdomen for two minutes, and aspirating the solution. The collected solution was centrifuged 325 x g to pellet cells. After resuspension in DMEM or PBS, the number and viability of cells were determined by Trypan blue exclusion and a hemacytometer.

2.2.5 Human Tissue Samples

All procedures performed in studies involving human participants were in accordance with the ethical standards of the institutional committee (University & Medical Center Institutional Review Board, 13-001654) and with the 1964 Helsinki declaration and its later amendments or comparable ethical standards. FFPE blocks of normal breast and breast cancer samples were obtained from an IRB-approved retrospective translational study (UMCIRB 13-001654) of breast cancer patients who received standard-of-care treatment at our center from 2000-2010. Samples from both IRB protocols were used for immunohistochemical staining for galectin-1. All human research studies were approved by the University and Medical Center Institutional Review Board (UMCIRB) and samples were obtained with authorized access under approved protocols.

2.3 Cell Culture

2.3.1 T11 Cell Culture

To adapt to tissue culture, an LDEV-free primary T11 tumor resected from a syngeneic Balb/c mouse was digested with DNase/collagenase II and passed through a 70 μm nylon filter to obtain a single cell suspension. Cells were maintained in RPMI with 10% FBS and 1% Penicillin-Streptomycin for the initial passage and 5% FBS without antibiotic for subsequent passages in a humidified incubator at 37°C, 5% CO2. Cells were passaged in culture 8-10 times before experimental use. For low serum and serum-free conditions, T11 cells were maintained in RPMI with 1% FBS or Mouse EpiCult-B Basal Medium with EpiCult-B Proliferation Supplement for up to three passages. Adherent cells were detached using 0.5 mM EDTA solution when cells reached 80-90% confluence and counted using a hemocytometer. Cell viability was determined by Trypan blue.

2.3.2 RAW 264.7 Cell Culture

RAW 264.7 cells were obtained from ATCC (TIB-71). Upon receipt, cells were thawed by gentile agitation in a 37°C water bath. Cells were washed in DMEM and centrifuged 325 x g for 5 minutes to pellet cells. Cells were resuspended in DMEM with 20% FBS and 1% Penicillin-Streptomycin for the initial passage and 10% FBS for subsequent passages in a humidified incubator at 37°C, 5% CO^2. Media was replaced every 2-3 days as needed. Adherent cells were detached using 0.5 mM EDTA solution when cells reached 80-90% confluence and counted using a hemocytometer. Cell viability was determined by Trypan blue. Cells were passaged in culture five times before experimental use.

2.4 Flow Cytometric Analysis

2.4.1 Sample Preparation for the Detection of Infiltrating Immune Cells in Primary Tumor and Metastatic Lung by Flow Cytometric Analysis

Primary tumors or lungs were placed in 1 mL DNase Collagenase type II and chopped into small pieces using a scalpel blade. Samples were placed in a 50 mL conical tube, and an additional 2 mL DNase Collagenase type II was added to the sample. Samples were placed on a shaker at room temperature for 1 hour. The digested tissue was strained through a 70 µm filter into a new centrifuge tube, washed with PBS, and centrifuged at 325 x g at 10°C for 10 minutes. Excess supernatant was removed from the sample, and 100-1000 µL of AKC Lysis Buffer was added for 1 minute at room temperature to remove red blood cells. Cells were washed in PBS, 0.2% BSA, 0.05% azide, centrifuged at 325 x g at 10°C for 10 minutes, and counted by hemocytometer with Trypan blue to determine viability. Cells were resuspended at $2x10^5$ cells/10 µL for antibody labeling.

Table 4: Antibodies used in flow cytometry

Antibody target	Fluorophore	Clone	Isotype	Host	Manufacturer	Catalog #
Mouse CD3e	APC	145-2C11	IgG1	Rat	BD Pharmingen	553066
Mouse CD3e	APC	145-2C11	IgG1	Hamster	BioLegend	100312
Mouse CD8a	FITC	53-6.7	IgG2a	Rat	BD Pharmingen	553030
Mouse CD11b	PE-Cy7	M1/70	IgG2b	Rat	Life Technologies	A15848
Mouse CD11b	APC	M1/70	IgG2b	Rat	eBioscience	17-0112-83
Mouse CD29	PE-Cy7	HMb1-1	IgG2b	Hamster	abCam	Ab95622
Mouse CD45	PerCP-Cy5.5	30-F11	IgG2b	Rat	BD Pharmingen	550994
Mouse CD68	APC	FA-11	IgG2a	Rat	BioLegend	137008
Mouse F4/80	APC-eFluor 780	BM8	IgG2a	Rat	ThermoFisher	47-4801-80
Mouse F4/80	PE-Cy5	BM8	IgG2a	Rat	BioLegend	123112
Mouse F4/80	SuperBright 780	BM8	IgG2a	Rat	eBiosciences	78-4801-80
Mouse Galectin-1	Alexa Fluor 647	RM0081-9J26	IgG2b	Rat	R&D Systems	NBP1-21721AF647
Mouse Ly6C	APC-Cy7	HK1.4	IgG2c	Rat	BioLegend	128026
Mouse Ly6G	PE	1A8	IgG2a	Rat	BD Pharmingen	551467 and 551461
Mouse MHCII	Alexa Fluor 488	M5/114.15.2	IgG2b	Rat	BioLegend	107616
Mouse Vimentin	Alexa Fluor 647	EPR3776	IgG	Rabbit	AbCam	Ab194719
	Alexa Fluor 647	EPR25A	IgG	Rabbit	AbCam	Ab199093
	Alexa Fluor 647	141945	IgG2b	Rat	R&D Systems	IC013R
	Alexa Fluor 647	RTK4530	IgG2b	Rat	BioLegend	400626
	APC	A110-1	IgG1	Rat	BD Pharmingen	553974
	APC	RTK2758	IgG2a	Rat	BioLegend	400512
	APC	aB149/10H5	IgG2b	Rat	eBioscience	17-0431-82
	APC-eFluor 780	eBM2a	IgG2a	Rat	eBioscience	47-4321-80
	APC-Cy7	RTK4174	IgG2c	Rat	BioLegend	400719
	FITC	R35-95	IgG2b	Rat	BD Pharmingen	553929
	PE	R35-95	IgG2a	Rat	BD Pharmingen	557076
	PE-Cy5	RTK2758	IgG2a	Rat	BioLegend	400510
	PE-Cy7	RTK4530	IgG2b	Rat	BioLegend	400617
	PE-Cy7	eBio299Arm	IgG2b	Hamster	eBiosciences	25-4888-81
	PerCP-Cy5.5	A95-1	IgG2b	Rat	BD Pharmingen	550764
	Super Bright 780	eBM2a	IgG2a	Rat	eBiosciences	78-4724-82

2.4.2 Flow Cytometric Analysis of Cell Surface and Intracellular Proteins

Cells prepared from mouse tissues or cell culture were treated with CD16/32 FcR blocker (BD Pharmingen, 553141) in staining buffer (PBS with 0.2% BSA, 0.05% Azide). Fluorophore-conjugated antibodies (**Table 4**) were added to 1-2x10^5 cells/10 µL staining buffer in round bottom culture tubes, and samples were incubated in the dark at 4°C for 30 minutes. For intracellular protein detection, such as galectin-1 and Vimentin, cells were fixed in 1% paraformaldehyde in PBS, followed by permeabilization with 0.1% Saponin in PBS for 15 minutes at room temperature. After washing with staining buffer, cells were incubated with fluorophore-conjugated antibodies

for 30 minutes on ice in the dark. Cells were washed with PBS 0.5% Azide to remove excess antibodies and were resuspended in 200 µL 1% paraformaldehyde while vortexing. Data was acquired using BD LSRII and analyzed using FACSDiva, FlowJo, or FCSExpress software, as indicated in the results. **Table 2** defines cell populations based on protein expression.

2.4.3 Flow Cytometric Analysis for the Detection of Apoptotic Cells after Treatment with Recombinant Galectin-1

Alexa Fluor® 488 annexin V/Dead Cell Apoptosis Kit with Alexa® Fluor 488 annexin V and PI for Flow Cytometry (Invitrogen, V13241) was used according to the manufacturer's protocol. Briefly, cells prepared from cell culture or peritoneal cell exudate were washed in PBS and centrifuged at 320 x g at 4°C for 10 minutes. Cells were counted and resuspended in annexin-binding buffer (50 mM HEPES, 700 mM NaCl, 12.5 mM CaCl2, pH 7.4) at $2x10^5$ cells/50 µL in round bottom culture tubes. Cells were treated with 50 µL of 15 µg/mL Concanavalin A with or without 4-100 mM lactose or mannose in annexin-binding buffer, 1.8-30 µg/mL recombinant galectin-1 with or without 4-100 mM sucrose, lactose, mannose, *N*-acetyllactosamine (LacNAc), or *N*-acetylglucosamine (GlcNAc) for 15 minutes at room temperature. In select experiments, where noted, to rule out potential lipopolysaccharide (LPS) contamination, samples were also treated with 0.1 µg/mL polymyxin B or CD16/32 FcR blocker followed by rat anti-mouse CD14 (M14-21; BioLegend, 150102) in staining buffer (PBS with 0.2% BSA, 0.05% Azide). Annexin V-Alexa Fluor 488 and 100 µg/mL propidium iodide (PI) were added to each sample, and samples were incubated at room temperature for 5-30 minutes. After incubation, 200 µL annexin-binding buffer was added to each sample. Samples were placed on ice, and data was acquired immediately using BD LSRII. FCSExpress software was used for data analysis.

2.4.4 Datura stramonium lectin (DSL)-labeling to determine N-acetyllactosamine (LacNAc)expression

Cells prepared from cell culture were washed with PBS, 1% BSA, and centrifuged at 320 x g at 10°C for 10 minutes. Cells were counted and resuspended in PBS at $1x10^5$/10 µL. Viability was determined by Trypan blue. Fluorescein-labeled Datura stramonium lectin (DSL-FITC, Vector, # FL-1181) was added to $2x10^5$ cells in round bottom culture tubes at a final concentration of 0.02 µM with or without 4-8 mM chitobiose or LacNAc. Samples were incubated in the dark at room temperature for 15 minutes. Cells were washed in PBS, 0.2% BSA, 0.05% Azide, centrifuged at 320 x g at 4°C for 10 minutes, and cells were resuspended in 200 µL PBS, 0.2% BSA, 0.05% Azide for immediate acquisition on immediately using BD LSRII. FCSExpress software was used for data analysis.

2.5 Multiplex Immunobead Assay

Flash frozen primary tumor, metastatic lungs, and control mammary fat pad and lungs were homogenized by polytron 0.05% Tween-20/Tris-HCl lysis buffer containing protease inhibitor cocktail (Sigma-Aldrich, P2714). After centrifugation at 4°C (12,000 x g, 10 minutes), the bicinchoninic acid (BCA) assay determined protein concentrations on supernatants. MILLIPLEX MAP Mouse Cytokine/Chemokine Immunology Multiplex Assay (Sigma, MCYPMX32-MAG) was used according to the manufacturer's instructions. Briefly, sample concentrations were adjusted to 1 mg/mL total protein in lysis buffer and combined in a 1:1 ratio of sample to assay buffer solution. Samples (25 µL) were loaded into a white 96-well plate, and then 25 µL magnetic Multiplex beads were added to each well. The plate was sealed, wrapped in aluminum foil, and placed on a shaker at 300 RPM at 4°C overnight. The next day, the plate was placed on a magnet to wash twice with 200 µL wash buffer. Detection antibodies (25 µL) were added to each well.

0The plate was sealed, wrapped in aluminum foil, and placed on a shaker at 300 RPM, room temperature, for 1 hour. After incubation, Streptavidin-Phycoerythrin (25 µL) was added to each well, the plate was sealed, wrapped in aluminum foil, and returned to the shaker at room temperature for an additional 30 minutes. The plate was washed twice on a magnet with wash buffer, and 150 µL of drive fluid was added to each well. Data was collected with MagPix and analyzed with the median fluorescent intensity (MFI) using a 5-parameter logistic curve-fitting method in xPONENT software. The assay included analytes for G-CSF, eotaxin, GM-CSF, IFNγ, IL-1α, IL-1β, IL-2, IL-4, IL-3, IL-5, IL-6, IL-7, IL-9, IL-10, IL-12 (p40), IL-12 (p70), LIF, IL-13, LIX, IL-15, IL-17, IP-10, KC, MCP-1, MIP-1α, MIP-1β, M-CSF, MIP-2, MIG, RANTES, VEGF, and TNFα.

2.6 RNA Sequencing of Mouse Lungs and Primary Tumors

2.6.1 RNA Isolation

Flash-frozen murine primary tumors were homogenized by polytron in 1 mL TRIzol reagent per 50 mg of tissue. Homogenized samples were incubated for 5 min in a 25°C water bath, then added 0.2 mL chloroform/1 mL of TRIzol reagent. Samples were mixed vigorously and centrifuged at 12,000 x g for 15 minutes at 4°C. The upper colorless, aqueous phase was removed, and then RNA was precipitated by adding equal volume isopropanol and incubating overnight at -20°C. The following day, samples were centrifuged at 12,000 x g for 10 min at 4°C, the supernatant was removed, and the RNA pellet was washed once with 75% ethanol. The pellet was air-dried and dissolved in RNase-free water. Nanodrop and Qubit determined RNA concentration.

2.6.2 RNA Sequencing of Mouse Primary Tumor and Lung Tissue

Samples with an RNA Integrity Number (RIN) ≥6.0 were sent to Novogene for RNA sequencing (RNA-Seq). RNA expression was normalized by the DEseq method implemented in

the DEseq2 R package; then, expression levels were extracted. Novogene performed downstream analysis using programs, including STAR, HTseq, Cufflink, and Novogene's wrapped scripts. Alignments were parsed using the Tophat program, and differential expressions were determined through DESeq2/edgeR. GO and KEGG enrichment were implemented by the ClusterProfiler. Gene fusion and the difference of alternative splicing events were detected by Star-fusion and rMATS software. For comparison of Lgals1 expression between the basal-like and claudin-low tumors, a student t-test was performed using Prism software (GraphPad). A p-value of 0.05 or less was considered significant.

2.6.3 RNA Sequencing of Human Primary Tumors

Data for RNA sequencing of human tumors was provided by Kevin Gardner from an IRB-approved retrospective translational study (UMCIRB 13-001654). Tissue cores were extracted from a subset of deceased patients (n=143). RNA expression was normalized using the DEseq normalization method implemented in the DEseq2 R package. RNA sequencing data was analyzed for breast cancer intrinsic subtypes and for published claudin-low signatures. Normalized data was mined for LGALS1 expression levels. Prism software (GraphPad) was used for analysis. One-way ANOVA Dunn's post hoc tests were used for multiple comparisons to compare expression to the claudin-low subtype. Nonparametric analysis was conducted using the Kruskal–Wallis test. P values of 0.05 or less were considered significant. All human research studies were approved by the University and Medical Center Institutional Review Board (UMCIRB) and samples were obtained with authorized access under approved protocols.

2.6.4 Data Mining from Published Microarray Data for Mouse and Human Tumor Samples

Mouse primary tumor microarray data from accession number GSE27101 for platform GPL4134 and human primary tumor microarray data from accession number GSE18229 for

platforms GPL885, GPL887, GPL1390, GPL1708, GPL5325, GPL6607, and GPL7504 were downloaded from the NIH GEO database repository. Data was mined for LGALS1 (Gal-1) expression levels using the field LOG_RAT2N_MEAN, which is the log2 ratio of (CH2IN_MEAN - CH2BN_MEDIAN) over (CH1_MEAN - CH1_BKD_MEDIAN) where CH2IN_MEAN and CH2BN_MEDIAN are global-normalized intensities.

2.7 Mass spectrometry

2.7.1 Sample Preparation for Nano-Liquid Chromatography Mass Spectrometry (Nano-LC-MS/MS) and Matrix-Assisted Laser Desorption Ionization Mass Spectrometry Imaging (MALDI-IMS)

A recombinant carrier-free mouse galectin-1 standard (rGal-1; R&D Systems, 1245-GA/CF) was diluted (0.5-250 ng/mL) in Optima grade water (Thermo Fisher Scientific, W6-4) to determine the lowest detection limit. Optima grade water, acetonitrile (ACN) (Thermo Fisher Scientific, A955-4), and formic acid (Thermo Fisher Scientific, A117-50) were used for standard preparation and as nano-LC-MS/MS mobile phases. For nano-LC-MS/MS, the rGal-1 standard was trypsin-digested (Promega, V5111) at a 1:50 protein concentration to trypsin weight: weight as described in section 2.4. For MALDI sample slides, 2 µL of trypsin digest was pipetted on an ITO-conductive slide (Delta Technologies Limited, CG-811N-S1159) with 1:1, 10 mg/mL sinapinic acid (SA) dissolved in 60:40 ACN: water, containing 0.07% trifluoroacetic acid (TFA) (Thermo Fisher Scientific, A116-10X1AMP). The trypsinized rGal-1 standard was analyzed using MALDI/TOF MS in positive ionization reflectron mode.

2.7.2 Nano-LC-MS/MS Sample Preparation

Cultured tumor cells and tissues were sonicated or polytron homogenized in 300-500 µL of 0.05% Tween-20/Tris-HCl lysis buffer containing protease inhibitor cocktail (Sigma-Aldrich,

P2714) followed by centrifugation for 10 minutes at 12,000 x g. Supernatants were collected for further processing. Samples with high albumin signals were re-analyzed following albumin precipitation as described.[328] The precipitation protocol was modified for tissue lysate, where 50 µL of the sample was mixed with 500 µL of 1% trichloroacetic acid: isopropanol (volume: volume). Precipitated pellets were resuspended in 50 µL of lysis buffer. In-solution digestion of proteins was conducted as described[329] with the following modifications. Protein concentrations were estimated spectrophotometrically (Nanodrop 1000) before and after precipitation. All samples were diluted 1:2.5 volume: volume in 6 M urea/50 mM Tris-HCl, pH 8.0. Dithiothreitol and iodoacetamide were added per the referenced protocol. 1 mM CaCl2/50 mM Tris-HCl, pH 7.6 was used in a 1:1 ratio volume: volume with 6 M urea/50 mM Tris-HCl, pH 8.0. Trypsin was added at recommended ratios of 1:20-1:100 trypsin weight: protein weight and incubated at 37°C for 17 hours. Trypsin concentrations and digestion times were optimized for each sample type. The trypsin reaction was stopped by adding 0.1% formic acid.

2.7.3 Nano-LC-MS/MS Data Acquisition

Recombinant carrier-free mouse galectin-1 (rGal-1; R&D Systems, 1245-GA/CF) was serial diluted (0.5-250 ng/mL) in water. Standards, cell, and tissue lysates were analyzed with an Eksigent 425 nanoLC/AB Sciex 5600+ Triple time-of-flight mass spectrometer (nano-LC-MS/MS). The samples were injected with a trap and elute method. The peptides were eluted using a gradient of up to 80% ACN with 0.1% formic acid. Samples were injected at 5 or 10 µL (1-2.5 µg protein) on a ChromXP C18CL column, 150 x 0.3 mm and 3 µm particle size, maintained at 25°C with a nano-flow rate of 300 nL/min. Both MS and MS/MS data were collected in positive ionization mode. The instrument settings were 100 V for the declustering potential, 10 for the collision energy, 10 for the source gas, 25 for the curtain gas, 2.8 kV on the ion spray, and 150°C

for the interface heater temperature. The MS parameters included scanning from 400 to 1500 Da with an accumulation time of 0.250 sec for 90 min. The MS/MS data were collected using an independent data acquisition (IDA) method. The IDA settings included selecting the top twenty masses within 400-1250 Da with a charge state of either +2, +3, or +4 and exceeded 150 counts/sec signal intensity. Mass calibration was conducted every five samples using a PepCal mix.

2.7.4 Nano-LC-MS/MS Data Analysis

Protein identifications for nano-LC/MS and LC/MS/MS data were conducted using Protein-Pilot v4.5 (Sciex) software. Samples were batched according to tissue type (i.e., mammary fat pad, tumor, control lung, metastatic lung) for 5 and 10 µL injections before and after albumin precipitation. For protein identification, the UniProt protein database containing 862,507 proteins for Mus musculus species was searched using the Paragon algorithm within Protein-Pilot. The bias correction option was executed. Global false discovery rate (FDR) and local FDR are reported to indicate the level of confidence in identified proteins. A decoy database search strategy was used to estimate the FDR, defined as the percentage of decoy proteins identified relative to the total proteins identified, with a threshold of 0.05 for local and 0.01 (corresponding to 95% and 99% confidence, respectively) for global protein identifications. All protein identifications obtained for each tissue were uploaded to the Reactome Knowledgebase (https://reactome.org) 18 for pathway analysis of Mus musculus using the UniProt protein accession numbers.

2.7.5 MALDI-IMS Sample Preparation

Flash-frozen primary tumor (n=3) and metastatic and control lung tissues (n=4 and n=3, respectively) were mounted to a cryostat chuck with HPLC-grade water in a dry ice container to freeze and fuse the tissue in place for sectioning. Tissue sections (10 µm) were thaw-mounted onto ITO-conductive microscope slides and maintained at -80°C until analysis. Slides were

sequentially washed in 70%, 90%, and 95% ethanol diluted in water for approximately 30 seconds each and then placed into a vacuum desiccator for 20-30 minutes. For trypsin digestion, a 0.025% trypsin solution prepared in a total volume of 460 µL with 20 µL, 1 µg/µL sequencing-grade trypsin, 330 µL 100 mM sodium bicarbonate containing 0.01% ammonium hydroxide, 40 µL acetonitrile, and 70 µL acetic acid. The solution was incubated at 30°C for 10 minutes to activate before application on the tissue using an HTXImaging TM-sprayer. Trypsin solution was deposited on the slide at 60 µL/min flow rate, 10 psi N2 gas pressure, 30°C nozzle temperature, 600 mm/min velocity, 2 mm track spacing, and two passes in a crisscross pattern. After trypsin application, the more porous lung samples were incubated at 37 °C for 30 minutes, 1 hour, and 2 hours. In contrast, denser primary tumor samples were incubated at 37°C for 2 and 4 hours to determine optimal trypsin application time. Spectra were analyzed using FlexAnalysis to assess the range of spectral peaks. All samples reported herein were trypsinized at the optimal digestion time (2 hours for lung tissue and 4 hours for tumor tissue). TM sprayer was used to apply SA matrix (10 mg/mL in 70:30 ACN: water with 0.3% TFA) to stop the trypsin reaction under the following conditions: 0.06 mL/min solvent flow rate, 10 psi N2 gas pressure, 30 °C nozzle temperature, 750 mm/min velocity, 2 mm spacing and 12 passes in a crisscross pattern.

2.7.6 MALDI-IMS Data Analysis

MALDI/IMS data was processed using SCiLS, FlexImaging (Bruker), and FlexAnalysis (Bruker) software. Images were normalized using TIC. Regions of metastases were determined by standard hematoxylin and eosin (H&E) staining of tissue sections used for MALDI/IMS after removing the SA matrix and/or by staining adjacent serial sections. Gal-1 peptides were determined by both MS-Bridge of theoretical Gal-1 trypsin-digest and normalized spectra from rGal-1 standard or tissue sections. Bridged Gal-1 peptides were searched using the mascot search

engine (Matrix Science Limited) and analyzed using BLAST (NCBI) to determine uniqueness. The parameters used to search the Uniprot database included two missed cleavages, Mus musculus taxonomy, no variable modifications, average mass, and a peptide tolerance of 1.0 Da.

2.8 SDS Page and Western Immunoblot

2.8.1 Galectin-1 Expression in Cultured Cells and Tissue Samples

Flash-frozen tissues were homogenized by polytron in 0.05% Triton-X /phosphate-buffered saline containing protease inhibitor cocktail (Sigma-Aldrich, P2714) at pH 7.0. After centrifugation at 4°C (12,000 x g, 10 minutes), the BCA assay determined protein concentrations on supernatants. SDS-PAGE was performed using NuPAGE™ 4-12% Bis-Tris Protein Gels. All samples (0.04 µg rGal-1 standard and 2-8 µg tissue lysate) were heated at 95°C for 5 minutes before electrophoresis. After SDS-PAGE, samples were transferred to a nitrocellulose membrane. We used a reversible total protein stain consistent with the currently recommended methodology to control for protein loading.[330-332] Membranes were stained with MemCode™ Reversible Protein Stain Kit (Thermo Scientific) per the manufacturer's protocol to visualize and quantify total protein. After scanning, de-staining, and blocking with 0.05% Tween 20/3% BSA/Tris Buffered Saline overnight at 4°C, membranes were incubated for 1 hour at room temperature with rabbit anti-galectin-1 (Abcam, ab138513, clone EPR3206). Protein bands were visualized after a 30-minute incubation with an alkaline phosphatase-conjugated anti-rabbit secondary antibody (Sigma, A9919) and developed with the BCIP/NBT Liquid Substrate System (Sigma). Both protein-stained membranes and Western immunoblots were scanned using the BioRad ChemiDoc™ Imaging System and analyzed with BioRad Image Lab™ Version 6.0 software. The Gal-1 signal intensity (Adjusted Total Band) was divided by the loading control intensity

(Memcode™ total protein; Adjusted Total Lane) to normalize Western blot signal intensity between samples.

2.8.2 Detection of recombinant galectin-1 protein aggregates

Recombinant carrier-free mouse galectin-1 (2-3.6 µg total protein; R&D Systems, 1245-GA/CF). Samples (10 µL) were applied to a 12-14% polyacrylamide separating gels (recipes in **Table 5**) and electrophoresed in 1X SDS-PAGE running buffer (25 mM Tris, 192 mM glycine) at 125 V for 3.5 hours. GelCode™ Blue Stain Reagent (ThermoFisher, 24590) was used to analyze the protein purity of the recombinant Gal-1 per the manufacturer's instructions. Gels were scanned using the BioRad ChemiDoc™ Imaging System.

Table 5: SDS-PAGE Solution Recipes

	Stacking gel (mL)	12% separating gel (mL)	14% separating gel (mL)
Distilled water	1.13	1.14	0.44
Gel buffer (0.5 M Tris-HCl, pH 8.8)	3.20	4.86	4.86
Acrylamide/bis-acrylamide solution (29:1)	0.670	4.00	4.70
20% ammonium persulfate	0.050	0.050	0.050
N, N, N', N'-tetramethylethylenediamine	0.005	0.005	0.005

2.9 Immunohistochemistry of Mouse and Human Tumors

Murine T11 primary tumors (n=2), lungs with T11 metastatic lesions (n=2), naïve mouse mammary fat pads (n=2), and lung tissues (n=2) were stained for Gal-1 protein expression by immunohistochemistry. Human breast tumors of varied intrinsic subtypes were also stained for Gal-1 protein expression by immunohistochemistry (n=4-6 tumors of each subtype). FFPE blocks were available for 4 of the eight human tumors classified as claudin-low. Both mouse and human FFPE tissue sections (5 µm) were deparaffinized and incubated in 3% hydrogen peroxide for 10 minutes to quench endogenous peroxidase. After three washes in PBS, non-specific binding sites were blocked (0.5% BSA/0.5% casein/PBS, pH 7.6 or Protein Block from Anti-Rabbit HRP DAB Detection System (Spring Bioscience). Sections were incubated with the primary rabbit anti-

galectin-1 antibody (Abcam, ab138513, clone EPR3206) diluted in a blocking solution at 4°C overnight. Negative controls were set with unlabeled control IgG isolated from normal rabbit serum (Abcam, EPR25A). The Anti-Rabbit HRP DAB Detection System (Spring Bioscience) was used for protein detection following the manufacturer's protocol. Sections were counter-stained with Mayer's hematoxylin, dehydrated, mounted with Permount, and scanned using an Aperio slide scanner. For human specimens, a pathologist evaluated slides for Gal-1 staining by blinded review.

2.10 ELISA for the quantification of galectin-1 expression in primary, metastatic tumors, and serum

Flash-frozen tissues were homogenized by polytron in 0.05% Triton-X /phosphate-buffered saline containing protease inhibitor cocktail (Sigma-Aldrich, P2714) at pH 7.0. After centrifugation at 4°C (12,000 x g, 10 minutes), the BCA assay determined protein concentrations on supernatants. Mouse Galectin-1 DuoSet ELISA kit (R&D Systems, DY1245) was used to quantify Gal-1 in the primary tumor, mammary fat pad, metastatic and normal tissue, and serum according to the manufacturer's protocol. Gal-1 levels were normalized to tissue weight (mammary fat pad tumor) or total protein concentration (tumor and lung tissues). Whole blood was collected through submandibular bleed into 500 µL conical test tubes and left at room temperature for 30 minutes to allow for clotting. Blood samples were centrifuged at 4°C and 1,500 x g for 10 minutes to remove the clot. The top serum layer was isolated by pipette, placed in a new conical tube, and stored at -80°C until testing. Serum samples were slowly thawed and diluted 1:20 in the reagent diluent provided in the kit.

2.11 Caspase 3/7 Glo Assays for the detection of caspase-dependent apoptosis in macrophages

RAW 264.7 and peritoneal exudate cells (10,000 cells/50 µL DMEM,10% FBS/ well) were plated into a 96-well white-walled plate. Cells were treated with 1-2 µM recombinant galectin-1 (R&D Systems, 1245-GA/CF), 5 µM camptothecin (positive control) or DMSO vehicle (negative control) for 15 min-4 hr. before testing caspase 3/7 activity using the Caspase-Glo 3/7 Assay (Promega, G8090) according to the manufacturer's instructions.

2.12 Fluorescent microscopy for the detection of apoptotic immune cells in T11 claudin-low primary tumors treated *in vivo* with or without galectin-1 inhibitor, OTX008

Harvested tumors were washed in PBS, fixed in formaldehyde, and embedded in paraffin. Tissue sections (5 µm) were cut using a microtome, deparaffinized, and boiled in citrate buffer, pH 6.0 for antigen retrieval before terminal deoxynucleotide transferase-dUTP nick end (TUNEL) and antibody labeling. TUNEL labeling was performed using Click-iT Plus TUNEL Assay Kit Alexa Fluor 597 (Invitrogen, C10618) according to the manufacturer's instructions and included a DNase I-treated (Thermo Fisher, 18068015) positive control and negative control lacking EdUTP. Protein blocking and antibody labeling were performed before the TUNEL enzyme reaction on sections co-stained with anti-CD3 labeled slides and after the enzyme reaction on sections co-stained for anti-CD11b. Tissue sections were blocked with 0.5% Sodium Casienate, 0.5% BSA, and 0.1% Azide for 30 minutes at room temperature. After blocking, CD3 Rabbit Anti-Mouse Monoclonal Antibody (Abcam ab16669, 1.3 µg/mL), CD11b rabbit anti-mouse monoclonal antibody (Abcam ab133357, 2.7 µg/mL), or an equal concentration of isotype-matched IgG (Abcam ab172730) was added to the slide and incubated overnight at 4°C in the dark. Slides were washed with 0.1% Triton X-100 in PBS followed by PBS alone before adding goat anti-rabbit IgG secondary Alexa Fluor 488 (Abcam, ab150077, 4.0 µg/mL) and incubating for 1

hour at room temperature in the dark. All antibodies were diluted in PBS with 3% BSA. Slides were washed with PBS, counterstained with DAPI (1 mg/mL) for 15 minutes in the dark, then cover slipped with ProLong™ Gold Antifade Mountant with DAPI (Thermo Fisher, P36941) or VECTASHIELD® Vibrance™ Antifade Mounting Medium with DAPI (Vector Labs, H-1800). Images were collected on blue (DAPI, 385 or 510 nm), green (CD3/CD11b, 470 or 488 nm), and red (TUNNEL, 567 or 580 nm) channels using a Zeiss Cell Discoverer 7 or a Zeiss LSM 700 Laser Scanning Fluorescence Inverted Confocal Compound Light Microscope. As described below, data was analyzed with Zeiss Blue and Fuji ImageJ software.

Seven random areas were selected on each tumor section for confocal microscopy imaging as z-stacked images at 20x. Images were converted to the maximum projected image (mpi). The total $CD3^+$, $CD11b^+$, $CD3^+TUNEL^+$, and $CD11b^+TUNEL^+$ cells were manually counted using Zeiss Blue software. The percent apoptotic $CD3^+$ or $CD11b^+$ cells were quantitated by dividing the number of $CD3^+TUNEL^+$ or $CD11b^+TUNEL^+$ cells by the total number of $CD3^+$ or $CD11b^+$ cells, respectively, and multiplying by 100. $CD11b^+$ cells were also counted using the colocalization plugin in Fuji ImageJ. Images were converted to 8-bit for automated quantitation, and thresholds were set for each channel. $CD11b^+$ and DAPI channels were analyzed for colocalization at a 10% ratio to determine the total $CD11b^+$ cells. The $CD11b^+$-DAPI colocalized image, and the TUNEL channel were analyzed for colocalization at a 10% ratio to determine the number of apoptotic cells. The percentage of apoptotic CD11b cells was determined by $(CD11b^+TUNEL^+)/(CD11b^+)*100$.

Overall apoptosis in a section was analyzed in sections labeled with anti-CD3 and TUNEL. Images were collected on seven randomly selected areas on confocal microscopy and across the entire tissue section on Cell Discoverer 7. Image files were converted to TIFF and analyzed in

Fuji Image J. The total fluorescence in the TUNEL and DAPI channels were collected independently. Total apoptosis in a section was calculated as (CD3 Channel)/(DAPI Channel).

CHAPTER 3: CHARACTERIZATION OF RELIABLY METASTATIC MURINE CLAUDIN-LOW CELL LINE

3.1 Rationale

The objective of this research was to leverage murine models of triple-negative breast cancer (TNBC) to pinpoint proteins and pathways with potential as therapeutic targets. To carry out these studies, triple-negative mouse tumors, 2225L and T11, were obtained from investigators at UNC-Chapel Hills and Baylor College of Medicine. These tumor lines were chosen based on their gene expression profiles, which were analogous to the human TNBC subtypes, basal-like and claudin-low.[16] However, when these tumor lines were first received, they could not be used for *in vivo* metastatic breast cancer research. When implanted into syngeneic mice, the original basal-like 2225L tumor line did not frequently nor reliably metastasize. To overcome this issue, 2225L was serial passaged in syngeneic mice at East Carolina University (ECU) with the final variant, 2225LM, consistently generating metastatic lesions in the lung. When examining the original T11 tumor line for viral pathogens, an infection with lactate dehydrogenase elevating virus (LDEV) was detected. LDEV is a murine RNA virus that infects macrophages. LDEV was eliminated by passing T11 primary tumors in athymic nude rats. This protocol was successful because the murine macrophages died off in the nude rat and LDEV in not able to infect rat macrophages. Subsequently, LDEV-free T11 tumors were implanted tumors into syngeneic mice to give rise to consistent T11 lung metastases. Serial passaging of primary tumors *in vivo* has several known factors that can contribute to differences in gene expression between passages, such as genetic instability, selective pressure by the host immune response, clonal evolution, and adaptive growth conditions based on how the tumor is passaged. Therefore, it was critical to characterize both tumor lines and compare their gene expression with the original tumors to ensure subtype stability and evaluate potential pathways for therapeutic targets.

This chapter describes the development of two reliably metastatic murine models of TNBC and subsequent characterization of the immune microenvironment in primary tumors and metastatic lungs by quantification of infiltrating $CD3^+$ and $CD11b^+$ immune cells and cytokine/ chemokines. Additionally, gene expression profiles from both the 2225LM and T11 lineages were compared to the respective source tumors. These characterized tumors were used for subsequent research studies.

3.2 Reliably Metastatic Basal-like and Claudin-low Murine Tumor Models

The 2225L murine tumor line was procured from Baylor College of Medicine to study metastasis in a syngeneic basal-like TNBC model with analogous gene expression to human basal-like TNBC.[16] Upon receipt, 2225L tumors were tested and cleared of mouse viral pathogens. Tumor fragments (1x1 mm^3) or cell suspensions in media ($5x10^5$ cells from a digested whole tumor) were initially implanted into the mammary fat pad of syngeneic Balb/c female mice (passages 1-3). Tumors were resected when they reached an average size of 1109 (±676) mm^3 (between 14-33 days post-implant or injection). These initial passages did not result in subsequent lung or liver metastases (on average of 28 (±17) and a maximum of 70 days post-tumor resection). Additionally, resectioning primary tumors from the mammary fat pad resulted in a high recurrence rate at the resection site and mortality rate. To improve outcomes, digested primary tumors suspended in media ($5x10^5$ cells) were injected subcutaneously. Initially, in passages 4-6, tumors were removed at an average size of 804 (±306) mm^3 (23±5 days post-tumor injections). The smaller tumor size allowed for more complete tumor resection and less recurrence at the resection site. Mice from these passages developed lung metastases 42% (8/19) of the time on average 43 (±20) days (range 1-71 days) post-tumor resection. One mouse was found dead after one-day post-tumor resection with several metastatic lung lesions, indicating that the mouse had progressive

disease at the time of surgery. However, in most cases, tumor resection was required to allow seeded metastases to develop in the lung. To generate a highly metastatic variant, selective passaging of primary or metastatic tumor digests ($5x10^5$-$1x10^6$ cells) or 1x1 mm^3 primary tumor fragments that resulted in high rates of metastatic disease were used for passages 6-11.

The final tumor variant, 2225LM, was chosen at passage 11 to establish a frozen tumor bank due to its high rate of metastatic lung disease (18/21; 86%) on 21 (±1) days post-tumor resection. These primary tumors were resected at an average volume of 775 (±260) mm^3 on day 19 (±4) post-implantation. In subsequent experiments, the 2225LM variant was transplanted onto the subcutaneous flank of syngeneic mice using banked 1x1 mm^3 tumor fragments. Resected primary tumors and metastatic lungs were used to investigate infiltrating $CD3^+$ and $CD11b^+$ immune cells and cytokine profiles. These mice maintained a high rate of lung metastases (85%) an average of 23 (±14) days post-tumor resection when tumors were removed at an average volume of 726 (±250) mm^3 20 (±5) days post-tumor implant.

In addition to the 2225L basal-like tumor line, the murine claudin-low tumor line, T11, was received from Baylor College of Medicine. The tumor was sent to Charles River Laboratories for mouse pathogen testing by polymerase chain reaction (PCR) and subsequently tested positive for LDEV. This murine single-stranded RNA virus infects and kills mouse macrophages.[333] Likewise, the University of North Carolina–Chapel Hill donated a banked T11 primary tumor from their institutions, which also tested positive for LDEV. To generate a reliable tumor model for future *in vivo* claudin-low breast cancer studies, virally infected T11 mouse tumors from both institutions were serially passaged into athymic nude rats three times (Britt, Pittman, and Verbanac, unpublished results). Due to the virus's specificity for mouse macrophages, the LDEV will not infect or replicate within rat macrophages. All tumors after passages 1, 2, and 3 were analyzed for

single-strand LDEV RNA by PCR at Charles River Laboratories and were found to be LDEV-free (**Figure 1**).[334]

In initial mouse studies (passages 1-5) using LDEV-free T11 tumors, after implanting a 1-4 mm^3 tumor fragment into the subcutaneous flank followed by resection 24 (±6) days post-tumor implant at an average volume of 706 (±202) mm^3, mice developed metastatic lung lesions 85% (22/26) of the time. Metastatic tumors from passage 4 were frozen and banked for future *in vivo* T11 experiments.

For a more clinically relevant T11 model, frozen tumor fragments 4 mm^3 were thawed and implanted into the mammary fat pad of syngeneic Balb/c mice. Primary tumors were removed when they reached an average volume of 506 (±300) mm3 by 14 (±8) days after implantation to reduce recurrence at the surgical site. This approach led to a recurrence rate of ≤5% in all subsequent *in vivo* experiments. Despite the smaller tumor size at removal, mice with mammary fat pad tumors developed metastatic lung disease in approximately 82% (18/22) of cases at 30±4 days post-tumor removal.

Additionally, to evaluate alternative implantation methods that may provide more consistent tumor growth and metastases, we conducted a comparative study using three mammary fat pad implantation methods: 4 mm^3 tumor fragment, $5x10^5$ cultured T11 cells in media, or $5x10^5$ cultured T11 cells in 50% Matrigel plus 50% media (n=7 in each group). Tumor size, days post-tumor injection or implant, and days from tumor resection to euthanasia were comparable across all three groups (**Table 6**). The most successful transplantation method was $5x10^5$ T11 cells in 50% Matrigel:50% media, which resulted in a metastatic rate of 86% (6/7), compared to 67% (5/6; 1/6 recurred) for the 4 mm^3 tumor fragment or 43% (3/7) for T11 cells in media alone. This method provides a more reliable procedure for T11 tumor transplantation with consistent outcomes that

result in high rates of metastases. Before this comparative investigation, various experiments examined immune cells and cytokine expression in primary and metastatic tumors and proteomic and genomic assessments. Consequently, a blend of orthotopic and subcutaneous tumor transplantation methods were used in these experiments. However, the outcomes from these investigations remained consistent irrespective of the implantation process. In all other experiments, T11 cultured cells were orthotopically transplanted using a 50: Matrigel:50% media suspension.

Table 6 Comparative study evaluating T11 transplantation methods into the mammary fat of syngeneic mice

Method	Days Post-Implant to Removal	Days Post-Removal to Euthanasia	Volume (mm^3) at Removal	Metastatic Rate (%)
$5x10^5$ cultured cells in media: Matrigel	15 (±1)	26 (±10)	496 (±61)	86 (6/7)
$5x10^5$ cultured cells in media	13 (±2)	30 (±4)	480 (±80)	43 (3/7)
2x2 mm tumor fragment	14 (±2)	28 (±12)	528 (±53)	67 (5/6)

Values for days and volume are expressed as the average (± standard deviation). The rate of metastases is defined as the percentage (n/total n)

3.3 Infiltrating $CD3^+$ and $CD11b^+$ Immune Cells in 2225LM and T11 Primary Tumors and Metastatic Lungs

Immune cells expressing CD11b and CD3 markers can indicate the immune response against cancer. In tumors, CD11b is expressed on monocytes, circulating macrophages, tumor-associated macrophages (TAM), mononuclear-myeloid-derived suppressor cells (M-MDSC), granulocytic-myeloid-derived suppressor cells (G-MDSC; also known as polymorphonuclear-myeloid-derived suppressor cells (PMN-MDSC)), neutrophils, and some subtypes of dendritic cells. CD11b-expressing cells can promote anti-tumor responses but can also promote tumor growth and metastases. Two $CD11b^+$ subsets known to promote tumor progression are M-MDSC and G-MDSC. In mice, M-MDSC express Ly6C in addition to CD11b, and G-MDSC express CD11b,

Ly6C, and Ly6G. These two MDSC populations can be distinguished from one another by the absence or presence of Ly6G; M-MDSC are $CD11b^+Ly6C^+Ly6G^-$ and G-MDSC are $CD11b^+Ly6C^+Ly6G^+$.

CD3 is a T-cell marker. T cells selectively recognize and destroy tumor cells. T cells expressing CD4 are known as T Helper cells and can activate other immune cells to respond to tumor cells. $CD3^+CD8^+$ T cells are cytotoxic T cells that can directly kill tumor cells. Measuring the presence of MDSC and T cells can provide valuable information about the immune response in the TME and the potential effectiveness of different therapeutic approaches.

The experiments discussed in this section aimed to determine the composition of $CD11b^+$ and $CD3^+$ cells in primary tumors and lungs with visible metastatic lesions. Flow cytometric analysis was used to conduct these studies, and IHC confirmed findings in primary tumors.

The first set of experiments aimed to quantify $CD11b^+$ and $CD3^+$ immune cells within the basal-like and claudin-low TNBC subtypes. Using 2225LM and T11 orthotopic or subcutaneous primary tumors of comparable weights (1.2 (±0.3) and 1.1 (±0.2) grams, respectively), tumors were digested and labeled with flow cytometry suitable, primary fluorescent antibodies for CD11b, Ly6C, and Ly6G or CD3, CD4, and CD8 in separate tubes (**Table 4**). Analysis showed that $CD11b^+$ cells comprised a significant proportion of the infiltrating immune cells, while $CD3^+$ cells were a minor component in both tumor types (n=6 and n=10, respectively). When gating on live cells, 54 (±11)% were $CD11b^+$ while 3 (±5)% were $CD3^+$ in the 2225LM tumor line, and 24 (±3)% were $CD11b^+$ while 6 (±5)% cells were $CD3^+$ in the T11 tumor line (**Figure 2a-b**). However, the 2225LM line had a 4.5-fold higher ratio of $CD11b^+$ cells to $CD3^+$ cells than the T11 line. Gating on live cells, $CD3^+$ populations were further classified into $CD3^+CD4^+$ T-helper and $CD3^+CD8^+$ cytotoxic T cells. Of the live cell population within 2225LM and T11 primary tumors, $CD3^+CD4^+$

T-helper were 2 (±4)% and 4 (±3)%, respectively, and $CD3^+CD8^+$ cytotoxic T cells comprised 1 (±1)% and 1 (±1)%, respectively. $CD11b^+$ cells included $CD11b^+Ly6C^+Ly6G^-$ monocytic and $CD11b^+Ly6C^+Ly6G^+$ granulocytic populations. When gating on live cells in the 2225LM line, only 4 (±3)% were classified as $CD11b^+Ly6C^+Ly6G^-$ monocytic and 11 (±6)% were $CD11b^+Ly6C^+Ly6G^+$ granulocytic; while in the T11 tumor line, 4 (±1)% were classified as $CD11b^+Ly6C^+Ly6G^-$ monocytic and 2 (±1)% were $CD11b^+Ly6C^+Ly6G^+$ granulocytic. In both tumor types, the $CD11b^+Ly6C^+Ly6G^-$ monocytic and $CD11b^+Ly6C^+Ly6G^+$ granulocytic subsets did not comprise the majority of $CD11b^+$ cells. Many unidentified $CD11b^+$ cells are likely TAM; smaller portions of the $CD11b^+$ subset may also include $CD11b^+$ dendritic cells or $F4/80^+$ macrophages. Furthermore, while these markers are commonly used to identify MDSC populations in murine tumors, they are not conclusively M-MDSC or G-MDSC based on their phenotypic expression of $CD11b^+Ly6C^+Ly6G^-$ and $CD11b^+Ly6C^+Ly6G^+$, respectively. For example, $CD11b^+Ly6C^+Ly6G^-$ is a phenotype shared with monocytes. It is possible to differentiate monocytes from M-MDSC by staining for F4/80 in addition to CD11b, Ly6C, and Ly6G. However, F4/80 was not used in these early experiments. It was added in later experiments to evaluate further tumor-infiltrating immune cells in T11 primary tumors. Likewise, $CD11b^+Ly6C^+Ly6G^+$ is the phenotype for G-MDSC, neutrophils, and TAN. Unfortunately, there are no additional surface markers that segregate these cells. Functional assays are required to identify and confirm the specific cell type for $CD11b^+Ly6C^+Ly6G^-$ and $CD11b^+Ly6C^+Ly6G^+$ cells. Due to the low numbers of $CD11b^+Ly6C^+Ly6G^-$ and $CD11b^+Ly6C^+Ly6G^+$ cells in 2225LM and T11 primary tumors, functional assays were not performed.

FFPE primary 2225LM (subcutaneous) and T11 (subcutaneous and orthotopic) tumors were cut into 5 μm sections and stained with anti-CD11b, CD3, or CD4 to confirm flow cytometry

findings. The results confirmed flow cytometry findings of a high proportion of $CD11b^+$ cells and low percentages of $CD3^+$ and $CD4^+$ cells in both tumor lines. (**Figure 2c**). Data from anti-CD4 IHC staining is data not shown.

Next, flow cytometry was used to determine the composition of $CD11b^+$ and $CD3^+$ cells in lungs with visible metastatic lesions originating from 2225LM or T11 resected primary tumors, compared to naïve control lungs. Control mice were age-matched and housed under the same conditions as tumor-bearing mice. Lungs from both metastatic and control mice were bifurcated into two halves. Lung halves that contained visible metastatic lesions or were from a non-tumor-bearing mouse were digested into a single-cell suspension, labeled with an antibody cocktail containing anti-CD45, CD11b, Ly6C, Ly6G, CD3, CD4, and CD8, and analyzed by flow cytometry (**Table 4**). To focus on immune cell subsets and exclude other cell types, such as lung epithelial and tumor cells, all live cells were first gated by positive CD45 expression. Consistent with primary tumors, $CD11b^+$ cells comprised a large portion of the lung-infiltrating immune cells (45 (±0.8)% and 47 (±16)% for 2225LM and T11, respectively). In contrast, $CD3^+$ cells were a minor component in lungs with 2225LM or T11 metastases (13% (±10%) and 5% (±4%), respectively; **Figure 3a-b**). The average percentage of $CD11b^+$ cells in normal lungs was more significant than in 2225LM or T11 metastatic lungs, although this did not reach statistical significance. However, 2225LM macrometastatic lungs showed a considerable elevation in $CD3^+CD8^+$ cell infiltration compared to control lungs ($p=0.04$), and the overall $CD3^+$ population was significantly lower in T11 macrometastatic lungs compared to control lungs ($p=0.007$). Comparative analysis between the normal lung and T11 metastatic lung showed significantly lower portions of $CD3^+CD4^+$ T-helper ($p=0.02$) and $CD3^+CD8^+$ cytotoxic T cells (0.006) in the metastatic lung.

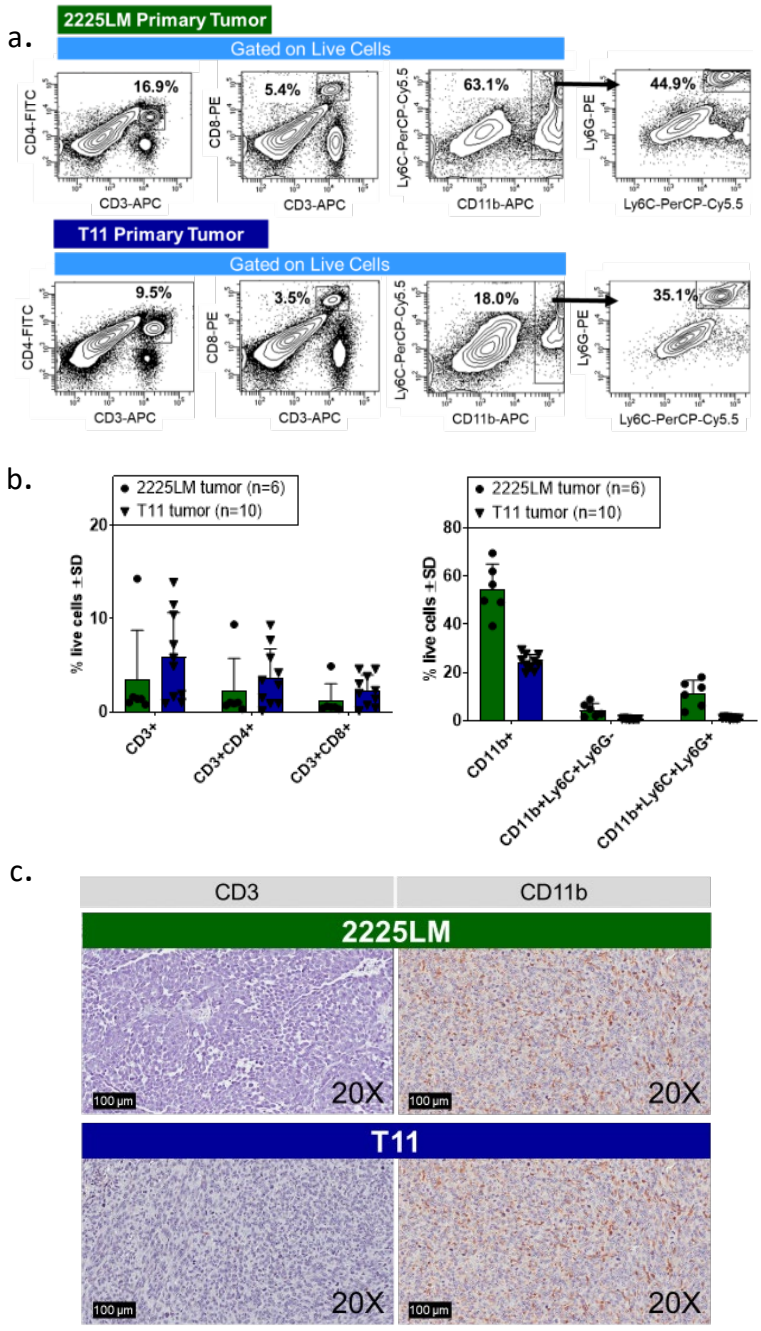

Figure 2: Identification of infiltrating immune cell subsets by flow cytometry in primary 2225LM and T11 tumors

$CD11b^+$ cells comprised most tumor immune cells, and $CD3^+$ cells were a minor component in both 2225LM and T11 primary tumors. (a.) Single-cell suspensions from whole tumor digests were labeled for CD11b (APC), Ly6C (PerpCP-Cy5.5), and Ly6G (PE) or CD3 (APC), CD4 (FITC), and CD8 (PE) in separate tubes and analyzed by flow cytometry. Images show the grating strategy and are representative of 2225LM (n=6) and T11 (n=10) primary tumors. All percentages are based on the total number of live cells. (b.) Bar charts summarize data 2225LM (n=6) and T11 (n=10) primary tumors. After gating on live cells, $CD11b^+$cells were 54 (±11)% and 24 (±3)%, respectively. $CD3^+$ cells comprised a smaller component of 2225LM and T11 primary tumors at 3 (±5) % and 6% (±5%) of total live cells, respectively. $CD3^+$ cells were further classified into $CD3^+CD4^+$ T-helper and $CD3^+CD8^+$ cytotoxic T cells.

$CD3^+CD4^+$ were 2 (±4)% in 2225LM primary tumors and 4 (±3)% of live cells in T11. $CD11b^+$ cells were subtyped into $CD11b^+Ly6C^+Ly6G^-$ monocytic and $CD11b^+Ly6C^+Ly6G^+$ granulocytic cells. In 2225LM these subsets comprised 4 (±3)% and 11 (±6)%, respectively. T11 showed lower infiltration of $CD11b^+Ly6C^+Ly6G^-$ monocytic (1 (±0.1)%) and $CD11b^+Ly6C^+Ly6G^+$ granulocytic (1±0.3)%) cells. (c.) Representative images from immunohistochemical staining with anti-CD3 (n=2 for each tumor type) or anti-CD11b (n=3 for 2225LM and n=4 for T11). Sections from each tumor type were also stained for anti-CD4 (n=2 for each tumor type) and showed low positivity (data not shown). This data confirms flow cytometry findings of low infiltrating $CD3^+$ cells and high infiltration of $CD11b^+$ cells in 2225LM and T11 primary tumors.

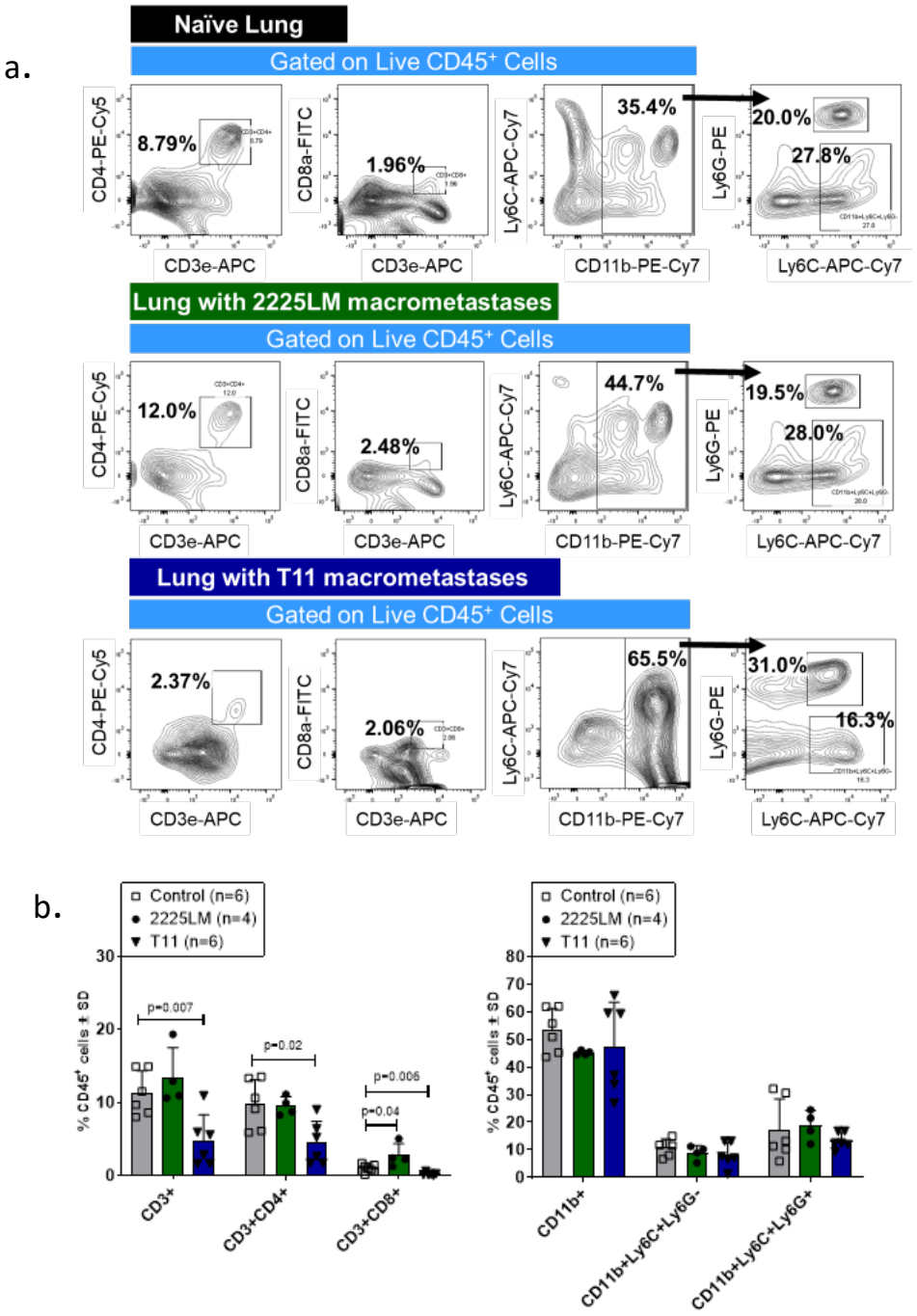

Figure 3 Identification of infiltrating immune cell subsets by flow cytometry in 2225LM and T11 metastatic lungs

(a.) Lungs were bifurcated into two halves; one half was digested into single-cell suspension and labeled with a cocktail of antibodies that included CD45 (PerCP-Cy5), CD11b (PE-Cy7), Ly6C (APC-Cy7), and Ly6G (PE), CD3 (APC), CD4 (PE-Cy5), and CD8 (FITC) and analyzed by flow cytometry. Images showing the gating strategy are representative of lung tissue digests from age-matched, naïve, non-tumor-bearing control mice (n=6) and mice with 2225LM (n=4) or T11 (n=6) visible lung metastases after primary tumor resection. All percentages are based on the total number of live $CD45^+$ cells. (b.) Bar charts summarize data from metastatic lungs (2225LM, n=4 and T11, n=6) and control lung (n=6). Both normal and metastatic lungs contained a high proportion of $CD11b^+$ cells and a lower

portion of $CD3^+$ cells. $CD11b^+$ cells were further classified into $CD11b^+Ly6C^+Ly6G^-$ and $CD11b^+Ly6C^+Ly6G^+$ subsets. There was no difference in the $CD11b^+$ populations when comparing 2225LM or T11 metastatic lungs to control. $CD3^+$ cells were analyzed for co-expression of CD4 or CD8. The overall average of $CD3^+$ cells was higher in 2225LM metastatic lungs (13 (±4)%) compared to contemporary controls (11 (±3)%), but it did not reach statistical significance. There was a significantly higher percentage of $CD3^+CD8^+$ cells in lungs with 2225LM metastases compared to controls (p=0.007 by Student's T-test) and no difference in $CD3^+CD4^+$ cells between the two groups. Lungs with T11 metastases had significantly lower $CD3^+$ cells compared to control lungs (p=0.007 by Student's T-test). $CD3^+CD4^+$ and $CD3^+CD8^+$ populations were also significantly lower in T11 lung metastases compared to control lungs (p=0.02 and 0.006 by Student's T-test, respectively)

3.4 Cytokine Expression in 2225LM and T11 Tumors and Metastatic Lungs

To further investigate immune responses in the microenvironment of 2225LM and T11 primary tumors and metastatic lungs, supernatants from homogenized tissue samples were measured by multiplex immunology assay using the Milliplex platform. Of 32 analytes tested, when comparing 2225LM or T11 primary tumor to control mammary fat pad, nine chemokines/cytokines showed increased expression, and six had decreased levels. (**Figure 4a, b** and **Table 7**). Compared to normal mammary fat pad (n=4), both 2225LM (n=14) and T11 primary tumors (n=7) displayed significantly higher expression of IL-6 (p=0.01 and 0.001, respectively), IP-10 (p=0.04 and <0.0001, respectively), MCP-1/CCL2 (p=0.002 and <0.0001, respectively), and VEGF (p=0.001 and 0.05, respectively), and significantly lower expression of IL-1α (p<0.0001 and p=0.0003, respectively) and LIX (p=0.001 and 0.003, respectively). Elevated expression of IL-6, IP-10, MCP-1/CCL2, and VEGF in 2225LM and T11 primary tumors indicate an inflammatory, pro-tumor microenvironment with suppression of immune responses due to lower expression levels of IL-1α and LIX.

2225LM primary tumors had increased expression of eotaxin (p=0.01), KC (p=0.02), and MIP-2 (p=0.02) and decreased expression of IL-2 (p=0.001), IL-9 (p=0.002), and IL-12 (p70) (p=0.001) compared to control mammary fat pad. T11 primary tumors showed increased expression of IL-12 (p40) (p=0.02) and M-CSF (p=0.03) and decreased expression in IL-1β (p=0.02) compared to mammary fat pad. Several of the detected cytokines are consistent with a

large infiltration of M-MDSC and G-MDSC or monocytes and granulocytes, such as eotaxin, KC, MIP-2, MCP-1, and MIP-2. Decreased levels of IL-2, IL-9, and IL-1β suggest lower $CD3^+$ T cells in primary tumor compared to control. Significant changes in expression were also observed for GM-CSF, IL-10, LIF, MIP-1β, RANTES, and TNF-α. However, there was high variability in expression levels among the tested samples. Several samples across all three groups (2225LM and T11 tumors and mammary fat pad) had expression levels below assay detectable limits. When samples exhibited values below detectable limits for a particular analyte, the lowest detectable limit for that analyte was used to conduct statistical analysis (Student's T-test) for comparing the primary tumor (2225LM or T11) to the control mammary fat pad. Overall, the differences in cytokine expression levels between the two tumors and the control mammary fat pad indicate a significant presence of innate immune cells, such as monocytes and granulocytes, in both 2225LM and T11 primary tumors.

Next, to determine potential cytokine activity that might contribute to metastatic seeding or disease progression within the metastatic microenvironment, analyte expression levels from lung tissues containing 2225LM or T11 metastases were compared to lungs from age-matched naïve, non-tumor-bearing mice. Results showed that 11 of 32 analytes tested had increased expression in either 2225LM or T11 metastatic lungs compared to control lungs. No cytokines had decreased expression in metastatic lungs compared to controls. G-CSF ($p=0.002$), eotaxin ($p=0.002$), IL-6 ($p=0.01$), LIF ($p=0.001$), IL-10 ($p=0.01$), MCP-1 (0.001), M-CSF (0.01), MIG ($p=0.03$) were elevated in 2225LM metastatic lungs compared to control lung tissue. These cytokines are indicative of a high pro-tumor response. They contribute to the progression of tumors by recruiting tumor-promoting innate immune cells, such as eosinophils, neutrophils, and macrophages. Compared to control lungs, T11 metastatic lungs showed increased expression of

G-CSF (p=0.02). IP-10 (p=0.02), and MCP-1 (p=0.04). G-CSF and MCP-1 support a pro-tumor microenvironment enriched with granulocytes, neutrophils, monocytes, and macrophages. IP-10 is a T cell chemoattractant expressed by T cells, NK cells, macrophages, fibroblasts, endothelial cells, and cancer cells.

Overall, the cytokine expression profiles in both primary tumors and metastatic lungs suggest an immunosuppressive and tumor-promoting microenvironment characterized by the recruitment of various immune cells that can contribute to disease progression and metastasis. The observed high variability in expression levels among samples indicates the complexity of the immune response and potential limitations in the assay sensitivity.

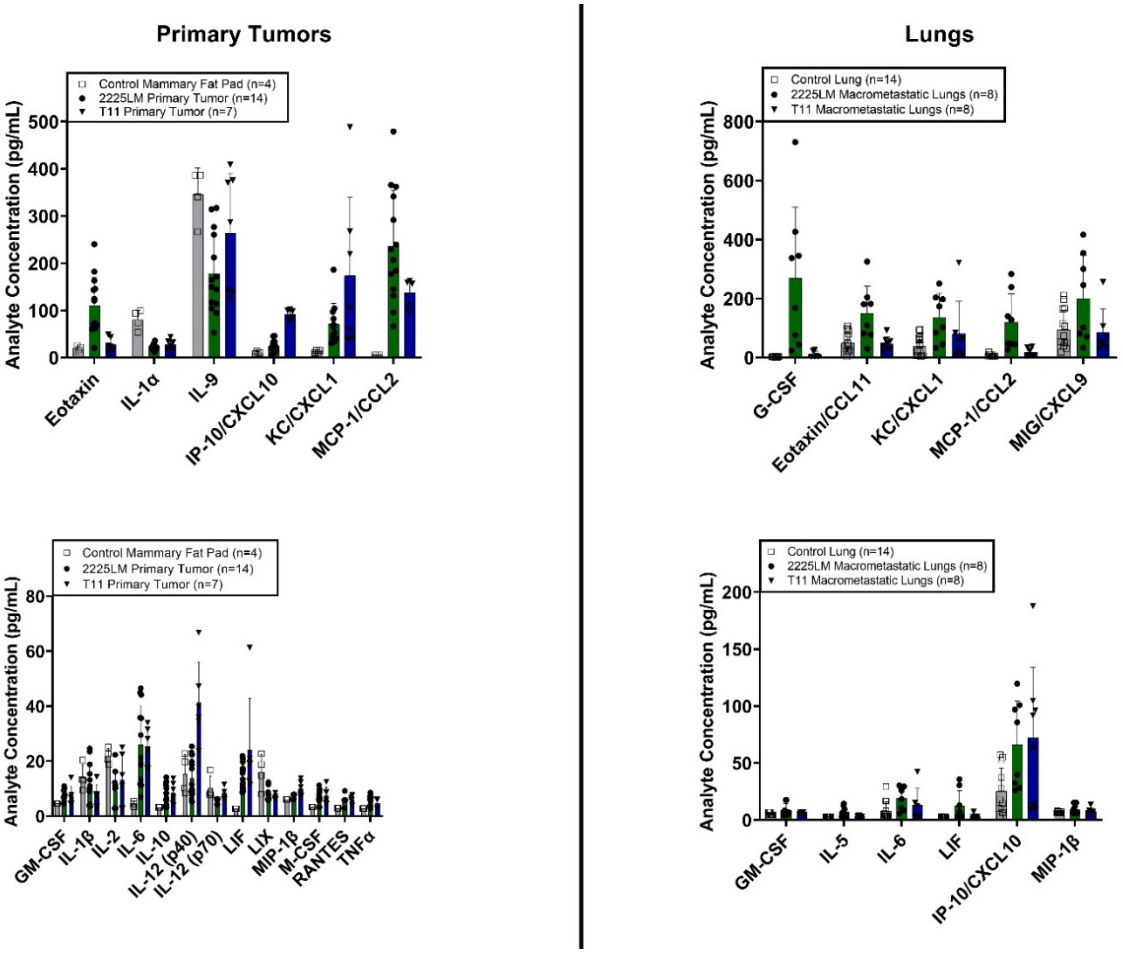

Figure 4 Differential cytokine levels measured by multiplex immunoassay in 2225LM and T11 primary tumors and metastatic lungs compared to control tissues

Multiplex analysis shows high expression of pro-tumor cytokines from tumor (left) and lung-containing metastatic lesions (right) compared to control tissues (mean and standard deviation are plotted). The graphs display the cytokines that were significantly different from control tissues. See Table 7: Comparison of cytokines measured by multiplex immunoassay in 2225L and T11 primary tumors, metastatic lungs, and control tissue for a list of p-values based on Student's T-test. Overall, although samples showed high variability results indicate an immunosuppressive and tumor-promoting microenvironment in both 2225LM and T11 primary and metastatic tumors.

Table 7: Comparison of cytokines measured by multiplex immunoassay in 2225L and T11 primary tumors, metastatic lungs, and control tissues

Chemokine/ Cytokine	Ctl MFP (n=4)	2225LM Tumor (n=14)	p-value*	T11 Tumor (n=7)	p-value*	Ctl Lung (n=14)	2225LM met lung (n=8)	p-value*	T11 met lung (n=8)	p-value*
G-CSF	175.52±118.16	177.07±134.77	0.98	65.59±64.90	0.07	2.62±0.57[a]	**268.94±240.80**	**0.002**	**10.72±10.96[a]**	**0.02**
Eotaxin	19.36±4.99	**110.53±59.80**	**0.01**	27.76±14.08	0.29	49.90±33.15[a]	**149.08±93.74**	**0.002**	46.14±23.76	0.78
GM-CSF	4.56±0.00[b]	**6.95±2.24[a]**	**0.05**	6.68±3.48[a]	0.26	5.14±1.04[b]	**8.87±5.55[a]**	**0.03**	5.95±1.16[a]	0.13
INF-y	4.53±1.53[a]	5.21±2.31[a]	0.60	4.49±1.39[a]	0.97	27.04±38.07[a]	2.68±0.58[b]	0.14	2.88±0.45[a]	0.11
IL-1α	80.09±20.97	**23.33±6.40**	**<0.0001**	**28.23±9.93**	**0.0003**	188.09±214.96	60.00±40.80	0.17	111.28±83.16	0.35
IL-1β	14.01±4.59	10.97±7.30[a]	0.45	**7.19±3.63[a]**	**0.02**	20.70±20.67	21.81±15.03	0.90	12.40±5.15[a]	0.32
IL-2	21.82±2.72	**9.16±6.12[a]**	**0.001**	13.15±9.44[a]	0.12	25.44±32.82[a]	21.50±21.92[a]	0.78	16.67±15.97[a]	0.49
IL-3	2.92±0.00[b]	3.88±0.74[b]	ND	3.67±0.80[b]	ND	2.31±0.85[a]	1.96±0.81[a]	0.36	2.12±0.88[a]	0.61
IL-4	0.81±0.00[b]	4.18±2.61[b]	ND	3.43±2.80[b]	ND	1.61±1.19[a]	1.81±0.95[a]	0.70	1.64±0.89[b]	0.94
IL-5	3.01±0.00[b]	4.97±1.61[b]	ND	4.60±1.70[b]	ND	2.94±0.17[a]	**7.16±4.62[a]**	**0.01**	3.23±0.61[a]	0.15
IL-6	4.14±0.95	**26.04±14.08**	**0.01**	**23.54±8.05**	**0.001**	8.02±8.07[a]	**19.37±10.05**	**0.01**	13.22±15.13[a]	0.34
IL-7	3.20±0.00[b]	4.55±1.04[b]	ND	4.10±1.12[a]	0.15	3.47±0.55[a]	4.60±1.88[a]	0.06	3.09±0.46[a]	0.14
IL-9	345.06±56.50	**178.07±84.88**	**0.002**	243.17±130.50	0.17	361.31±358.65	235.95±184.62	0.40	191.35±132.02	0.22
IL-10	3.14±0.00[b]	**7.41±3.94[a]**	**0.05**	7.72±4.11	0.06	5.70±5.34[a]	7.83±6.53[a]	0.45	3.59±0.80[a]	0.32
IL-12 (p40)	15.27±7.08	13.79±6.97	0.71	**38.78±14.92**	**0.02**	21.34±25.01[a]	18.18±16.18[a]	0.77	19.03±11.82[a]	0.81
IL-12 (p70)	10.14±4.42	**5.51±1.00[a]**	**0.001**	7.46±2.02[a]	0.19	3.82±0.99[a]	3.26±0.93[a]	0.21	3.49±1.25[a]	0.50
LIF	2.68±0.00[b]	**13.97±4.65**	**0.0002**	**24.58±16.97**	**0.03**	2.57±.0.26[a]	**12.48±13.27[a]**	**0.01**	3.37±1.93[a]	0.15
IL-13	12.11±0.00[b]	19.27±5.54[b]	ND	16.88±5.95[a]	0.15	9.20±4.50[a]	6.09±5.64[a]	0.19	6.75±5.74[b]	0.28
IL-15	16.00±0.00[b]	43.08±20.95[b]	ND	37.07±22.52[b]	ND	41.35±35.30[b]	56.57±37.95[b]	ND	51.50±37.95[b]	ND
LIX	16.03±6.32	**7.47±2.21[a]**	**0.001**	**6.63±0.90[a]**	**0.003**	6.41±0.59[a]	8.60±3.96[a]	0.08	6.48±2.10[a]	0.92
IL-17	2.82±0.00[b]	4.86±1.58[b]	ND	4.41±1.69[b]	ND	15.20±18.62[a]	6.62±6.75[a]	0.26	7.19±5.76[a]	0.25
IP-10	10.35±2.51	**24.59±12.18**	**0.04**	**89.76±11.01**	**<0.0001**	25.18±20.36[a]	**66.14±38.35**	**0.01**	**72.02±61.71**	**0.02**
KC	12.85±2.96	**70.96±43.65**	**0.02**	173.12±153.16	0.07	39.05±33.50[a]	**136.59±80.82**	**0.001**	80.90±110.2	0.20
MCP-1	5.44±0.00[b]	**236.87±117.92**	**0.001**	**135.41±27.82**	**<0.0001**	8.21±4.34[a]	**119.67±97.16**	**0.001**	**18.58±14.83[a]**	**0.04**
MIP-1α	46.09±3.64	29.07±19.24[a]	0.10	36.86±12.66	0.20	45.73±49.27	32.19±22.79	0.50	32.89±21.81[a]	0.50
MIP-1β	6.04±0.00[b]	**7.15±0.91[a]**	**0.03**	**9.68±2.55[a]**	**0.02**	6.60±0.72[a]	**9.71±3.96[a]**	**0.02**	7.74±2.61[a]	0.17
M-CSF	3.26±0.02[a]	5.94±2.62[a]	0.06	**7.09±3.00**	**0.03**	3.68±1.00[a]	**6.65±3.97[a]**	**0.01**	4.71±1.99[a]	0.14
MIP-2	19.22±4.79[a]	**32.81±9.63[a]**	**0.02**	159.30±230.89	0.27	24.02±9.39[a]	21.48±8.82[a]	0.56	18.18±7.17[a]	0.20
MIG	63.56±14.82	152.02±103.80	0.12	52.44±9.40	0.18	94.58±65.43[a]	**200.69±146.72**	**0.03**	85.68±79.12	0.79
RANTES	2.86±0.00[b]	**4.74±1.46[a]**	**0.04**	**5.59±1.63[a]**	**0.01**	8.19±6.95[a]	7.94±7.56[a]	0.94	7.09±4.36[a]	0.69
VEGF	5.18±1.78	**34.62±14.74**	**0.001**	**183.28±158.26**	**0.05**	16.34±10.40[a]	22.12±14.34	0.30	37.33±47.13	0.12
TNFα	2.74±0.00[b]	**5.94±1.65[a]**	**0.002**	4.46±1.83[a]	0.10	3.49±1.04[b]	4.37±1.19[a]	0.10	3.79±1.12[b]	ND

Concentrations are expressed as pg/mL (± standard deviation)

[a] For samples below detection limits, the lowest detectable concentration for each analyte was used to complete statistical analysis.

[b] All samples were below detectable limits. Statistical analysis was not performed when all samples in both groups were below detectable limits (ND).

* p-value is based on a T-test comparing tumor or macrometastatic lung tissue to the control mammary fat pad or lungs, respectively.

3.5 Gene expression analysis of the 2225L murine model of basal-like TNBC

As described in section 3.1, 2225LM tumors were serially passaged to develop a syngeneic basal-like TNBC murine tumor model that frequently and reliably metastasized to the lung. Serial passaging of primary tumors *in vivo* has several known factors contributing to observed differences in gene expression between passages, such as genetic instability, selective pressure by the host immune response, clonal evolution, and adaptive growth conditions. To determine if gene expression changes occurred during *in vivo* serial passaging of 2225L, RNA sequencing analysis was conducted on the original 2225L received from Baylor (n=1), early passages of 2225L tumors (passage 5-9; n=4) and the reliably metastatic variant, designated 2225LM (passage 11; n=5).

RNA of sufficient quantity, concentration, and quality for RNA-Seq analysis was isolated from all samples. The samples had a mean RNA concentration of 1.5±1.1 µg/µL (0.040-2.804 µg/µL), and the mean RNA integrity number (RIN) value was 8.8±0.8 (7.2-9.4). Libraries were prepared, and RNA was sequenced by Novogene using the Illumina high-throughput sequencing platform. An average of 90.5±25.5 million clean reads were obtained, and most reads (>93%) reached Phred-like quality scores (Q-scores) at the Q30 level with a base error rate ≤0.03%. After alignment using Tophat, an average of 87.6±1.5% (86-91%) uniquely aligned reads were mapped to the mouse reference genome. Read counts were normalized using the method fragments per kilobase of transcript per million mapped reads (FPKM), which normalizes read counts based on gene length and the total number of mapped reads.

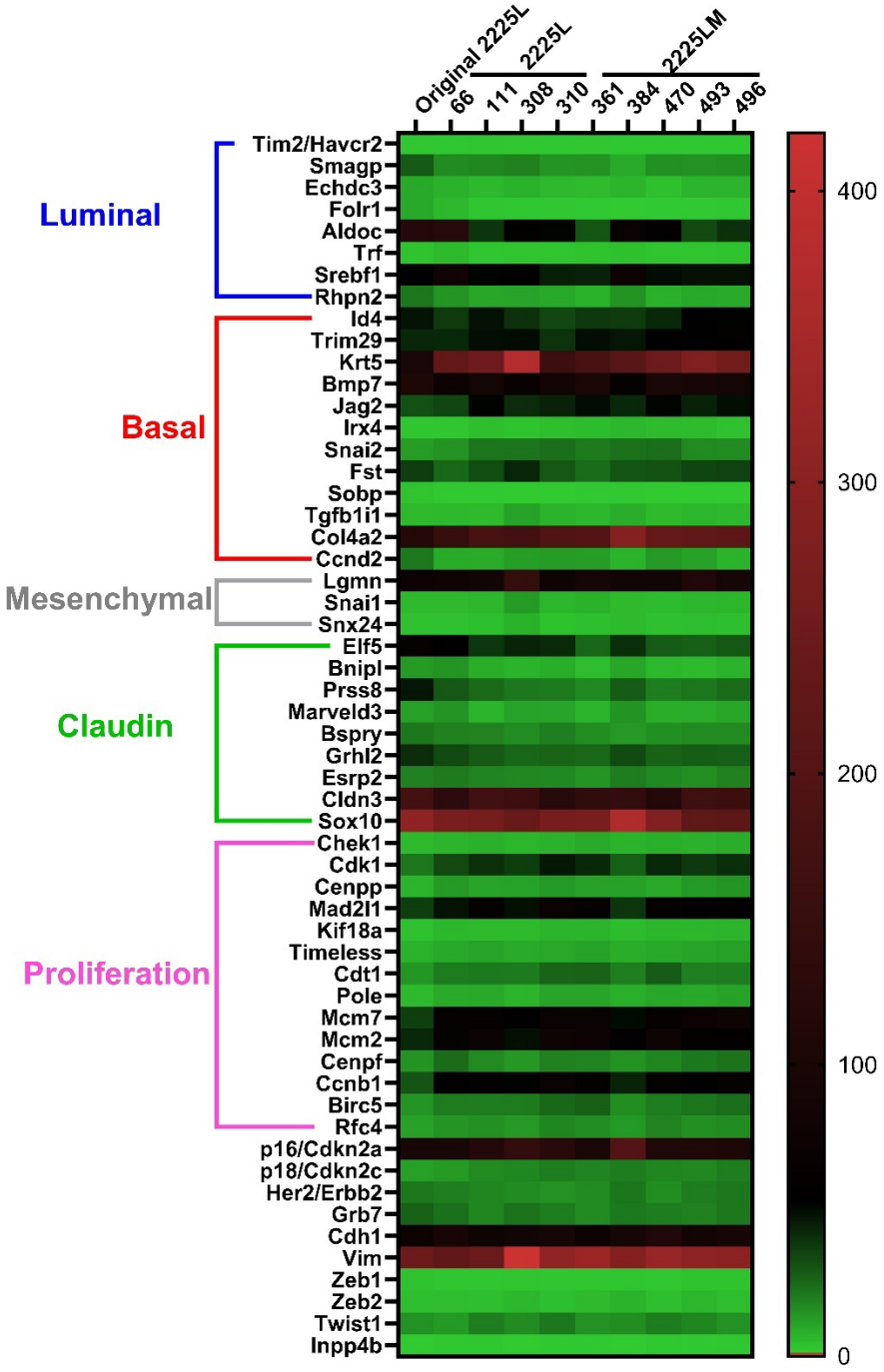

Figure 5 2225LM variants-maintained expression of basal-like subtype identifying genes
Normalized RNA-Seq expression levels of subtype identifying genes for 2225L previously described by Herschkowtiz et al.[32] Genes for each identifying subtype are listed on the left side of the graph. They are grouped according to the associated breast cancer subtype. Normalized gene expression levels are graphed in the heatmap by individual tumor and grouped according to the original tumor, early passages (5-9), and final variant (passage 11). The basal epithelial expression pattern, including K5, was highly expressed in all 2225L and 2225LM tested tumors.

Using FPKM normalized counts from Novogene RNASeq analysis, genes that were previously described as being characteristic of the 2225L basal-like tumor line[32] were graphed in a heatmap to compare expression levels of characteristic genes in the original 2225L, early passages of 2225L (passage 5-9) and the final 2225LM variant (passage 11) (**Figure 5**). These characteristic genes were found to have similar expression levels across all tumors tested. This indicates that both the 2225L and 2225LM variant contains a gene expression profile consistent with a murine basal-like tumor line.

Next, differential gene expression analysis was performed on normalized read counts from the original tumor received from Baylor, early passages of 2225L, and the 2225LM metastatic variant using DESeq2. Results showed 12,763 shared genes among the three groups (**Figure 6**). Each group had unique genes from the other two; the original 2225L had 492 individual genes, 2225L early passages contained 139 unique genes, and the 2225LM variant had 175 unique genes. The unique genes from each group were uploaded to Reactome (www.reactome.org) to determine the characteristics of differentially expressed genes.

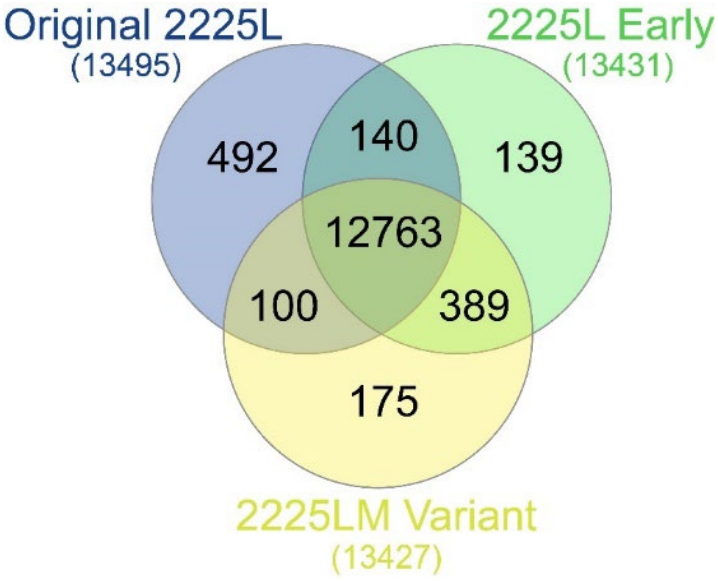

Figure 6 Number of genes expressed in each 2225L tumor subgroup

Venn diagram of the number of differentially genes expressed by passage subgroup. Comparisons were made from the original tumor (n=1), early 2225L passages (n=4), and the final 2225LM variant (n=5). The number in parentheses is the total number of genes identified for each tumor group. Each group had unique genes from the other two; the original 2225L had 492 unique genes, 2225L contained 139 unique genes, and the 2225LM variant had 175 unique genes.

In the original 2225L, the pathway with the highest entity ratio (i.e., the total number of identified entities divided by the total number of entities in the pathway) was the "metabolism of proteins." In the early 2225L passages and the final 2225LM variant, the pathway with the highest entity ratio was "metabolism" (0.24 for both). A significant number of genes in the 2225L early passages and 2225LM variant were associated with the immune system. Genes unique to the 2225L early passage and 2225LM variant groups within the metabolism and immune system pathways are listed in **Table 8**. Interestingly, RNASeq analysis showed that IL1α, IL6, and MIP2ß are expressed uniquely in 2225L early passages and not in the 2225L original tumor or the 2225LM final variant. However, as described in section 3.3, previous multiplex data showed that IL1α, IL6, and MIP-2 were expressed at the protein level in primary 2225LM tumors; IL6 and MIP-2 were significantly higher in 2225LM primary tumors compared to control mammary fad pad tissues, and IL-1α was reduced considerably (see **Figure 4** and **Table 7**). The reason for the differences in cytokine detection at the RNA and protein levels may be attributed to several biological and technical factors, such as the rate of translation, post-translation regulation of proteins, low levels of cytokine expression, and assay sensitivity. Additionally, the time between tumor implantation and resection, the tumor size, and the tissue processing time could influence the cytokine levels detected in each assay. As the average primary tumor volume (749±271 and 775±260 mm^3, respectively) and days between primary tumor implant and resection (21±5 and 19±4) were comparable between the tumors in the 2225L early passages and 2225LM variant groups, the size and timing of tumor removal are less likely to be contributing variables compared to other biological or technical factors, such as the rate of translation or assay sensitivity. Since

cytokines are often produced in limited quantities to activate a specific cellular response, RNA levels of these cytokines may be too low to detect by RNA sequencing. At the same time, the multiplex assay was designed with high sensitivity and specificity for low levels of cytokines. IL1α, IL6, and MIP-2 proteins are present in the 2225LM variant primary tumor, but RNA levels for these cytokines are below detection limits for RNA sequencing.

Table 8 Genes in metabolism and immune system pathways unique to 2225L early passages and the 2225LM variant

Sample Group	Pathway	Gene ID	Gene Name
2225L early passages (5-9)	Metabolism	Cox6a2	Cytochrome c oxidase subunit Via polypeptide 2
		Upp2	Uridine phosphorylase 2
		Agpat9	1-acylglycerol-3-phosphate O-acyltransferase 9
		Dpep2	Dipeptidase 2
		Gng8	Guanine nucleotide-binding protein (G protein) gamma 8
		Lalba	Lactalbumin alpha
		Ankrd1	Ankyrin repeat domain 1 (cardiac muscle)
		Aspa	Aspartoacylase (aminoacylase) 3
		Bcat1	Branched-chain aminotransferase 1 cytosolic
		Tshb	Thyroid stimulating hormone beta subunit
2225L early passages (5-9)	Immune System	Ighg1	immunoglobulin heavy constant gamma 1 (G1m marker)
		Il11	Interleukin 11
		Cd79b	CD79b antigen
		Tslp	Thymic stromal lymphopoietin
		Trac	Epidermal growth factor-containing fibulin-like extracellular matrix protein 2
		Trbc1	T cell receptor beta constant region 1
		Ppbp	Pro-platelet basic protein
		Glycam1	Glycosylation-dependent cell adhesion molecule 1
		Il1a	Interleukin 1 alpha
		Myh2	Myosin heavy polypeptide 2 skeletal muscle adult
		IL6	Interleukin 6
		Igkc	Immunoglobulin kappa constant
		Sell	Selectin lymphocyte
		Rsad2	Radical S-adenosyl methionine domain containing 2
		Il1r2	Interleukin 1 receptor type II
		Serpinb1a	Serine (or cysteine) peptidase inhibitor clade B member 1a
		Cish	Cytokine inducible SH2-containing protein
		Klhl41	Kelch-like 41
		Cxcl3	Chemokine (C-X-C motif) ligand 3 (also known as MIP-2ß)

2225LM variant (passage 11)	Metabolism	Sult1e1	Sulfotransferase family 1E member 1
		Slc35d2	Solute carrier family 35 member D2
		Elovl4	Elongation of very long chain fatty acids (FEN1/Elo2 SUR4/Elo3 yeast)-like 4
		Pip	Prolactin induced protein
		Pipox	Pipecolic acid oxidase
		Brip1	BRCA1 interacting protein C-terminal helicase 1
2225LM variant (passage 11)	Immune System	Mb21d1	Mab-21 domain containing 1
		Cst6	Cystatin E/M
		Cd300lb	CD300 antigen-like family member B
		Krt1	Keratin 10
		Padi2	Peptidyl arginine deiminase type II
		Tlr8	Toll-like receptor 8
		C2	Complement component 2 (within H-2S)

Differential expression analysis comparing the original 2225L tumor to the 2225LM variant was conducted on normalized read counts using DESeq2. The resulting p-values were adjusted using Benjamini and Hochberg's approach for controlling the False Discovery Rate (FDR), and genes with an adjusted p-value (padj) <0.05 were considered differentially expressed. The padj and an absolute fold change of 1.0 were set as the threshold for significant differential expression. There were 534 genes with upregulated expression compared to the original 2225L and 562 downregulated genes. These genes were analyzed for enrichment by Gene Ontology (GO) and Kyoto Encyclopedia of Genes and Genomes (KEGG) to determine the functional significance of the differentially expressed genes. Gene length bias was corrected and GO and KEGG terms with padj < 0.05 were significantly enriched by differentially expressed genes.

In the 2225LM variant compared to the original 2225L tumor, "positive regulation of cellular component movement" (n=42 genes; padj ≤0.0001), "positive regulation of cell motility" (n=40 genes; padj ≤0.0001), and "positive regulation of cell migration" (n=39 genes; padj ≤0.0001) were the top three GO terms that were significantly overexpressed (**Figure 7a**). Leukocyte (n=29; padj ≤0.0001), myeloid leukocyte (n=21 genes; padj ≤0.0001), and granulocyte (n=18; padj ≤0.0001) migration were also significantly upregulated in 2225LM compared to the original 2225L. Among the 2225LM upregulated cytokines identified in these pathways were

VEGF, CXCL1 (KC), and CCL2 (MCP-1). This data was consistent with multiplex chemokine analysis, which showed increased levels of these proteins in 2225LM primary tumors compared to the control mammary fat pad (refer to **Figure 4** and **Table 7** for multiplex cytokine values). On the other hand, GO terms for "transmembrane transporter complex" (n=26 genes; padj ≤0.0001), "transporter complex" (n=26; padj ≤0.0001), "ion channel complex" (n=24 genes; padj ≤0.0001) were significantly downregulated in 2225LM compared to the original 2225L tumor (**Figure 7b**).

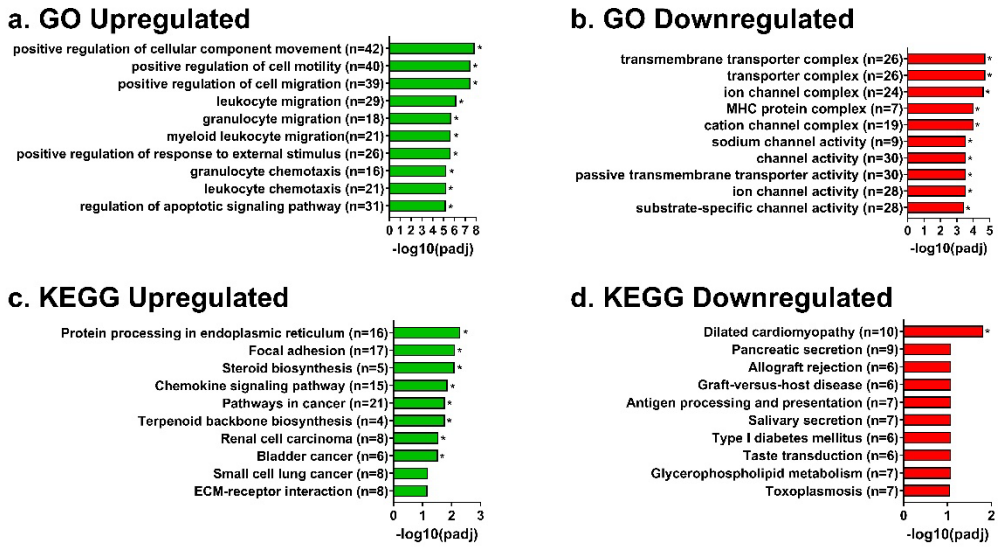

Figure 7 GO and KEGG enrichment analysis of differentially expressed genes in 2225LM verses the original 2225L murine primary tumors.
Bar graph of the top ten significantly (padj < 0.05) enriched GO terms using (a) upregulated or (b) downregulated differentially expressed genes in the 2225LM variant compared to the 2225L original tumor. Bar graph of the top ten significantly (padj< 0.05) enriched KEGG terms using (c) upregulated or (d) downregulated differentially expressed genes in the 2225LM variant compared to the 2225L original tumor. In all graphs, the y-axis shows the enriched GO or KEGG terms with the number of identified genes in parenthesis. The x-axis shows the -$\log_{10}$ of the p-value adjusted by Benjamini and Hochberg's approach for controlling the False Discovery Rate (FDR). Padj >0.05 was considered significant. GO or KEGG pathways that were significantly enriched are indicated with an asterisk.

.

KEGG enrichment analysis was also used to determine the functional significance of the differentially expressed genes. Genes were differentially expressed with a padj of <0.05 and an absolute fold change of 1. This analysis showed that "protein processing in endoplasmic reticulum" (n=16 genes; padj=0.0004), "focal adhesion" (n=17 genes; padj=0.0008), and "steroid biosynthesis" (n=5; padj=0.0008)) were upregulated in 2225LM variant compared to the original

2225L received from Baylor (**Figure 7c**). "Chemokine signaling pathway" (n=15; p=0.01) was also significantly enriched and identified CXCL1 (KC) and CCL2 (MCP-1) as chemokines differentially expressed 2225LM and 2225L original tumor. This data supports findings in the GO differential enrichment and multiplex immunoassay analyses. There was only one significantly downregulated pathway by KEGG enrichment analysis in the 2225LM variant compared to the original tumor, "dilated cardiomyopathy" (n=10; p=0.02) (**Figure 7d**). Other pathways were identified, but they did not reach statistical significance.

Next, the computational model, seq-ImmuCC, was used to analyze further potential differences in infiltrating immune cell composition between the original 2225L and the 2225LM variant tumors. The model was developed by Chen *et al.* to infer the relative proportions of 10 major immune cell types in mouse tissues from RNA-Seq data sets.[335] Normalized RNASeq transcriptional data from the 2225L original tumor (n=1), early passages of 2225L (passage 5-9; n=4), and the 2225LM metastatic variant (passage 11; n=5) were uploaded to the seq-ImmuCC server (http://218.4.234.74:3200/immune/). Results from individual tumors showed high variability in the immune signatures observed in all tumors (**Figure 8a**). The original tumor (22%) and early passages of 2225L (17 (±14)%) showed higher proportions of infiltrating macrophages compared to the 2225LM metastatic variant (1 (±2)%). Early 2225L passages had the highest proportion of infiltrating CD8 T cells (33 (±19)%) compared to the original 2225L (12%) and the 2225LM variant (9 (±12)%), which may have contributed to the observed low rate of metastases in early tumor passages. The highest percentage of dendritic cells was observed in the 2225LM variant (31 (±15)% compared to 19% and 2 (±3)% in the original and early passages, respectively). Recall from section 3.2, flow cytometry analysis showed that in 2225LM primary tumors, 54 (±11)% of live cells were $CD11b^{+,}$ and 3 (±5)% were $CD3^{+}$. Even when considering other immune

cells that are $CD11b^+$, such as monocytes and neutrophils, the percentage is much lower than observations from flow cytometry experiments. Conversely, when considering immune cells that could potentially express CD3, the combined populations of computed CD4 and CD8 T cells surpass what was anticipated based on flow cytometry data. While the flow cytometry experiments were analyzed based on all cells, including epithelial, endothelial, and tumor cells, ImmuCC outputs specify the percentage of total immune cells. If flow cytometry data were to be gated specifically on immune cells using a pan-immune cell marker such as CD45, the percentages for $CD11b^+$ and $CD3^+$ cells would likely be proportionally higher. One reason for this observation is differences in assay sensitivity. RNA transcription data can be less sensitive than traditional protein and immune cell detection assays due to low transcription levels of immune-specific genes. Also, post-transcriptional or translational modifications can affect the stability or activity of characterizing RNA or proteins. The half-lives of RNA and protein differ, and their levels of expression are influenced by various factors in cell activation, the tumor microenvironment, and alternative signaling pathways; therefore, protein levels detected by antibody-based assays (e.g., multiplex assays, flow cytometry, and IHC) may not correlate directly with gene expression. This could be why there are significant differences among tumors in the cell populations calculated from the RNA transcriptome.

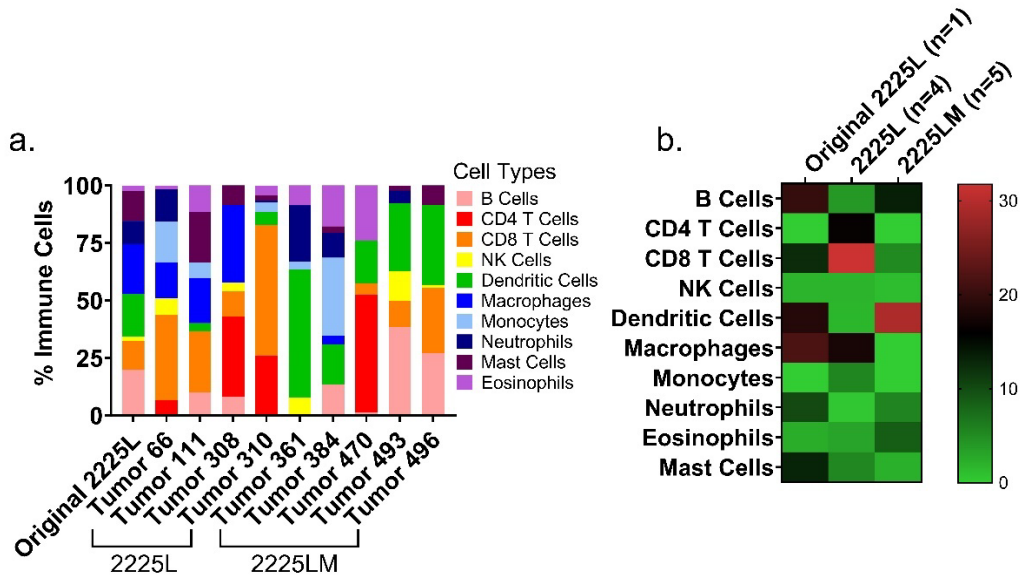

Figure 8 Immune cell composition of 2225L and 2225LM primary tumors using RNA Sequencing transcriptome

(a) Stacked bar plot showing the cellular compositions of the immune microenvironment in the original 2225L tumor received from Baylor, early passages of 2225L (passage 5-9; n=4) that were less reliably metastatic, and 2225LM variant (passage 11-12; n=5) that reliably metastasized to the lung. Analysis was conducted from mouse RNA-seq data collected on primary tumors. It was computed using the seq-ImmuCC tool to determine each tumor group's relative proportions of immune cells. Results showed high variability among all tumors analyzed. (b) Tumors were grouped by original, early, and variant types, and each cell type's average percentage was compared across all groups in a heatmap. The results indicate a high infiltration of Cytotoxic T cells in the early 2225L passages, and the 2225LM passages had the highest infiltration of dendritic cells. These changes in the immune microenvironment within the primary tumor may influence the reliability of lung metastases.

3.6 Gene expression analysis of the LDEV-free T11 murine model of claudin-low breast cancer

As described in section 3.1, tumors received from both institutions (Baylor and UNC) tested positive for a murine single-stranded RNA virus that infects and kills mouse macrophages, lactate dehydrogenase elevating virus (LDEV).[333] Subsequently, virally infected T11 mouse tumors were serially passaged into athymic nude rats to eliminate the virus (Britt, Pittman, and Verbanac, unpublished results); however, LDEV cannot replicate within rat macrophages due to its specificity for mouse macrophages. To assess any potential changes in gene expression due to LDEV infection, RNA was isolated from the original T11 tumors received from Baylor and UNC (n=1 each), tumors passaged into nude rats (n=4, one from each institution from passages 1 and

3), and LDEV-free tumors passaged into mice (n=7). Isolated RNA was sent to Novogene for gene expression analysis.

All samples were successfully processed and had sufficient RNA for RNA-Seq transcript quantification. The samples had a mean RNA concentration of 2.4±1.4 µg/µL (0.367-5.836 µg/µL), and the mean RIN value was 9.1±0.5 (7.8-10.0). An average of 93.3±13.9 million clean reads were obtained, and most reads (>94%) reached Phred-like quality scores (Q-scores) at the Q30 level with a base error rate ≤0.03%. After alignment using Tophat, an average of 90±7% (74-96%) uniquely aligned reads were mapped to the mouse reference genome.

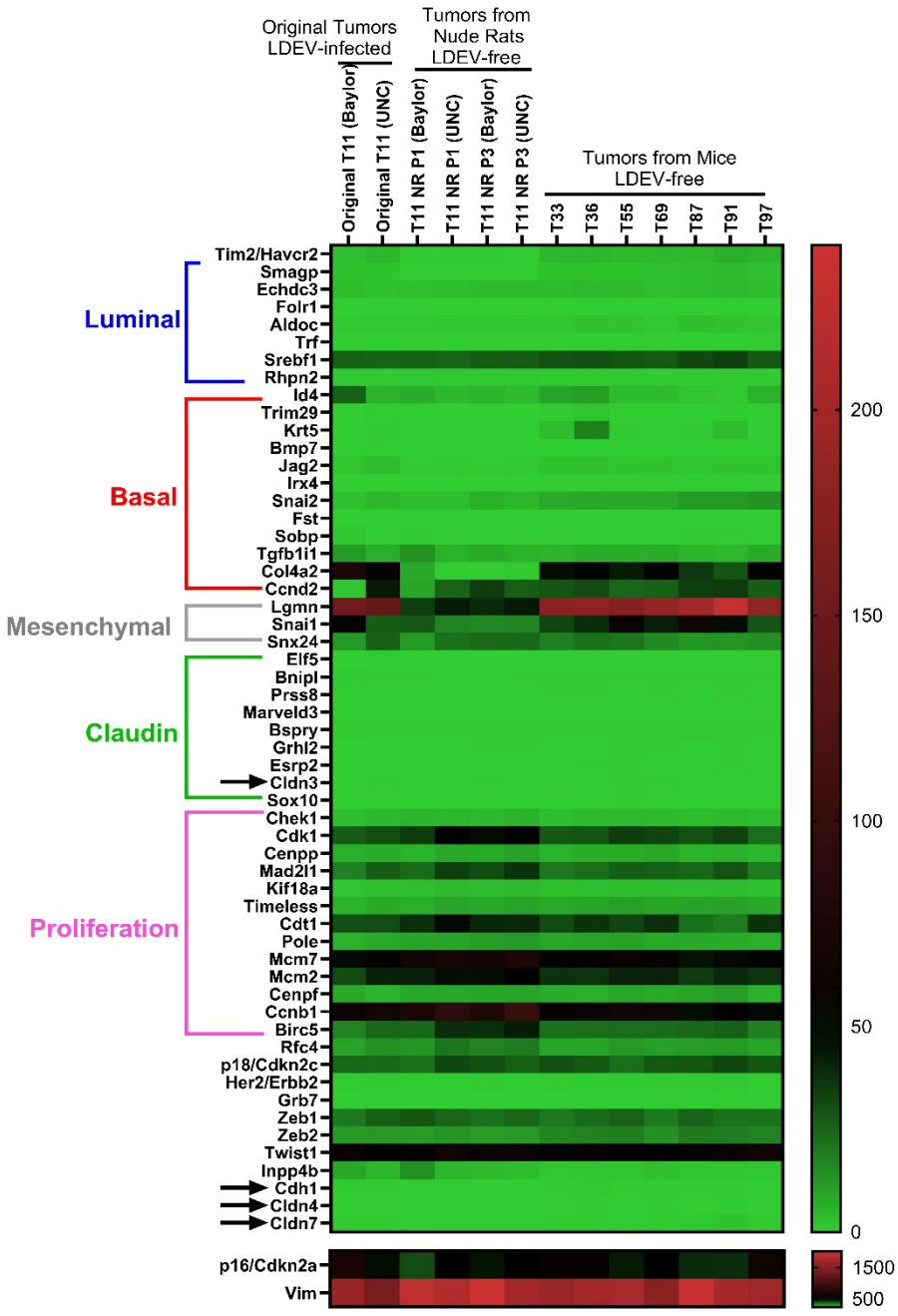

Figure 9 Intrinsic gene set analysis of T11 LDEV-infected and LDEV-free tumors passaged in nude rats and mice.

Normalized RNA-Seq expression levels of subtype-identifying genes previously described by Herschkowitz et al.[32] Genes are listed on the left side of the heatmap. They are grouped by the intrinsic subtype identified by Herschkowitz. et al. Mouse numbers or descriptors are listed at the top of the heatmap. They are grouped according to how they were passaged (original tumor received from Baylor or UNC or passaged in rats or mice) and the LEDV infection as noted above the tumor number. All T11 tumors tested show low expression of claudin-3, -4, -7, and E-cadherin (indicated by the black arrows). Low or absent expressions of these four genes are characteristic of claudin-

low tumors. Results showed that genes with reduced or elevated expression in the original primary tumors maintained similar expression levels in the LDEV-free tumor. Tumors in nude rats showed reduced gene expression levels in Col4a2 and Lgmn. The original T11 tumor received from Baylor showed low levels of Ccn2 expression. Still, after serial passaging in nude rats and mice, expression levels were comparable to the original tumor received from UNC.

Differential gene expression analysis was performed on FMPK normalized read counts from the original LDEV-infected tumors, which were passaged into nude rats, and LDEV-free tumors passed into mice using DESeq2. Genes previously described as characteristic of the murine tumor subtypes[32] were graphed in a heatmap to compare expression levels of intrinsic genes. Gene expression patterns for all tested T11 tumors were consistent with previous reports for T11 claudin-low tumor lines, which are known for low expression cell-cell adhesion protein, E-cadherin, and tight junction proteins, claudins 3, 4, and 7 (**Figure 9**).[16, 18, 21] However, there were a few intrinsic genes that showed different expression patterns between tumor groups. For example, tumors passaged in nude rats showed reduced gene expression levels in collagen α2 IV chain (Col4a2), one of the six subunits of collagen IV, a major structural component of basement membranes (normalized count range 0.09-8.8 compared to 29.1-74.1 for all other tumors tested) and legumain (Lgmn), a cysteine protease that assists in extracellular matrix degradation (normalized count range 34.8-43.8 compared to 143.2-230.4 for all other tumors tested). Collagen is produced by fibroblasts, which infiltrate the tumor to support extracellular matrix deposition. Tumors implanted into the rats would have infiltration of rat fibroblasts in the primary tumor. It is possible that fibroblasts from the nude rat do not produce Col4a2 or Lgmn at the same levels as the normal syngeneic Balb/c mouse host. When comparing the original T11 tumor received from Baylor to all other T11 tumors tested, Cyclin D2 (Ccnd2), a D-type cyclin that regulates the G1-S transition of cell division, was another gene with differential expression (normalized read count=1.7 compared to range 9.3-43.6 in all other tumors tested). Tumors from nude rats and syngeneic mice showed expression levels comparable to the original tumor received from UNC. Reduced

expression of Ccnd2 in the original tumor from Baylor may be due to the size or timing of tumor resection. Tumor growth is dependent on the rate of cell division. If the tumor growth had slowed at the time of tumor resection, cell division and the transition of tumor cells from G1 to the S phase would also be reduced, resulting in lower expression of CCnd2. Despite these minor differences between individual tumors, tumors within each group share a high level of like gene expression; therefore, tumors were clustered according to their source (i.e., original tumors (n=2), LDEV-free tumors passaged in rats (n=4), and LDEV-free tumors passaged in mice (n=7)) and were considered biological replicates.

To evaluate the potential effect of LDEV-infection on tumor biology, differential expression analysis was conducted on the original tumors (LDEV-infected; n=2, one from each institution) and the LDEV-free tumors passaged in mice (n=7) using DESeq2. Results showed that 12,171 genes were shared between LDEV-infected and LDEV-free tumors (**Figure 10a**). However, each group contained a unique set of genes not expressed in the other tumors. LDEV-infected tumors exhibited 452 individual genes, while LDEV-free tumors had 473 genes not expressed in LDEV-infected tumors. To discern variations in upregulated and downregulated genes between these two tumor types, the p-values resulting from DESeq2 analysis were subjected to adjustment using the Benjamini and Hochberg method to control the False Discovery Rate (FDR). Genes with an adjusted p-value (padj) <0.05 were deemed to be differentially expressed. The padj and an absolute fold change of 1.0 were set as the threshold for significant differential expression. The data was graphed in a volcano plot comparing LDEV-free tumors (n=7) to the original tumors containing LDEV (n=2) (**Figure 10b**). LDEV-free tumors had 495 upregulated and 794 downregulated genes compared to LDEV-infected tumors. The top 3 most differentially expressed genes were Zinc Finger DHHC-Type Palmitoyltransferase 15 (Zdhhc15), Insulin-like

growth factor 2 mRNA-binding protein 3 (Igf2bp3), and cat eye syndrome chromosome region candidate 2 (Cecr2). All 3 of these genes were upregulated in LDEV-free tumors compared to the original LDEV-infected tumors.

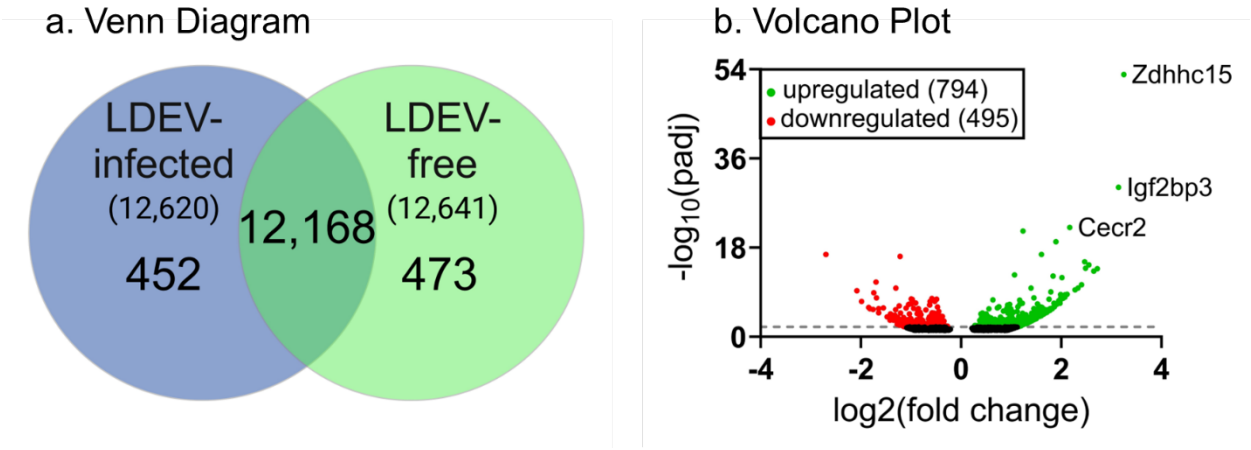

Figure 10 Differentially expressed genes between the original LDEV-infected tumors and LDEV-free tumors passages in syngeneic mice

(a) Venn diagram of the number of differential genes expressed between the original tumors received from donating institutions that were infected with LDEV (n=2) and tumors that were cleared of LDEV and subsequently passaged into syngeneic, immunocompetent mice (n=7). The number in parentheses is the total number of genes identified for each tumor group. Both groups shared 12,168 like genes but expressed 452 and 473 unique genes in the LDEV-infected and LDEV-free tumors, respectively. (b) A volcano plot of the differentially expressed genes for LDEV-infected and LDEV-free tumors. DESeq2 was used to conduct differential expression analysis on the two tumor groups. The resulting p-values were adjusted using Benjamini and Hochberg's approach for controlling the False Discovery Rate (FDR), and genes with an adjusted p-value (padj) <0.05 were considered differentially expressed. The padj and an absolute fold change of 1 were set as the threshold for significant differential expression (gray line). The red dots indicate downregulated genes, and the green dots indicate upregulated genes. As shown on the volcano plot in parenthesis, 794 upregulated genes and 495 downregulated genes were identified. The top 3 most differentially expressed genes are noted on the volcano plot: Zinc Finger DHHC-Type Palmitoyltransferase 15 (Zdhhc15), Insulin-like growth factor 2 mRNA-binding protein 3 (Igfnbp3), and Cecr2 Histone Acetyl-Lysine Reader. All three genes were upregulated in LDEV-free tumors compared to the original LDEV-infected tumors.

The highest differential expression was Zdhhc15, one of 23 in a family of S-acyltransferase enzymes that share a conserved zinc finger DHHC (Asp-His-His-Cys) cysteine-rich domain. These enzymes catalyze S-palmitoylation, the transfer of palmitic acid (C16:0) or other long-chain saturated fatty acids to internal cysteine residues of proteins on the cytoplasmic face of cellular membranes through unstable thioester linkages, leading to alterations in their physiological properties. This dynamic and reversible process has significant implications for the accumulation, secretion, localization, stability, and function of proteins in cells by modulating their membrane affinity.[336] Emerging evidence suggests that palmitoylation of proteins is involved in carcinogenesis, tumor cell growth, survival, and treatment resistance.[337] Significant upregulation of Zdhhc15 in LDEV-free tumors compared to LDEV-infected tumors may contribute to the consistent and reliable lung metastases observed after virus removal.

Igf2bp3 had the second highest differential expression with significant upregulation in LDEV-free tumors compared to LDEV-infected tumors. It is one of three insulin-like growth factor-2 mRNA-binding proteins that bind RNA to influence various protein functions, such as localization, stability, and embryonic development. Igf2bp3 is largely absent from adult tissues but is present in reproductive organs developing fetal tissues and is highly expressed in many aggressive cancers.[338, 339] Several publications have investigated the role of Igf2bp3 in TNBC. These studies have demonstrated Igf2bp3 plays a role in cell proliferation through the EGFR-AKT axis using the *in vitro* human TNBC claudin-low cell line, MDA-MB-231.[340] Additionally, in other *in vitro* and *in vivo* TNBC models, studies have shown Igf2bp3 plays a role in the regulation of the epithelial to mesenchymal transition, metastasis, and chemoresistance.[339, 341, 342] Two small retrospective studies using human tumor samples correlated tumor characteristics with Igf2bp3 IHC staining. These studies showed a significant association with higher tumor grade and stage

and a basal-like TNBC phenotype.[343, 344] One of the human retrospective studies also demonstrated a significant correlation between high levels of Igf2bp3 and disease-free and overall survival.[344] In addition to the previously investigated roles of Igf2bp3, a recent study conducted using *in vitro* and *in vivo* TNBC models showed Igf2bp3 is involved in the immune escape of TNBC cells. Results from this study demonstrated that the gene coding for N6-adenosine-methyltransferase (Mettl3), an enzyme involved in the post-transcriptional methylation of mRNA internal adenosine residues, increased PD-L1 mRNA stability and was dependent on Igf2bp3 expression. As previously discussed in section 1.2.2, high tumor PD-L1 expression suppresses T-cell activation and aids in tumor immune escape. Therefore, this data indicates that the knockdown of Igf2bp3 can enhance T cell-mediated anti-tumor immunity by downregulating PD-L1 expression in TNBC.[339, 345] These combined data suggest that tumors expressing higher levels of Igf2bp3 have a more aggressive phenotype and support the observation that LDEV-free tumors have reliable progressive disease.

The third most significant differentially expressed protein between LDEV-free and LDEV-infected tumors was Cecr2, an epigenetic factor with a bromodomain that recognizes acetylated lysine residues. There are few reports about the role of Cecr2 in cancers; however, one recent study described Cecr2 regulation of breast cancer metastasis and macrophage-promoted immune suppression through NF-κB signalling.[346] Using matched pairs of human primary and distant metastatic breast tumors, gene expression analysis revealed that Cecr2 was highly expressed in breast cancer metastases, and correlated with M2 macrophage abundance and worse metastasis-free survival. In an immunocompetent, syngeneic basal-like TNBC (4T1) mouse model, Cecr2 was required for breast cancer metastasis. NF-κB was shown to recruit Cecr2 to increase chromatin accessibility and activate the expression of target genes, such as VEGFA, CSF-1 (M-

CSF), and CXCL1 (KC). Inhibition of Cecr2 bromodomain impeded NF-κB-promoted immune suppression by macrophages and inhibited breast cancer metastasis. Though limited, this information further supports our data, suggesting that removing LDEV from murine T11 tumors improved its ability to metastasize to the lung reliably and consistently.

For a deeper exploration into the pathways associated with the variations in gene expression, an analysis was conducted on 794 upregulated and 495 downregulated genes in LDEV-free tumors compared to LDEV-infected tumors. This analysis aimed to identify enrichment patterns using Gene Ontology (GO) and Kyoto Encyclopedia of Genes and Genomes (KEGG) databases. Gene length bias was corrected and GO and KEGG terms with an adjusted p-value of <0.05 were considered significantly enriched by differentially expressed genes. There were 602 GO terms and 17 KEGG pathways that were significantly upregulated in LDEV-free T11 primary tumors compared to the original T11 (**Figure 11a, c**). The most significant upregulated GO term was "cell-cell junction" (n=53; padj ≤ 0.0001), while "focal adhesion" was the most significant KEGG pathway upregulated in LDEV-free tumors (n=29; padj ≤ 0.0001). Nine genes were shared among these two enrichment terms: alpha actin1 (Actn1), alpha-actin 4 (Actn4), cyclin D1 (Ccnd1), Integrin alpha-5 (Itga5), Laminin Subunit Alpha 1 (Lama1), Serine/threonine-protein kinase (Pak4), protein phosphatase 1, catalytic subunit, alpha isoform (Ppp1ca), talin 2 (Tln2), Zyxin (Zyx). Upregulation of these genes suggests the LDEV-free tumor has a higher rate of cell proliferation that is likely to play a role in increased cell growth and higher rates of lung metastases. Additionally, of the 602 upregulated GO terms, 25 are associated with regulating immune response, and 27 are related to angiogenesis or blood vessel formation (data not shown). "Angiogenesis" was the most significant GO term related to angiogenic pathways (n=42; padj ≤ 0.0001), and among the immune response-related GO terms, "myeloid leukocyte migration" was

the most significant (n=21; 0.0002). These upregulated pathways are critical to tumor growth and metastases and support the premise that T11 tumors have more aggressive disease progression without LDEV.

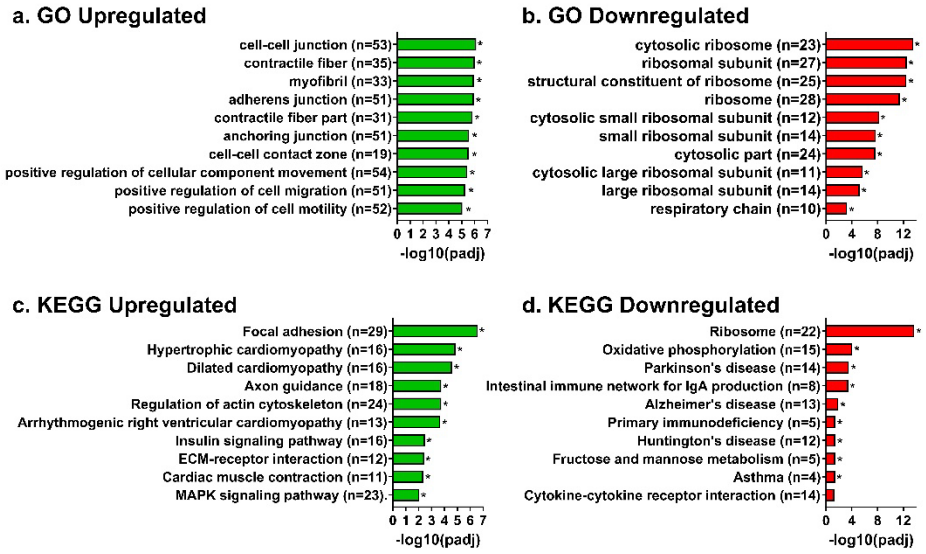

Figure 11 GO and KEGG enrichment analysis of differentially expressed genes in the LDEV-free tumor compared to the original LDEV-infected primary tumors.
Bar graph of the top ten significantly (padj < 0.05) enriched GO terms using (a) upregulated or (b) downregulated differentially expressed genes in the LDEV-free compared to the LDEV-infected original T11 tumors. Bar graph of the top five significantly (padj< 0.05) enriched KEGG terms using (c) upregulated or (d) downregulated differentially expressed genes in the 2225LM variant compared to the 2225L original tumor. In all graphs, the y-axis shows the enriched GO or KEGG terms with the number of identified genes in parenthesis. The x-axis shows the -$\log_{10}$ of the p-value adjusted by Benjamini and Hochberg's approach for controlling the False Discovery Rate (FDR). Padj >0.05 was considered significant. GO or KEGG pathways that were significantly enriched are indicated with an asterisk. There were 602 GO terms and 17 KEGG pathways that were significantly upregulated in LDEV-free T11 primary tumors compared to the original T11, and106 GO terms and 9 KEGG pathways were significantly downregulated.

Downregulated genes also play a critical role in cellular processes and signaling pathways related to tumor progression. In the analysis of LDEV-free compared to LDEV-infected tumors, 106 GO terms and 9 KEGG pathways were significantly downregulated (padj<0.05) (**Figure 11b, d**). The cytosolic ribosome GO term exhibited the most noteworthy downregulation (n=23; padj≤0.0001), and the corresponding KEGG pathway was ribosome (n=22; padj≤0.0001). As indicated by the descriptions, both analyses showed a significant decrease in 22 ribosomal proteins, implying that tumors infected with LDEV experienced substantial disturbances in ribosome

assembly, changes in cellular metabolism, and diminished protein production. These modified mechanisms would predictably influence tumor cell growth and progression.

Interestingly, within the 106 GO terms showing significant downregulation, 65 terms were linked to immune response mechanisms. As indicated in **Table 9,** several immune pathways are downregulated that are enriched with genes, such as CD40, CD83, CD84, and toll-like receptor 9 (TLR9), suggesting a strong downregulation of antigen presentation in LDEV-free tumors. After clearing the LDEV infection from T11 primary tumors, the presentation of viral antigens to T cells would expectedly decline. This decrease in the immunostimulatory tumor microenvironment would likely reduce the activation of tumor-specific T cells, thereby dampening the anti-tumor immune response. As a result, the tumor would gain the opportunity to evade immune surveillance, leading to a more aggressive tumor phenotype.

The most significant GO term among the 65 immune regulation terms was "regulation of leukocyte activation" (n=29; padj=0.0007). As indicated in **Table 9**, several leukocyte-affected pathways are enriched with genes, such as CD40, CD83, CD84, and toll-like receptor 9 (TLR9), suggesting a strong downregulation of antigen presentation in LDEV-free tumors. After clearing the LDEV infection from T11 primary tumors, the presentation of viral antigens to T cells would expectedly decline. This would reduce the activation of tumor-specific T cells, thereby dampening the anti-tumor immune response. As a result, the tumor would gain the opportunity to evade immune surveillance, leading to a more aggressive tumor phenotype.

Table 9 Significantly downregulated GO term associated with immune responses in LDEV-free primary tumors compared to the original T11 primary tumors infected with LDEV

GO Term	n	padj
regulation of leukocyte activation	29	0.0007
regulation of lymphocyte proliferation	18	0.0011
regulation of mononuclear cell proliferation	18	0.0011
regulation of leukocyte proliferation	18	0.0013
leukocyte mediated immunity	21	0.0014

lymphocyte proliferation	20	0.0029
positive regulation of leukocyte activation	19	0.0029
regulation of lymphocyte activation	23	0.0029
regulation of chemotaxis	15	0.0029
positive regulation of the immune effector process	15	0.0035
leukocyte proliferation	20	0.0035
cytokine receptor activity	10	0.0042
myeloid cell activation is involved in the immune response	9	0.0060
antigen processing and presentation of peptide antigen via MHC class II	5	0.0060
regulation of antigen processing and presentation	5	0.0060
regulation of leukocyte-mediated immunity	14	0.0068
myeloid leukocyte-mediated immunity	9	0.0086
positive regulation of lymphocyte activation	16	0.0086
regulation of leukocyte cell-cell adhesion	18	0.0105
leukocyte cell-cell adhesion	19	0.0111
positive regulation of immune response	24	0.0116
myeloid leukocyte activation	13	0.0116
regulation of the immune effector process	19	0.0116
negative regulation of the immune system process	22	0.0131
positive regulation of lymphocyte proliferation	11	0.0137
regulation of T cell activation	17	0.0137
positive regulation of leukocyte cell-cell adhesion	13	0.0146
negative regulation of leukocyte activation	12	0.0162
positive regulation of leukocyte proliferation	11	0.0168
regulation of T cell proliferation	12	0.0168
T cell activation	23	0.0169
leukocyte activation is involved in the immune response	15	0.0172
leukocyte chemotaxis	13	0.0175
cell activation involved in immune response	15	0.0186
leukocyte migration	17	0.0191
positive regulation of B cell proliferation	6	0.0191
negative regulation of mononuclear cell proliferation	8	0.0191
negative regulation of lymphocyte proliferation	8	0.0191
T cell proliferation	13	0.0191
phagocytosis, engulfment	6	0.0191
positive regulation of the production of molecular mediator of immune response	8	0.0191
adaptive immune response	19	0.0191
positive regulation of cell migration	22	0.0191
negative regulation of cell adhesion	15	0.0191
positive regulation of T cell activation	12	0.0191
granulocyte activation	5	0.0191
positive regulation of neutrophil chemotaxis	5	0.0191

positive regulation of cellular component movement	23	0.0191
regulation of leukocyte degranulation	6	0.0201
negative regulation of leukocyte proliferation	8	0.0207
myeloid leukocyte migration	12	0.0207
regulation of B cell proliferation	7	0.0214
leukocyte degranulation	7	0.0225
production of molecular mediator of immune response	12	0.0225
negative regulation of T-cell activation	9	0.0225
positive regulation of granulocyte chemotaxis	5	0.0225
negative regulation of cell activation	12	0.0229
T cell migration	6	0.0245
negative regulation of T cell proliferation	7	0.0253
regulation of myeloid leukocyte-mediated immunity	6	0.0263
positive regulation of chemotaxis	10	0.0263
negative regulation of lymphocyte activation	10	0.0327
negative regulation of leukocyte cell-cell adhesion	9	0.0338
regulation of neutrophil chemotaxis	5	0.0339
positive regulation of neutrophil migration	5	0.0339

n is the number of significantly downregulated genes identified in the GO term. Genes were considered significantly differential when the adjusted p-value was <0.05 and the absolute fold change was 1.0.
padj is the p-value adjusted using Benjamini and Hochberg's approach for controlling the False Discovery Rate (FDR)

To further elucidate the immune changes between LDEV-free and LDEV-infected T11 primary tumors, the seq-ImmuCC computational model was used to infer the relative proportions of 10 major immune cell subsets in mouse tissues from the RNA-Seq data.[335] To estimate the relative immune cell compositions in each of the primary tumor groups, the normalized RNASeq transcriptional data was uploaded to the seq-ImmuCC server (http://wap-lab.org:3200/immune/) The percentage of each immune cell type was plotted by the individual tumor in a bar graph to depict the high variability among all tumors analyzed (**Figure 12a**). The T11 tumor from UNC showed the highest macrophage composition among the tumors, with 80% of total immune cells, in contrast to 18% in the Baylor T11 tumor, and a range of 13-44% (average 32±10%) in tumors passaged in mice after the removal of LDEV. Primary tumors that were passaged in mice were categorized into two groups: those containing LDEV infections (n=2, one original T11 tumor from

each institution) and tumors that were eliminated of LDEV and then passaged into mice (n=7). To assess differences in immune composition between these two tumor groups, the average relative immune cell compositions for each group were depicted in a heatmap (**Figure 12b**). Tumors with LDEV infection exhibited a more significant average proportion of antigen-presenting cells (i.e., dendritic cells and macrophages) than tumors without LDEV. Conversely, tumors free of LDEV demonstrated a more significant average T cell infiltration than those with LDEV infection. It is worth noting that the extrapolated percentages in the ImmuCC results are based on tumor gene expression. They may not directly correlate with protein or immune assays due to variations in transcription rates, translation, post-translational modifications, and protein regulation. The two original tumors also showed significant variability in their extrapolated immune cell compositions. Notably, the makeup of immune cells within the tumor microenvironment doesn't automatically indicate a particular immune response. Understanding the intricate immune cell interactions in the TME requires deeper exploration. Further analysis is needed to confirm the differences between the two tumor groups' immune cell composition differences and mechanisms.

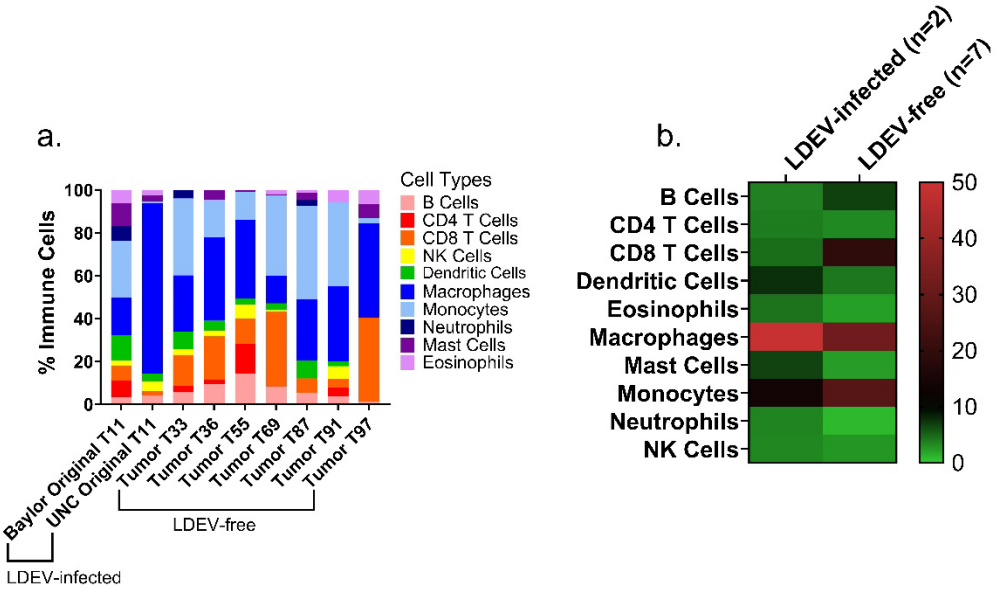

Figure 12 Immune cell composition of LDEV-infected and LDEV-free T11 primary tumors from immunocompetent, syngeneic mice using the RNASeq transcriptome
(a) Stacked bar plot showing RNA-seq seq-ImmuCC calculated cellular compositions of the immune microenvironment in LDEV-infected (n=2) and LDEV-free (n=7) murine primary tumors harvested from immunocompetent, syngeneic mice. (b) Heat map displaying the mean percent of each immune cell type for each tumor group. Results showed high variability among all tumors analyzed. The original T11 tumor from UNC had a macrophage composition of 80% compared to 18% total macrophages in the Baylor T11 and a range of 13-44% (average 32±10%) in tumors passaged in mice after LDEV removal. LDEV-infected tumors had a higher mean percentage of antigen-presenting cells (i.e., dendritic cells and macrophages) than LDEV-free tumors.

3.7 Gene expression analysis of T11 claudin-low breast cancer lung metastases

The next series of evaluations was conducted to unveil relevant pathways and mechanisms governing the mechanisms of CLBC metastasis. LDEV-free primary tumors were resected from syngeneic, immunocompetent, female Balb/c mice when they reached an average of 678±202 mm^3. Mice were sutured and housed for an additional 23±7 days post-resection (n=3 total), euthanized, and lungs were evaluated for visible metastatic lesions. Two of the three mice had small identifiable lesions, and one had extensive metastases covering much of the lung surface area. Naïve lung tissue (n=2) from contemporary, age-matched mice was used as the control. The age of all mice at the time of euthanasia was approximately 10-11 weeks.

All samples were successfully processed and had sufficient RNA for RNA-Seq transcript quantification. The samples had a mean RNA concentration of 0.278±0.329 µg/µL (0.057-0.930 µg/µL), and the mean RIN value was 8.6±1.6 (6.0-10.0). An average of 75.2±11.2 million clean reads were obtained, and most reads (>94%) reached Phred-like quality scores (Q-scores) at the Q30 level with a base error rate ≤0.02%. After alignment using Tophat, an average of 92±1% (92-93%) uniquely aligned reads were mapped to the mouse reference genome.

Using DESeq2, differential expression analysis was conducted on FMPK-normalized read counts to compare normal lungs (n=2) to lungs containing T11 metastatic lesions (n=3). The resultant p-values were adjusted using the Benjamini and Hochberg method for False Discovery Rate (FDR) control. Genes with an adjusted p-value (padj) <0.05 were deemed to be differentially expressed, with the criteria of padj and an absolute fold change of 1.0 served as the benchmarks for determining significant differential expression.

Upon comparing the gene profiles of both normal and metastatic lungs, the results revealed a common set of 12,462 genes shared by both groups (**Figure 13a**). Within normal lungs, 1,936 were unique, whereas lungs with T11 metastases featured 789 distinct genes. Analyzing differential gene expression in lung tissues showed 6,414 upregulated genes and 7,676 downregulated genes in T11 metastatic lungs compared to control (**Figure 13b**). This assessment identified four upregulated genes with the most pronounced and significant differential expression in T11 metastatic lungs: cyclin-dependent kinase inhibitor 2a (Cdkn2a), Myc proto-oncogene (Myc), S100 calcium-binding protein a4 (S100a4), and cellular retinoic acid binding protein 2 (Crabp2). Altered expression of these genes within metastatic lung tissues indicates they play a crucial role in the metastasis of CLBC.

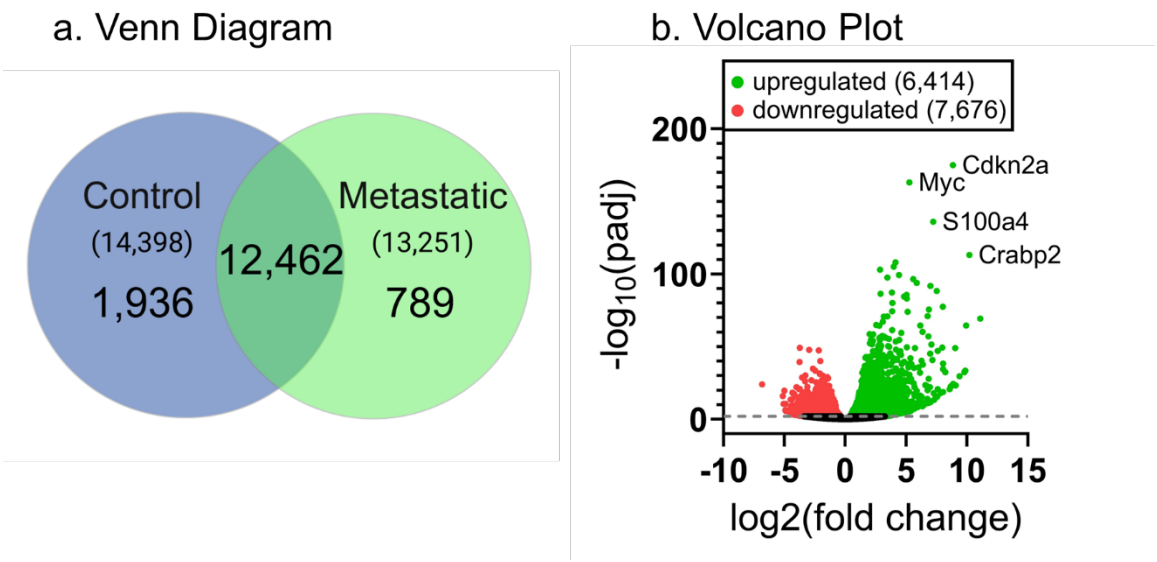

Figure 13 Differentially expressed genes between lungs with T11 claudin-low breast cancer metastases and control lungs.

(a) Venn diagram of the number of differential genes expressed between the control lungs (n=2) and lungs with T11 metastases (n=3). The number in parentheses is the total number of genes identified for each tumor group. Both groups shared 12,462 like genes but expressed 1,936 and 789 unique genes in control and T11 metastatic lungs, respectively. (b) A volcano plot of the differentially expressed genes for control and metastatic lungs. DESeq2 was used to conduct differential expression analysis on the two tumor groups. The resulting p-values were adjusted using Benjamini and Hochberg's approach for controlling the False Discovery Rate (FDR), and genes with an adjusted p-value (padj) <0.05 were considered differentially expressed. The padj and an absolute fold change of 1.0 were set as the threshold for significant differential expression (gray line). The red dots indicate downregulated genes, and the green dots indicate upregulated genes. As indicated on the volcano plot in parenthesis, there were 6,414 upregulated and 7,676 downregulated differentially expressed genes identified. The top 4 most differential genes are noted on the volcano plot: Cyclin-Dependent Kinase Inhibitor 2A (Cdkn2a), Myc proto-oncogene (Myc), S100 Calcium Binding Protein A4 (S100a4), and Cellular Retinoic Acid Binding Protein 2 (Crabp2). All 4 of these genes were upregulated in metastatic lungs compared to the control.

Cdkn2a exhibited the most notable differential expression in T11 metastatic lungs compared to the control. Cdkn2a encodes the p16 protein, a key regulator of cell cycle progression that functions as a tumor suppressor by impeding unchecked cell growth through interactions with cyclin-dependent kinases.[347] Ideally, the upregulation of Cdkn2a should enhance p16 activity, inhibiting cyclin-dependent kinases and subsequent slowdown of cell cycle progression. This attenuation of cell cycle progression should restrain unrestricted cell growth, potentially resulting in a less aggressive tumor phenotype. However, the tumor and metastatic microenvironments are dynamic and complex. Despite the upregulation of Cdkn2a, T11 tumor cells do not appear to have

reduced tumor growth. Therefore, mechanisms might have been developed to evade Cdkn2a cell cycle regulation, inhibiting tumor growth less effectively.

Following Cdkn2a, Myc was the second-highest gene with differential expression between T11 metastatic and control lungs. Myc is a widely recognized cell proliferation and differentiation driver, frequently implicated in cancer development and stem cells. Previous studies have shown that Myc is amplified in TNBC and the claudin-low subtype.[18] The genetic changes seen in T11 lung metastases, which result in elevated Myc expression, correspond with genetic findings previously documented in human and mouse primary claudin-low breast tumors, including T11.

S100a4 ranked as the third most significantly differentially expressed gene. The S100A4 gene-encoded protein has been identified as having the ability to regulate cell cycle progression, modulate intercellular adhesion, and enhance the invasive and metastatic characteristics of cancer cells while also having the potential to bind and inactivate the p53 suppressor protein, which governs both the G1-S transition and the transition of cells from the S phase to mitosis (G2-M).[348] Recent studies in TNBC human and mouse models have demonstrated a positive correlation between the inhibition of S100a4 and the rate of metastases.[349, 350]

Lastly, Crabp2 is an integral component of retinoic acid signaling, a pathway with diverse effects on cell differentiation and proliferation. Abnormal expression of Crabp2 has been observed in various tumor types, acting as both a tumor suppressor and promoter.[351] Within TNBC, emerging data suggest that Crabp2 exerts a significant influence on regulating invasion and metastasis, correlating with a poorer prognosis.[349, 352] The presence of these four upregulated genes in metastatic lungs highlights their potential relevance in driving the aggressive phenotype of CLBC.

For a more in-depth exploration of the pathways associated with T11 CLBC metastases, the set of 6,414 upregulated genes and 7,676 downregulated genes in T11 metastatic lungs compared to control underwent analysis for enrichment using GO and KEGG. Normalization for gene length bias was applied and GO and KEGG terms with an adjusted p-value of <0.05 were considered significantly enriched by differentially expressed genes. Results showed that 1,232 GO terms and 30 KEGG pathways were significantly upregulated. Downregulated genes were enhanced considerably in 1,380 GO terms and 48 KEGG pathways when comparing metastatic lungs to controls (data not shown). The most significant upregulated GO term and KEGG pathway were "ribonucleoprotein complex biogenesis" (n=277; padj≤0.0001) and "ribosome" (n=85; padj≤0.0001), respectively. The most significantly downregulated GO term and KEGG pathway were "side of membrane" (n=168; padj≤0.0001) and "cell adhesion molecules (CAMs)" (n=59; padj≤0.0001), respectively. Interestingly, the GO term "angiogenesis" (n=148; padj≤0.0001) came in second for the most significant downregulated, suggesting that there was less angiogenesis occurring in the metastatic compared to control lungs. Overall, the GO terms and KEGG pathways suggest substantial increases in protein production, metabolic activity, matrix remodeling, and a decrease in angiogenesis, immune responses, and cell adhesion. Follow-up experiments should focus on genes involved in these pathways to hone in on potential TNBC therapies.

Using the RNA-Seq datasets from T11 metastatic and control lungs, the seq-ImmuCC computational model was applied to analyze potential changes in immune cell subsets.[335] To estimate these tissues' relative immune cell compositions, the normalized RNASeq transcriptional data was uploaded to the seq-ImmuCC server (http://wap-lab.org:3200/immune/). The percent compositions were graphed in a bar chart by individual lung samples and were grouped for comparison in a heat map (**Figure 14**). Results showed high variability among the samples, with

macrophage cell derivation showing the lowest variability within each group. A low number of samples for analysis likely contributed to these observations. Despite this limitation, the data suggested that there was a substantial increase in the percentage of infiltrating macrophages and CD8 T cells in metastatic lungs compared to the control (32±11% vs. 1±0.3% and 19±29% vs. 6±9%, respectively). Alternatively, B cells and CD4 T cells were lower in metastatic versus control lungs (13±13% vs. 24±4% and 4±5% vs. 21±26%, respectively). Derivation results from seq-ImmuCC did not align with previous flow cytometry results showing that T11 metastatic lungs had 47 (±16)% $CD11b^+$and 5% (±4%) $CD3^+$ cells, while control lungs contained 53% (±8%) $CD11b^+$ and 11 (±3)% $CD3^+$ cells. As previously discussed with primary tumors in sections 3.4 and 3.5, there are many reasons why these two assays would yield different results. When considering all analyses conducted on T11 primary tumors and metastatic lungs, it is apparent that a complex and dynamic series of immune responses are occurring that are helping to drive tumor progression. Future experiments will continue to focus on pathways and mechanisms that are helping to drive tumor progression.

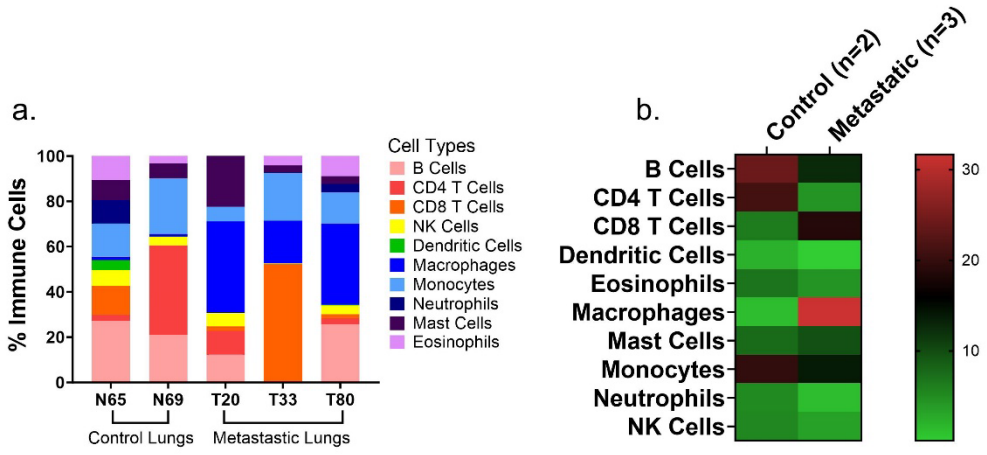

Figure 14 Immune cell composition derived from the RNA-Seq transcriptome of normal lungs and lungs with T11 metastatic lesions

(a) Stacked bar plot showing RNA-seq seq-ImmuCC calculated cellular compositions of the immune microenvironment in normal control lung from contemporary, age-matched mice (n=2) and lungs with T11 metastatic

lesions (n=3)(b) Heat map displaying the mean percent of each immune cell type for each group. Results showed high variability among all tissues analyzed. Data suggested that there is a substantial increase in the percentage of infiltrating macrophages and CD8 T cells in metastatic lungs compared to the control (32±11% vs. 1±0.3% and 19±29% vs. 6±9%, respectively). B cells and CD4 T cells were lower in metastatic versus control lungs (13±13% vs. 24±4% and 4±5% vs. 21±26%, respectively)

3.8 Summary and Discussion

The evasion of immune surveillance is an accepted hallmark of tumor progression, and treatment strategies for targeting immune-suppressive pathways have led to enhanced survival in breast cancer patients.[353-355] In TNBC, normal immune cells are suppressed, and immune-suppressing cells, such as TAMS and MDSC, are heavily recruited into the TME. TAMS and MDSC inhibit the activity of T cells and induce T cell apoptosis, which allows tumors to progress. Since 2011, when the first immune checkpoint inhibitor was FDA-approved, drug discovery for cancer treatments has focused on overcoming tumor mechanisms for immune cell evasion. However, while these inhibitors are effective with chemotherapy for TNBC, response to this combination therapy is inconsistent and unpredictable across this tumor subtype.[354] The overall aim of this research was to identify proteins that could be targeted in TNBC by using a reliably metastatic murine model. We used two murine models of TNBC to begin our investigation but focused on the TNBC subtype of CLBC. In this chapter, two murine models of TNBC, 2225L (basal-like) and T11 (claudin-low), were developed and characterized. These models were generated with the goal of providing clinically relevant, immunocompetent, and syngeneic murine tumor models for studying TNBC therapeutic targets.

Reliably metastatic murine tumor models for basal-like (2225L) and CLBC (T11) were characterized in the first part of this dissertation. The 2225L and T11 tumor lines were suitable for immunocompetent Balb/c mice and were syngeneic to the host. When the 2225L was received from the donating institution and transplanted into mice, it was not reliably metastatic. However, our lab produced a highly metastatic variant (2225LM) through serial passaging in syngeneic

hosts. The T11 tumor line could not be immediately transplanted into mice because it was positive for LDEV, a virus that infects macrophages. The LDEV infection was successfully removed by serial transplantation into nude rats. The mice developed consistent lung metastases when the clean tumor line was implanted into the syngeneic host's mammary fat pad or subcutaneous flank. Genomic testing was conducted on the original and subsequent passaged tumors for both tumor lines. The original and passaged tumors' genomic profiles were comparable in their tumor subtype-defining gene profiles. Similarly, the gene expression profile of T11 tumor cells derived from transplanted tumors was consistent with claudin-low primary tumors. In the T11 tumor lines, the findings of lung metastases were significant because other labs reported they were unable to achieve metastases using this model up to 90 days post-tumor implant with or without resection.[23] This suggests macrophage function may be necessary in tumor metastasis for CLBC.

RNA sequencing analysis performed on the original 2225L tumor, early passages of 2225L, and the 2225LM metastatic variant showed characteristic gene expression profiles consistent with murine basal-like tumor lines were observed, despite the potential for genetic instability and clonal evolution with serial passaged tumors. Differential gene expression analysis revealed significant shifts non-intrinsic basal-like genes, with hundreds of unique genes within each group. Enrichment analysis identified vital pathways and functions affected by these changes, including cellular movement, migration, metabolism, and immunological pathways. Computational modeling further explored immune cell proportions and demonstrated variability in immune signatures across tumor samples. The genes and potential pathways identified through this analysis should be further investigated to better understand their role in basal-like tumor progression, which will be further discussed in Chapter 6.

Next, RNA sequencing analysis was used to assess the impact of LDEV infection on gene expression patterns in murine T11 tumors. Tumors sourced from Baylor and UNC and tumors propagated in nude rats and syngeneic mice were analyzed for alterations in gene expression following the removal of LDEV. Overall, LDEV-free tumors maintained consistent characteristics of T11 claudin-low tumor lines based on their expression of intrinsic claudin-low genes. A deeper analysis compared LDEV-free tumors to the original LDEV-infected tumors. Results showed significant differential expression of numerous genes. Notably, three highly upregulated genes were identified in LDEV-free tumors: Zinc Finger DHHC-Type Palmitoyltransferase 15 (Zdhhc15), Insulin-like growth factor 2 mRNA-binding protein 3 (Igf2bp3), and cat eye syndrome chromosome region candidate 2 (Cecr2). These genes are known to affect tumor growth, survival, metastasis, and immune response regulation. Enrichment analysis showed upregulated pathways in LDEV-free tumors associated with cell-cell junctions, focal adhesion, angiogenesis, and immune response regulation. Conversely, downregulated pathways were linked to ribosome assembly, immune response regulation, and antigen presentation. The immune cell composition within the tumor microenvironment showed variations, with LDEV-free tumors having more infiltrating T cells than infected tumors. These pathways and mechanisms will be further discussed in Chapter 6 and should be considered for future investigations for identifying targetable proteins and pathways for CLBC.

Differential expression analysis highlighted significant alterations, with 6,414 upregulated and 7,676 downregulated genes in metastatic lungs compared to controls. Four key upregulated genes were identified in metastatic lungs: Cdkn2a, Myc, S100a4, and Crabp2. These genes are implicated in the regulation, proliferation, invasion, and metastatic processes in CLBC. Enrichment analyses uncovered pathways associated with increased protein production, metabolic

activity, matrix remodeling and decreased angiogenesis, immune responses, and cell adhesion in metastatic lungs. The seq-ImmuCC model was applied to estimate changes in immune cell subsets. The data indicated variations in immune cell compositions, with increased infiltrating macrophages and CD8 T cells and decreased B cells and CD4 T cells in metastatic lungs compared to controls. These findings underscore the complex and dynamic immune responses contributing to tumor progression in CLBC.

Herschkowitz et al. first characterized tumor lines 2225L and T11 in 2011 using DNA microarray data to evaluate mouse models of TNBC. The publication described the 2225L tumor line as having high basal cytokeratins expression and epidermal growth factor receptor (EGFR) overexpression and the T11 tumor line as having low expression of tight junction and cell-cell adhesion genes. The T11 tumors also expressed mesenchymal features and showed low expression of luminal genes, inconsistent basal gene expression, and expression of lymphocyte and endothelial cell markers, like human CLBC.[21] Compared to other TNBC murine tumors, T11 tumors have a high percentage of the stem cell markers CD29 and CD24 (70– 85% vs. 14% max).[32] Consistent with the original lines evaluated by Herschkowitz et al. using DNA microarray, our RNA sequencing results showed that 2225LM had analogous keratin -5, -6, -17, and EGFR expression levels. Similarly, the LDEV-infected and LDEV-free T11 tumors were alike, with low expression of tight junction and cell-cell adhesion proteins, claudin -3, -4, -7, occludin, and E-cadherin, as well as high expression of mesenchymal markers such as vimentin and snail, and stem cell markers, CD29 and CD24.[16, 32]

To understand the immune cell profiles of the T11 and 2225LM tumors, immune cells were evaluated for their expression of $CD3^+$ and $CD11b^+$ using flow cytometry. $CD3^+$ cells were further subclassified into $CD3^+CD4^+$ and $CD3^+CD8^+$. $CD3^+CD4^+$ are T helper cells that help to coordinate

the immune response by stimulating other immune cells. At the same time, $CD3^+CD8^+$ are known as cytotoxic T cells because they directly kill cells through cell-regulated cytotoxicity. Both T cell subsets correlate with improved responses to therapy and better outcomes. $CD11b^+$ cells were classified into $CD11b^+Ly6C^+Ly6G^-$ and $CD11b^+Ly6C^+Ly6G^+$. $CD11b^+Ly6C^+Ly6G^-$ are monocyte precursor cells for macrophages and dendritic cells. $CD11b^+Ly6C^+Ly6G^+$ are considered neutrophils. Cells with $CD11b^+Ly6C^+Ly6G^-$ expression could be monocytes or M-MDSC, and G-MDSC and TAN share expression of $CD11b^+Ly6C^+Ly6G^+$. These definitions were first proposed by Gabrilovich et al. in 2008 to identify MDSC subsets, which play a significant role in regulating the tumor immune response in the TME and have been widely accepted as important MDSC markers by the larger cancer community.[356-359] For the purposes of the research presented in this dissertation, these markers were used to determine the primary types of infiltrating T cells (T helper and cytotoxic T cells) and MDSC (myeloid or granulocytic) present in 2225LM and T11 tumors.

Flow cytometry showed that $CD11b^+$ cells were the predominant immune cell type in 2225LM and T11 primary tumors compared to $CD3^+$ cells. Previous evaluations of human claudin-low tumors by Prat et al. indicate that CLBC have genes suggestive of high lymphoid infiltration.[18] However, Singh et al. showed that TAM highly infiltrate the murine T11 tumor line compared to basal-like or luminal-like murine tumor lines (2225L and 2208L, respectively).[360] For this analysis, they used the marker F4/80, expressed on macrophages, such as TAMS, and has a low expression on both M-MDSC and G-MDSC. This marker alone does not differentiate TAMS from dendritic cells or monocytes expressing various levels of F4/80. TAMS markers, such as CD68 and CD206, were not considered in our characterization of T11 or 2225LM, as our focus was on MDSC and T cells. However, flow cytometry results showed that 2225LM tumors had a

significantly higher infiltration of $CD11b^+$ cells compared with T11. CD11b is a standard surface marker for all myeloid lineages. Based on what has previously been published on T11 and 2225L, it is expected that there would be a higher $CD11b^+$ population in the T11 tumor line compared to 2225LM. However, other cell types that could be considered among the CD11b population are MDSC, neutrophils, monocytes, and some populations of dendritic cells. All these cell types are expected to be present in the TME and could be present at various levels throughout the tumor and may change with tumor progression. The definition of key markers used to define immune cell populations is critical to the analytical results. It is also important to note that niches can form throughout the tumor. Different proportions of immune cells may be present in distinct areas of the tumor, aiding in cell growth or death within that region. To obtain the most information from each sample, tumors were dissected into tumor chunks, and only a portion of the tumors were used for flow cytometry analysis. Additionally, this experiment evaluated the protein expression of markers on the cell surface. In contrast, Singh et al. used gene expression profiles of the two tumor lines to assess the presence of immune cells. All these considerations could explain the differences observed between this data and Singh et al. when comparing the two tumor lines.

To better understand our results compared to Singh et al., normalized RNASeq data were uploaded to seq ImmuCC to determine the relative proportions of infiltrating immune cells in parental lines and the variants established by our lab. Compared to 2225L tumors, the 2225LM variant had a reduction in the proportion of macrophages and CD8 T cells and an increase in the proportion of dendritic cells. The gene profile of T11 tumors showed a significant proportion of immune cells were identified as macrophages. Since seq-ImmuCC does not subdivide the macrophage population from this data, it cannot be concluded that these are TAMS. However, when comparing the relative proportions of immune cells between 2225L, 2225LM, and T11, T11

had the highest proportion of macrophages. Despite using different analytical methods for evaluating the transcriptome data, these results are consistent with the transcriptome immune profile results comparing T11 and 2225L reported by Singh et al.[360] Overall, the immune profile and flow cytometry data from 2225LM and T11 suggest that the immune response within the TME is enriched to promote tumor growth through the action of immune-suppressing myeloid cells. TAMS and MDSC are suppressive to $CD3^+$ cells, which may explain why there are significantly fewer $CD3^+$ cells in T11 and 2225LM tumors compared to $CD11b^+$ cells. Likewise, the transcriptome data suggests that T11 may have a more suppressive TME than 2225LM.

A multiplex cytokine assay provided insight into cytokines that may regulate the immune response in the TME of 2225LM and T11 tumors and may regulate tumor seeding at metastatic sites. This data showed elevated levels of pro-inflammatory cytokines, such as MCP-1 and KC, which are involved in myeloid cell recruitment and further supported the flow cytometry and genomic evaluations of the types of infiltrating immune cells. However, this data was highly variable and limited to the specific cytokines assayed. To further expand on this exploratory approach for identifying potential key protein regulators of CLBC progression, we deployed two mass spectrometry techniques, nano-liquid chromatography-tandem mass spectrometry (nano-LC-MS/MS) and matrix-assisted laser desorption ionization imaging mass spectrometry (MALDI-IMS). From this point on, the CLBC T11 tumor line was the primary focus of our investigations.

This study provides insights into the intricate mechanisms driving CLBC metastasis and identifies critical genes and pathways contributing to the aggressive phenotype and metastatic potential of CLBC. Further research is warranted to elucidate the underlying mechanisms driving these observed changes and to explore potential therapeutic implications. Expansion on these key pathways for future areas of research in CLBC will be discussed in Chapter 6.

CHAPTER 4: PROTEOMIC IDENTIFICATION OF TUMOR AND METASTASIS-ASSOCIATED GALECTIN-1 IN MURINE CLAUDIN-LOW BREAST CANCER

4.1 Rationale

TNBC claudin-low tumors are clinically aggressive and exhibit high rates of metastasis and recurrence. Additionally, these tumors are chemoresistant and lack targeted therapies, which results in poor patient prognosis. In this chapter, two proteomic approaches, nano-LC/MS/MS and MALDI/IMS, were used to examine primary orthotopic and metastatic CLBC using murine T11 syngeneic, transplantable tumors in immunocompetent Balb/c female mice. Nano-LC/MS/MS was chosen for its ability to improve detection limits and provide accurate peptide masses over traditional protein detection methods. MALDI/IMS integrated spatial mapping of mass spectra with histological methods to visualize peptide and protein distribution in tissue samples.

This research aimed to use discovery-based proteomic approaches to identify proteins associated with CLBC to gain insight into pathways and mechanisms that could lead to targets for intervention. Most of the findings presented in this chapter were published in Biochim Biophys Acta Gen Subj, 1865, Balestrieri et al., Proteomic identification of tumor- and metastasis-associated galectin-1 in claudin-low breast cancer, Page 129784, Copyright Elsevier (2021) by our group.[321]

4.2 Proteomic profile of T11 claudin-low TNBC

The overall study approach and workflow, including proteomics, validation studies, and data analysis, are depicted in **Figure 15**. Proteomic profiling of murine claudin-low tumors and control tissues was first conducted by nano-LC-MS/MS methodology (**Figure 15a**). The local and global Protein Pilot False Discovery Report (FDR) of the number of proteins and peptides identified in T11 cultures, primary and metastatic tumor samples, and control tissues are summarized in **Table**

10. Accession numbers for all proteins identified with >90% confidence were used to generate a Venn diagram (Figure 17a) to reveal the number of differentially expressed proteins. Regions outlined in bold highlight two protein groups: 1) 19 proteins shared by cultured T11 cells, T11 primary tumors, and T11 metastatic tumors (but not identified in control mammary fat pad or lung), and 2) 170 proteins unique to metastatic T11 tumors.

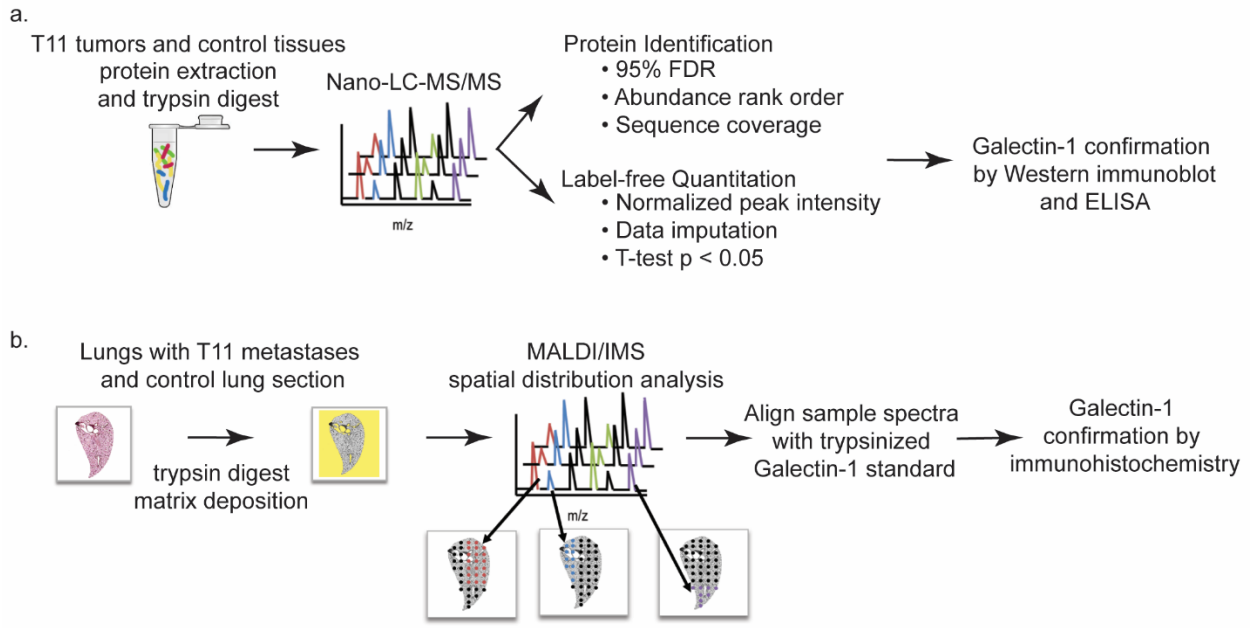

Figure 15 Proteomics Approach, Validation Studies, and Data Analysis Workflow
(a) Nano-LC-MS/MS Proteins extracted from T11 tumor, metastatic lung, control breast, and lung tissues were trypsin digested and analyzed by nano-LC-MS/MS, as described in the Methods. Protein Pilot software was used to identify proteins in each sample. Intensity-based label-free quantitation of proteins from normal and metastatic lung tissues identified Gal-1 as a differentially expressed protein in claudin-low tumors. Western immunoblot and ELISA confirmed Gal-1 identification. (b) MALDI imaging MS frozen T11 metastatic and control lung sections were trypsin-digested on ITO-slides. A rGal-1 standard was spotted on the slide with the samples as a positive control. Spectra from tissue sections and rGal-1 standard were aligned, and Gal-1 peptides overlaid onto tissue sections to qualitatively assess their spatial localization. The most intense peptides appeared in the tumor region of metastatic lung sections. Immunohistochemistry confirmed Gal-1 spatial distribution.

Table 10: Summary of proteins and peptides detected after nano-LC/MS analysis of T11 tumor tissues and controls

Sample Description [c]	# Proteins		# Peptides	
	5% local FDR [a]	1% global FDR	5% local FDR	1% global FDR
T11 claudin-low cultures	113	114	431	460
Primary tumors [b] (n=3)	187	191	877	936
Metastatic lung (n=2)	66	84	1003	1004

Control lung (n=3)	88	101	1384	1390

[a] FDR = False Discovery Rate
[b] Includes untreated samples and samples treated to deplete albumin and globin
[c] Mammary fat pad tissue (not shown) had significant lipid interference, resulting in only six proteins identified (n=2).

We first focused on the 19 identified proteins shared by claudin-low T11-containing samples (T11 cultures, primary tumor, and metastatic tissue) but not identified in control mammary fat pads or control lung tissues. **Table 11** summarizes the nine resulting T11 parent protein identifications after accounting for variant and isoform redundancies. The STRING database analysis determined that seven of the nine proteins are related through protein-protein binding or co-expression **(Figure 17b).** Furthermore, three of the nine proteins identified in T11-containing samples are reported to have a role in cancer metastasis: heat shock cognate (Hspa8), myosin-9 (Myh9), and galectin-1 (Lgals1).[274, 361, 362] Galectin-1 shares a reported direct relationship with protein disulfide-isomerase A6 (Pdia6).[363]

We also compared the 170 proteins only detected in metastatic tumors with the 638 proteins only expressed by primary tumors. The 63 proteins explicitly found in metastatic lungs were uploaded to the STRING Database to determine potential relationships. The identified relationships are depicted in **Figure 16**. T11 lung metastases had a higher percentage of proteins involved in pathways of the immune system, and most of these proteins had roles in innate immunity and/or neutrophil degranulation. After removing variant and isoform redundancies, the proteins found only in metastatic lung tissues were reduced to 61 unique protein identities.[364]

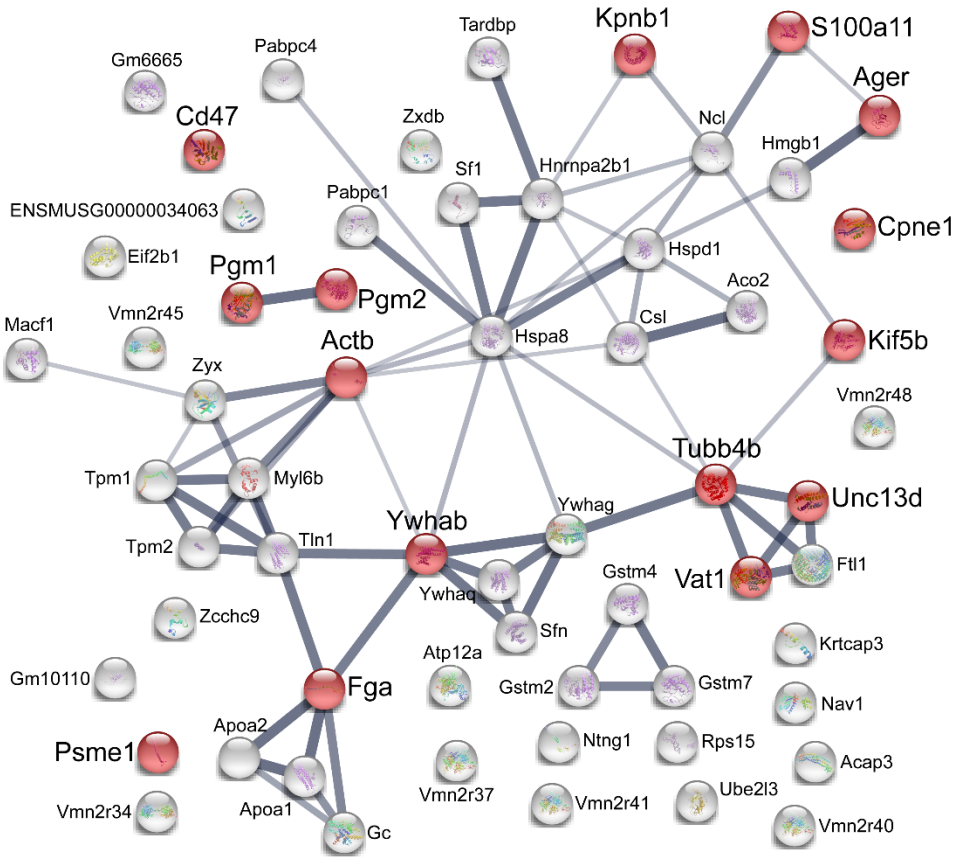

Figure 16 Protein interactions identified only in T11 metastases
After removing protein redundancies, 63 proteins found specifically in metastatic lungs were uploaded to the STRING Database to determine potential relationships. The gray lines indicate a solid possible relationship between the two proteins. The red spheres highlight proteins of the immune system pathway, which was significantly elevated in metastatic lungs compared to primary tumors; most of these proteins were involved in innate immunity. CD47, S100a11, Ager/RAGE, and Kif5b have been previously reported as playing a role in metastasis.

Table 11: Nano-LC/MS identification of shared proteins in claudin-low T11 tumor-containing samples, but not detected in control tissue[a,b]

		Cultured T11 Cells			Primary T11 Tumors			Metastatic Lung		
Gene ID	**Protein ID**	**Unique peptides**	**Rank [c]**	**Percent Coverage**	**Unique peptides**	**Rank [c]**	**Percent Coverage**	**Unique peptides**	**Rank [c]**	**Percent Coverage**
Lgals1	Galectin-1	15	13/119	88	26	21/240	72	8	36/130	47
Hspa8	Heat shock cognate 71 kDa protein	14	6/119	29	24	4/240	35	14	11/130	27
Myh9	Myosin-9	1	75/119	3	12	22/240	7	8	34/130	7
Actb	beta-actin	17	59/119	52	36	2/240	70	49	112/130	78
Eef2	Eukaryotic elongation factor 2	10	11/119	20	22	5/240	25	7	40/130	11
Tuba3a	Tubulin alpha chain	6	21/119	23	9	123/240	25	14	113/130	45
Hnrnpab	Heterogeneous nuclear ribonucleoprotein A/B	3	40/119	16	3	63/240	10	1	80/130	3
Pdia6	Protein disulfide-isomerase A6	2	46/119	10	2	77/240	6	1	69/130	3
Gpi	Glucose-6-phosphate isomerase	1	115/119	5	5	59/240	11	1	63/130	5

[a] All proteins listed were identified with ≥95% confidence except for Glucose-6-phosphate isomerase in cultured T11 cells and beta-actin and tubulin alpha chain in the metastatic lung, which were identified with ≥90% confidence.

[b] Of the 19 T11-specific proteins, 10 were redundant variants or isoforms of heterogenous nuclear ribonuclear protein A/B, protein disulfide isomerase A6, and tubulin alpha chain, which resulted in nine unique proteins not identified in control tissues.

[c] Rank of the specified protein relative to other proteins detected in the ProteinPilot Report.

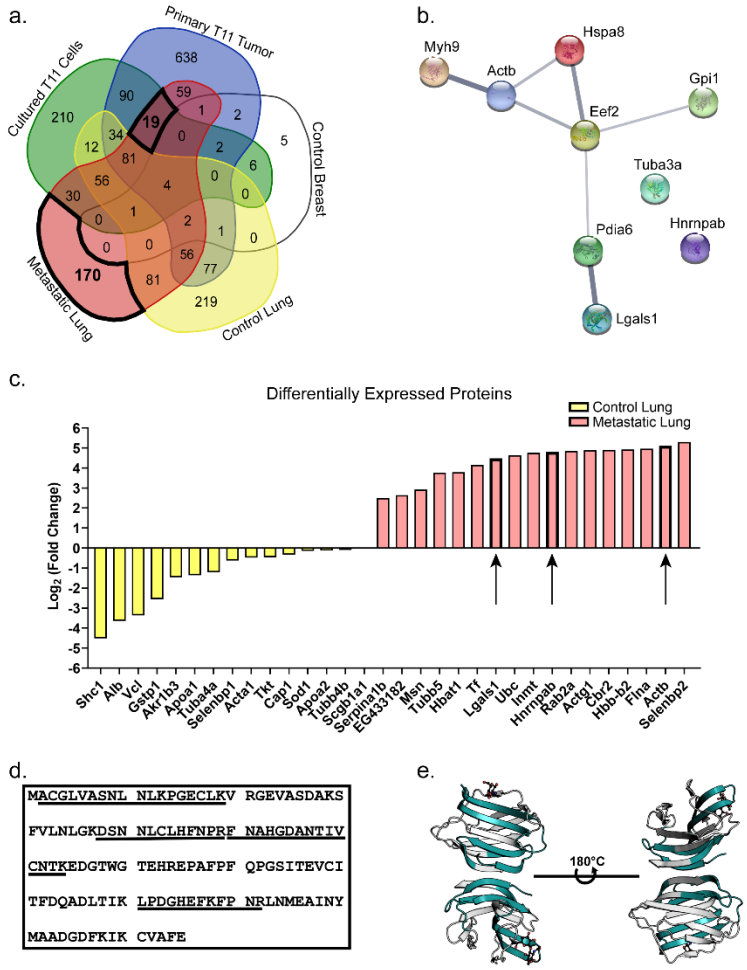

Figure 17 Proteins identified in claudin-low T11 cells, primary tumors, metastatic lung, and control tissues
(a) Venn diagram of proteins (ungrouped) identified by nano-LC-MS/MS with >95% confidence. Bold outlines indicate unique and overlapping protein groups of particular interest: the proteins found in all T11 samples but not in control tissues and the proteins found only in T11 lung metastases (b) After accounting for variant and isoform redundancies, there were nine proteins with common to T11 cells and tumors but not identified in control tissues, as detailed in Table 11. Gene identifications were uploaded into the STRING Database to determine potential relationships. The gray lines indicate a strong potential relationship between two proteins. Galectin-1 (Lgals1) shares a reported direct relationship (dark thick line) with protein disulfide-isomerase A6 (Pdia6). (c) Intensity-based label-free quantitation was used to determine differential protein expression between metastatic and control lungs ($p<0.05$), as described in Methods. The black arrows designate the highly expressed and differentially expressed proteins of interest shared by primary T11 tumors, metastases, and cultures (also shown in Table 11 and Figure 17b). (d) Nano-LC-MS/MS-identified consistent Galectin-1 tryptic peptides (underlined sequences) from digests of primary and metastatic T11 tumors were mapped within the Gal-1 primary structure (e) Consistent Galectin-1 tryptic peptides (highlighted in teal) were mapped to the Gal-1 quaternary structure (Gal-1 homodimer). The 3D image was reconstructed using the human Gal-1 sequence using Pymol (The PyMOL Molecular Graphics System, Version 2.0, Schrödinger, LLC), and the N-acetyllactosamine disaccharide is included to map its binding sites. The Gal-1 protein is highly conserved between mice and humans with ~98% conserved and ~89% identical sequences.

We next used intensity-based label-free quantitation methodology (LFQ) to quantitate differential protein expression and enable assessment of the statistical significance of protein fold

changes between normal and metastatic lung tissues.[365] **Figure 17c** displays the log2 fold change of proteins significantly ($p \leq 0.05$) different between control and metastatic lungs. None of the proteins we had found to be solely associated with metastatic tumors were significantly differentially expressed by LFQ. However, three of the nine proteins identified as highly and differentially expressed in all three categories of T11 claudin-low tumors (compared to normal tissue) were found to be significantly increased by LFQ (see arrows, **Figure 17c**). Both ß-actin and heterogeneous nuclear ribonucleoprotein A/B have been extensively studied; they serve housekeeping functions, are ubiquitously expressed in normal tissue, and upregulated in proliferating cells, including cancers. Notably, LFQ also documented a significant (4.5 log2) fold increase in the differential expression of galectin-1 in lung metastases. For the remainder of this study, we focused on validating the identification, expression, and tissue distribution of galectin-1 (Gal-1), an N-acetyllactosamine-binding protein. Gal-1 is a multifunctional protein overexpressed in other cancers and has been implicated in pathways associated with cancer progression. However, to our knowledge, Gal-1 overexpression has not been investigated in claudin-low breast cancer, which is in dire need of targeted therapies.

4.3 Galectin-1 peptides identified in murine claudin-low TNBC

Galectin-1 exhibited the highest sequence coverage and high abundance rank order among nano-LC-MS/MS-identified proteins shared by T11 claudin-low tumors but not normal tissue (Protein Pilot FDR report at >95% confidence, **Table 11**). Gal-1 was below detection limits (17.2 pmol, as described in Methods) in both control mammary and control lung tissue from naïve age-matched healthy mice. This detection limit was determined by diluting rGal-1 in water, as described in Methods, rather than a matrix representing the peptide complexity in cell and tissue lysates. Gal-1 placed in the top 9% of identified proteins in T11 primary tumors (by abundance

rank order), with 26 distinct peptides covering 72% of the protein. Likewise, Gal-1 was ranked within the top 11% of identified proteins in T11 tumor cultures and the top 28% of identified proteins in metastatic lung tissues. Protein coverage for T11 cultures was 88% and 47% for metastatic lungs, with 15 and 8 distinct Gal-1 peptides identified, respectively. No other members of the galectin family were identified within tissue homogenates.

Nano-LC-MS/MS consistently identified four Gal-1 tryptic peptides in T11 cell cultures, T11 tumors, and metastatic lung tissue (underlined within the 135-amino acid Gal-1 sequence in **Figure 17d**). The reconstructed 3D image of a Gal-1 homodimer showing the location of the tryptic peptides consistently identified by nano-LC-MS/MS (highlighted in teal) is presented in **Figure 17e**. Despite the presence of two lysine residues within the C-terminal beta-strand (gray arrowhead), they are not consistently cleaved; this strand is at the interface of dimer formation, and thus trypsin access may be blocked by steric hindrance. The *N*-acetyllactosamine disaccharide is included in the image to map its binding sites; the location on the protein periphery demonstrates the potential of the Gal-1 homodimer to crosslink glycoproteins and form multivalent complexes.

4.4 Validation of differentially expressed galectin-1

Western immunoblot analysis for Gal-1 was conducted on cell and tissue lysates to verify the identity and differential expression of Gal-1. After protein fractionation by SDS-PAGE and membrane transfer, specific antibodies detected Gal-1 expression at varying levels in all samples (**Figure 18a**). The immunoblots revealed a ~14 kDa protein that co-migrated with the rGal-1 standard and is consistent with the mass of monomeric Gal-1. As expected from nano-LC-MS/MS peak intensities, Gal-1 expression was highest in cultured T11 cells and primary tumors. It is important to note that the metastatic lung lysate analyzed in the example shown was from a lung containing only three metastatic lesions (each ≤3 mm in diameter). Western blot image intensities

were quantitated and compared after normalization for the total protein analyzed in each sample (using a reversible total protein stain as described). On quantitative image analysis, compared to control lung tissue, Gal-1 expression was significantly higher in the metastatic lung ($p \leq 0.01$; **Figure 18b**). ELISA was also conducted on tumor, metastatic lung, and control tissues to quantitate Gal-1 expression (**Figure 18c**). After normalization for tissue or protein mass, both tumor and metastatic lung had significantly higher Gal-1 levels compared to mammary fat pad ($p \leq 0.004$) or normal lung ($p \leq 0.005$). ELISA results are consistent with the nano-LC-MS/MS and Western immunoblot data and further support the identification of Gal-1 as an overexpressed protein in claudin-low tumors.

The Gal-1 concentration in metastatic lung tissues was also correlated with the total volume of the visible metastatic lesions in each lung sample (**Figure 19a**). After sacrifice, tumor volumes were measured by caliper and calculated for the volume of an ellipse. Caliper could not measure one lung sample because of the high tumor burden (i.e., massive mets). This sample was included in the initial Pearson's correlation coefficient test to evaluate the concentration of Gal-1 and the volume of the tumor burden. Results showed a significant positive correlation between these two variables ($r = 0.95$, $p=0.013$). Pearson's analysis was also run without the massive met sample, which showed a positive correlation between the Gal-1 concentration and measurable tumor volume ($r=0.97$, $p=0.034$).

To evaluate circulating levels of Gal-1, whole blood was collected from tumor-burden mice (n=8) and contemporary age-matched controls (n=9) by submandibular bleeding before euthanasia. The serums were thawed on ice, observed for hemolysis, and diluted 1:20 in reagent diluent before Gal-1 ELISA quantification. Analysis by student's T-test showed that serum

galectin-1 was significantly reduced in mice with macrometastases compared to serum galectin-1 concentrations from non-tumor-bearing mice (p=0.05). (**Figure 19b**)

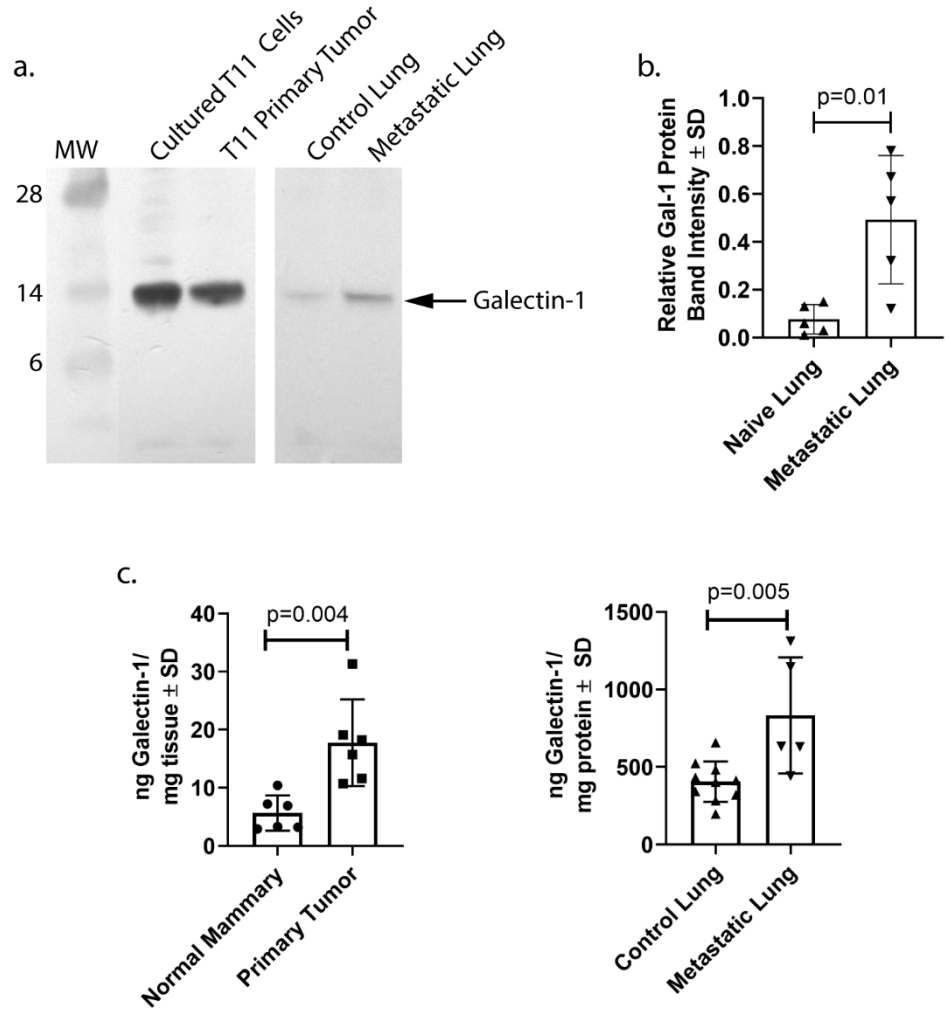

Figure 18 Confirmation and Quantification of Gal-1 by Western Immunoblot and ELISA
(a) Representative Western immunoblot. Protein lysates of T11 tumor samples and control tissues were fractionated by SDS PAGE on the same gel, transferred to nitrocellulose membranes, and incubated with an anti-Gal-1 antibody. To improve detection sensitivity, the section of the membrane with control and metastatic lung tissue was incubated with a 10-fold greater concentration of secondary antibody (right panel) than used for the blot with lysates from T11 tumor cultures and primary T11 tumor (left panel). (b) Quantitative image analysis of five Gal-1 immunoblots in control and metastatic lung tissue after normalization for total protein loading using a reversible total protein stain as described in the Methods. (c) Galectin-1 ELISA results from tissue lysates (Left) after normalization of primary tumors and control mammary fat pad to tissue weight; (Right) after normalization of metastatic and control lungs to total protein. A student's t-test was used to determine statistical significance between samples; error bars represent standard deviation.

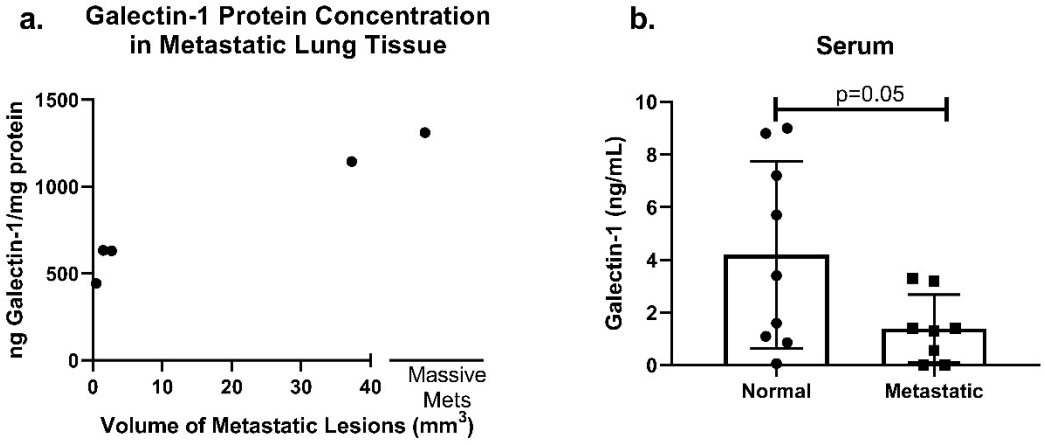

Figure 19 Galectin-1 expression is dependent on the level of tumor burden, but galectin-1 serum levels are significantly reduced in metastatic mice compared to controls.
(a) Galectin-1 ELISA results from lung tissue lysates containing visible metastatic lesions after normalization to total protein. Data were correlated to the caliper-measured volume of the metastatic lesions. Pearson's correlation coefficient test was used to analyze the Gal-1 concentration against the tumor burden with (n=5) and without (n=4) the sample that contained massive mets. The caliper measured metastatic lesions ranged from 0.5-37.3 mm^3. Both analyses showed a positive correlation between Gal-1 concentration and tumor burden. (r=0.95, p=0.013 and r=0.97, p=0.034, respectively). (b) Whole blood samples were collected from mice at their endpoint via submandibular puncture and processed for serum collection. The serum was diluted 1:20 and quantified by ELISA. Student T-test shows that serum galectin-1 is significantly reduced in mice with macrometastases compared to serum galectin-1 concentrations in normal mice (p=0.05).

4.5 Spatial mapping of galectin-1 expression within claudin-low metastatic tumors

To further understand the tissue distribution of Gal-1 expression at metastatic sites, we used MALDI/IMS facilitated spatial peptide mapping (**Figure 15b**). Representative average mass spectra for Gal-1 tryptic peptides are highlighted in **Figure 20a** for rGal-1 standard, primary T11 tumor, and lung tissue with and without metastases. The identified Gal-1 peptides and m/z ratio are listed in the table next to the spectra. A Mascot database search for the identified masses of the Gal-1 peptides in all rGal-1 standard concentrations and all samples analyzed returned Gal-1 as the top protein with scores greater than >106, indicating high confidence in identifying Gal-1. The identified Gal-1 peptides were uploaded to FlexImaging™ to map their expression in a normal control lung sample and a lung with a macrometastatic lesion (**Figure 20b**). Although Gal-1 was detected in all tissue sections by this method, focal areas of metastases within the lung

demonstrated increased intensity in 8 Gal-1 peptides compared to adjacent normal tissue and the control lung. In these samples, the most intense peptide signals were found at the edges of the metastatic foci compared to adjacent normal lung tissue.

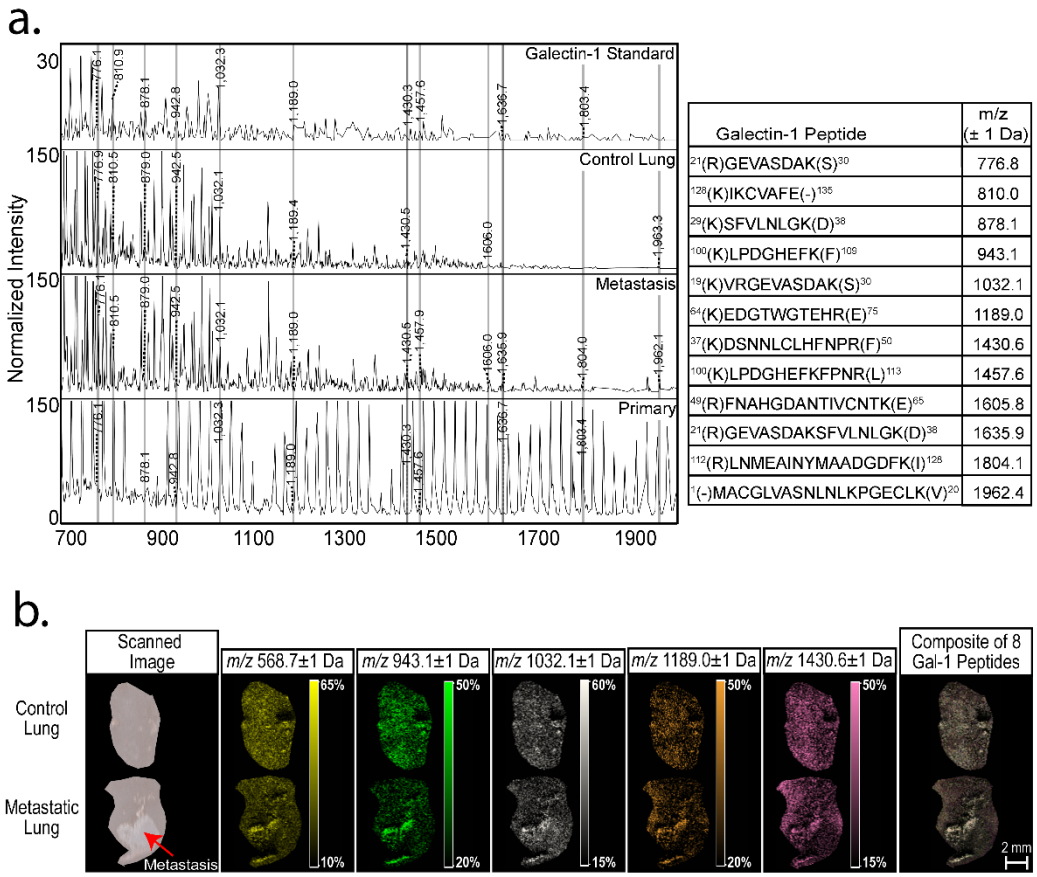

Galectin-1 Peptide	m/z (± 1 Da)
[21](R)GEVASDAK(S)[30]	776.8
[128](K)IKCVAFE(-)[135]	810.0
[29](K)SFVLNLGK(D)[38]	878.1
[100](K)LPDGHEFK(F)[109]	943.1
[19](K)VRGEVASDAK(S)[30]	1032.1
[64](K)EDGTWGTEHR(E)[75]	1189.0
[37](K)DSNNLCLHFNPR(F)[50]	1430.6
[100](K)LPDGHEFKFPNR(L)[113]	1457.6
[49](R)FNAHGDANTIVCNTK(E)[65]	1605.8
[21](R)GEVASDAKSFVLNLGK(D)[38]	1635.9
[112](R)LNMEAINYMAADGDFK(I)[128]	1804.1
[1](-)MACGLVASNLNLKPGECLK(V)[20]	1962.4

Figure 20 MALDI/IMS mass spectra of Gal-1 tryptic peptides

(a) Representative average mass spectra of Gal-1 peptides from the rGal-1 analytical standard and tissue samples. Vertical lines demarcate the m/z values corresponding to the Gal-1 peptides in the adjacent table. Relative abundance was greatest in primary tumors, as shown by normalized intensity (b) Spatial distribution of MALDI/IMS-detected Gal-1 peptides across control and metastatic lung tissue. The extracted chemical ion tissue images of 5 different Gal-1 tryptic peptides (5 different masses) and a final composite image of 8 Gal-1 peptides. The location of metastasis within the lung tissue section is noted on the scanned image (lower panel, red arrow). Images were generated in FlexImaging™ and are representative of two independent experiments.

Serial sections of murine tissue were stained using immunohistochemistry (IHC) to verify the spatial distribution of Gal-1. Primary T11 tumors and metastatic lung lesions exhibited intense staining for Gal-1 (**Figure 21**, right panels), further supporting nano-LC-MS/MS, Western blot, and MALDI/IMS findings. Gal-1 was detected in the cell nucleus, cytoplasm, membrane, and interstitial spaces, consistent with other reports.[289, 292] To investigate Gal-1 expression at the protein level in molecularly classified human tumors, we also performed immunohistochemistry on human breast tumors and control mammary tissue. **Figure 22** shows representative tumor sections: the most intense staining was observed in claudin-low tumors. The surgically resected claudin-low breast tumors (n=4) displayed intermediate to high Gal-1 staining in both stroma and tumor cells. Gal-1 staining of other breast cancer subtypes ranged from low to high, with most tumors showing intensity within both the tumor and stroma. These data indicate that both murine and human claudin-low tumors have increased expression of the Gal-1 protein.

4.6 Galectin-1 gene expression in claudin-low tumors compared to other breast cancer subtypes

Genomic analysis compared Gal-1 RNA expression in claudin-low tumors to other breast cancer subtypes. We first analyzed published mouse and human microarray data to compare LGALS1 (Gal-1) gene expression at the mRNA level in claudin-low tumors to other breast cancer subtypes. Our murine gene expression data source comes from a study that showed that murine tumors segregate into intrinsic subtypes like human tumors.[32] These data include the T11 tumor used in our study as well as two claudin-low murine tumor lines, 2151R and 2247R (**Figure 23a**). To evaluate LGALS1 expression in tumors, we extracted data from the first publication to molecularly characterize human claudin-low tumors compared to other breast cancer subtypes (**Figure 23b**).[18] In both species, the claudin-low subtype had the highest LGALS1 expression levels compared to normal breast or other breast cancer subtypes. Finally, we sought to

corroborate these findings based on data generated by our lab. We analyzed RNA-Seq data from two murine mouse models, 2225L (basal-like) and T11 (claudin-low), and from 143 tumor samples obtained from patients treated at our center (**Figure 23c-d**). In both species and using published microarray and RNA-Seq data, the claudin-low subtype had the highest LGALS1 expression compared to normal breast or other breast cancer subtypes.

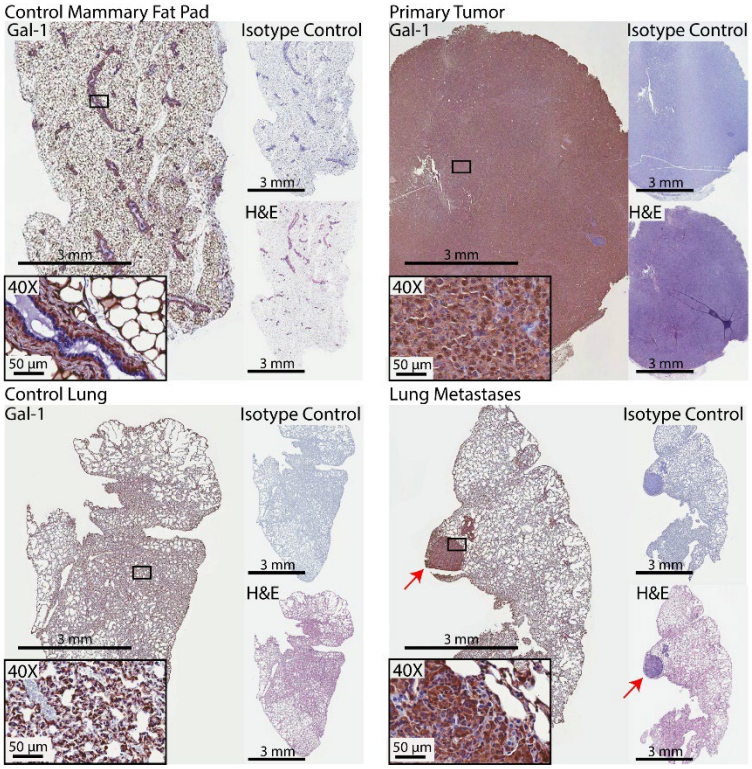

Figure 21 Immunohistochemistry analysis of Gal-1 expression in mouse tissues
Images from serial sections of control mammary fat pad (top left), T11 primary tumor (top right), control lung (bottom left), and metastatic lung (bottom right) stained with anti-Gal-1 IgG, isotype control IgG or H&E. Images are representative from two independent experiments.

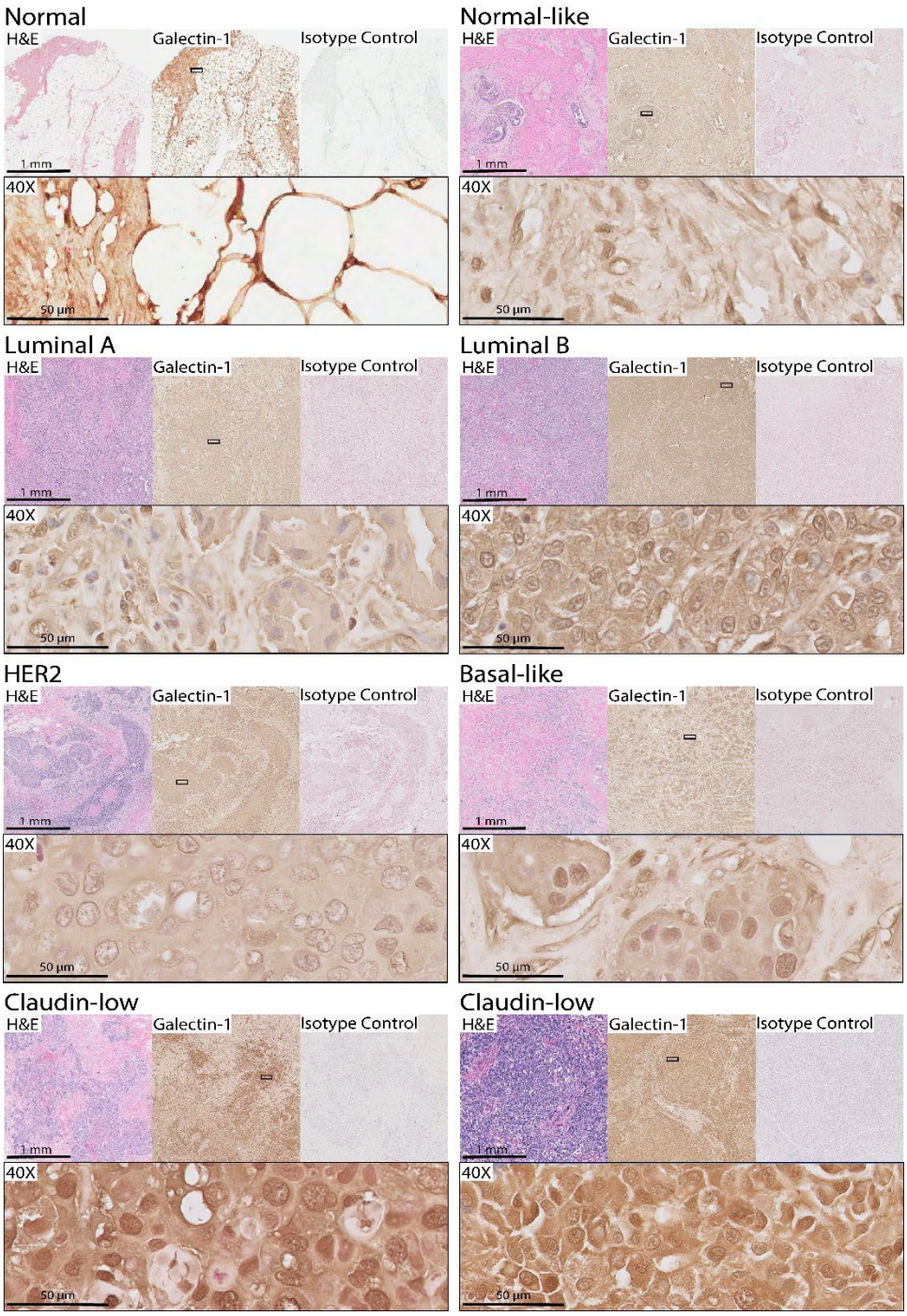

Figure 22 Immunohistochemical analysis of Gal-1 expression in human breast tissue
Representative images of normal breast tissue and breast tumors of different molecular subtypes. Serial sections within each tissue were stained with H&E, anti-Gal-1 IgG, or isotype control IgG. Images are representative of multiple independent experiments and 28 specimens. Samples were blinded and reviewed by a pathologist.

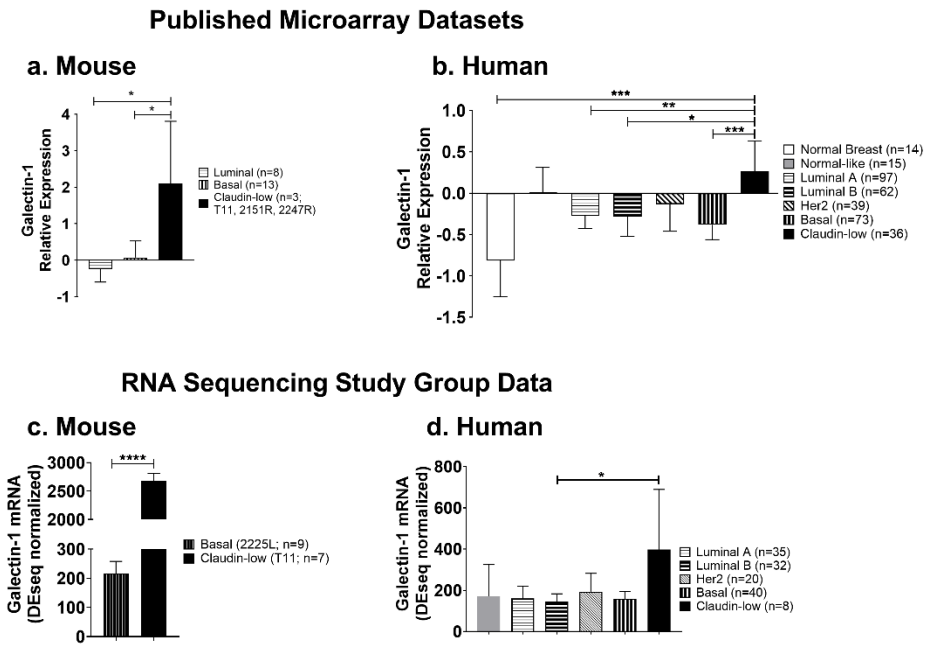

Figure 23 Analysis of tumor microarray data set for differential expression of Gal-1 in breast cancer subtypes (a) Mouse data analyzed from NIH GEO Accession Number GSE2710. The data includes the T11 tumor and two other claudin-low murine tumor lines, 2247R and 2151R. (b) Human data was analyzed from NIH GEO Accession Number GSE18229. For both data sets, the mean expression of the gene) is plotted for each subtype, together with the upper or lower 95% confidence interval (whiskers above or below the bars, respectively). Statistical analysis was performed by comparing all subtypes to claudin-low using the Kruskal-Wallis test with Dunn's post-hoc analysis (*p $\leq$ 0.05, **p $\leq$ 0.01, ***p $\leq$ 0.001). (c) Mouse basal-like (2225L) and claudin-low (T11) tumors were analyzed by RNA sequencing. Data were normalized by the DEseq method, and LGALS1 levels were plotted in a bar graph. A student t-test was performed to compare expression between the two subtypes, ***p $\leq$ 0.0001. (d) DEseq normalized human RNA-Seq data was mined for LGALS1 expression. Data were plotted in a bar graph, and statistical analysis was performed by comparing all subtypes to claudin-low using the Kruskal-Wallis test with Dunn's post-hoc analysis (*p $\leq$ 0.05, **p $\leq$ 0.01, ***p $\leq$ 0.001).

4.7 Summary and Discussion

Nano-LC/MS/MS identified Gal-1 as an overexpressed protein in murine T11 CLBC. MALDI/IMS, overlaying Gal-1 peptides in metastatic T11 lung samples, showed significant differential Gal-1 expression in the metastatic lesions than in normal adjacent tissue. Gal-1 overexpression in primary and metastatic tumors was validated by Western immunoblot, ELISA, IHC, and gene expression analysis in T11. These findings were extended to translational studies investigating Gal-1 expression in human tissue samples by IHC and transcriptome analysis. This was the first publication to use these proteomic approaches to identify and subsequently validate Gal-1 overexpression in claudin-low tumors.

Proteomic research approaches, such as nano-LC-MS/MS and MALDI/IMS, have enabled the identification of promising diagnostic and prognostic biomarkers in various diseases, including cancer.[366, 367] Nano-LC-MS/MS utilizes low-flow chromatography separation combined with nano-electrospray ionization to improve detection limits and provide accurate peptide masses to enhance protein identification.[368-370] MALDI/IMS integrates spatial distribution maps of mass spectra with histopathological methods, which can be used to identify the distribution of proteins and peptides within tissues,[371] and is particularly useful to capture heterogeneity both within primary tumors and within distant tissues with varying metastatic burdens. Several studies have employed electrospray ionization and MALDI techniques to measure treatment responses and to identify potential biomarkers in primary tumors and sera from TNBC patients.[372-374] Balestrieri *et al.* 2021 was the first use of MALDI/IMS to determine the spatial distribution of tumor- and metastasis-associated proteins in claudin-low breast cancer.[321] Since this original publication, these results have been referenced in two review articles on MALDI/IMS.[375, 376]

When compared to normal tissue from healthy control mice, Gal-1, an N-acetyllactosamine binding protein, was documented by mass spectrometry as overexpressed in claudin-low primary tumors and lung metastases, with the highest protein coverage of all identified T11 metastasis-associated proteins and a high abundance rank order. Label-free quantitation, Western immunoblot, and ELISA confirmed galectin-1 identity and significant differential expression in claudin-low orthotopic, and metastatic tumors compared to normal tissue. Immunohistochemistry and gene expression analysis confirmed that, compared to other breast cancer subtypes and normal breast tissue, Gal-1 is highly expressed in both murine and human claudin-low breast tumors. In addition to Gal-1, galectin-3 was identified in cultured T11 cells (although with a lower protein

coverage of 11.9%), but galectin-3 was not detected in any of the tumor tissue lysates by either nano-LC-MS/MS or MALDI/IMS. No other members of the Galectin family were identified.

Gal-1 was first identified by Teichberg et al. in 1975 when it was isolated from an electric eel and has been the most studied galectin since its discovery.[377] In 1988, dimeric Gal-1 was shown to bind to N-acetyllactosamine residues preferentially,[378] then in 1993, was found to bind with a higher affinity to poly-N-acetyllactosamine sequences.[379] Since these original findings, additional studies have sought to understand further how Gal-1 protein interacts with different LacNAc constructs on glycoproteins and glycolipids.[170, 203, 207, 380-382] It is well-known that Gal-1 has both monomeric and dimeric conformations that are dependent on concentration and oxidation state. Both forms can bind to LacNAc; however, the avidity increases when Gal-1 is dimerized and poly-LacNAc residues are in a branched conformation.[207, 210] Interactions with cell surface glycoconjugates can result in the formation of multivalent complexes or lattices which can control a variety of biological processes and cell functions, in both normal and pathological conditions, including cancer.[383] [205]

Gal-1 is overexpressed in many cancers and has been implicated in pathways associated with cancer progression. As early as 1981, it was speculated that a galactoside-specific lectin on the surface of tumor cells could regulate metastasis through the interaction of tumor cells with endothelial or immune system cells.[384] In recent years, tumor-secreted Gal-1 has been shown to be involved in tumor cell immune escape, indicating that Gal-1 is a critical molecular target in cancer and could be a potential therapeutic target for cancer treatment. Evidence from several *in vitro* studies and *in vivo* mouse models have indicated that Gal-1 promotes tumor proliferation, invasion, metastasis, angiogenesis, and immune evasion in various cancers, including breast cancer. [205, 274] Gal-1 is known to be a highly expressed protein in murine [180-182, 291, 294, 385, 386] and

human [289, 292, 387] TNBC; however, these studies did not molecularly subtype tumors or classify tumors as claudin-low and Gal-1 expression in claudin-low tumors may be a dominant contributor to these observations.[180] Three studies have examined the effect of Gal-1 inhibition on metastasis in the 4T1 basal-like murine model and have shown that knockdown of Gal-1 in tumor cells reduced the number of metastatic lesions in the lung and increased the percentage of tumoricidal T cell populations at metastatic sites, [180, 182, 386] supporting the premise that Gal-1 is an important mediator of metastasis in TNBC.

Published studies of Gal-1 function in claudin-low breast cancers are limited to several *in vitro* studies of tumor cell migration, invasion, and drug resistance using the human cancer cell line MDA-MB-231.[295, 298] The nano-LC-MS/MS findings reported herein were consistent with two other studies that used mass spectrometry-based discovery approaches and reported overexpression of Gal-1 in the human claudin-low cell line, MDA-MB-231, and in a highly metastatic MDA-MB-231 variant.[387, 388] In contrast to our study, these investigations used cell cultures, not primary or metastatic tumors, and additional methods did not confirm Gal-1 identity and overexpression. Using a direct proteomic approach without pre-fractionation of tryptic peptides, we consistently identified Gal-1 protein with high confidence in cultured tumor cells, primary tumors, and metastatic lungs. An alternative and more common approach for nano-LC-MS/MS analysis of complex samples employs fractionation of the peptide mixture before mass spectrometry analysis, which would allow for more in-depth analysis and is thus better suited for identifying less abundant proteins.

IHC analysis verified Gal-1 overexpression at the protein level in mouse and human claudin-low tumors compared to other breast cancer subtypes and control tissues. Expression was found throughout the tumor and stroma and was high in both the nucleus and cytoplasm. The biological

activity of Gal-1 differs depending on its intracellular, membrane-bound, and extracellular locations, as well as its subcellular localization. It has been proposed that Gal-1 may bind to LacNAc-decorated proteins on cell surfaces to regulate adherence to the extracellular matrix, whereas cytoplasmic Gal-1 may bind to Hras, causing cell transformation. One limitation of IHC studies with human breast tumors is that they are hampered by the limited availability of molecularly subtyped tumors with tissue blocks. They are further restricted when focusing on the claudin-low cancer subset. In the human tumor samples reported herein, Gal-1 expression was evident and varied across all subtypes, but the most intense staining was observed in claudin-low tumors. Future studies using larger sample sizes and H-scores could be used to quantify staining in subcellular compartments. They would provide further perspective into the activity of Gal-1 in claudin-low tumors.

In addition to evaluating Gal-1 at the protein level, *in silico* analysis of primary tumor microarray data sets were used to confirm Gal-1 overexpression at the mRNA level in the claudin-low subtype compared to other breast cancer subtypes and to normal mammary tissue in both mice and humans. For this analysis, individual studies of published microarray data were used. Our lab conducted RNA sequencing analysis on mouse and human tumors using Illumina platforms to confirm findings from *in silico* analysis. Consistent with published microarray data, RNA results from our lab showed similar trends in Gal-1 RNA levels among breast cancer subtypes. The number of breast cancer samples available to our lab was limited. More extensive data sets from multiple sources would increase the power of this analysis and would likely further delineate differences in Gal-1 expression between breast cancer molecular subtypes.

Specific mechanisms for how overexpression of Gal-1 may contribute to breast cancer progression are lacking, and no studies have been conducted specifically on the mechanisms of

Gal-1 in CLBC. In one report, the intensity of Gal-1 expression by immunohistochemical staining of breast cancer specimens correlated with tumor invasiveness and progression. [125, 288] These investigators did not correlate Gal-1 staining with hormone receptor status; there were few TNBC patients in this study. In more recent studies, TNBC samples exhibited diverse immunohistochemical staining patterns, highlighting the heterogeneity of Gal-1 expression within this subtype. [180, 289, 292] In a recent *in silico*, retrospective analysis of Gal-1 mRNA expression, high expression of LGALS1 was a significant prognostic factor for poor survival in TNBC.[289] Since the publication by Balestrieri et al. in 2021 showing that Gal-1 has a significantly higher elevation in CLBC, one lab collaborated the findings of elevated LGALS1 using next-generation sequencing in cancer stem cell populations isolated from MDA-MB-231 claudin-low xenografts.[389]

Murine studies using the 4T1 basal-like murine model have shown that knockdown of Gal-1 in tumor cells reduced the number of metastatic lesions in the lung and increased the percentage of tumoricidal T cell populations at metastatic sites,[180, 182, 386] One study showed decreased frequency and low immunosuppressive function in Treg cells in Gal-1 knockdown tumor cells compared to wild-type tumor cells.[180] Other murine TNBC studies have suggested that Gal-1 promotes tumor growth through its effect on effector T cell apoptosis.[182, 192] In breast cancer patients, tolerogenic DC populations were demonstrated to be higher in patient serum samples compared to healthy donors, and conditioned medium containing recombinant Gal-1 or Gal-1 secreted from cultured MDA-MB-231 claudin-low cell line induced tolerogenic DC differentiation. Furthermore, the murine 4T1 breast cancer cell line enhanced IL-10 expression in DC compared to the 4T1 Gal-1 knockdown cell line.[294] These studies suggest that Gal-1 may contribute to the progression of CLBC by regulating the immune response.

CHAPTER 5: *IN VITRO* AND *IN VIVO* INVESTIGATIONS OF GALECTIN -1 EFFECTS ON CD11b$^+$ MYELOID CELLS AND CLAUDIN LOW BREAST CANCER

5.1 Rationale

Chapter 3 described developing a reliable, metastatic model for claudin-low breast cancer using the T11 tumor line. We showed that T11 tumors have a high infiltration of CD11b$^+$ cells and a protumor cytokine profile. We know in breast cancer that macrophages aid in immune escape and can assist tumor cells to intravasate into circulation and extravasate at metastatic sites.[105, 390, 391] Additionally, in Chapter 4, we have shown that T11 claudin-low tumors have significantly higher differential Gal-1 expression compared to normal tissue and other breast cancer subtypes. Based on our findings and reports in the literature, in this chapter we report our studies to investigate Gal-1 effects on myeloid cells.

Research has shown that Gal-1 has an impact on macrophages in relation to several diseases. Gal-1 seems to encourage an anti-inflammatory state in monocytes and macrophages. When introduced exogenously, Gal-1 reduces the production of pro-inflammatory cytokines in murine macrophages and prompts a shift towards an M2-like profile by blocking IFNγ-induced MHCII expression and MHCII-dependent antigen presentation.[252, 253] Macrophages treated with Gal-1 also induce 12/15-lipoxygenase expression, which is an enzyme involved in the metabolism of polyunsaturated fatty acids during the resolution of inflammation.[254] Gal-1 promotes the differentiation of macrophages into an M2-like phenotype by controlling L-arginine metabolism, either by reducing NO levels or favoring the arginase pathway.[258] However, in an alternate *in vitro* study, Gal-1 inhibited monocyte migration and induced apoptosis, but did not impact macrophages.[260] These findings indicate that Gal-1 may influence macrophages to have an M2-like phenotype, potentially promoting tumor growth and progression.

To assess whether galectin-1 had an effect on $CD11b^+$ myeloid cells, we used the *in vitro* macrophage cell line RAW 264.7. This model is widely used for evaluating macrophage biology and immune responses. Cultured RAW 264.7 cells were treated with recombinant Gal-1 (rGal-1) in the presence or absence of a competing disaccharide or a monosaccharide that lacks Gal-1 specificity, after which agglutination and apoptosis were assayed. Since RAW 264.7 cells are isolated from a tumor, are transformed, and cultured, they may not accurately represent the biological activity and phenotype of *in vivo* macrophages. Therefore, we assayed for apoptosis in an alternative macrophage model using peritoneal macrophages. We obtained these macrophages by injecting thioglycolate into the peritoneum of normal Balb/c mice to induce a localized inflammatory response in the peritoneal cavity. We then collected peritoneal exudate cells and tested them *ex vivo* in the presence and absence of exogenous rGal-1 for Annexin V and PI by flow cytometry. The results from these experiments are discussed in this chapter.

Next, to assess if targeting Gal-1 would have an impact on CLBC growth, we used a Gal-1 allosteric inhibitor, OTX008, to block Gal-1 binding to its ligands *in vivo*. Both control and treated primary tumors were assayed to determine the effect of Gal-1 inhibition on tumor growth, tumor cell apoptosis, infiltration of $CD3^+$ and $CD11b^+$ cells, and the level of apoptosis in these immune cells.

Three studies conducted by other labs have examined the effect of Gal-1 inhibition on metastasis in the 4T1 basal-like murine model and have shown that knockdown of Gal-1 in tumor cells reduced the number of metastatic lesions in the lung and increased the percentage of tumoricidal T cell populations at metastatic sites.[180, 182, 386] One study showed decreased frequency and low immunosuppressive function in Treg cells in Gal-1 knockdown tumor cells compared to wild-type tumor cells.[180] Other murine TNBC studies have suggested that Gal-1 promotes tumor

growth through its effect on effector T cell apoptosis.[182, 192] Since a couple of reports in breast and other cancer types have showed Gal-1 can reduce the number of T cells in primary tumors and induce T cell apoptosis, we also evaluated the effect of Gal-1 inhibition on the infiltration and apoptosis of $CD3^+$ cells in addition to $CD11b^+$ myeloid cells. Although research from others has shown Gal-1 has pro-tumor effects on cancer cells in other types of cancers, including the inhibition of immune cells and the induction of apoptosis in activated T cells, its protumor effects have yet to be explored in CLBC.

Here we investigate the effects of a Gal-1 allosteric inhibitor, OTX008, in an *in vivo* setting for insights into the role of Gal-1 in CLBC. Based on our findings and those of others, studies were designed to determine if systemic treatment with a Gal-1 inhibitor would 1) inhibit CLBC tumor development and growth and 2) induce apoptosis in $CD8^+$ T cells (the predominant $CD3^+$ cell type) or macrophages (the predominant $CD11b^+$ cell type) in the T11 mouse model of CLBC.

OTX008 is a peptide topomimetics of the β-peptide mimic, Anginex, which has been shown to inhibit angiogenesis by diminishing affinity of galectins toward their carbohydrate ligands. While Anginex cross-reacts with other known galectins, OTX008 is specific for Gal-1 and has been shown to have a binding affinity of 50 μm. OTX008 prevents Gal-1 glycoprotein interactions by acting as an allosteric inhibitor by binding the beta-sheet on the opposite side of the carbohydrate-recognition domain.[317, 318] The half-life of OTX008 is approximately 31.4 hours. When intravenously administered to tumor-bearing nude mice, the maximum systemic concentration was 1.76 μM at 0.5 hours after administration. Intratumor concentrations were calculated as 2.3 μM after repeated intravenous administration of 5mg/kg every other day for 21 days.[319] As a monotherapy, OTX008 was found to be a potent inhibitor of angiogenesis in ovarian and melanoma mouse models.[314] In combination with chemotherapeutics *in vitro* and *in vivo*,

OTX008 has shown synergistic effects slowing tumor growth and reducing angiogenesis.[318, 319] OTX008 has been registered with the FDA in a Phase I clinical trial for human solid tumors (NCT01724320).[320]

Other researchers have conducted *in vivo* mouse studies using OTX008 to explore the effects of Gal-1 inhibition on tumor biology. However, various methods of administration have been employed. For instance, in one study, ovarian tumors (MA148 cells) were allowed to grow to 100 mm^3 before OTX008 was administered subcutaneously via an implanted osmotic minipump at 10 mg/kg daily.[318] In *in vivo* experiments involving human ovarian cancer (A2780-1A9 cells) and glioblastoma (U87-MG cells) injected subcutaneously, athymic mice received intraperitoneal or intravenous doses of 5 mg/kg OTX008 every other day to three times per week starting when tumors became palpable.[319, 392] Meanwhile, in a xenograft mouse model of human head and neck cancer (SQ20B), mice were injected intraperitoneally with 10 mg/kg OTX008 daily when tumors reached approximately 100 mm^3.[393] These studies served as references for the design of the mouse study outlined in this chapter.

Our laboratory has discovered that T11 tumors differentially express Gal-1 which is higher than normal tissue and other breast cancer subtypes in mice. Additionally, we and others have observed that $CD11b^+$ cells heavily infiltrate T11 tumors. As a result, we chose to use this model to investigate the impact of inhibiting Gal-1 on tumor cell growth, the frequency of $CD11b^+$ cell subsets in the tumor, and apoptosis of infiltrating $CD3^+$ and $CD11b^+$ cells. Additionally, we aimed to quantify overall tumor.

5.2 Carbohydrate-dependent apoptosis of recombinant mouse galectin-1-treated RAW 267.7 murine macrophage line

From the studies conducted in Chapter 4 and publications from other labs, we know that many types of cells express Gal-1. Before testing whether exogenous Gal-1 binds to RAW 264.7 cells, we first needed to determine endogenous intracellular and membrane-associated Gal-1 expression levels in RAW 264.7 cells. Cultured RAW 264.7 macrophages and T11 tumor cells (as a positive control) were harvested and assayed on the same day once they reached ≥80% confluence. Viable cells were counted using Trypan blue, then 1-2 x 10^5 cells were labeled with anti-mouse galectin-1-AF647 or an isotype-matched control. For intracellular protein detection, cells were fixed in 1% paraformaldehyde in PBS, followed by Saponin permeabilization before labeling with anti-galectin-1. Data was collected on a BDSRII flow cytometer and analyzed using FSC Express software.

As expected, based on our proteomic and Western blot analysis (**Chapter 4, Figure 18**), most cultured T11 cells (89-92%) displayed high intracellular galectin-1 (mean fluorescent intensity (MFI)=387-617; **Figure 24a, c**). Furthermore, T11 cells expressed membrane-associated Gal-1 (58-78% Gal-1^+ cells, MFI=56-100), indicating that secreted galectin-1 binds to LacNAc residues on the surface of the tumor cells (**Figure 24b, d**). In comparison, the majority (71-76%) of RAW 264.7 cells also had intracellular expression of Gal-1, but the MFI was significantly lower than that of cultured T11 cells (**Figure 24a, e**). Similarly, a minor shift was observed in membrane-associated Gal-1 expression on RAW 264.7 (11-17%) compared to the isotype-matched control antibody, but the MFI was very low (MFI=10-12), indicating that the observed shift may not reflect a positive signal (**Figure 24b, f**).

For these initial experiments, T11 cells were grown in complete media containing 5% FBS which is known to contain Gal-1 protein. To confirm that the observed Gal-1 surface expression was not related to the presence of FBS in the media, T11 cells were cultured in RPMI with low (1%) FBS or mouse EpiCult-B basal media with proliferation supplement (serum-free) for three passages. T11 cells grown using serum-free, 1%, and 5% FBS were assayed by flow cytometry for intracellular and membrane-associated expression of Gal-1. Overall, the average percentage of Gal-1^{+} cells with intracellular and membrane-associated staining in both 1% FBS and serum-free media was comparable to cells grown in the presence of 5% FBS (**Figure 25a-b**). Additionally, cell yield and viability by Trypan blue were assessed for all media conditions to determine if different serum concentrations affected cell growth or viability. Cells grown in serum-free media had slower growth ($1.2e^{6}$±$5.1e^{5}$ cells) at 5-day harvest compared to cells grown in the presence of 1% or 5% FBS ($3.5e^{6}$±$1.1e^{6}$ and $3.7e^{6}$±$1.3e^{6}$ cells, respectively), the cell viability as determined by Trypan blue was ≥80% across all groups.

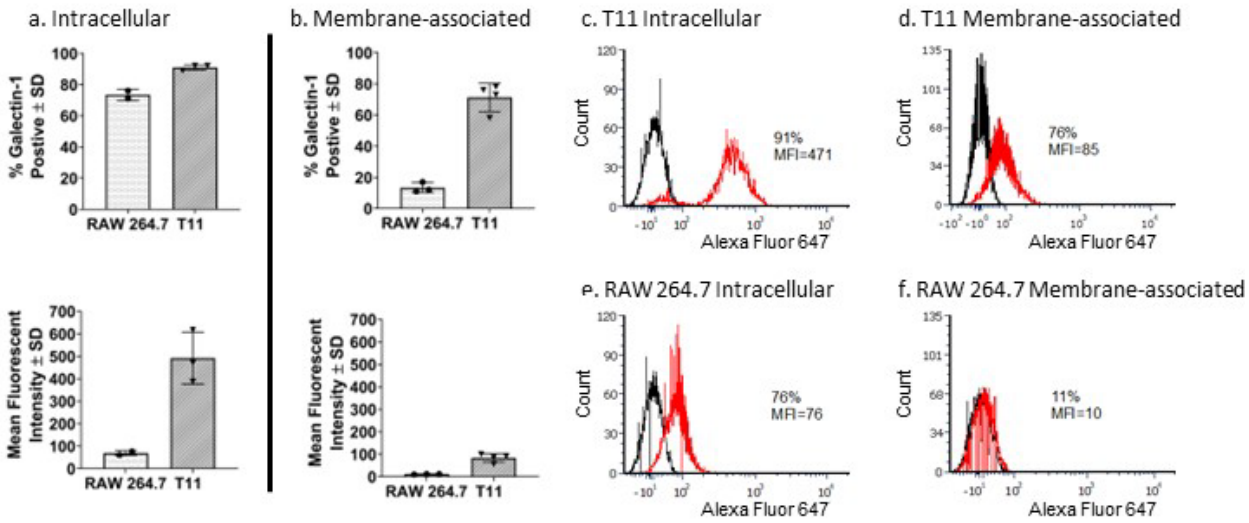

Figure 24 Endogenous expression of Galectin-1 in Cultured T11 and RAW 264.7 cells
Flow cytometry analysis was conducted on cultured RAW 264.7 macrophages and T11 claudin-low tumor cells to determine the intracellular (RAW 264.7 cells n=2; T11 cells n=3) and membrane-associated (RAW 264.7 cells n=3; T11 cells n=4) expression of Gal-1. Cells were harvested at ≥80% confluence on the same day. Cells were counted by Trypan blue, then 1-2 $x10^{5}$ were placed in a culture tube and stained with an anti-mouse galectin-1-Alexa Flour

647. Isotype control was used to determine non-specific-binding and set positive gates. For intracellularly stained cells, cells were fixed in 1% paraformaldehyde in PBS, followed by Saponin permeabilization prior to staining. Bar graphs summarize data from two to four independent experiments conducted to determine endogenous (a) intra- and (b) extra-cellular galectin-1 expression in cultured T11 tumor cells and RAW 264.7 macrophages. Representative histograms of galectin-1 intracellular and membrane-associated staining of (c, d) T11 and (e, f) RAW 264.7 cells. The red line represents positive galectin-1-AF647 staining, and the black line represents the isotype matched control. T11 cells display high expression of galectin-1 intracellularly and on the membrane-associated surface, indicating that galectin-1 is expressed by T11 cells and secreted galectin-1 binds to LacNAc residues on the cell surface. RAW 264.7 macrophages show intracellular expression of galectin-1 but has minimal to no galectin-1 detected on the cell surface.

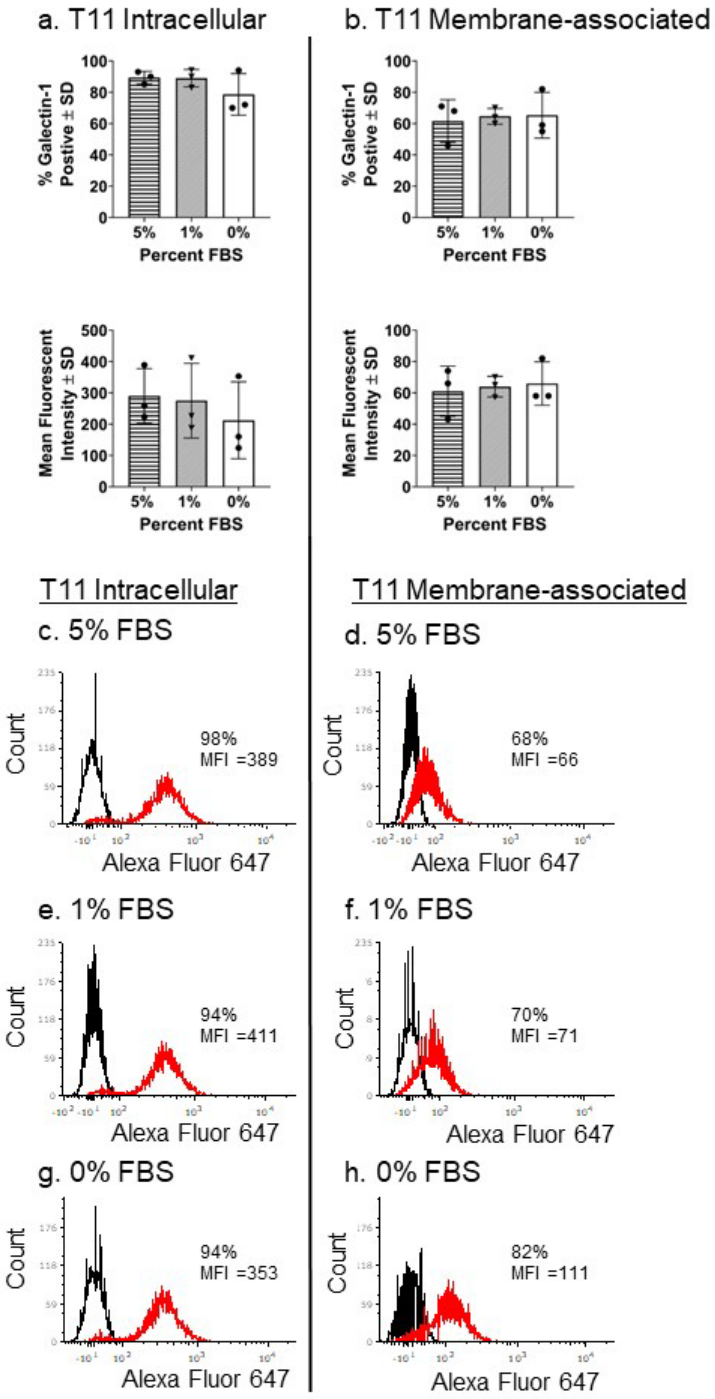

Figure 25 Fetal calf serum supplemented media does not affect the detection of galectin-1 in T11 tumor cell cultures.

For initial experiments to assess the intracellular and membrane-associated expression of Gal-1 in T11 tumor cells, cultured cells were growth in 5% FBS which contains Gal-1. To determine if the Gal-1 expression observed in these samples was from the Gal-1 in the FBS, T11 tumor cells were cultured in reduced serum and serum-free media, then stained with anti-mouse galectin-1-AlexaFlour 647 (AF647) or a matched isotype control and assayed by flow cytometry. (a) Bar graphs representing three independent experiments show (a, c) intracellular and (b, d) membrane-associated endogenous galectin-1 expression is not affected by the presence of fetal calf serum in complete media. (e,

f, g, h) Representative histograms show the shift in AF647 intensity when labeled with anti-mouse galectin-1 (red line) compared to isotype control (black line) in media supplemented with 5%, 1%, and serum-free, respectively.

5.3 Recombinant galectin-1-induced apoptosis of RAW 264.7 macrophages is caspase 3/7-independent

One of the common functions of galectin-1 is its ability to form complexes that crosslink glycosylated ligands to form a dynamic lattice structure. Galectin-1 crosslinking can regulate the selection, activation and arrest of T cells, receptor kinase signaling and the functionality of membrane receptors, including cadherins and integrins.[167] In the initial studies described herein, we used the $CD11b^+$ murine macrophage cell line RAW 264.7 to determine the level of Gal-1 agglutination in $CD11b^+$ RAW 264.7 cells *in vitro*. In the first set of experiments, RAW 264.7 cells were treated with serial dilutions (0-1.0 μM) of recombinant murine Gal-1 (rGal-1) in the presence or absence of lactose or mannose for over a time course of 0-15 minutes and were imaged on a Zeiss Cell Discoverer 7 microscope. For reference, physiological Gal-1 serum concentrations in normal Balb/c female mice were on average 0.28 μM (**Chapter 4, Figure 19**). Gal-1 specifically recognizes and binds to the lactose disaccharide; thus, lactose was expected to inhibit specific binding and subsequent activity of the rGal-1 protein. Gal-1 does not bind the monosaccharide mannose which serves as a negative control sugar. In method development assays, we found that mouse red blood cells (positive control) hemagglutinated at a concentration of 1.0 μM rGal-1 after a 15-minute incubation period. However, no cell agglutination was observed in RAW 264.7 cells treated with the same rGal-1 concentrations and timepoints (data not shown).

In an alternative flow cytometric method for evaluating agglutination, RAW 264.7 cells were treated with serial dilutions (0-1.0 μM) of rGal-1. The rGal-1 dilutions were incubated with 2 mM lactose or mannose for at a minimum of 30-minutes at room temperature prior to adding to

$2x10^5$ RAW 264.7 cells. Cells were incubated with rGal-1 with or without lactose or mannose at room temperature for 15 minutes, then cells were assayed by flow cytometry to determine the percentage of doublet cells. While there was no change in the percentage of doublet cells (data not shown), we observed a significant decrease in cell viability based on forward and side scatter (**Figure 26a-b**). These experiments demonstrated that Gal-1 induced cell death in RAW 264.7 cells in a carbohydrate-dependent manner. Viability was significantly reduced in cells treated with Gal-1 alone or Gal-1 with 1-2 mM mannose, but this effect was blocked when treated with Gal-1 plus 1-2 mM lactose.

Follow-up flow cytometry experiments were conducted using annexin V as a marker for apoptosis and propidium iodide as an indicator for cell membrane leakage. In normal live cells, phosphatidyl serine (PS) is located on the cytoplasmic surface of the cell membrane. However, in apoptotic cells, PS is translocated from the inner to the outer leaflet of the plasma membrane, thus exposing PS to the external cellular environment. The human anticoagulant, annexin V, is a calcium-dependent phospholipid-binding protein that has a high affinity for PS. Red-fluorescent propidium iodide (PI) is a nucleic acid binding dye. PI is impermeant to live cells and early apoptotic cells but stains necrotic, dead cells by binding tightly to nucleic acids. It is expected that early apoptotic cells will not be positive for PI staining (red fluorescence) but will be positive for annexin V-Alexa Fluor 488 (AF488; green fluorescence). Late apoptotic cells will stain positively for PI, when the plasma membrane becomes more permeable; therefore, late apoptotic cells will be double positive for AF488 and PI. Likewise, live cells will be negative for any fluorescence. Flow cytometry experiments using annexin v-AF488 and PI showed that Gal-1 treatment increased the percentage of Annexin V^+PI^+ RAW 264.7 cells in a concentration-dependent manner (**Figure**

26c). This effect could be blocked with lactose, but mannose was not protective against Gal-1-induced apoptosis.

The recombinant mouse Gal-1 protein purchased for these experiments was made using an *Escherichia coli* (*E. coli*) expression system. When considering the apoptotic assays' results on RAW 264.7 cells, this elicits two potential concerns. The first concern is that the rGal-1 may have formed protein aggregates, which could reduce cell viability when added to the RAW 264.7 cells, as this has been reported for other recombinant eukaryotic proteins in bacterial expression systems. To assay for protein aggregation, rGa1-1 protein was run on a native SDS-Gel and stained with Coomassie blue for visualization. In three independent assays with recombinant protein masses of 1-3 μg and concentrations of 6.9-20.7 μM, rGal-1 presented predominantly as a dimer at 29 kDa, consistent with other reports.[394] Larger aggregates were not detected (**Figure 27a**). This data suggests that the rGal-1 protein was not aggregating. Therefore, it is unlikely that the apoptosis observed in cultured RAW 264.7 cells after incubation with rGal-1 is a reaction to rGal-1 protein aggregates.

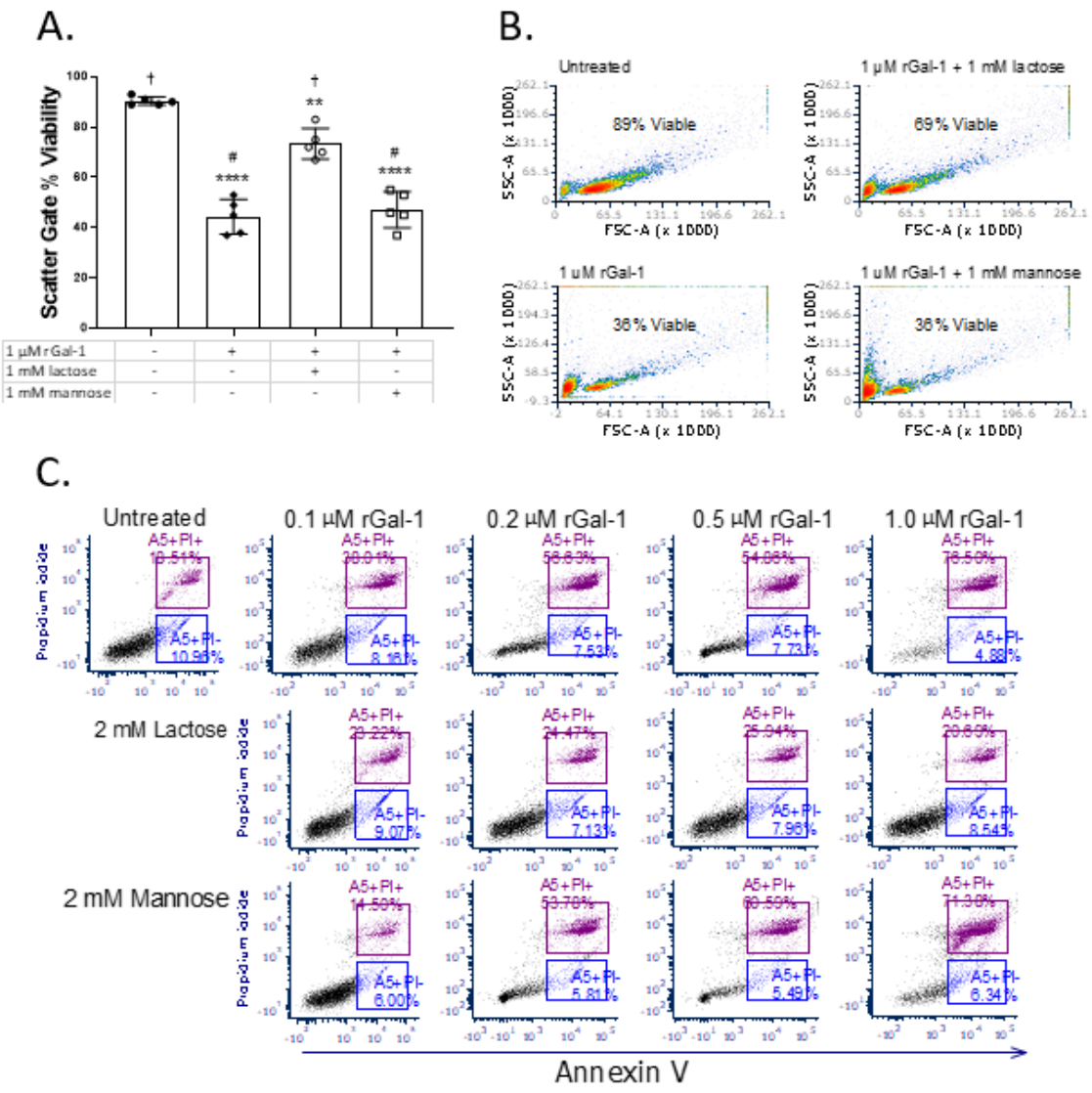

Figure 26 Galectin-1 reduces viability of RAW 264.7 macrophages through carbohydrate-dependent ligand binding

Cultured RAW 264.7 cells were harvested, aliquoted in culture tubes at a cell density of $2x10^5$ per 50 µL, then incubated with serial dilutions of 0.1-1.0 µM rGal-1 with 1-2 mM lactose, sugar with a high affinity for rGal-1, or, mannose, sugar with no rGal-1 affinity, for 15 minutes at room temperature. Sugars were preincubated with rGal-1 for a minimum of 30 minutes at room temperature prior to adding to the cells. (a) Bar graphs summarizing forward-side scatter viability from five independent experiments. The viability of RAW 264.7 macrophages is reduced after treatment with 1.0 µM recombinant galectin-1. This effect is blocked when cells are treated with the same concentration of galectin-1 plus 1.0 mM lactose. Mannose is not protective against galectin-1-induced apoptosis. **** $p < 0.0001$, ** $p < 0.01$ compared to untreated, † $p < 0.0001$ compared to galectin-1-treated, # $p < 0.0001$ compared to 1.0 µM galectin-1 plus 1 mM lactose (b.) Representative dot plots displaying a shift in cell viability determined by forward-side scatter gating. (c.) Representative dot plots of Annexin V-AF488 and propidium iodide (PI) staining. Data demonstrates that galectin-1-induced cell death is concentration and carbohydrate-dependent. After 15 minutes of incubation with 1.0 µM recombinant galectin-1, RAW 264.7 macrophages are in the late stage of apoptosis, indicated by double positive staining with Annexin V-AF488 and PI. Lactose is protective against rGal-1-induced apoptosis, while mannose does not inhibit apoptosis.

It was also possible that *E. coli.* byproducts caused the observed rGal-1-induced apoptosis. *E. coli.* are gram-negative bacteria with a high concentration of lipopolysaccharides in their cell wall. These endotoxins will elicit an inflammatory response in macrophages, which can activate apoptotic pathways. To assess endotoxin activity in the recombinant protein, we used two separate methods for inhibiting endotoxins: polymyxin B, an antibiotic that scavenges and neutralizes endotoxin and is used to treat infections with gram-negative bacteria, and anti-CD14, an antibody that blocks the cell surface receptor for lipopolysaccharides. In 2-3 separate experiments using 83 or 831 µM polymyxin B to block endotoxin activity, cells were treated with 1.0 µM rGal-1 and stained for Annexin V and PI analysis by flow cytometry. Polymyxin B did not affect apoptosis (the percentage of $Annexin^{+}PI^{+}$ cells; **Figure 27b**). Likewise, after blocking the LPS receptor with anti-CD14, treating with rGal-1, and staining for Annexin V and PI, there was no change in the percentage of $Annexin^{+}PI^{+}$ cells compared to the isotype control (**Figure 27c**). Together, this data indicates that Gal-1-induced apoptosis is independent of potential endotoxin contamination in recombinant *E. coli*-produced Gal-1.

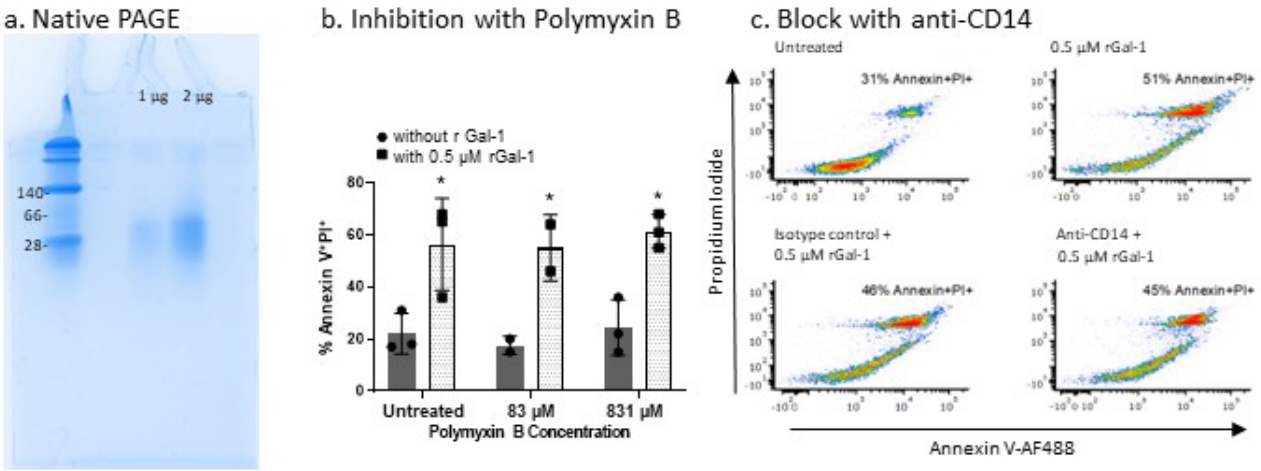

Figure 27 Galectin-1 induced apoptosis is not attributed to protein aggregation or endotoxin contamination in recombinant protein

(a) Representative native PAGE of *E. coli* recombinant galectin-1 (rGal-1). rGal-1 is present predominantly as a dimer at 29 kDa. Larger aggregates were not detected in 3 independent tests using 1-3 µg recombinant protein. (b.)

Polymyxin B does not reduce the percentage of galectin-1 induced AnnexinV^{+}PI^{+} RAW 264.7 macrophages in 2-3 independent experiments with 83 or 831 μM polymyxin B. (c.) Representative dot plots from two independent experiments of Annexin V and propidium iodide (PI) staining after blocking LPS co-receptor with anti-CD14. Combined, these experiments indicate that the observed galectin-1-induced apoptosis is independent of protein aggregation and potential endotoxin contamination in recombinant *E. coli*-produced galectin-1.

Finally, as an alternative to using rGal-1, RAW 264.7 cells were treated with conditioned media from T11 tumor cells, which we have shown express intracellular Gal-1, secrete and display surface expression of Gal-1. (**Section 5.1, Figure 24**) There was no difference in apoptotic activity between cells treated with media or with media containing lactose (inhibitor) or sucrose (negative control). Consistent, significant apoptosis was previously observed in RAW 264.7 cells at concentrations of 1 μM rGal-1, with lesser effects observed at concentrations as low as 0.1 μM (**Figure 26**). Media concentrations of Gal-1 were determined to be 2 nM on average (range 0.6-3.3 nM) by ELISA (data not shown). RAW 264.7 cells were treated with 70 nM r Gal-1, which did not induce apoptosis, and 1.0 μM as a positive control which did cause apoptosis (data not shown). This experiment was only conducted one time. However, previous experiments used concentrations as low as 100 nM, which showed an increase in apoptosis compared to controls, but this effect was reduced compared to higher concentrations. The most consistent apoptosis of RAW 264.7 cells was observed in concentrations greater than 0.4 μM (435 nM). Thus, the media concentrations of Gal-1 (range 0.6-3.3 nM) were insufficient to induce apoptotic activity in RAW 264.7 cells.

5.4 Recombinant galectin-1 induces apoptosis in RAW 264.7 macrophages by a caspase-independent pathway

Caspases (cysteine-aspartic proteases, cysteine aspartases, or cysteine-dependent aspartate-directed proteases) are a family of cysteine proteases that act in concert in a cascade triggered by apoptotic signaling. Caspases are inactive proenzymes that undergo proteolytic

processing by upstream caspases (caspase-8, -9). Caspase-3 is activated during the early stages of apoptosis and proteolytically cleaves caspase-7 to propagate the caspase signaling cascade. To assess the effect of exogenous Gal-1 on the activity of caspase-3 and -7 in $CD1b^{+}$ cells *in vitro*, RAW 264.7 cells were treated with 1 μM rGal-1 for various time ranging from 5 min-4 hr. As a positive control, cells were treated with 5 μM camptothecin for 4 hr. Caspase activity was evaluated with cell-based homogenous Caspase Glo Assay in media with 10% FBS. The results showed that the positive control worked, but RAW 264.7 cells treated with rGal-1 at all-time points were negative for caspase-3 and -7 activity (**Figure 28**). These data suggested that the apoptosis observed in RAW 264.7 cells treated with rGal-1 is not dependent on a caspase pathway.

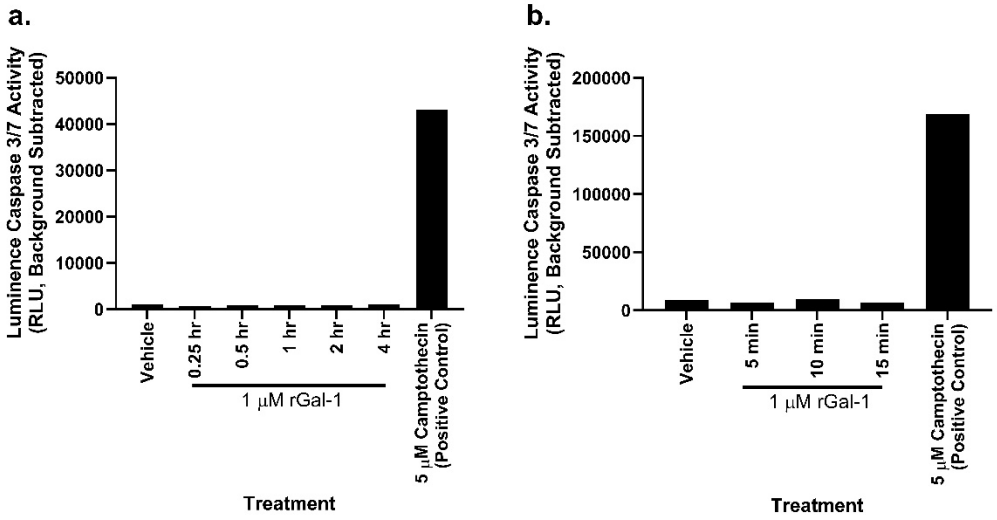

Figure 28 Recombinant galectin-1-induced apoptosis of RAW 264.7 cells is caspase 3/7-independent
RAW 264.7 were seeded at 1600 cells per well in 200 μL DMEM/10% FBS in a 96-well white wall plate and placed in incubator at 37°C, 5% CO2 48 hours prior to assaying. After 48 hours, the plate was removed from the incubator and the media was replaced with 100 μL of fresh media. Cells were treated with 1.0 μM rGal-1 for 5 min to 4 hr. 5 μM camptothecin was used as a positive control at treatment time of 4 hr. (a) rGal-1 failed to activate caspases 3/7 in RAW 264.7 cells following the treatment with 1.0 μM rGal-1 for 15 min-4 hr. (b) To ensure the window of caspase activity was not missed, RAW 264.7 cells were treated with 1.0 μM rGal-1 for 5-15 min. rGal-1 failed to activate caspases 3/7 at all-time points assayed, indicating that RAW 264.7 cell rGal-1-induced apoptosis acts through a caspase-independent pathway. Each time course assay was conducted independently one time.

5.5 Differences in LacNAc expression on myeloid cells

We next assessed the apoptotic effect of rGal-1 in myeloid cells from peritoneal exudate rather than a cell line. Mice were injected intraperitoneally with 2 mL thioglycolate, which is known to elicit an ascitic fluid exudate rich in macrophages and neutrophils. Peritoneal exudate cells (PEC) were removed by injecting PBS into the abdomen 4 days post-thioglycolate inoculation. Before analyzing the effects of rGal-1 on PEC, the cells were stained with myeloid markers for CD11b, MHCII, F4/80, Ly6C, CD68, and Ly6G to determine the composition by flow cytometry. PEC consisted of 62±15% $CD11b^+$, 32±15% $MHCII^+$, 26±16% $F4/80^+$, 26±16% $Ly6C^+$, 45±25% $CD68^+$, and 5±4% $Ly6G^+$. To further enrich $CD11b^+F4/80^+$ cells (macrophages), PEC were plated in complete media for 2-3 hours prior to assaying for apoptosis. After rinsing cells thoroughly with PBS, attached cells were gently scraped off the plate and assessed for post-plate enrichment by flow cytometry. Cells were gated on the forward and side scatter to exclude cell debris and dead cells. All other cells were considered live cells and were gated for each myeloid cell marker. Plating PEC reduced the average cell viability and did not significantly enrich the cell populations for $CD11b^+$ or $F4/80^+$ cells (**Figure 29a-b**). Therefore, the intact PEC preparation was used to assess the effect of rGal-1 on apoptosis. In three independent experiments, no significant increase in Annexin V^+ or Annexin V^+PI^+ cells were observed in PEC treated with rGal-1 compared to untreated cells (**Figure 29c**). Although the average Annexin V positive cells were lower in untreated cells compared to cell treated with 1.0 μM rGal-1. We speculated that this may be attributed to lower levels of LacNAc expression on the surface of PEC compared to RAW 264.7 cells, where significant apoptosis was consistently observed. To evaluate LacNAc surface expression, a heterodimer plant-derived lectin with high affinity for (β-1,4) -linked LacNAc (Gal-GlcNAc) residues known as *Datura stramonium* lectin (DSL) conjugated to FITC

was used to stain RAW 264.7 cells and PEC. Results from one experiment showed that PEC expressed significant cell surface LacNAc residues, however with lower density (lower MFI DSL-FITC staining) than RAW 264.7 cells (**Figure 29d**).

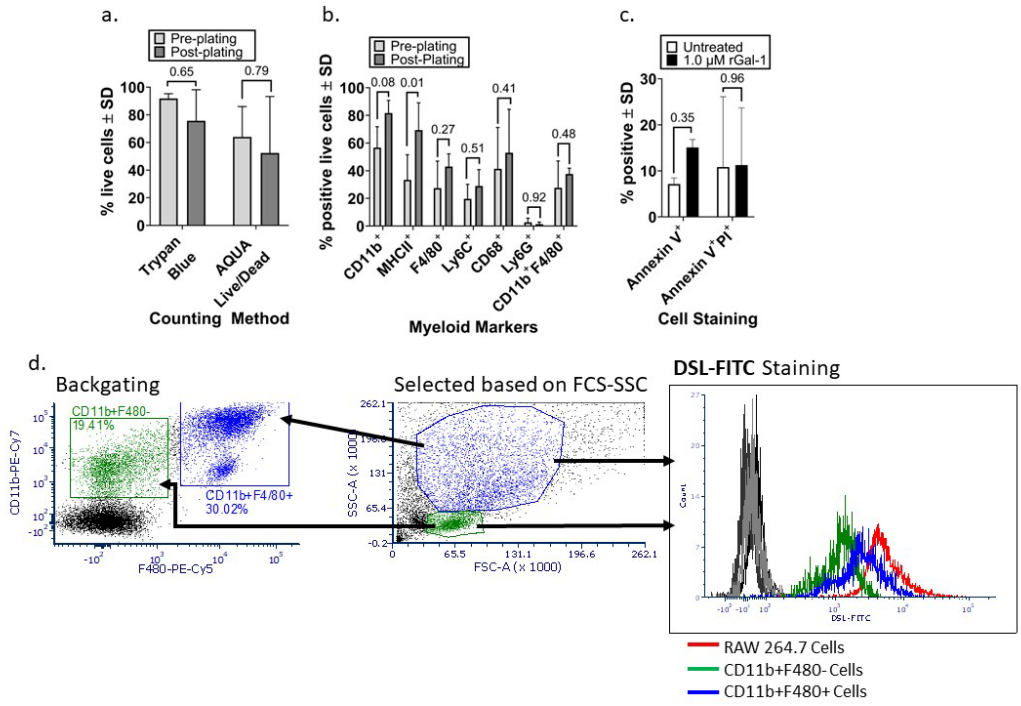

Figure 29 Galectin-1 induced apoptosis is not significant in peritoneal exudate cells which may be attributed to lower LacNAc expression compared to RAW 264.7 cells

Peritoneal exudate cells (PEC) were isolated from thioglycolate-treated Balb/c mice. Cells were counted by Trypan blue and AQUA Live /Dead stain before and after staining for myeloid cell markers. (a) Bar graph of the percent of live cells as determined by Trypan blue or AQUA Live/Dead stain before and after plating PEC in temperature and humidity-controlled incubator for 48 hours prior to staining for myeloid cell markers. Data is a summary of three independent experiments. Statistical analysis was conducted using a Two-way ANOVA with a post-hoc Sidak's multiple comparisons test. The light gray bars indicate pre-plated cell viability and dark gray bars represent cell viability post-48-hour plating. (b) Bar graphs show the average percentage from three independent experiments of each myeloid cell marker after gating on live cells by forward and side scatter. Light gray bars represent the average percent of live cells before plating PEC for 48-hours, while the dark gray bars represent the percentage of live cells after plating. Two-way ANOVA with a post-hoc Fisher's test showed that $MHCII^+$ cells were significantly enriched post-plating ($p=0.01$), but there was not a significant increase in any other PEC population. (c) Whole PEC exudate cells were treated with 1.0 µM rGal-1 or PBS vehicle and stained with Annexin V-AF488 and PI to determine the apoptotic effect of rGal-1 on these cells. PECs treated with rGal-1 have a higher mean of Annexin V^+ cells but it was not statistically significant in a two-way ANOVA with a post-hoc Fisher's test ($p=0.35$). There was no change in the percent of Annexin V^+PI^+ cells between the untreated and 1.0 µM rGal-1 treated PEC. (d) To determine differences in LacNAc residues among $CD11b^+$ macrophages, cells were labeled with DSL-FITC. PEC populations were identified based on forward and side scatter. High and low forward and side scatter populations were selected and backgated on cells that were positive for CD11b-PE-Cy7 and F480-PE-Cy5. The selected populations were graphed in a histogram and compared to DSL-FITC expression levels on RAW 264.7 cells. The gray line represents isotype control for RAW 264.7 cells, the black line is the isotype control for PEC, the red line shows DSL-FITC positivity on RAW 264.7 cells; while the green and blue lines show $CD11b^+F4/80^-$ and $CD11b^+F4/80^+$ PEC,

respectively. This suggests that the low observance of apoptosis in PEC may be attributed to lower LacNAc expression compared to RAW 264.7 cells.

To resolve the discrepant *in vitro* and *ex vivo* apoptosis findings and to further investigate the effects of Gal-1 on $CD11b^+$ myeloid lineage cells and CLBC, we moved to an *in vivo* orthotopic T11 CLBC model. The transition to *in vivo* experiments was guided by the need for more physiologically relevant conditions to comprehensively evaluate the apoptotic effects of Gal-1 on $CD11b^+$ myeloid cells in the tumor microenvironment. Gal-1 was inhibited *in vivo* through intraperitoneal injection of a phenol-linked Anginex peptide topomimetic, OTX008, when all tumors reached an average tumor volume of 100 mm^3 at 7 days post-tumor implant. Refer to the publication by Dings et al. 2012 for a representative image of OTX008 binding to Gal-1 when lactose is bound in the carbohydrate binding region.[395] Based on our findings and those of others, this *in vivo* study was designed to determine if systemic treatment with a Gal-1 inhibitor would 1) reduce CLBC tumor growth and 2) induce apoptosis in tumor cells, T cells (the predominant $CD3^+$ cell type) or macrophages (the predominant $CD11b^+$ cell type) in the T11 mouse model of CLBC. This shift to an in vivo model using murine T11 CLBC allowed for the exploration of Gal-1 inhibition with OTX008 and its effects on tumor growth, tumor cell apoptosis, and apoptosis of immune cells to obtain a more comprehensive understanding of Gal-1 functions in a physiological context.

5.6 *In vivo* galectin-1 inhibition with OTX008 slows tumor growth

To begin our *in vivo* study to explore the effects of Gal-1 inhibition on tumor growth, we implanted cultured T11 tumor cells into the mammary fat pad of syngeneic, Balb/c female mice. Eight-week-old T11 tumor-bearing Balb/c female mice were randomly assigned to groups that received either 10 mg/kg OTX008 (treatment) or sterile PBS (control) every three days until

euthanasia on day 14 or 15 post-tumor implant (10 per group). Two mice in the treatment group and one mouse in the control group had palpable tumors growing deep below the skin (15%; 3/20), making it difficult to initially measure the tumor by calipers. These mice did not receive an injection on day seven but received injections on days 10 and 13 post-tumor implant. One mouse in the PBS group did not have primary tumor growth and did not receive any treatment (5%; 1/20). All four mice were excluded from the overall analysis of primary tumor growth. Tumors were removed by day 15 post-tumor implant due to advanced tumor burden in control mice. All mice appeared bright, alert, and responsive throughout the study. Mouse body condition and calculated body weight indicate no apparent toxicity from OTX008 administration (**Figure 30a-c**). Neither the primary tumor nor overall body weight (with the primary tumor) significantly differed between the two groups. The average tumor and body weight were lower for OTX008-treated mice than for PBS-treated mice.

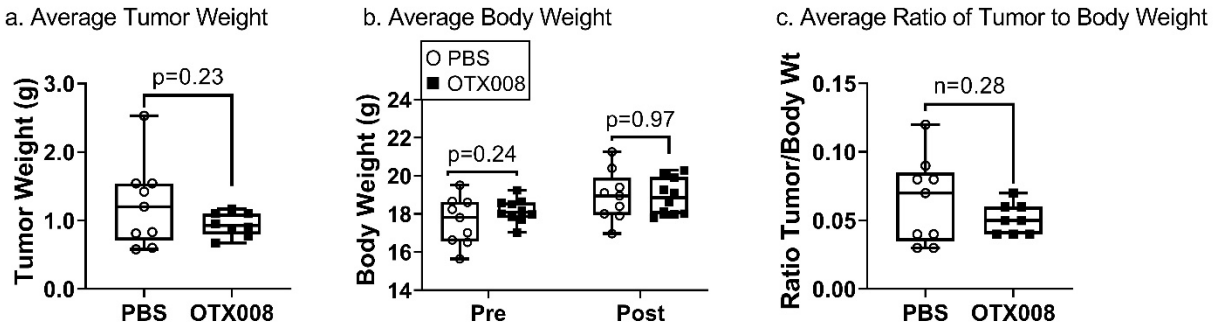

Figure 30 Galectin-1 inhibition does not significantly reduce tumor or body weight.
(a) Tumor weight, (b) body weight before (day 4) and after (day of sacrifice, 14 or 15) OTX008 or PBS administrations, and (c) the ratio of tumor to body weight were analyzed by Student's T-test (n=8 per group). OTX008-treated mice had a lower average tumor weight and tumor-to-body weight ratio than PBS-treated mice, but these differences were not statistically significant. Initial body weights (Pre) were collected four days post-tumor injection, and final body weights were collected just before euthanasia on day 14 or 15, depending on the sacrifice date. Tumors were removed 15 days post-tumor implant due to advanced tumor burden in the control group (PBS). All body weights were collected with the primary tumor burden. The control group had a lower starting weight on day 4 (Pre) than OTX008-treated mice, but there was no difference between the two groups post-treatment (days 14-15). Body weight data suggests that there was no apparent toxicity from OTX008 treatment.

The control group started with lower mean body weight (17.6 vs. 18.2 g) before injections, but both groups had an equivalent average body weight by the end of the study (both averages were 18.9 g). There was higher variability in the control group than in the treatment group in tumor, body weight, and tumor growth. Cell yield by Trypan blue staining assessed the number of cells per gram of tumor as another measure of comparison, but there was no significant difference between the two groups (data not shown). Tumor measurements from OTX008-treated mice compared to control showed a considerable difference in growth over treatment. In comparison to the mice who received sterile PBS (n=8), the mice who were given at least two doses of OTX008 (n=8) showed a smaller average tumor size after 12 days of tumor implantation (**Figure 31a, c, and d**). The results of the two-way ANOVA revealed that the treatment effect was significant in the OTX008-treated mice compared to the control group ($p= 0.05$). Further, the post-hoc Sidak's test indicated a considerable decrease in the average tumor volume on day 14 post-tumor implant in the OTX008-treatment group ($p=0.003$). Additionally, a linear regression analysis on both groups was performed, and the slope of the best-fitting regression lines was compared to determine statistical significance. It was found that from days 6-15, the slope of the linear regression line for the OTX008 treatment is significantly lower compared to the PBS-treated group ($p=0.0003$). (**Figure 31b**) If the three largest tumors in the PBS-treated group are removed from the dataset, the data loses statistical significance by both ANOVA and linear regression. However, these three tumors in the PBS treated group were not determined as outliers using interquartile range, ROUT, nor Grubbs' outlier analysis.

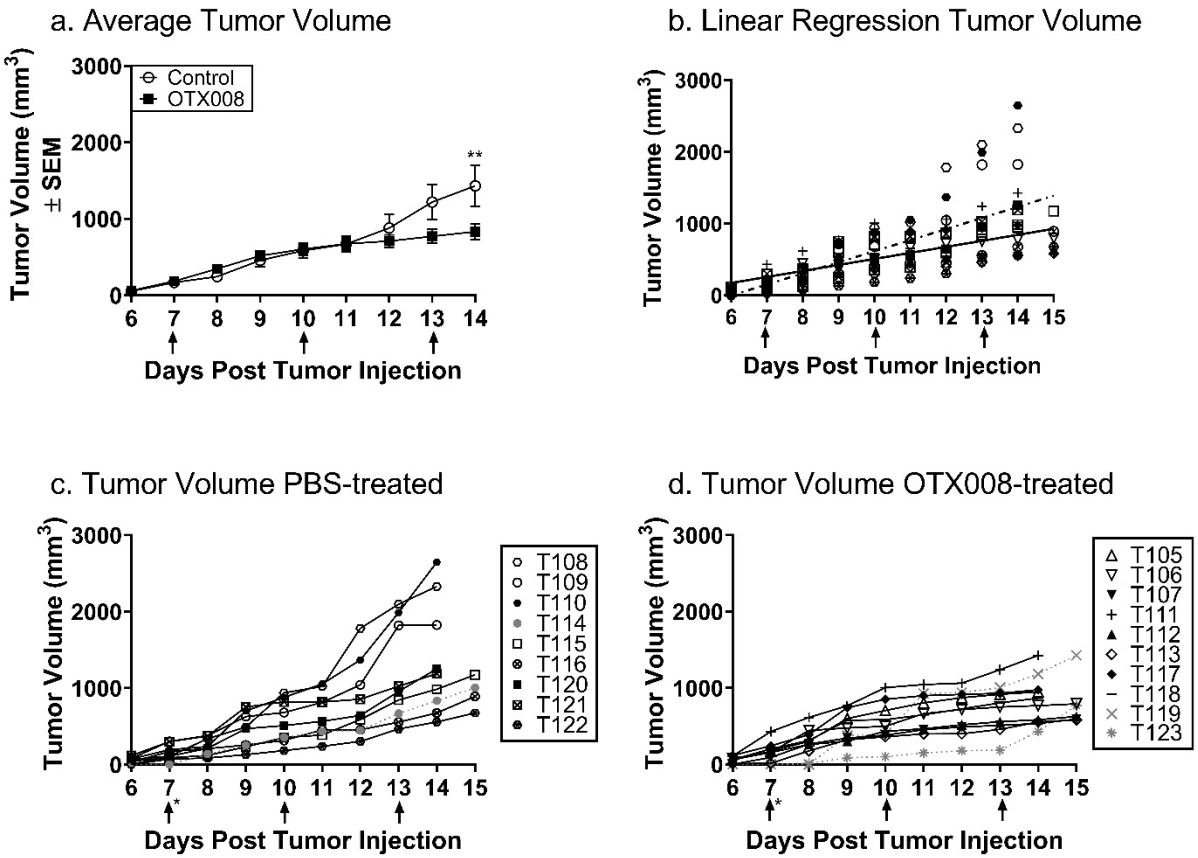

Figure 31 Galectin-1 inhibition with OTX008 slows tumor growth
T11 tumor-bearing mice were injected with 10 mg/kg OTX008 (n=8) or PBS (n=8) every three days beginning 7 days post-tumor injection. Black arrows indicate injection days. Initially, ten mice were randomized to each group, but three mice (n=2 OTX008 and n=1 PBS) had delayed treatment due to inaccurate estimation of tumor volume (i.e., these tumors were too deep to measure externally *in vivo* by calipers). These three mice were excluded from the overall analysis of tumor growth but are shown on the graphs displaying tumor growth curves for the individual mice (T114, T119, T123). One mouse from the PBS group did not have primary tumor growth. This mouse was excluded from all analyses. (a) Average tumor volume ± standard error of the mean was plotted from 6 days post-tumor injection when most tumors were palpable to the day of sacrifice, 14- or 15-days post-implant. Separation between the two treatment groups begins on day 12. OTX008 significantly reduces tumor growth at day 14 post-tumor injection compared to the PBS-treated cohort ($p=0.003$ by a 2-way ANOVA ($p=0.05$) with a post-hoc Sidak's multiple comparison test. (b) Linear regression analysis of PBS- and OTX008-treated mice. The linear regression lines of best fit are shown as dotted (PBS, $R^2=0.52$) and solid (OTX008, $R^2=0.54$) black lines. The slopes significantly differed from day 6 to day 15 ($p=0.0003$). (c) Tumor growth curve for each mouse (n=9) in the PBS-treatment group. T114 (gray symbol and dotted line) did not receive an injection on day 7 (asterisk) and was not included in the overall tumor growth analysis due to deep tumor growth. (c) Tumor growth curve for each mouse (n=10) in the OTX008 treatment group. T119 nor T123 (gray symbol and dotted line) did not receive an injection on day 7 (asterisk) and were not included in the overall analysis due to deep tumor growth. Dr. Kathryn Verbanac and Moses McDaniel conducted the drug injections and blinded tumor volume assessments.

5.7 Evaluation of infiltrating myeloid subsets after treatment with OTX008

The impact of Gal-1 inhibition on $CD11b^+$ cell infiltration in the tumor microenvironment was assessed using tumors removed from euthanized mice 14 or 15 days after tumor injection. The tumors were weighed and cut into 2-3 pieces for flow cytometry and fluorescent microscopy analysis. The weights of each tumor section used for flow cytometry were recorded and graphed (PBS control n=9 and OTX008 treatment n=8, **Figure 32a**). The tumor segments used for flow cytometry were placed in a digestion buffer on a shaker at room temperature for one hour, then strained through a 70 µm nylon filter to obtain a single-cell suspension. After lysing red blood cells, the remaining cells were manually counted using a hemocytometer and Trypan blue viability dye. Cell quantification and viability counts were compared for each tumor to ensure that cell viability did not contribute to any observations (**Figure 32b-c**). Before staining for flow cytometric analysis, both groups had an average live cell count of $3x10^7$ ($\pm 2x10^7$) cells and viability ≥80%. Cells were resuspended in staining buffer, incubated with CD16/32 FcR blocker, and then labeled with an antibody cocktail containing anti-.CD11b, Ly6C, Ly6G, F4/80, and CD68 to determine the frequency of $CD11b^+$ subsets (cell types associated with these markers are defined in **Table in Figure 33**). It is important to note that the expression of immune markers can differ depending on the tumor microenvironment and stage of tumor development. These markers were chosen based on previously published studies showing their expression on $CD11b^+$ subsets. To determine the percentage of each $CD11b^+$ subpopulation, cells were first gated on AQUA viability die to select viable cells. Doublet cells were then excluded by plotting forward scatter height versus area. Cellular debris was removed by gating on forward and side scatter, and then subpopulations were determined by gating on their respective markers. Isotype controls were used to determine where to set gates for specific antibody binding. As determined by AQUA staining

and flow cytometric analysis, the average viability for each group was 75.3 (±7.6)% for control and 75.6 (±4.3)% for OTX008 treated mice. Tumors consisted of the following $CD11b^+$ populations in PBS- and OTX008-treated mice, averages and standard deviations are reported respectively: $CD11b^+CD68^-F4/80^+Ly6C^+Ly6G^+$ (G-MDSC/ TAN) 2.6 (±1.0)% and 2.8 (±0.8)%, $CDllb^+CD68^-F4/80^+Ly6C^+Ly6G^-$ ($Ly6C^+$ monocytes) 11.3 (±3.5)% and 11.2 (±3.3)%, $CD11b^+CD68^-F4/80^-Ly6C^+Ly6G^-$ (M-MDSC) 5.5 (±2.5)% and 6.3 (±2.9)%, and $CD11b^+CD68^{High}F4/80^-Ly6C^+Ly6G^-$ ($CD68^{High}$ TAM) 52.9 (±7.3)% and 54.7 (±7.6)%, $CD11b^{+/Low}CD68^{Low}F4/80^+Ly6C^-Ly6G^-$ ($CD68^{Low}$ TAM) 41.6 (±6.9)% and 40.2 (±6.6)% (**Figure 33a**). The results indicate that there was no notable difference in the $CD11b^+$ subsets of mice that were treated with PBS and those that were treated with OTX008. Two separate populations of CD11b+CD68+F4/80—Ly6C+Ly6G— cells were detected. One population showed low levels of CD11b and CD68 expression, while the other showed high levels of CD11b and CD68. Based on the literature, some TAMs may exhibit low CD11b and CD68 expression, while others may have higher expression levels. While CD11b and CD68 are commonly expressed on TAM, the expression levels can vary depending on the specific microenvironment and activation state. They may be influenced by tumor type, stage, and location factors. The specific roles and functions of TAM with low CD11b and CD68 expression are not well-defined and require further investigation.

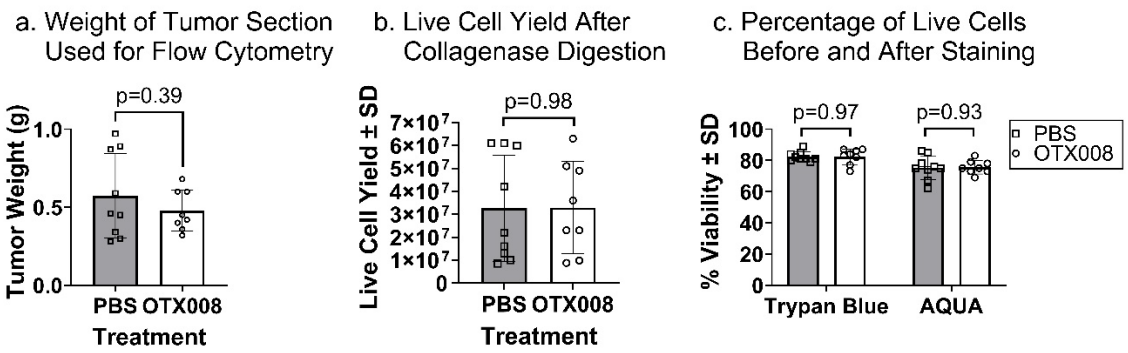

Figure 32 Tumor-derived Cells: Cell Count and Viability for Flow Cytometric Assessment following *in vivo* treatment with OTX008 or PBS

Cells were isolated from a portion of each tumor by collagenase digestion. There were no observable differences between PBS- and OTX008-treated tumors when comparing (a) tumor weight of each section used for analysis, (b) cell yield after tumor digestion: live cell counts by Trypan blue, and (c) overall percent cell viability after tumor digestion. Trypan blue was used to determine cell viability before staining with antibodies for flow cytometry, and AQUA was used in flow cytometry to evaluate viability after staining. Cell counts include all cells isolated from the tumor after digestion, including tumor, immune, and epithelial cells.

Since Gal-1 is known to bind LacNAc residues on cell surface proteins, we sought to understand the level of LacNAc expression on each of the $CD11b^+$ subsets within the tumor microenvironment with and without *in vivo* Gal-1-inhibition with OTX008. A plant-derived lectin with a known affinity for LacNAc, DSL, was used to measure LacNAc expression on $CD11b^+$ cells. Cells stained with the antibody cocktail were also incubated with DSL-FITC, and the median fluorescent intensity (MFI) was calculated for each gated population of interest (n=4 in each group). Treatment with OTX008 did not influence LacNAc expression in any of the CD11b subsets. $CD11b^+CD68^{High}F4/80^+Ly6C^-Ly6G^-$ ($CD68^{High}$ TAM) had the highest LacNAc expression, and $CD11b^+CD68^-F4/80^+Ly6C^+Ly6G^+$ (G-MDSC/ TAN) had the second highest abundance of LacNAc residues (**Figure 33b**). $CD11b^+CD68^-F4/80^-Ly6C^+Ly6G^-$ (M-MDSC) have the lowest LacNAc expression among the CD11b subsets.

Results from Chapter 3 showed that treating the $CD11b^+$ RAW264.7 immortal macrophage cell line *in vitro* with exogenous mouse recombinant Gal-1 changed the forward scatter side scatter pattern and induced carbohydrate-specific, caspase-independent apoptosis. Based on these

observations, we examined the cells isolated from primary tumors treated with PBS or OTX008. We analyzed the flow cytometry for a change in forward and side scatter (**Figure 34**), as an indication of cells undergoing apoptosis. There was no change in the percentage of doublet cells (data not shown) or the low or high forward scatter percentage in all live or CD11b^{+} cells.

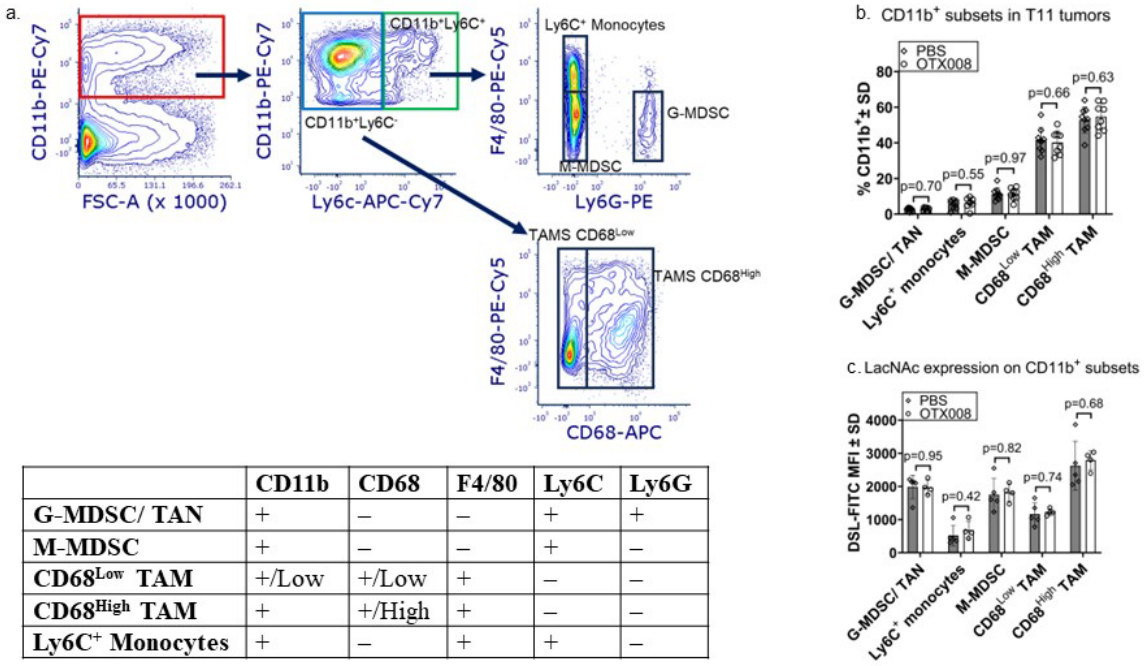

	CD11b	CD68	F4/80	Ly6C	Ly6G
G-MDSC/ TAN	+	–	–	+	+
M-MDSC	+	–	–	+	–
CD68^{Low} TAM	+/Low	+/Low	+	–	–
CD68^{High} TAM	+	+/High	+	–	–
Ly6C^{+} Monocytes	+	–	+	+	–

Figure 33 Flow cytometric analysis of infiltrating myeloid cells in tumors treated with OTX008 or PBS
Single-cell suspension from digested tumors were labeled with (a) anti-CD11b, CD68, F4/80, Ly6C, and Ly6G to determine CD11b^{+} subsets present in T11 primary tumors (n= 9 (PBS) and 8 (OTX008)). After selecting for live cells, cells were selected for positive CD11b expression. Double positive CD11b and Ly6C cells were further gated for expression of F4/80 and Lyc6G, while cells that were CD11b positive and Ly6C negative were further gated by F4/80 and CD68. The table below the representative flow diagrams defines cell types by their expression of the selected markers. (b) Bar graph represents DSL-FITC (n=4 each) staining to test for cell surface LacNAc expression. No differences were observed in the percentage of infiltrating CD11b^{+} cell subtypes with and without Gal-1 inhibition with OTX008. CD68^{High} TAM were the most abundant tumor CD11b^{+} cell type and expressed the highest LacNAc residues level. G-MDSC/ TAN had the lowest percentages of CD11b^{+} cells and expressed the second highest level of LacNAc residues.

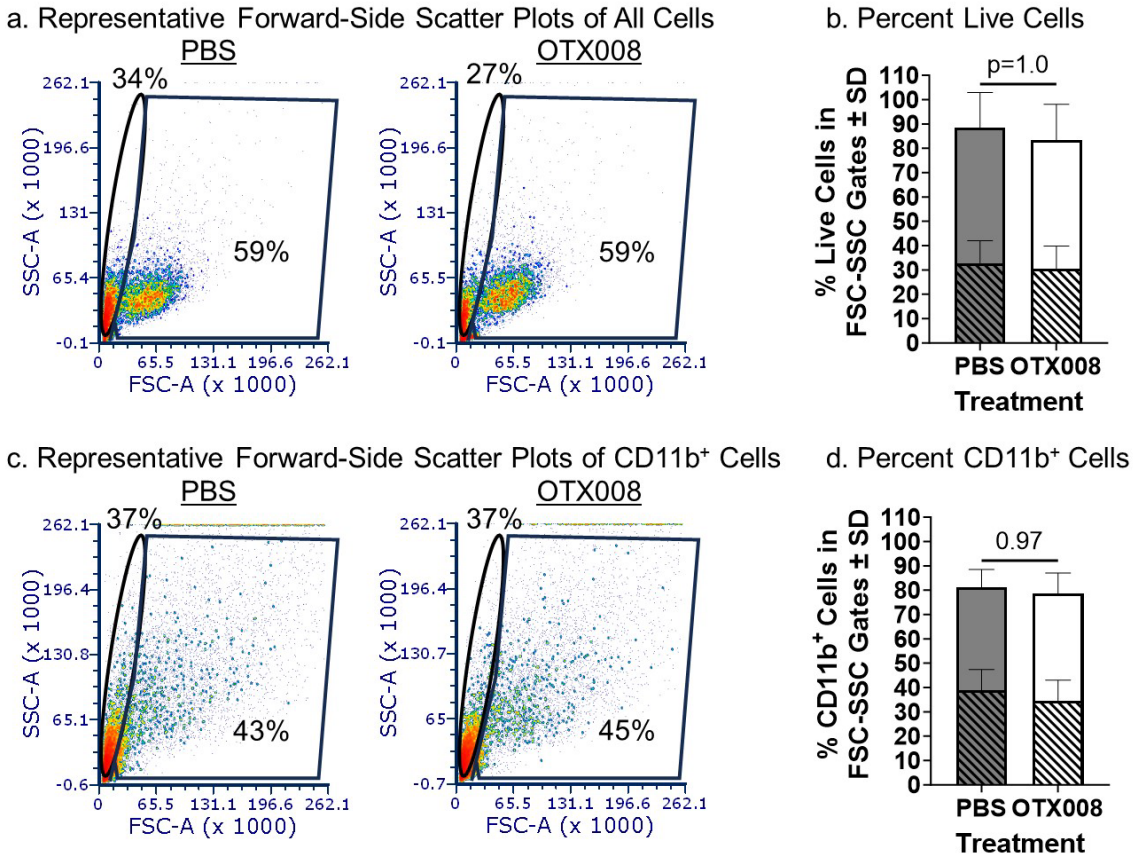

Figure 34 OTX008 Gal-1 inhibition did not change the forward and side scatter pattern in cells isolated from primary tumors

Single-cell suspension from digested tumors were evaluated for a change in forward and side scatter. Cells were gated to remove dead cells by positive AQUA stain and doublet cells by plotting forward scatter height versus area (data not shown). Forward and side scatter was evaluated on PBS (n=9) and OTX008 (n=8) treated tumors to determine a shift in forward scatter based on treatment with OTX008 or PBS. Based on RAW 264.7 cell data, we would expect more cells in the high forward scatter gate when treated with a Gal-1 inhibitor compared to tumors treated with PBS. (a) Representative images of all live cells from PBS and OTX008 treated tumors analyzed for forward and side scatter. Cells were gated by low and high forward scatter. (b) Bar graph of the low and high forward scatter in all live cells. The gray and white bars represent the average of cells with high forward scatter, and the two bars with diagonal stripes show the percentage of cells with low forward scatter. Two-way ANOVA with post-hoc Tukey's analysis showed no significant difference between either low or high forward scatter in PBS compared to OTX008 treated tumors (p=1.0). (c.) Representative images of $CD11b^+$ cells from PBS and OTX008 treated tumors analyzed for forward and side scatter. Cells were gated by low and high forward scatter. (d.) Bar graph of the low and high forward scatter in all $CD11b^+$ cells. The gray and white bars represent the average of cells with high forward scatter, and the two bars with diagonal stripes show the percentage of cells with low forward scatter. Two-way ANOVA with post-hoc Tukey's analysis showed no significant difference between either low or high forward scatter in PBS compared to OTX008 treated tumors (p=0.97).

5.8 Fluorescent microscopy analysis of intratumoral apoptosis in OTX-008-treat tumors

Tumors removed from mice were cut into 2-3 pieces to be processed for downstream assays. These assays aimed to assess the impact of OTX008 Gal-1 inhibition on $CD3^+$ and $CD11b^+$

cell tumor infiltration and apoptosis and overall tumor apoptosis. One of two or three tumor pieces was placed in formalin and embedded in paraffin for fluorescent microscopy experiments. FFPE tumors were sectioned into 5 μm. Three sections throughout the tumor were selected for staining. Samples were deparaffinized, antigens were unmasked, and sections were stained with anti-CD3-AF488 or CD11b-AF488, TUNEL-AF594, and DAPI. Overall tumor apoptosis was assessed by two fluorescent microscopy instruments, confocal microscopy and Zeiss Cell Discoverer 7 microscope. In both methods, the fluorescent intensity of TUNEL-AF594 (red) and DAPI (blue) were collected and calculated by determining the ratio of TUNEL: DAPI MFI across the selected region of interest (ROI). Using confocal microscopy, seven ROIs were chosen in each tumor section, and total fluorescence was collected across the ROI (**Figure 35a-b**). The average MFI was calculated across the entire tumor by averaging all ROI collected and within each section by averaging MFI from all ROI within a tumor section. Likewise, using Cell Discoverer 7, the entire tissue section was imaged and selected as the ROI for analysis (**Figure 35c**). Results showed that the mean for the OTX008-treated mice was lower compared to control mice in all analyses for total tumor apoptosis, but these figures did not reach statistical significance by Student's T-test. This indicates that the slower tumor growth in the OTX008-treated mice could not be conclusively attributed to an increase in apoptosis of tumor cells due to Gal-1 inhibition.

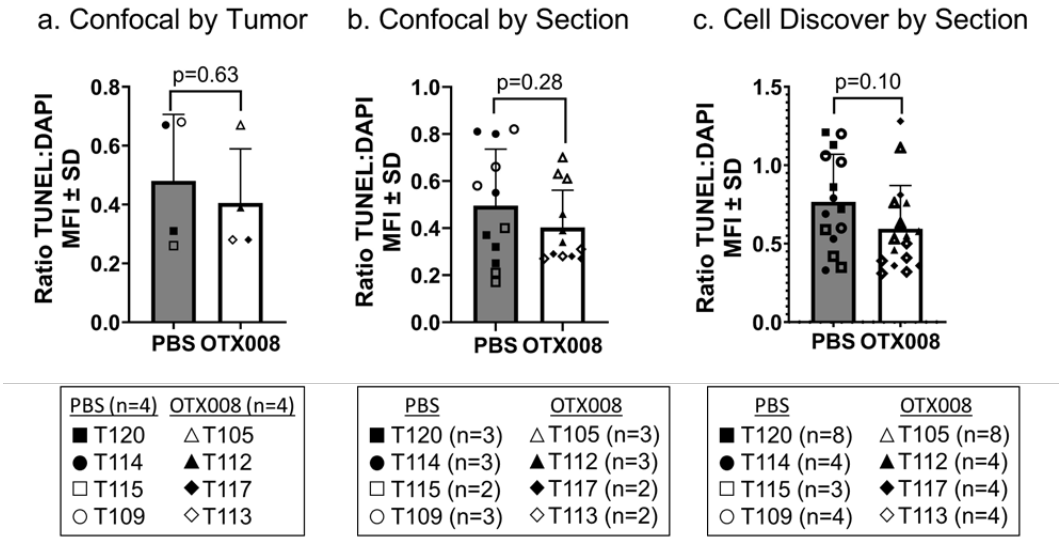

Figure 35 Gal-1 inhibition did not significantly decrease overall tumor apoptosis
Tumor sections were stained for TUNEL and DAPI, and data was collected by confocal microscopy to evaluate overall tumor apoptosis. The results were calculated by averaging the MFI for TUNEL-AF594 (red) and DAPI (blue) across seven ROI within 2-3 tumor sections per tumor and graphed by tumor (a) and by section (b). Images of whole tumor sections were collected on a Zeiss Cell Discoverer 7 microscope. The ratio of TUNEL to DAPI was calculated across the entire tissue section and graphed in (c) by section. In all analyses, OTX008-treated tumors had lower TUNEL: DAPI ratios, but these results were not statistically significant by the Student's T-test. Dr. Elizabeth Ables advised on the overall approach and TUNEL assay and acquired confocal images and data. Cindy Kukoly and Amanda Petritsch acquired the fluorescent images and data on the Cell Discoverer 7 and advised on the data acquisition and analysis.

To analyze the effects of Gal-1-induced apoptosis on infiltrating $CD3^+$ and $CD11b^+$ cells, FFPE tumor sections were deparaffinized, and antigens were unmasked, then sections were stained with anti-CD3-AF488 or anti-CD11b-AF488, TUNEL-AF594, and DAPI. Images of three selected ROI were collected using confocal microscopy. Positive cell counts were performed by automated colocalization analysis in Fiji or by manually counting using Zeiss-Blue software. Samples stained for CD3 cells were analyzed by manual cell counting alone because the low number of CD3 cells caused software errors when attempting to use automated counts. Results showed no significant difference in the number of $CD3^+$ or $CD3^+TUNEL^+$ cells between samples treated with PBS or OTX008 (**Figure 36a-c**). There was a high degree of variability in the number

of $CD3^+$ cells identified within each tumor. CD3-positive cells were scarce throughout tumors from both treatment groups.

The same analysis was collected for samples stained with CD11b and TUNEL. Both manual and automated counts were performed on these sections. A significantly larger number of CD11b cells were identified throughout all tumor sections compared to CD3, which is expected based on previous characterization analyses conducted and described in Chapter 3. Automatic counts were performed in Fiji software, but the quality control of automated counts resulted in low confidence in identifying double and triple-positive cells (data not shown). Neither the manual nor automated counts were able to detect a significant difference in the target cell populations from either treatment group. Manual counts for $CD11b^+$ cells and the percentage of $CD11b^+TUNEL^+$ cells are shown in **Figure 37a-d**. Representative images from confocal microscopy analysis of $CD11b^+TUNEL^+$ stained tumor samples are shown in **Figure 37e**.

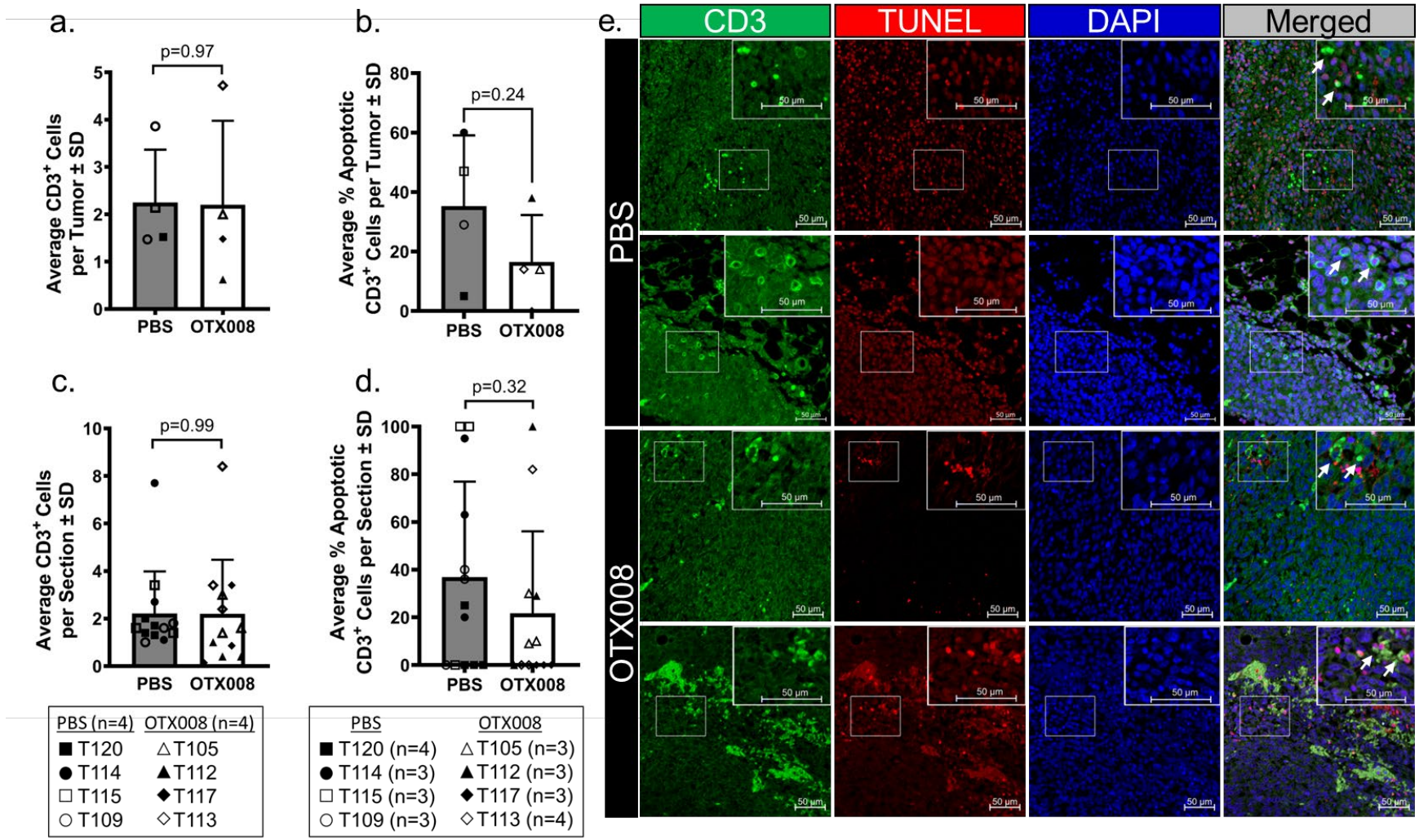

Figure 36 Apoptosis of CD3$^+$ cells in tumors treated with OTX008 or PBS

Four FFPE tumors from each treatment group were sectioned into 5 µm sections, and 3-4 sections from each tumor were stained with anti-CD3 (green), TUNEL (red), and DAPI (blue). Seven ROI within each tumor section were imaged on a confocal microscope at 20X. CD3$^+$DAPI$^+$ and CD3$^+$TUNEL$^+$DAPI$^+$ were manually counted in each ROI. The average CD3$^+$DAPI$^+$ cells for all ROI collected in 3-4 sections are graphed in (a) by tumor, and the average of double positive cells within each tissue section is graphed in (c). The average percentage of apoptotic CD3$^+$ cells was calculated by dividing the CD3+TUNEL+DAPI+ by the total

$CD3^+DAPI^+$ cells and multiplying by 100. The average percentage of positive apoptotic $CD3^+$ cells in each ROI from 3-4 tissue sections is graphed by tumor in (b) and the average percentage across ROI within each tissue section is graphed in (d). Each tumor is represented by a different symbol to show the variability of CD3 quantitation and CD3 apoptosis among tissue sections from the same tumor. Treatment groups were analyzed for statistical significance by a Student's T-test. The mean of the OTX008 group was lower compared to controls in all analyses, but these findings were not significant. (e) Representative confocal microscopy ROI images from tumor sections in each treatment group. These images show zoomed-in regions within the ROI that display the variability of CD3 staining.

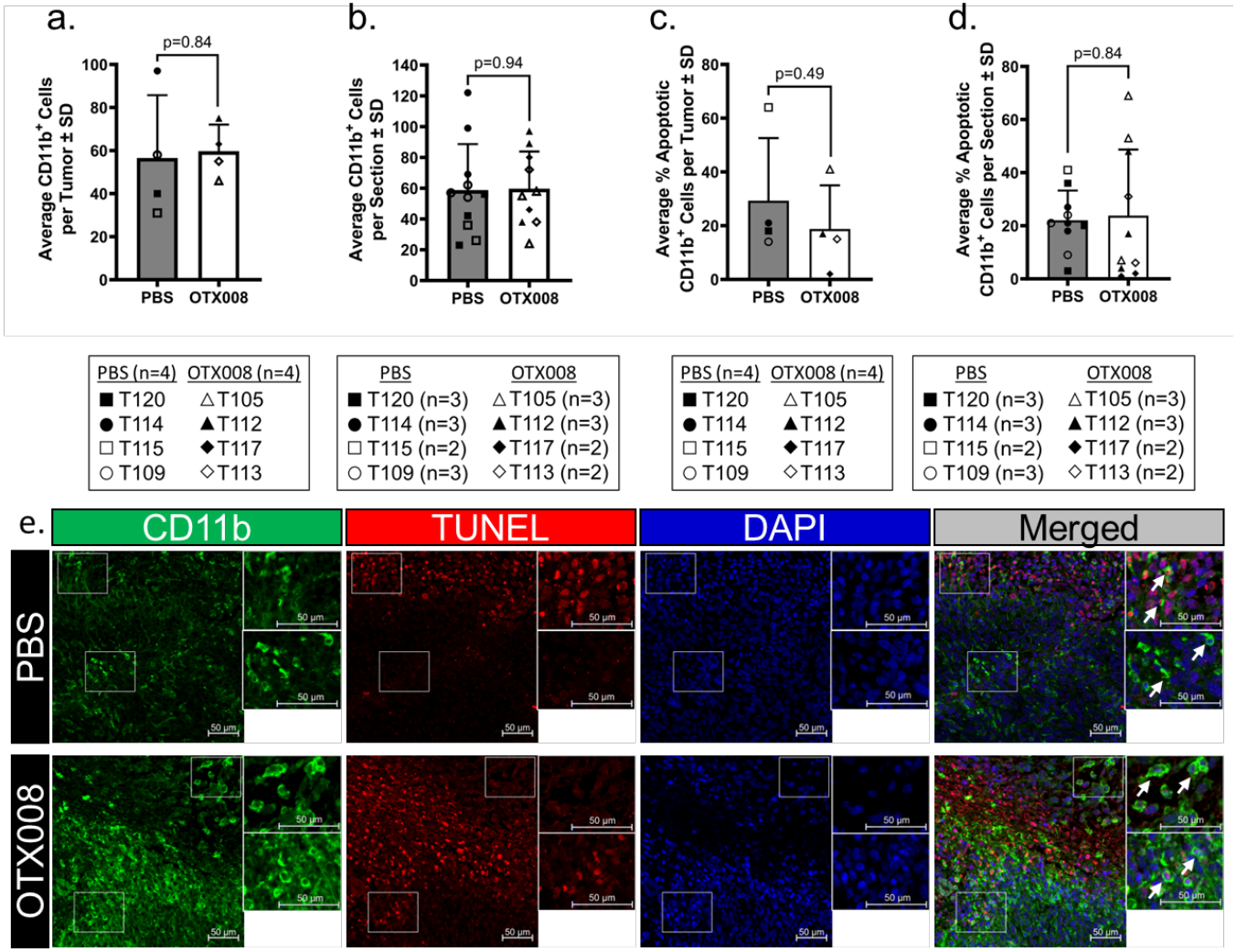

Figure 37 Apoptosis of CD11b$^+$ cells in tumors treated with OTX008 or PBS

Four FFPE tumors from each treatment group were sectioned into 5 µm sections, and three sections from each tumor were stained with anti-CD11b-AF488 (green), TUNEL-AF594 (red), and DAPI (blue). Seven ROI within each tumor section were imaged on confocal microscopy at 20X. CD11b$^+$DAPI$^+$ and CD11b$^+$TUNEL$^+$DAPI$^+$ were manually counted in each ROI. The average CD11b$^+$DAPI$^+$ cells for all ROI collected in 2-4 sections are graphed in (a) by tumor and the average of double positive cells within each tissue section is graphed in (b). The average percentage of apoptotic CD11b$^+$ cells was calculated by dividing the

$CD11b^+TUNEL^+DAPI^+$ by the total number of $CD11b^+DAPI^+$ cells and multiplying by 100. The average percentage of positive cells in each ROI from 2-4 tissue sections is graphed by tumor in (c) and the average percentage across ROI within each tissue section is graphed in (d). Each tumor is represented by a different symbol to show the variability of CD11b quantitation and CD11b apoptosis among tissue sections from the same tumor. Treatment groups were analyzed for statistical significance by a Student's T-test. The mean of the OTX008 group was comparably equal to controls in all analyses except when comparing the percentage of apoptotic $CD11b^+$ cells by tumor. The mean was lower in the OTX008 group compared to the control in this analysis. However, the results did not reach statistical significance (e) Representative confocal microscopy ROI images from tumor sections in each treatment group. One zoomed area within each ROI from each treatment group is an example of double-positive ($CDllb^+DAPI^+$) cells, and one area contains triple-positive cells ($CDllb^+TUNEL^+DAPI^+$).

5.9 Summary and Discussion

Our investigation into the effect of Gal-1 on macrophages began with determining whether Gal-1 crosslinks $CD11b^+$ cells through agglutination using an *in vitro* model of murine $CD11b^+$ cells, the RAW 264.7 cell line. These immortal macrophage cells, isolated from an Abelson murine leukemia virus-induced tumor, are commonly used to assess in vitro macrophage responses to stimuli. RAW 264.7 cells were co-incubated with recombinant mouse Gal-1 (rGal-1) in the presence or absence of lactose, an inhibitor, or mannose, a sugar not expected to block Gal-1 binding. Cells were analyzed by flow cytometry for agglutinated doublet cells (data not shown). The results showed no increase in doublet cells but there was a decrease in forward and side scatter in RAW 264.7 cells treated with rGal-1 compared to cells treated with rGal-1 plus lactose. These findings prompted us to assay rGal-1-treated RAW 264.7 cells for apoptotic markers, Annexin V and propidium iodide (PI), by flow cytometry.

When RAW 264.7 cells were incubated with recombinant Gal-1 in the presence and absence of lactose or mannose and stained with annexin-v, a Ca^{2+}-dependent phospholipid-binding protein that has a high affinity for phosphatidyl serine and propidium iodide, which binds tightly to nucleic acids when cells are in late-stage apoptosis or are necrotic. When cells are double positive for annexin-v and propidium iodine, the results indicate that the cells are in late-stage apoptosis. This result was observed in all assays with concentrations ranging from and at time points as early as 5 minutes. A series of qualifying assays determined that the apoptosis observed was not due to macrophage-expressed Gal-1, cell agglutination, recombinant Gal-1 protein aggregation, or endotoxin contamination. Isolated PEC were used as an alternative *ex vivo* model for determining the apoptotic effect of Gal-1 on macrophages. From three independent experiments, results did not show that exogenous recombinant Gal-1 could induce apoptosis in these cells. Knowing that

glycosylation moieties are influenced by various environmental factors,[396] an experiment using a plant lectin with high affinity for (β-1,4) -linked LacNAc (Gal-GlcNAc) was conducted to determine the level of Gal-1 ligands on the surface of RAW 264.7 cells and PEC. The results suggested that RAW 264.7 cells had higher expression of LacNAc on their cell surface than $CD11b^{+}F4/80^{-}$ and $CD11b^{+}F4/80^{+}$ cells. The higher expression of LacNAc on RAW 264.7 cells may be one explanation for observing apoptosis in these cells but not in PEC.

Previous studies on Gal-1-induced apoptosis in macrophages are limited, and no studies have evaluated the apoptosis of RAW 264.7 or PEC treated with Gal-1. One study assessed the effect of exogenous Gal-1 on monocytes isolated from the peripheral blood of human patients and macrophages isolated from surgical specimens of patients with Crohn's disease or ulcerative colitis. This study treated samples with 1.0 μM recombinant Gal-1 for 24 hours before staining with annexin-v and propidium iodine. Results revealed that Gal-1 induced apoptosis in monocytes but failed to induce cell death in macrophages.[260] This would suggest that monocytes have more Gal-1 ligands on their cell surface than macrophages. Differences in glycoprotein or glycolipid expression were not evaluated in this study. However, comparative differences in glycoconjugate expression have been evaluated in microglia, resident macrophages of the central nervous system, in M1 and M2-like polarized states. After inducing microglia polarization using IL-4 (M2-like) or INFγ (M1-like), cells were treated with exogenous Gal-1. Results showed that Gal-1 binding was significantly higher in cells that were polarized towards the M1 phenotype compared to unpolarized and M2-polarized microglia. Further evaluation was conducted using different plant lectins to determine glycoconjugate specificity. Compared to M2-like microglia, M1-like microglia had higher expression of terminal β-galactoses, which are the structures required for glycan elongation, LacNAc incorporation, and Gal-1 binding.[397] These data suggest that different

polarization states change the glycan structures present on macrophages, which could be one explanation for observing differences in DSL-binding and Gal-1-induced apoptosis in the RAW 264.7 and PEC macrophage models.

The observed apoptotic effect of Gal-1 on RAW 264.7 cells could be caspase-dependent or caspase-independent programmed cell death. Caspases are a family of cysteine proteases that act in concert in a cascade triggered by apoptotic signaling. They are inactive proenzymes that undergo proteolytic processing by upstream caspases (caspase-8 and-9). Caspase-3 is activated during the early stages of apoptosis and proteolytically cleaves caspase-7 to propagate the caspase signaling cascade. To determine if the observed apoptosis of RAW 264.7 cells treated with exogenous Gal-1 was caspase-dependent, cells treated over 5 minutes to 4 hours were assayed for caspase -3 and -7 presence. At the time points assessed, caspase-3 and -7 were not detected in Gal-1-treated cell populations. This data suggested that the late-stage apoptosis observed in RAW 264.7 cells treated with recombinant Gal-1 was not caspase-dependent. However, this evaluation is limited to early and mid-stage markers of apoptosis. The observation of double-positive staining for annexin v and propidium iodine after a short incubation period with Gal-1 indicates that the macrophages are undergoing an alternative programmed cell death pathway, such as necroptosis. Necroptosis allows cells to undergo necrosis in a programmed fashion. It is most studied in the innate immune system as a means for cells to subvert the spreading of pathogens by facilitating cellular suicide. Like necrosis, cells undergoing necroptosis rupture and leak their contents into the intracellular space. This signaling pathway begins by engaging the TNF receptor on the cell surface. The most reliable method for confirming necroptosis is measuring the downstream phosphorylation status of the kinase domain protein, MLKL, by antibody-based assays, such as

Western immunoblot, IHC, or flow cytometry. Future studies evaluating the effect of Gal-1 on macrophages, mainly using the RAW 264.7 model, should include an evaluation of necroptosis.

Our early studies focused on discovery-based approaches for identifying a targetable pathway for CLBC and led to identifying Gal-1 overexpression at the protein and RNA level in both murine and human claudin-low tumors. Flow cytometry apoptosis experiments assaying Annexin V and PI demonstrated that treatment of RAW 264.7 cells with recombinant galectin-1 led to dose- and carbohydrate-dependent apoptosis. To conduct studies on the effect of T11 tumor-derived galectin-1 on $CD11b^+$ cells, we tested the concentration of galectin-1 in cultured T11 media by ELISA. However, the concentration of tumor-expressed Gal-1 in the cultured media did not appear to be sufficient to induce rGal-1-induced apoptosis. One publication on Gal-1-induced immune cell apoptosis, secreted Gal-1 bound to the cell surface or extracellular matrix had a more substantial effect than soluble Gal-1. Gal-1 on Matrigel was found to kill T cells at ten-fold less concentration compared to soluble Gal-1.[398] The Gal-1 concentration from whole tumor lysate were estimated to be 1.4 nM (**Chapter 4, Figure 18**), which is 71-fold lower than the lowest dose range tested *in vitro* on RAW 264.7 cells (**Chapter 5, Figure 26**) Collectively, these findings suggest that Gal-1 is not at a high enough concentration within primary tumors to induce $CD11b^+$ cell apoptosis.

To determine if Gal-1 could be a suitable target for CLBC therapy, an *in vivo* study was conducted using an allosteric Gal-1 inhibitor known as OTX008. OTX008 is a topomimetic of galectin-1-targeting peptide Anginex, a potent angiogenic inhibitor developed in 2001.[312] OTX008 is more chemically stable, more resistant to hydrolysis, and has higher Gal-1 specificity than Thiodigalactoside (TDG) and Anginex. TDG has previously been used in TNBC *in vivo* murine studies but has cross-reactivity with galectins-3, -8, and -9, and Anginex can interact with

Gal-2, -7, -8 and 9 but at a lower specificity compared to Gal-1.[181, 313] OTX008 is specific for Gal-1 with no known cross-reactivity with other galectins. It prevents Gal-1 from interacting with its ligands by binding to dimerized Gal-1 at a site more distant from the CRD.[318]

OTX008 or PBS was administered to tumor-bearing mice through an intraperitoneal injection every three days once the average tumor size for all mice reached approximately 100 mm^3. This experimental design was based on previous *in vivo* experiments using OTX008 to treat various cancers.[274, 393, 399] Tumor volume was measured daily, and body weight was measured on injection days. The OTX008 treatment group showed a significant decrease in tumor growth compared to PBS-treated mice 12 days after tumor injection and after two injections. Overall body weight and condition were not significantly different between the two groups, suggesting no apparent toxicity.

This study was the first to use OTX008 as an inhibitor of Gal-1 in breast cancer. One previous 4T1 basal-like mouse model study used TGD to inhibit Gal-1. This study showed a decrease in tumor growth at nine days post-tumor injection after just one administration of TDG.[181] Due to the lack of specificity of TDG for Gal-1, it is unclear from this data whether the decrease in tumor size results from Gal-1, another form of galectin, or a combined effect from inhibiting multiple galectins. This study also used direct intertumoral injections of TDG at 40-120 mg/kg to achieve these results.

OTX008 efficacy was evaluated in several cancer cell lines *in vitro* and *in vivo* using a murine ovarian carcinoma model. In these studies, epithelial-derived ovarian cancers were shown to be more sensitive to OTX008 than cells of mesenchymal origin.[392] This could be due to the significantly higher expression of Gal-1 in mesenchymal cancers compared to other cancers and breast cancer subtypes.[400] To achieve more significant tumor growth reduction, CLBC may require a higher dose or more frequent injections than we used in this study design. High Gal-1

expressing CLBC may require alternative injection methods, such as intratumoral injection, to achieve a higher inhibitor concentration at the target site. Most of the studies that have previously used OTX008 in murine models used an intraperitoneal injection method at doses of 5-10 mg/kg. In human ovarian cancer (MA148) and murine melanoma (B16), injections were given daily, while human ovarian carcinoma (A2780-1A9 and SQ20B) received injections only three times per week.[274, 393, 399] Given that these tumors arise from different source tissues, their biological activity will differ significantly from the T11 CLBC model. Therefore, leveraging this data for the development or enhancement of a protocol to inhibit Gal-1 in the T11 CLBC model poses a considerable challenge. *In vivo* growth inhibition hinges on numerous variables, encompassing the drug's capacity for absorption into the bloodstream and the tumor, its permeability within the tumor, tumor metabolism, the extent of tumor vascularization, and the composition of the tumor extracellular matrix. Achieving systemic concentrations that surmount these physiological barriers is imperative to optimizing the protocol.

Additionally, there are no reports of Gal-1 protein concentrations in the cell lines MA148, A2780-1A9 or SQ20B to compare with our Gal-1 ELISA or Western blot data from T11 primary tumors. While one study presented Gal-1 Western blot data for the murine B16 melanoma cultured cell line, the relative Gal-1 concentrations were calculated as a ratio of Gal-1 to β-actin rather than using the relative concentration based on Gal-1 band intensity and total protein concentration. Astorgues-Xerri et al. showed differential RNA fold changes determined by comparing Gal-1 expression levels to the housekeeping gene, TBP, in several *in vitro* cell lines, including A2780-1A9 and SQ20B. However, as OTX008 targets the translated protein rather than the RNA, these expression levels fail to provide insight into the amount of OTX008 needed to inhibit Gal-1 protein effectively.[392]

Intratumoral injection is not the ideal method for administering anti-tumor therapy as it could lead to ulceration of the tumors at the injection site and is unlikely to be reproducible in a clinical setting. Daily intraperitoneal or systemic intravenous injections would be preferred to maintain a higher concentration of OTX008 and a more substantial level of inhibition. Additionally, injections were started in the protocol used for our *in vivo* experiment when the average tumor size for all mice was approximately 100 mm^3. Tumor growth varies among mice. On the first day of injection, the average tumor size was comparable between the two treatment groups (167.3±91.6 mm^3 PBS and 183.5±121.3 mm^3 OTX008) with the largest tumors in the OTX008 group; however, measurable tumors ranged from 14.0-429.4 mm^3 across both groups. Additionally, if the three largest tumors in the control group are removed from the overall dataset, the OTX008 and PBS treated mice are not significantly different by 2-way ANOVA nor by testing the slope of the lines by linear regression. However, these three tumors in the PBS treated group were not determined as outliers using interquartile range, ROUT, nor Grubbs' outlier analysis. The biological variability in tumor growth is consistent with previous studies using this transplant method. Several factors may contribute to the biological variability in tumor growth. The likely explanation for the observed disparity in tumor growth is that variations in syringe loading or leakage from the tumor injection site result in an unequal implantation of viable tumor cells across mice.

While there is not enough power in this dataset to conduct a subanalysis evaluating the growth rate differences, beginning treatment when the tumors are smaller than 100 mm^3 would likely show a more prominent difference in growth rate between the two groups. Due to the high variability in tumor growth, a larger sample size would also show more substantial group differences in the treatment effect. A post-hoc power analysis was conducted using a z-based model. The calculation was conducted using the sample size, mean and standard deviation from each group on

day 14 of the *in vivo* study. The effect size was determined using a one-tailed test assuming an alpha (α, type I error probability) of 0.05 and a sigma (σ, population variance) value of 1. Results showed the study was powered at 47.3% with an α=0.05, indicating that this study did not have high statistical power, which may result in a Type I error with a false conclusion that OTX008 has a significant treatment effect. Future studies will require a minimum of 30 mice per group to achieve 80% power at a significance criterion of α=0.05.

Mice from our *in vivo* study were euthanized 14-15 days post-tumor injection after three treatments. Tumor tissue was collected to test the hypothesis that the presence of Gal-1 results in quantitative differences in the types of $CD11b^+$ myeloid-derived cells in CLBC. Flow cytometry analysis determined the percentage of each infiltrating myeloid cell type defined in **Figure 33**. There was no significant difference in the percentage of the populations between PBS- and OTX008-treated mice. M-MDSC were approximately 6.3±2.9% (PBS) and 5.5±2.5% (OTX008) of the total $CD11b^+$ cells. In this assay, F4/80 was added to delineate M-MDSC from monocytes compared to previous flow cytometry analysis on T11 tumors, which only used Ly6C and Ly6G to differentiate M-MDSC from G-MDSC. Despite this difference, the percentage of M-MDSC and neutrophils detected in this experiment was comparable to the previous analysis. TAM were the largest population of infiltrating myeloid cells with an average of 52.9±7.3% (PBS) and 54.7±7.6% (OTX008). Neutrophils were the lowest population of infiltrating $CD11b^+$ myeloid cells, with an average of 2.6±1.0% (PBS) and 2.8±0.9% (OTX0008). Publications on the effect of exogenous Gal-1 on neutrophils are limited, and there have been no publications on this subject in cancer. Under inflammatory conditions, exogenous Gal-1 has been shown to inhibit activation, chemotaxis, and extravasation of neutrophils and promote phosphatidylserine exposure, promoting apoptosis and phagocytic removal of neutrophils.[243, 244, 248] There was no significant change in the

level of LacNAc ligands, as determined by DSL-binding when comparing PBS- to OTX008-treated tumors. TAM expressed had the highest MFI, while M-MDSC displayed the lowest. Monocytes displayed a significantly higher MFI than macrophages, consistent with previous findings that show exogenous Gal-1 can interact with monocytes but has a lower affinity to macrophages.[260]

To determine if OTX008 inhibition would make a quantitative difference in the number of $CD11b^+$ or $CD3^+$ cells *in vivo,* T11 tumors treated with OTX008 or PBS were sectioned and stained with TUNEL and anti-CD11b or anti-CD3. TUNEL assays identify apoptotic cells by detecting fragmented DNA within a cell. Two different fluorescent microscopy data collection methods were utilized to obtain the most information from each sample. Overall, TUNEL MFI data was collected using the CD7 Cell Discoverer, which provided an overall tissue image that could be used to determine the $TUNEL^+$ MFI signal across the entire tumor section. Confocal microscopy evaluated the number of $CD3^+$ and $CD11b^+$ cells and the percentage of each apoptotic immune cell type. Neither analysis detected a statistical difference in the number of infiltrating $CD3^+$ or $CD11b^+$ cells or the amount of detectable apoptosis in PBS- or OTX008-treated tumors. There are two reports of Gal-1 knockdown or inhibition in the TNBC 4T1 model. Both studies were reported from the same laboratory and show a significant increase in the percentage of T cells after Gal-1 knockdown or inhibition. Using thiodigalactoside to competitively inhibit Gal-1 binding to its carbohydrate ligands, Ito et al. showed that Gal-1 inhibition increased $CD8^+$ infiltration into primary tumors, reduced lung metastases, and increased $TUNEL^+$ apoptotic cancer cells and $CD3^+$ T cells in lung metastases.[181, 182] Likewise, using a 4T1 Gal-1 knockdown model, $CD3^+$ cell infiltration into the primary tumor and at metastatic sites was increased in mice implanted with Gal-1 knockdown tumors compared to vector controls.[182] Our discrepant findings may be due to

differences in the tumor models and methodologies (e.g., basal-like tumors versus CLBC, metastatic tumors versus primary tumor, primary tumor size at start of treatment, or intratumoral versus intraperitoneal injection method, or method of Gal-1 inhibition.)

Despite our data being contradictory to the two previous reports showing an increase in the percentage of T cells after Gal-1 knockdown or inhibition, our data is reliable. To determine overall apoptosis in tumor sections, we used two different florescent microscopes to collect data on the tissue sections, Cell Discoverer 7 and Confocal, and evaluated the average MFI at the tumor (n=4) and section level (n=2-8 per tumor). The data was highly variable, but the distribution of the data in both treatment groups is similar. The variability in samples from immunofluorescence is due to the nature of the technique. The tumor sections are a snapshot of the tumor in a 5 μm section. The differences observed across sections are due to differences in cell types and densities and the spatial distribution throughout the tumor, which is largely unpredictable and can be affected by tumor stage and size. For confocal, data was collected on a high enough number of sections and analyzed regions of interest that give us enough evidence to conclude that Gal-1 in the *in vivo* tumor microenvironment is not causing apoptosis of $CD3^+$ or $CD11b^+$ positive cells. Similarly, in the flow data, we did not observe a difference in the percentage of infiltrating $CD11b^+$ cells. The flow data has less variability compared to the confocal data because it is a larger area of the tumor that is dissociated into single-cell suspensions. This reduces the influence of tissue heterogeneity because we are no longer observing the cells within the spatial distribution of the tumor. None of the data described herein was compromised. In the florescent microscopy experiments, DNase-treated samples were used as positive controls for TUNEL staining. Likewise, isotype-matched controls were used for antibody staining controls. In the flow data, samples were appropriately compensated using single-stained tumor cells, and isotype-matched

controls were used to help determine levels of non-specific staining in the samples. There were no unexpected observations in the flow dot plots or histograms. Samples were kept on ice throughout the staining process and assayed immediately after staining. Additionally, the overall percentage of infiltrating $CD11b^+$ cells was comparable to the percentages obtained in flow analysis for T11 cells discussed in Chapter 3.

The effect of Gal-1 expression on myeloid subtypes in breast cancer has not previously been evaluated. While OTX008 inhibition suggests inhibiting Gal-1 may decrease tumor growth, it does not appear to affect the immune cell response in the TME. This is the first study evaluating the impact of Gal-1 inhibition in CLBC. However, there have been only two studies in cancer to determine the effect of tumor-derived Gal-1 on myeloid cells; both were conducted in glioblastoma. Verschuere et al. showed that the silencing of glioma-derived Gal-1 significantly decreased the number of brain-infiltrating macrophages and MDSC in a mouse glioma model. In another glioblastoma study, Chen et al. showed that the knockdown of LGALS1 inhibited the immunosuppressive microenvironment by down-regulating M2 macrophages and MDSC cells and by decreasing immunosuppressive cytokines such as CCL2, VEGFA, and TGF-β.[401] The TME is unique to the tumor type and subtype, as we observed in the early characterization studies of 2225LM and T11. While this data does not show any changes in the infiltrating immune cells after Gal-1 inhibition, it should not prevent future studies from evaluating this further with alternative, possibly more effective Gal-1 inhibitors. Alternatively, future studies should consider the effect of Gal-1 inhibition on angiogenesis. One study in the 4T1 model of TNBC showed a significant decrease in angiogenesis when Gal-1 was inhibited. A reduction in angiogenesis would slow tumor cell growth and could be an alternative explanation for this study's observed slowed tumor

growth. Additional Gal-1 pathways to consider for future experiments in CLBC are discussed in **Chapter 6**.

CHAPTER 6: DISCUSSION AND FUTURE DIRECTIONS

Triple negative claudin-low breast cancer (CLBC) is a subtype of breast cancer that lacks expression of estrogen, progesterone, and human epidermal growth factor 2 receptors. Since it does not express these receptors, it is not responsive to therapies targeting these receptors. Therefore, the standard of care involves toxic chemotherapies. CLBC is frequently accompanied by increased invasiveness and a poor prognosis; therefore, patients have a shorter overall survival and are at a higher risk of recurrence compared to other breast cancer subtypes. Approximately 7-14% of breast cancer patients have the claudin-low phenotype.[3, 20] CLBC has low mutational burden and low level of genomic instability compared to the other subtypes.[402] Additionally, there is a greater variation in the mutational burden, degree of copy number aberration, and no specific genomic aberrations accurately delineate claudin-low tumors.[403] Claudin-low tumors can be BRCA-deficient, but these tumors display lower expression of epithelial-to-mesenchymal transition features and align strongly with the basal-like phenotype.[404]

A comprehensive understanding of CLBC progression and metastasis requires models for investigating potential targets for therapy. In this work, we developed a reliably metastatic model of CLBC using the murine T11 claudin-low tumor (see Chapter 3). When transplanted into a syngeneic mouse with an intact immune system, T11 gene expression mirrors human claudin-low gene profiles. Through RNA sequencing analysis, we showed that the tumors maintained expression of intrinsic claudin-low genes with demonstrated low expression of tight junction proteins, claudins -3, -4, -7, and cell-cell adhesion protein, E-cadherin, despite serial passaging in nude rats and syngeneic mice. Additionally, the tumors had high expression of markers indicative of stem-cell like properties and the epithelial-to-mesenchymal transition, such as Vimentin and Snai1. To identify potential targets for therapy, we conducted differential expression analysis on

RNASeq data from three lung samples that contained metastatic lesions compared to two normal control lungs. Volcano plots four differentially expressed genes with the highest statistical significance and fold change that could be of interest in future studies investigating CLBC. The most differentially upregulated proteins were cyclin-dependent kinase inhibitor 2a (Cdkn2a), Myc proto-oncogene (Myc), S100 calcium-binding protein a4 (S100a4), and cellular retinoic acid binding protein 2 (Crabp2). All these proteins have been reported as having roles in other types of cancer. Cdkn2a encodes the p16 protein, a key regulator of cell cycle progression that functions as a tumor suppressor by impeding unchecked cell growth through interactions with cyclin-dependent kinases.[347] Ideally, the upregulation of Cdkn2a should enhance p16 activity, inhibiting cyclin-dependent kinases and subsequent slowdown of cell cycle progression. This attenuation of cell cycle progression should restrain unrestricted cell growth, potentially resulting in a less aggressive tumor phenotype. Despite the upregulation of Cdkn2a, T11 tumor cells do not appear to have reduced tumor growth. Therefore, mechanisms might have been developed to evade Cdkn2a cell cycle regulation, inhibiting tumor growth less effectively.

Myc is a widely recognized cell proliferation and differentiation driver, frequently implicated in cancer development and stem cells. Previous studies have shown that Myc is amplified in TNBC and the claudin-low subtype.[18] The genetic changes seen in T11 lung metastases, which result in elevated Myc expression, correspond with genetic findings previously documented in human and mouse primary claudin-low breast tumors, including T11.

The S100A4 gene-encoded protein has been identified as having the ability to regulate cell cycle progression, modulate intercellular adhesion, and enhance the invasive and metastatic characteristics of cancer cells while also having the potential to bind and inactivate the p53 suppressor protein, which governs both the G1-S transition and the transition of cells from the S

phase to mitosis (G2-M).[348] Recent studies in TNBC human and mouse models have demonstrated a positive correlation between the inhibition of S100a4 and the rate of metastases.[349, 350] Crabp2 is an integral component of retinoic acid signaling, a pathway with diverse effects on cell differentiation and proliferation. Abnormal expression of Crabp2 has been observed in various tumor types, acting as both a tumor suppressor and promoter.[351] Within TNBC, emerging data suggest that Crabp2 exerts a significant influence on regulating invasion and metastasis, correlating with a poorer prognosis.[349, 352]

The presence of these four upregulated genes in metastatic lungs highlights their potential relevance in driving the aggressive phenotype of CLBC and should be further investigated to better understand their role in driving CLBC metastatic progression. Our analysis included two normal control lungs and three lungs with metastatic lesions. In the lung samples with metastases, two samples contained one to two small metastases while the third sample was covered in metastatic lesions. The lung tissue with large, widespread metastases had a significantly higher number of tumor cells compared to the samples with only one or two small lesions. This significantly impacts the differential expression analysis due to the variability in the amount of tumor present in the sample. A more comprehensive differential expression analysis should be conducted with more samples with similar levels of tumor burden. It would also be of interest to analyze lungs from different time points before and after tumor resection to provide additional insights to how the metastatic site changes throughout tumor progression.

Chapter 4 describes our subsequent discovery-based proteomic approach to identifying targetable proteins or pathways in CLBC. We found that compared to normal tissue from healthy control mice, Gal-1, an N-acetyllactosamine binding protein, was highly differentially expressed in claudin-low primary tumors and lung metastases. Label-free quantitation, Western immunoblot,

and ELISA confirmed galectin-1 identity and significant differential expression in claudin-low orthotopic and metastatic tumors compared to normal tissue. Immunohistochemistry and gene expression analysis confirmed that, compared to other breast cancer subtypes and normal breast tissue, Gal-1 is highly expressed in both murine and human claudin-low breast tumors. We were the first to report overexpression of Gal-1 RNA and protein in primary and metastatic claudin-low tumors.[321]

Gal-1 is overexpressed in other cancers and has been implicated in pathways associated with cancer progression (refer to **Chapter 1, Table 3**). As early as 1981, it was speculated that a galactoside-specific lectin on the surface of tumor cells could regulate metastasis through the interaction of tumor cells with endothelial or immune system cells.[384] In recent years, in a few isolated studies, tumor-secreted Gal-1 has been shown to potentially be involved in tumor cell immune escape.[405] Our data and other reports suggest that Gal-1 could be a critical molecular target in cancer and a potential therapeutic target for cancer treatment. As part of this study, we conducted STRING analysis to determined protein-protein binding or co-expression between the nine unique proteins present in tumors but not control tissues **(Figure 17b).** Three of the nine proteins are reported to have a role in cancer metastasis: heat shock cognate (Hspa8), myosin-9 (Myh9), and Gal-1 (Lgals1).[274, 361, 362] Seven proteins identified with differential expression in tumor samples contain the acceptor sequence required for N-linked glycosylation, except Pdai6, and all contain potential O-linked glycosylation sites, they could theoretically be ligands for Gal-1. However, there are no reports in the literature that these proteins have LacNAc residues, nor that Gal-1 interacts with or binds to these proteins. Perhaps most interestingly, Gal-1 shares a reported direct relationship with protein disulfide-isomerase A6 (Pdia6). Though, no reports discuss the specific interactions between Gal-1 and Pdia6; it is likely that their interaction is related

to the enzymatic function of Pdia6, which catalyzes the rearrangement of disulfide bonds to aid in protein folding, prevent protein aggregation and regulate protein redox states. Since Gal-1 has multivalent functions dependent on its oxidation state,[216, 287, 406, 407] Pdia6 may serve as a chaperone for Gal-1 or as a regulator of Gal-1 function. Further examination of these proteins and their interrelationships with Gal-1 in claudin-low tumors may help elucidate Gal-1 function.

Gal-1 was found to be differentially expressed in both proteomic and genomic analyses of lungs with T11 metastases compared to normal control tissue. Normalized RNASeq read counts of *Lgals1* had counts of 1525 in normal controls (n=2) and 53,764 (n=3) in lungs with T11 metastases, a 5 $\log_2$ fold increase with a p-value ≤ 0.0001. *Lgals1* was not the most differentially expressed gene in these samples, but it was within the top 113 differentially upregulated genes. Similarly, our published proteomic data showed high levels of Gal-1 protein expression in lung samples with T11 metastases compared to normal lungs. Gal-1 exhibited the highest sequence coverage and high abundance rank order among nano-LC-MS/MS-identified proteins shared by CLBC but not normal tissue and placed in the top 9% of identified proteins in T11 by abundance rank order. Notably, label-free quantitation documented a significant 4.5 log2 fold increase in the differential expression of Gal-1 in lung metastases.

Review articles have summarized the evidence from a small number of *in vitro* studies and *in vivo* mouse models of various cancers have suggested that Gal-1 promotes tumor proliferation, invasion, metastasis, angiogenesis, and immune evasion.[205, 274] While the mechanism of action for Gal-1 remains unclear, the notable overexpression of Gal-1 in cancer progression suggests it plays a significant role in cancer-related processes. Three studies have examined the effect of Gal-1 inhibition on metastasis in the 4T1 basal-like murine model and have shown that knockdown of Gal-1 in tumor cells reduced the number of metastatic lesions in the lung and increased the

percentage of tumoricidal T cell populations at metastatic sites,[180, 182, 386] supporting the premise that Gal-1 is an important mediator of metastasis in TNBC. Prior to our work, there were no reports showing overexpression of Gal-1 RNA and protein in primary or metastatic CLBC or investigations of Gal-1 inhibition in CLBC.

As previously discussed, in characterization studies of the T11 tumor line, we found that macrophages were a significant component of the TME. The prevalence of the type of immunosuppressive mechanism depends on the type of macrophages or MDSCs present in the TME and the stage and site of the suppression. MDSCs are heterogeneous due to the presence of various immature myeloid-derived cell subsets and immunosuppressive independent of their diverse phenotypes, while TAMs possess a greater capacity for functional and phenotypic adaptation and assume pro- or anti- tumor activities dependent on the tumor microenvironment. Both MDSCs and pro-tumor TAMs aid in tumor growth and progression and share commonalities in secretion of immunoregulatory mediators, which are like those involved in wound repair, such as arginase, IL-10, G-CSF, MCP-1, KC, and VEGF.[88-90] Gal-1 has been shown to influence monocyte and macrophage function in other types of diseases and MDSC activity in many types of cancer.[408, 409] However, the effect of tumor-expressed Gal-1 on $CD11b^+$ myeloid-derived cells in breast cancer has not been investigated.

To evaluate Gal-1 as a potential target for therapy and the potential effect of Gal-1 on $CD11b^+$ myeloid cells, we conducted an *in vivo* study with the Gal-1 OTX008 inhibitor. OTX008 is a topomimetic of galectin-1-targeting peptide Anginex, a potent angiogenic inhibitor developed in 2001.[312] OTX008 is more chemically stable, more resistant to hydrolysis, and has higher Gal-1 specificity than Thiodigalactoside (TDG) and Anginex. TDG has previously been used in TNBC *in vivo* murine studies but has cross-reactivity with galectins-3, -8, and -9, and Anginex can interact

with Gal-2, -7, -8 and 9 but at a lower specificity compared to Gal-1.[181, 313] OTX008 is specific for Gal-1 with no known cross-reactivity with other galectins. It prevents Gal-1 from interacting with its ligands by binding to dimerized Gal-1 at a site more distant from the CRD as compared to Anginex.[318]

Our results on tumor growth showed a statistically significant decrease in tumor volume at day 14 post-tumor implant in the OTX008-treated group compared to vehicle control. Although not identified as outliers by three separate methods (interquartile range, ROUT, and Grubbs'), three of the eight mice in the vehicle control group had high volume tumors that significantly contributed to these results. If these three mice were removed from the dataset, the statistical differences in tumor volume and the rate of tumor growth (slopes) between the test and control groups would be lost. The differences in biological response may have been due to technical variations in the tumor cell injection process (e.g., variability in syringe loading or leakage from the injection site) that can contribute to the different biological responses in syngeneic littermates. Larger numbers of mice in both groups would help address this concern and are needed to validate these initial findings.

The use of field standard caliper measurements and calculations for tumor volume is most frequently used in murine tumor growth studies. These measurements were conducted by blinded personnel, but this type of assessment remains susceptible to bias. Upon weighing the tumors after sacrifice and resection, there were no differences in tumor weight between the two groups, but this method is also susceptible to bias and technical limitations. The tumor weights may be affected by factors such as the extent of necrosis, the types of infiltrating cells, dissection accuracy, precision, and the handling of tissues during dissection. Scale accuracy and environmental conditions, such as temperature and humidity, can also contribute to variations. To minimize

technical variations in the dissection for these experiments, measures were taken to ensure consistency. Dissections were conducted over two consecutive days at the same time of day, utilizing the same calibrated scale. Furthermore, the removal of tumors was performed by a single operator, and a separate operator was responsible for weighing the tumors. More robust techniques are available for tumor *in vivo* tumor volume assessments, such as bioluminescence imaging or small animal MRI, and should be utilized in future studies for more accurate tumor measurements.

Our *in vivo* studies focuses on OTX008, which acts as a non-competitive Gal-1 allosteric inhibitor and prevents carbohydrate binding. It has been suggested that it may inactive Gal-1 via oxidation, leading to a major conformational change and proteasomal degradation.[392] While there are no published reports on the association or dissociation measurements for OTX008 to Gal-1, we can speculate on the molar ratios of OTX008 to Gal-1 that are required to inhibit Gal-1-carbohydrate interactions. Protein-protein interactions are known to exhibit high affinity, particularly when they are involved in critical cellular processes, such as enzyme substrate interactions, signal transduction pathways, or the formation of protein complexes. Likewise, certain lectins, such as Gal-1, have high affinity and specificity for their target carbohydrate. As previously mentioned in **Chapter 1, Section 1.3.2**, avidity between LacNAc and Gal-1 increases when Gal-1 is dimerized and poly-LacNAc residues are branched. [207, 210] For example, the dissociation constant (Kd) of monomeric Gal-1 with a single LacNAc motif is approximately 81±12 μM as determined by isothermal titration calorimetry (ITC), but dimerized Gal-1 binds to CD45, a glycoprotein with poly-branched LacNAc residues, with a Kd of 2.3 nM.[211, 212] For comparison, the ITC determined Kd of PD-1 to PD-L1 is reported as 3.90±0.07 μM[410], which is higher than the Kd for monomeric Gal-1 to a single LacNAc motif but lower than dimerized Gal-1 binding to CD45. It is important to note that the Kd for an interaction can vary based on

experimental conditions, techniques, and specific reagents used. Likewise, biological conditions within a localized environment *in vivo* will influence binding affinities for proteins to their ligands. Therefore, the results from these studies should not be directly compared, and rather, this information should be used to generate hypotheses about the interactions between Gal-1 and LacNAc then subsequently tested.

Similarly, insights extracted from a laboratory report detailing the OTX008 to Gal-1 molar ratios to prevent Gal-1 interactions on the surfaces of target cells, including $CD4^+$ and $CD8^+$ T cells, and $CD31^+$ endothelial cells, provide a valuable reference for the design and understanding of *in vivo* Gal-1 inhibition. Specifically, the molar ratio of 200:1 (20 μM OTX008 to 0.1 μM Gal-1) was identified as necessary to reduce Gal-1 binding to $CD4^+$ or $CD8^+$ T cells by 80%. For $CD31^+$ endothelial cells, a 200:1 molar ratio decreased binding by 50% and by increasing the ratio to 1000:1 (100 μM OTX008 to 0.1 μM Gal-1) further improved the percentage of unbound ligand to 70%.[395] While this experimental data aids in the design and interpretation of study outcomes, it's essential to recognize the limitations inherent in its *in vitro* nature, preventing direct extrapolation to *in vivo* studies.

Based on ELISA data from whole primary tumors lysates (**Chapter 4, Figure 18**), where the average concentration of Gal-1 was measured at 17.8 ng Gal-1/mg tissue and considering an average tumor weight of 940 mg from OTX008-treated tumors, we calculated that each tumor contains approximately 1.2 nmol of Gal-1 (using the molecular weight of 14,000 g/mol). With a drug administration volume of 10 mg/kg in an average 18.5-gram mouse; each mouse received approximately 197 nmol OTX008 (with a molecular weight of 937.18 g/mol). Consequently, the molar ratio of OTX008 to Gal-1 in our study was 164:1. This ratio closely aligns with the *in vitro* molar ratio determined by Dings et al. (200:1), which was effective in preventing Gal-1 from

binding to 70% of T cells and 50% endothelial cells. This suggests that we employed a molar ratio significant enough to impede Gal-1 interactions with its ligand.[395] However, as previously discussed in this chapter, *in vitro* concentrations cannot be directly correlated to *in vivo* dosing. *In vivo* calculations of OTX008 to Gal-1 molar ratios are theoretical because we did not directly evaluate tumor concentrations of OTX008. Nano-LC-MS/MS analysis on trypsin-digested tumor lysates after OTX008 administration should be included in these studies to provide precise determination of the OTX008 concentration in primary tumors and systemic blood. Flash frozen tumors collected as part of the *in vivo* study reported herein could be used to conduct these analyses. This information could help guide future *in vivo* experiments and would allow for more robust data acquisition and hypothesis testing to determine the roles of Gal-1 in CLBC, such as evaluating the effect of Gal-1 inhibition on metastatic disease.

Off-target effects have not been reported by others. Although the off-target effects of OTX008 on ligand binding and cell viability have not been determined, it is assumed that the primary action of OTX008 is on Gal-1 since a dose-dependent response is observed in studies conducted by Dings et al.[315, 317, 318, 395] When higher concentrations of Gal-1 are present, more OTX008 is required to observe similar inhibitory effects on surface binding, agglutination, and cell proliferation. In one study evaluating the effect of OTX008 on cell viability using an *in vitro* model of oral squamous cell carcinoma, dose ranges of 55-186 μg/mL (59-198 μM) were required to reach IC50. Results showed that the observed decrease in viability was dose and time dependent and resulted in an upregulation of FOS. The authors hypothesized that the observed tumor cell apoptosis occurred through early induction of MAPK pathway; however, the study provided no evidence of Gal-1 binding.[411] Another study showed higher Gal-1 expression levels correlated with mesenchymal markers, such as Vimentin, and low RNA levels of epithelial markers, such as E-cadherin.[392]

These markers are consistent with the CLBC phenotype, which is characterized by low expression of tight-junction proteins, claudin-3, -4, and -7, and cell-cell adhesion protein, E-cadherin.[17] Our RNASeq data confirmed expression of these markers in the murine claudin-low T11 tumors, as well as high expression of Vimentin. One study evaluated the effect of Gal-1 inhibition with OTX008 on mesenchymal phenotypes by using two pairs of *in vitro* epithelial to mesenchymal models, COLO205-S/ COLO205-R (human colorectal cancer) and MCF7/ MCF7-shWISP (human luminal A breast cancer). Results showed OTX008 had more potent antiproliferative effects on the epithelial models compared to their mesenchymal counterparts, both mesenchymal cells lines requiring ≥300 μM OTX008 to reduce cell proliferation by 50%.[274] This suggests that OTX008 may not be a potent enough inhibitor for the high expression levels of Gal-1 observed in the claudin-low T11 mouse model. However, it is difficult to correlate these *in vitro* concentrations to *in vivo* dosing. In addition, OTX008 in our studies was injected systemically (i.p.) and most certainly would bind to Gal-1 protein encountered prior to reaching the tumor, thus reducing the actual molar ratio within the primary tumor.

Existing *in vitro* studies by other laboratories indicate that Gal-1 induced apoptosis in immune cells requires higher concentrations than those anticipated under physiological conditions, typically ranging from 1 to 30 μM.[219] Our own *in vitro* apoptotic studies on the immortal macrophage cell line RAW 264.7, conducted with Gal-1 concentrations ranging from 0.1-1 μM, revealed concentration-dependent, carbohydrate-specific apoptosis at all dilutions. However, when RAW 264.7 cells were cultured in T11 cell conditioned media (with lower concentration ranging from 0.6-3.3 nM), *in vitro* apoptosis was not observed. Given the inability to observe apoptosis in non-transformed PEC, we transitioned to an *in vivo* model to assess the effects of Gal-1 inhibition on tumor and immune cells. Despite administering OTX008 concentrations similar to

other published *in vivo* studies in different tumor models, we did not observe alterations in immune cell infiltration or apoptosis.

While a few studies have reported changes in immune cell numbers in primary tumors and metastases following Gal-1 inhibition, these low numbers might be attributed to alternative mechanisms, such as a lack of proliferation or migration into the tumor.[180, 182, 188] It's important to acknowledge that we did not evaluate the effect of Gal-1 on immune cell function. Future investigations should consider these alternative mechanisms for immune cell regulation in the tumor microenvironment, such as immune cell migration, immune suppressive activity, and proliferation. Additionally, studies on the impact of Gal-1 on immune cell phenotypes should be thoroughly explored. Analyzing cytokine production and conducting *ex vivo* functional assays for immune cell migration and immune suppressive activity across a range of Gal-1 concentration in the nM range and at various time points is advisable. Therefore, at this juncture, the potential influence of Gal-1 on immune cell activity should still be considered a plausible mechanism of Gal-1 activity in CLBC, and further exploration is warranted in future *in vivo* studies. Additionally, future studies should include a minimum of 30 mice per group to achieve 80% power at a significant criterion of α=0.05 in addition to increasing the dosage and/or dose frequency for OTX008 administration.

OTX008 (also known as Calixarene-0118) has been in phase 1 clinical trials to treat solid tumors;[395] however, the last update on this study was in 2013.[319] The data presented in 2013 reported that 22 patients with solid tumors (50% colorectal carcinoma) received a daily subcutaneous injection of OTX008 from March 2012-March 2013, six patients received 65 mg, seven patients were dosed with 120-130 mg with 2/7 experience a dose limiting toxicity; therefore, an additional 9 patients were enrolled at 65 mg dose. The stage of disease was not reported.

Additionally, it is unknown from the data reported if all patients had primary tumor resection, but it is assumed that tumors were removed as part of the standard of care prior to administration of first-line therapy. The most common adverse events were transient and reversible neurological events, which were more common and frequent at the higher dose range. Unfortunately, the primary outcome of objective response was not obtained.[412] This suggests that OTX008 may not be a potent enough inhibitor of Gal-1 to observe improved clinical outcomes. However, there is not sufficient detail in the reported data to draw conclusions. For example, if all patients had stage IV disease, the metastatic burden may have been too high for this dose escalation regimen to be effective. Local injection site tolerance of subcutaneous administration was poor; therefore, alternative administration methods could be explored, such as limb profusion, and may result in improved outcomes and drug tolerance. It is still anticipated that high-affinity Gal-1-specific inhibitors would benefit cancer research and may introduce treatment options for certain types of cancer, especially those expressing high Gal-1.

There are other therapeutic approaches that have been explored in mouse models to target Gal-1. Several studies report that anti-Gal-1 monoclonal antibodies (mAb) could provide therapeutic benefits. These studies have shown decreased tumorigenesis in mouse models of Kaposi's sarcoma, oral squamous carcinoma, and prostate cancer.[290, 413, 414] Antibodies are expensive to produce and would require stratified dosing depending on the amount of Gal-1 the tumor produces. As an alternative, one recent study showed success when vaccinating mice against Gal-1 proteins in a B16 melanoma mouse model. Gal-1 vaccination suppressed tumor growth, inhibited angiogenesis, increased infiltration of $CD8^+$ T cells and M1-type macrophages (defined by CD11c positivity), and decreased infiltration of M2-type TAMS (defined by CD206-positivity).[415] One downside to this study was that the mice were vaccinated before tumor implantation. While tumor

growth was suppressed, the mice still developed tumors, suggesting that Gal-1 vaccination must be combined with another therapy. In the clinical setting, the level of potential benefit for vaccination against Gal-1 would not be known until after the patient has developed a tumor and the tumor has been tested for Gal-1 expression. However, Gal-1 vaccination after primary tumor resection may have an improved benefit over peptide inhibitors and mAbs because the patient's immune system would be activated to target Gal-1 for destruction and prevent the downstream effects of Gal-1 tumor-promoting activities.

Targeting the enzymes that regulate LacNAc addition to the carbohydrate sidechains of glycoproteins may also provide therapeutic benefit. The addition of LacNAc residues onto proteins is outlined in chapter 1, section 1.3.2. It is well known that increased Golgi expression of β-1,6-N-acetylglucosaminiltranserfase V (Mgat5) increases during carcinogenesis, resulting in branched, complex N-glycans on the surface of glycoproteins. This increase in enzyme production leads to an increase in the number of high affinity Gal-1 ligands.[416] Additionally, the secreted form of Mgat5 is also known to promote angiogenesis. Although Mgat5 is known to be critical in tumor development, the specific mechanisms are not fully understood.[416] In one murine breast cancer study, silencing Mgat5 was shown to decrease tumor progression and stimulate an anti-tumor immune response , similar to the effects observed when Gal-1 was inhibited in a 4T1 murine model of breast cancer.[417, 418] Additionally, the small molecule peracetylated 4-fluoro-glucosamine has been shown to reduce the biosynthesis of LacNAc by reducing UDP-GlcNAc synthesis, which has the downstream effect of increased anti-tumor immune cell activity and reduced tumor growth in melanoma and lymphoma in mouse models.[419] These data suggest that either the targeting the LacNAc ligand or direct targeting of Gal-1 could be suitable pathways for intervention.

Interestingly, in a panel of cell lines, Gal-1 expression was shown to positively correlate with mesenchymal markers, such as vimentin, and negatively correlate with epithelial markers, like E-cadherin.[395] This is consistent with the EMT markers and stemlike characteristics of CLBC. In our mouse and human RNA datasets, we observed tumors with high Gal-1 expression also had high expression of vimentin and low expression of E-cadherin based on the intrinsic claudin-low gene profile.[392]

A few studies have shown a decrease in angiogenesis by inhibiting Gal-1, either through knock down in primary tumors or by pharmaceutical intervention. One of these studies was conducted using the murine 4T1 basal-like breast cancer model, as previously described in the introduction. In our study, we did not evaluate the effect of Gal-1 inhibition on angiogenesis, although it is warranted in future studies. As discussed in the Chapter 1 (Introduction), others have reported that overexpression of VEGF is a characteristic of TNBC and high expression of Gal-1 correlates with expression levels of Gal-1 and CCL2. We reported in Chapter 3 that VEGF and CCL2 has significantly higher expression in 2225LM and T11 tumors compared to normal tissue. OTX008 is a derivative of the potent angiogenic inhibitor, Anginex. Anginex inhibits the formation of new blood vessels, but does not affect pre-existing blood vessels, lending to its ability to specifically target tumors.[313] In one study, Anginex was reported to significantly decrease membrane-bound H-Ras, but not K- or N-Ras with a specific reduction in Raf/Mek/Erk signaling activation in vascular endothelial cells.[316] Interestingly, another study showed that Ras signals were found to be highly expressed in CLBC, suggesting a potential correlation between Ras and Gal-1 expression.[403] Gal-1 has previously been reported in one study to directly bind with H-Ras at the cell membrane to stabilize the interaction between H-Ras and GTP. It has been proposed that this interaction alters the orientation of the H-Ras globular domain and promote the lateral segregation

of H-Ras to initiate MAPK signaling. Overexpression of Gal-1 enhances this signaling cascade.[420] The downstream effect of constituently active H-Ras is promotion of epithelial-mesenchymal transformation, which causes breast epithelial cells to become malignant. This transition is linked to increased expression of ZEB1, which is another intrinsic gene of the claudin-low phenotype.[421]

Our findings support further investigations focusing on the function, role, and significance of Gal-1 overexpression in claudin-low tumor progression. Our publication was the first to employ advanced proteomic approaches for the identification and subsequent validation of Gal-1 overexpression in claudin-low tumors. The implications of our findings suggest a compelling prospect for the use of Gal-1 inhibitors to treat this aggressive tumor subtype. Understanding the pharmacokinetics and biodistribution of OTX008 in the tumor and throughout the body would be critical to evaluate the continued potential of this specific drug. New studies should also focus on finding improved inhibitors for tumors expressing the highest levels of Gal-1. Furthermore, follow-up studies need to reassess the impact of Gal-1 inhibition on infiltrating immune cell populations, specifically probing into how Gal-1 influences immune cell phenotype and functional activity. Exploring the role of Gal-1 in angiogenesis also warrants attention. Innovative techniques like multiplex immunohistochemistry can provide spatial insights into the cellular localization of Gal-1 and its interactions with distinct cell types. In essence, our research advocates for a robust and comprehensive exploration of Gal-1 inhibition as a pivotal avenue for advancing therapeutic strategies against claudin-low tumors.

CHAPTER 7: REFERENCES

1. Fallahpour S, Navaneelan T, De P, Borgo A. Breast cancer survival by molecular subtype: a population-based analysis of cancer registry data. CMAJ Open. 2017;5(3):E734-E9.

2. Foulkes WD, Smith IE, Reis-Filho JS. Triple-negative breast cancer. N Engl J Med. 2010;363(20):1938-48.

3. Kumar P, Aggarwal R. An overview of triple-negative breast cancer. Arch Gynecol Obstet. 2016;293(2):247-69.

4. Harrell JC, Prat A, Parker JS, Fan C, He X, Carey L, et al. Genomic analysis identifies unique signatures predictive of brain, lung, and liver relapse. Breast Cancer Res Treat. 2012;132(2):523-35.

5. Badowska-Kozakiewicz AM, Budzik MP. Immunohistochemical characteristics of basal-like breast cancer. Contemp Oncol (Pozn). 2016;20(6):436-43.

6. Medina MA, Oza G, Sharma A, Arriaga LG, Hernandez Hernandez JM, Rotello VM, et al. Triple-Negative Breast Cancer: A Review of Conventional and Advanced Therapeutic Strategies. Int J Environ Res Public Health. 2020;17(6).

7. Gadi VK, Davidson NE. Practical Approach to Triple-Negative Breast Cancer. J Oncol Pract. 2017;13(5):293-300.

8. Gierach GL, Burke A, Anderson WF. Epidemiology of triple negative breast cancers. Breast Dis. 2010;32(1-2):5-24.

9. McVeigh TP, Kerin MJ. Clinical use of the Oncotype DX genomic test to guide treatment decisions for patients with invasive breast cancer. Breast Cancer (Dove Med Press). 2017;9:393-400.

10. Parker JS, Mullins M, Cheang MC, Leung S, Voduc D, Vickery T, et al. Supervised risk predictor of breast cancer based on intrinsic subtypes. J Clin Oncol. 2009;27(8):1160-7.

11. Tafreshi NK, Morse DL, Lee MC. Narrowing the focus: Therapeutic cell surface targets for refractory triple-negative breast cancer. World J Clin Oncol. 2020;11(4):169-79.

12. Reyal F, van Vliet MH, Armstrong NJ, Horlings HM, de Visser KE, Kok M, et al. A comprehensive analysis of prognostic signatures reveals the high predictive capacity of the proliferation, immune response and RNA splicing modules in breast cancer. Breast Cancer Res. 2008;10(6):R93.

13. Burstein MD, Tsimelzon A, Poage GM, Covington KR, Contreras A, Fuqua SA, et al. Comprehensive genomic analysis identifies novel subtypes and targets of triple-negative breast cancer. Clin Cancer Res. 2015;21(7):1688-98.

14. Teschendorff AE, Journée M, Absil PA, Sepulchre R, Caldas C. Elucidating the altered transcriptional programs in breast cancer using independent component analysis. PLoS Comput Biol. 2007;3(8):e161.

15. Lehmann BD, Bauer JA, Chen X, Sanders ME, Chakravarthy AB, Shyr Y, et al. Identification of human triple-negative breast cancer subtypes and preclinical models for selection of targeted therapies. J Clin Invest. 2011;121(7):2750-67.

16. Herschkowitz JI, Lubet R. Mouse models of triple negative [basal-like/claudin low] breast cancer. Breast Dis. 2010;32(1-2):63-71.

17. Perou CM. Molecular stratification of triple-negative breast cancers. Oncologist. 2011;16 Suppl 1:61-70.

18. Prat A, Parker JS, Karginova O, Fan C, Livasy C, Herschkowitz JI, et al. Phenotypic and molecular characterization of the claudin-low intrinsic subtype of breast cancer. Breast Cancer Res. 2010;12(5):R68.

19. Sabatier R, Finetti P, Guille A, Adelaide J, Chaffanet M, Viens P, et al. Claudin-low breast cancers: clinical, pathological, molecular and prognostic characterization. Mol Cancer. 2014;13:228.

20. Dias K, Dvorkin-Gheva A, Hallett RM, Wu Y, Hassell J, Pond GR, et al. Claudin-Low Breast Cancer; Clinical & Pathological Characteristics. PLoS One. 2017;12(1):e0168669.

21. Herschkowitz JI, Simin K, Weigman VJ, Mikaelian I, Usary J, Hu Z, et al. Identification of conserved gene expression features between murine mammary carcinoma models and human breast tumors. Genome Biol. 2007;8(5):R76.

22. Matossian MD, Burks HE, Bowles AC, Elliott S, Hoang VT, Sabol RA, et al. A novel patient-derived xenograft model for claudin-low triple-negative breast cancer. Breast Cancer Res Treat. 2018;169(2):381-90.

23. Knezevic J, Pfefferle AD, Petrovic I, Greene SB, Perou CM, Rosen JM. Expression of miR-200c in claudin-low breast cancer alters stem cell functionality, enhances chemosensitivity and reduces metastatic potential. Oncogene. 2015;34(49):5997-6006.

24. Usary J, Zhao W, Darr D, Roberts PJ, Liu M, Balletta L, et al. Predicting drug responsiveness in human cancers using genetically engineered mice. Clin Cancer Res. 2013;19(17):4889-99.

25. Curtis C, Shah SP, Chin SF, Turashvili G, Rueda OM, Dunning MJ, et al. The genomic and transcriptomic architecture of 2,000 breast tumours reveals novel subgroups. Nature. 2012;486(7403):346-52.

26. Pereira B, Chin SF, Rueda OM, Vollan HK, Provenzano E, Bardwell HA, et al. The somatic mutation profiles of 2,433 breast cancers refines their genomic and transcriptomic landscapes. Nat Commun. 2016;7:11479.

27. Hennessy BT, Gonzalez-Angulo AM, Carey MS, Mills GB. A systems approach to analysis of molecular complexity in breast cancer. Clin Cancer Res. 2009;15(2):417-9.

28. Fougner C, Bergholtz H, Kuiper R, Norum JH, Sørlie T. Claudin-low-like mouse mammary tumors show distinct transcriptomic patterns uncoupled from genomic drivers. Breast Cancer Res. 2019;21(1):85.

29. Choi Y, Lee S, Kim K, Kim SH, Chung YJ, Lee C. Studying cancer immunotherapy using patient-derived xenografts (PDXs) in humanized mice. Exp Mol Med. 2018;50(8):1-9.

30. Jerry DJ, Kittrell FS, Kuperwasser C, Laucirica R, Dickinson ES, Bonilla PJ, et al. A mammary-specific model demonstrates the role of the p53 tumor suppressor gene in tumor development. Oncogene. 2000;19(8):1052-8.

31. Usary J, Darr DB, Pfefferle AD, Perou CM. Overview of Genetically Engineered Mouse Models of Distinct Breast Cancer Subtypes. Curr Protoc Pharmacol. 2016;72:14.38.1-14.38.11.

32. Herschkowitz JI, Zhao W, Zhang M, Usary J, Murrow G, Edwards D, et al. Comparative oncogenomics identifies breast tumors enriched in functional tumor-initiating cells. Proc Natl Acad Sci U S A. 2012;109(8):2778-83.

33. Deepak KGK, Vempati R, Nagaraju GP, Dasari VR, S N, Rao DN, et al. Tumor microenvironment: Challenges and opportunities in targeting metastasis of triple negative breast cancer. Pharmacol Res. 2020;153:104683.

34. Taylor CT, Colgan SP. Regulation of immunity and inflammation by hypoxia in immunological niches. Nat Rev Immunol. 2017;17(12):774-85.

35. O'Meara T, Safonov A, Casadevall D, Qing T, Silber A, Killelea B, et al. Immune microenvironment of triple-negative breast cancer in African-American and Caucasian women. Breast Cancer Res Treat. 2019;175(1):247-59.

36. Gallego-Ortega D, Ledger A, Roden DL, Law AM, Magenau A, Kikhtyak Z, et al. ELF5 Drives Lung Metastasis in Luminal Breast Cancer through Recruitment of Gr1+ CD11b+ Myeloid-Derived Suppressor Cells. PLoS Biol. 2015;13(12):e1002330.

37. Kaplan RN, Riba RD, Zacharoulis S, Bramley AH, Vincent L, Costa C, et al. VEGFR1-positive haematopoietic bone marrow progenitors initiate the pre-metastatic niche. Nature. 2005;438(7069):820-7.

38. Weigelt B, Peterse JL, van 't Veer LJ. Breast cancer metastasis: markers and models. Nat Rev Cancer. 2005;5(8):591-602.

39. Denkert C, Loibl S, Noske A, Roller M, Müller BM, Komor M, et al. Tumor-associated lymphocytes as an independent predictor of response to neoadjuvant chemotherapy in breast cancer. J Clin Oncol. 2010;28(1):105-13.

40. Mohammed ZM, Going JJ, Edwards J, McMillan DC. The role of the tumour inflammatory cell infiltrate in predicting recurrence and survival in patients with primary operable breast cancer. Cancer Treat Rev. 2012;38(8):943-55.

41. Soysal SD, Tzankov A, Muenst SE. Role of the Tumor Microenvironment in Breast Cancer. Pathobiology. 2015;82(3-4):142-52.

42. Karn T, Pusztai L, Rody A, Holtrich U, Becker S. The Influence of Host Factors on the Prognosis of Breast Cancer: Stroma and Immune Cell Components as Cancer Biomarkers. Curr Cancer Drug Targets. 2015;15(8):652-64.

43. Yu X, Guo J, Zhou Q, Huang W, Xu C, Long X. A novel immune-related prognostic index for predicting breast cancer overall survival. Breast Cancer. 2021;28(2):434-47.

44. Adams S, Gray RJ, Demaria S, Goldstein L, Perez EA, Shulman LN, et al. Prognostic value of tumor-infiltrating lymphocytes in triple-negative breast cancers from two phase III randomized adjuvant breast cancer trials: ECOG 2197 and ECOG 1199. J Clin Oncol. 2014;32(27):2959-66.

45. Loi S, Michiels S, Salgado R, Sirtaine N, Jose V, Fumagalli D, et al. Tumor infiltrating lymphocytes are prognostic in triple negative breast cancer and predictive for trastuzumab benefit in early breast cancer: results from the FinHER trial. Ann Oncol. 2014;25(8):1544-50.

46. Loi S, Sirtaine N, Piette F, Salgado R, Viale G, Van Eenoo F, et al. Prognostic and predictive value of tumor-infiltrating lymphocytes in a phase III randomized adjuvant breast cancer trial in node-positive breast cancer comparing the addition of docetaxel to doxorubicin with doxorubicin-based chemotherapy: BIG 02-98. J Clin Oncol. 2013;31(7):860-7.

47. Taylor NA, Vick SC, Iglesia MD, Brickey WJ, Midkiff BR, McKinnon KP, et al. Treg depletion potentiates checkpoint inhibition in claudin-low breast cancer. J Clin Invest. 2017;127(9):3472-83.

48. Bos PD, Plitas G, Rudra D, Lee SY, Rudensky AY. Transient regulatory T cell ablation deters oncogene-driven breast cancer and enhances radiotherapy. J Exp Med. 2013;210(11):2435-66.

49. Bates GJ, Fox SB, Han C, Leek RD, Garcia JF, Harris AL, et al. Quantification of regulatory T cells enables the identification of high-risk breast cancer patients and those at risk of late relapse. J Clin Oncol. 2006;24(34):5373-80.

50. Bohling SD, Allison KH. Immunosuppressive regulatory T cells are associated with aggressive breast cancer phenotypes: a potential therapeutic target. Mod Pathol. 2008;21(12):1527-32.

51. Ohara M, Yamaguchi Y, Matsuura K, Murakami S, Arihiro K, Okada M. Possible involvement of regulatory T cells in tumor onset and progression in primary breast cancer. Cancer Immunol Immunother. 2009;58(3):441-7.

52. Pruneri G, Gray KP, Vingiani A, Viale G, Curigliano G, Criscitiello C, et al. Tumor-infiltrating lymphocytes (TILs) are a powerful prognostic marker in patients with triple-negative breast cancer enrolled in the IBCSG phase III randomized clinical trial 22-00. Breast Cancer Res Treat. 2016;158(2):323-31.

53. Kroemer G, Senovilla L, Galluzzi L, André F, Zitvogel L. Natural and therapy-induced immunosurveillance in breast cancer. Nat Med. 2015;21(10):1128-38.

54. Gao ZH, Li CX, Liu M, Jiang JY. Predictive and prognostic role of tumour-infiltrating lymphocytes in breast cancer patients with different molecular subtypes: a meta-analysis. BMC Cancer. 2020;20(1):1150.

55. Muenst S, Schaerli AR, Gao F, Däster S, Trella E, Droeser RA, et al. Expression of programmed death ligand 1 (PD-L1) is associated with poor prognosis in human breast cancer. Breast Cancer Res Treat. 2014;146(1):15-24.

56. Pedoeem A, Azoulay-Alfaguter I, Strazza M, Silverman GJ, Mor A. Programmed death-1 pathway in cancer and autoimmunity. Clin Immunol. 2014;153(1):145-52.

57. O'Donnell JS, Teng MWL, Smyth MJ. Cancer immunoediting and resistance to T cell-based immunotherapy. Nat Rev Clin Oncol. 2019;16(3):151-67.

58. Muenst S, Soysal SD, Gao F, Obermann EC, Oertli D, Gillanders WE. The presence of programmed death 1 (PD-1)-positive tumor-infiltrating lymphocytes is associated with poor prognosis in human breast cancer. Breast Cancer Res Treat. 2013;139(3):667-76.

59. Chapon M, Randriamampita C, Maubec E, Badoual C, Fouquet S, Wang SF, et al. Progressive upregulation of PD-1 in primary and metastatic melanomas associated with blunted TCR signaling in infiltrating T lymphocytes. J Invest Dermatol. 2011;131(6):1300-7.

60. Dong H, Strome SE, Salomao DR, Tamura H, Hirano F, Flies DB, et al. Tumor-associated B7-H1 promotes T-cell apoptosis: a potential mechanism of immune evasion. Nat Med. 2002;8(8):793-800.

61. Alsuliman A, Colak D, Al-Harazi O, Fitwi H, Tulbah A, Al-Tweigeri T, et al. Bidirectional crosstalk between PD-L1 expression and epithelial to mesenchymal transition: significance in claudin-low breast cancer cells. Mol Cancer. 2015;14:149.

62. Gao M, Wang T, Ji L, Bai S, Tian L, Song H. Therapy With Carboplatin and Anti-PD-1 Antibodies Before Surgery Demonstrates Sustainable Anti-Tumor Effects for Secondary Cancers in Mice With Triple-Negative Breast Cancer. Front Immunol. 2020;11:366.

63. Huang W, Ran R, Shao B, Li H. Prognostic and clinicopathological value of PD-L1 expression in primary breast cancer: a meta-analysis. Breast Cancer Res Treat. 2019;178(1):17-33.

64. Freeman GJ, Long AJ, Iwai Y, Bourque K, Chernova T, Nishimura H, et al. Engagement of the PD-1 immunoinhibitory receptor by a novel B7 family member leads to negative regulation of lymphocyte activation. J Exp Med. 2000;192(7):1027-34.

65. Lipson EJ, Forde PM, Hammers HJ, Emens LA, Taube JM, Topalian SL. Antagonists of PD-1 and PD-L1 in Cancer Treatment. Semin Oncol. 2015;42(4):587-600.

66. Nanda R, Chow LQ, Dees EC, Berger R, Gupta S, Geva R, et al. Pembrolizumab in Patients With Advanced Triple-Negative Breast Cancer: Phase Ib KEYNOTE-012 Study. J Clin Oncol. 2016;34(21):2460-7.

67. Plitas G, Konopacki C, Wu K, Bos PD, Morrow M, Putintseva EV, et al. Regulatory T Cells Exhibit Distinct Features in Human Breast Cancer. Immunity. 2016;45(5):1122-34.

68. Li CW, Lim SO, Xia W, Lee HH, Chan LC, Kuo CW, et al. Glycosylation and stabilization of programmed death ligand-1 suppresses T-cell activity. Nat Commun. 2016;7:12632.

69. Lee HH, Wang YN, Xia W, Chen CH, Rau KM, Ye L, et al. Removal of N-Linked Glycosylation Enhances PD-L1 Detection and Predicts Anti-PD-1/PD-L1 Therapeutic Efficacy. Cancer Cell. 2019;36(2):168-78.e4.

70. Li CW, Lim SO, Chung EM, Kim YS, Park AH, Yao J, et al. Eradication of Triple-Negative Breast Cancer Cells by Targeting Glycosylated PD-L1. Cancer Cell. 2018;33(2):187-201.e10.

71. Chung W, Eum HH, Lee HO, Lee KM, Lee HB, Kim KT, et al. Single-cell RNA-seq enables comprehensive tumour and immune cell profiling in primary breast cancer. Nat Commun. 2017;8:15081.

72. Azizi G, Abolhassani H, Kiaee F, Tavakolinia N, Rafiemanesh H, Yazdani R, et al. Autoimmunity and its association with regulatory T cells and B cell subsets in patients with common variable immunodeficiency. Allergol Immunopathol (Madr). 2018;46(2):127-35.

73. Mahmoud SM, Lee AH, Paish EC, Macmillan RD, Ellis IO, Green AR. The prognostic significance of B lymphocytes in invasive carcinoma of the breast. Breast Cancer Res Treat. 2012;132(2):545-53.

74. Arias-Pulido H, Cimino-Mathews A, Chaher N, Qualls C, Joste N, Colpaert C, et al. The combined presence of CD20 + B cells and PD-L1 + tumor-infiltrating lymphocytes in inflammatory breast cancer is prognostic of improved patient outcome. Breast Cancer Res Treat. 2018;171(2):273-82.

75. Eiró N, Pidal I, Fernandez-Garcia B, Junquera S, Lamelas ML, del Casar JM, et al. Impact of CD68/(CD3+CD20) ratio at the invasive front of primary tumors on distant metastasis development in breast cancer. PLoS One. 2012;7(12):e52796.

76. Thompson E, Taube JM, Elwood H, Sharma R, Meeker A, Warzecha HN, et al. The immune microenvironment of breast ductal carcinoma in situ. Mod Pathol. 2016;29(3):249-58.

77. Murray PJ, Wynn TA. Obstacles and opportunities for understanding macrophage polarization. J Leukoc Biol. 2011;89(4):557-63.

78. Gautier EL, Shay T, Miller J, Greter M, Jakubzick C, Ivanov S, et al. Gene-expression profiles and transcriptional regulatory pathways that underlie the identity and diversity of mouse tissue macrophages. Nat Immunol. 2012;13(11):1118-28.

79. Schupp J, Krebs FK, Zimmer N, Trzeciak E, Schuppan D, Tuettenberg A. Targeting myeloid cells in the tumor sustaining microenvironment. Cell Immunol. 2019;343:103713.

80. Ugel S, De Sanctis F, Mandruzzato S, Bronte V. Tumor-induced myeloid deviation: when myeloid-derived suppressor cells meet tumor-associated macrophages. J Clin Invest. 2015;125(9):3365-76.

81. Leek RD, Lewis CE, Whitehouse R, Greenall M, Clarke J, Harris AL. Association of macrophage infiltration with angiogenesis and prognosis in invasive breast carcinoma. Cancer Res. 1996;56(20):4625-9.

82. Tsutsui S, Yasuda K, Suzuki K, Tahara K, Higashi H, Era S. Macrophage infiltration and its prognostic implications in breast cancer: the relationship with VEGF expression and microvessel density. Oncol Rep. 2005;14(2):425-31.

83. Mahmoud SM, Lee AH, Paish EC, Macmillan RD, Ellis IO, Green AR. Tumour-infiltrating macrophages and clinical outcome in breast cancer. J Clin Pathol. 2012;65(2):159-63.

84. Qian BZ, Pollard JW. Macrophage diversity enhances tumor progression and metastasis. Cell. 2010;141(1):39-51.

85. Michea P, Noël F, Zakine E, Czerwinska U, Sirven P, Abouzid O, et al. Adjustment of dendritic cells to the breast-cancer microenvironment is subset specific. Nat Immunol. 2018;19(8):885-97.

86. Treilleux I, Blay JY, Bendriss-Vermare N, Ray-Coquard I, Bachelot T, Guastalla JP, et al. Dendritic cell infiltration and prognosis of early stage breast cancer. Clin Cancer Res. 2004;10(22):7466-74.

87. Veglia F, Perego M, Gabrilovich D. Myeloid-derived suppressor cells coming of age. Nat Immunol. 2018;19(2):108-19.

88. Condamine T, Gabrilovich DI. Molecular mechanisms regulating myeloid-derived suppressor cell differentiation and function. Trends Immunol. 2011;32(1):19-25.

89. Kim IS, Zhang XH. One microenvironment does not fit all: heterogeneity beyond cancer cells. Cancer Metastasis Rev. 2016;35(4):601-29.

90. Kitamura T, Pollard JW. Therapeutic potential of chemokine signal inhibition for metastatic breast cancer. Pharmacol Res. 2015;100:266-70.

91. Niu H, Hadwiger G, Fujiwara H, Welch JS. Pathways of retinoid synthesis in mouse macrophages and bone marrow cells. J Leukoc Biol. 2016;99(6):797-810.

92. Markowitz J, Wesolowski R, Papenfuss T, Brooks TR, Carson WE, 3rd. Myeloid-derived suppressor cells in breast cancer. Breast Cancer Res Treat. 2013;140(1):13-21.

93. Maenhout SK, Thielemans K, Aerts JL. Location, location, location: functional and phenotypic heterogeneity between tumor-infiltrating and non-infiltrating myeloid-derived suppressor cells. Oncoimmunology. 2014;3(10):e956579.

94. Yu YR, Hotten DF, Malakhau Y, Volker E, Ghio AJ, Noble PW, et al. Flow Cytometric Analysis of Myeloid Cells in Human Blood, Bronchoalveolar Lavage, and Lung Tissues. Am J Respir Cell Mol Biol. 2016;54(1):13-24.

95. Mishalian I, Granot Z, Fridlender ZG. The diversity of circulating neutrophils in cancer. Immunobiology. 2017;222(1):82-8.

96. Dolcetti L, Peranzoni E, Ugel S, Marigo I, Fernandez Gomez A, Mesa C, et al. Hierarchy of immunosuppressive strength among myeloid-derived suppressor cell subsets is determined by GM-CSF. Eur J Immunol. 2010;40(1):22-35.

97. Templeton AJ, McNamara MG, Šeruga B, Vera-Badillo FE, Aneja P, Ocaña A, et al. Prognostic role of neutrophil-to-lymphocyte ratio in solid tumors: a systematic review and meta-analysis. J Natl Cancer Inst. 2014;106(6):dju124.

98. Keskinov AA, Shurin MR. Myeloid regulatory cells in tumor spreading and metastasis. Immunobiology. 2015;220(2):236-42.

99. Moses K, Brandau S. Human neutrophils: Their role in cancer and relation to myeloid-derived suppressor cells. Semin Immunol. 2016;28(2):187-96.

100. Iwase T, Sangai T, Sakakibara M, Sakakibara J, Ishigami E, Hayama S, et al. An increased neutrophil-to-lymphocyte ratio predicts poorer survival following recurrence for patients with breast cancer. Mol Clin Oncol. 2017;6(2):266-70.

101. Medrek C, Pontén F, Jirström K, Leandersson K. The presence of tumor associated macrophages in tumor stroma as a prognostic marker for breast cancer patients. BMC Cancer. 2012;12:306.

102. Solito S, Marigo I, Pinton L, Damuzzo V, Mandruzzato S, Bronte V. Myeloid-derived suppressor cell heterogeneity in human cancers. Ann N Y Acad Sci. 2014;1319:47-65.

103. Ferrara N. Role of myeloid cells in vascular endothelial growth factor-independent tumor angiogenesis. Curr Opin Hematol. 2010;17(3):219-24.

104. Lin L, Chen YS, Yao YD, Chen JQ, Chen JN, Huang SY, et al. CCL18 from tumor-associated macrophages promotes angiogenesis in breast cancer. Oncotarget. 2015;6(33):34758-73.

105. Qian B, Deng Y, Im JH, Muschel RJ, Zou Y, Li J, et al. A distinct macrophage population mediates metastatic breast cancer cell extravasation, establishment and growth. PLoS One. 2009;4(8):e6562.

106. Ahn GO, Tseng D, Liao CH, Dorie MJ, Czechowicz A, Brown JM. Inhibition of Mac-1 (CD11b/CD18) enhances tumor response to radiation by reducing myeloid cell recruitment. Proc Natl Acad Sci U S A. 2010;107(18):8363-8.

107. Fang Z, Wen C, Chen X, Yin R, Zhang C, Wang X, et al. Myeloid-derived suppressor cell and macrophage exert distinct angiogenic and immunosuppressive effects in breast cancer. Oncotarget. 2017;8(33):54173-86.

108. Yu J, Wang Y, Yan F, Zhang P, Li H, Zhao H, et al. Noncanonical NF-κB activation mediates STAT3-stimulated IDO upregulation in myeloid-derived suppressor cells in breast cancer. J Immunol. 2014;193(5):2574-86.

109. Bergenfelz C, Larsson AM, von Stedingk K, Gruvberger-Saal S, Aaltonen K, Jansson S, et al. Systemic Monocytic-MDSCs Are Generated from Monocytes and Correlate with Disease Progression in Breast Cancer Patients. PLoS One. 2015;10(5):e0127028.

110. Diaz-Montero CM, Salem ML, Nishimura MI, Garrett-Mayer E, Cole DJ, Montero AJ. Increased circulating myeloid-derived suppressor cells correlate with clinical cancer stage, metastatic tumor burden, and doxorubicin-cyclophosphamide chemotherapy. Cancer Immunol Immunother. 2009;58(1):49-59.

111. Montero AJ, Diaz-Montero CM, Kyriakopoulos CE, Bronte V, Mandruzzato S. Myeloid-derived suppressor cells in cancer patients: a clinical perspective. J Immunother. 2012;35(2):107-15.

112. Gabrilovich DI. Myeloid-Derived Suppressor Cells. Cancer Immunol Res. 2017;5(1):3-8.

113. Yang M, Liu F, Higuchi K, Sawashita J, Fu X, Zhang L, et al. Serum amyloid A expression in the breast cancer tissue is associated with poor prognosis. Oncotarget. 2016;7(24):35843-52.

114. Wolfe AR, Trenton NJ, Debeb BG, Larson R, Ruffell B, Chu K, et al. Mesenchymal stem cells and macrophages interact through IL-6 to promote inflammatory breast cancer in pre-clinical models. Oncotarget. 2016;7(50):82482-92.

115. Zhao X, Qu J, Sun Y, Wang J, Liu X, Wang F, et al. Prognostic significance of tumor-associated macrophages in breast cancer: a meta-analysis of the literature. Oncotarget. 2017;8(18):30576-86.

116. Al-Raawi D, Abu-El-Zahab H, El-Shinawi M, Mohamed MM. Membrane type-1 matrix metalloproteinase (MT1-MMP) correlates with the expression and activation of matrix metalloproteinase-2 (MMP-2) in inflammatory breast cancer. Int J Clin Exp Med. 2011;4(4):265-75.

117. Mohamed MM, El-Ghonaimy EA, Nouh MA, Schneider RJ, Sloane BF, El-Shinawi M. Cytokines secreted by macrophages isolated from tumor microenvironment of inflammatory breast cancer patients possess chemotactic properties. Int J Biochem Cell Biol. 2014;46:138-47.

118. Chen Y, Zhang S, Wang Q, Zhang X. Tumor-recruited M2 macrophages promote gastric and breast cancer metastasis via M2 macrophage-secreted CHI3L1 protein. J Hematol Oncol. 2017;10(1):36.

119. Ueno T, Chow LW, Toi M. Increases in circulating VEGF levels during COX-2 inhibitor treatment in breast cancer patients. Biomed Pharmacother. 2006;60(6):277-9.

120. Moraes LA, Kar S, Foo SL, Gu T, Toh YQ, Ampomah PB, et al. Annexin-A1 enhances breast cancer growth and migration by promoting alternative macrophage polarization in the tumour microenvironment. Sci Rep. 2017;7(1):17925.

121. Gwak JM, Jang MH, Kim DI, Seo AN, Park SY. Prognostic value of tumor-associated macrophages according to histologic locations and hormone receptor status in breast cancer. PLoS One. 2015;10(4):e0125728.

122. Yang J, Li X, Liu X, Liu Y. The role of tumor-associated macrophages in breast carcinoma invasion and metastasis. Int J Clin Exp Pathol. 2015;8(6):6656-64.

123. Yuan ZY, Luo RZ, Peng RJ, Wang SS, Xue C. High infiltration of tumor-associated macrophages in triple-negative breast cancer is associated with a higher risk of distant metastasis. Onco Targets Ther. 2014;7:1475-80.

124. Zhang Y, Cheng S, Zhang M, Zhen L, Pang D, Zhang Q, et al. High-infiltration of tumor-associated macrophages predicts unfavorable clinical outcome for node-negative breast cancer. PLoS One. 2013;8(9):e76147.

125. Jhaveri K, Teplinsky E, Silvera D, Valeta-Magara A, Arju R, Giashuddin S, et al. Hyperactivated mTOR and JAK2/STAT3 Pathways: Molecular Drivers and Potential Therapeutic Targets of Inflammatory and Invasive Ductal Breast Cancers After Neoadjuvant Chemotherapy. Clin Breast Cancer. 2016;16(2):113-22.e1.

126. Campbell MJ, Tonlaar NY, Garwood ER, Huo D, Moore DH, Khramtsov AI, et al. Proliferating macrophages associated with high grade, hormone receptor negative breast cancer and poor clinical outcome. Breast Cancer Res Treat. 2011;128(3):703-11.

127. Richardsen E, Uglehus RD, Johnsen SH, Busund LT. Macrophage-colony stimulating factor (CSF1) predicts breast cancer progression and mortality. Anticancer Res. 2015;35(2):865-74.

128. Fridlender ZG, Sun J, Kim S, Kapoor V, Cheng G, Ling L, et al. Polarization of tumor-associated neutrophil phenotype by TGF-beta: "N1" versus "N2" TAN. Cancer Cell. 2009;16(3):183-94.

129. Granot Z, Henke E, Comen EA, King TA, Norton L, Benezra R. Tumor entrained neutrophils inhibit seeding in the premetastatic lung. Cancer Cell. 2011;20(3):300-14.

130. Polyak K, Haviv I, Campbell IG. Co-evolution of tumor cells and their microenvironment. Trends Genet. 2009;25(1):30-8.

131. Ethier JL, Desautels D, Templeton A, Shah PS, Amir E. Prognostic role of neutrophil-to-lymphocyte ratio in breast cancer: a systematic review and meta-analysis. Breast Cancer Res. 2017;19(1):2.

132. Koh CH, Bhoo-Pathy N, Ng KL, Jabir RS, Tan GH, See MH, et al. Utility of pre-treatment neutrophil-lymphocyte ratio and platelet-lymphocyte ratio as prognostic factors in breast cancer. Br J Cancer. 2015;113(1):150-8.

133. Wei B, Yao M, Xing C, Wang W, Yao J, Hong Y, et al. The neutrophil lymphocyte ratio is associated with breast cancer prognosis: an updated systematic review and meta-analysis. Onco Targets Ther. 2016;9:5567-75.

134. Chen J, Deng Q, Pan Y, He B, Ying H, Sun H, et al. Prognostic value of neutrophil-to-lymphocyte ratio in breast cancer. FEBS Open Bio. 2015;5:502-7.

135. Wang Y, Ding Y, Guo N, Wang S. MDSCs: Key Criminals of Tumor Pre-metastatic Niche Formation. Front Immunol. 2019;10:172.

136. Katoh H, Wang D, Daikoku T, Sun H, Dey SK, Dubois RN. CXCR2-expressing myeloid-derived suppressor cells are essential to promote colitis-associated tumorigenesis. Cancer Cell. 2013;24(5):631-44.

137. Steele CW, Karim SA, Leach JDG, Bailey P, Upstill-Goddard R, Rishi L, et al. CXCR2 Inhibition Profoundly Suppresses Metastases and Augments Immunotherapy in Pancreatic Ductal Adenocarcinoma. Cancer Cell. 2016;29(6):832-45.

138. Highfill SL, Cui Y, Giles AJ, Smith JP, Zhang H, Morse E, et al. Disruption of CXCR2-mediated MDSC tumor trafficking enhances anti-PD1 efficacy. Sci Transl Med. 2014;6(237):237ra67.

139. Di Mitri D, Toso A, Chen JJ, Sarti M, Pinton S, Jost TR, et al. Tumour-infiltrating Gr-1+ myeloid cells antagonize senescence in cancer. Nature. 2014;515(7525):134-7.

140. Zhu H, Gu Y, Xue Y, Yuan M, Cao X, Liu Q. CXCR2(+) MDSCs promote breast cancer progression by inducing EMT and activated T cell exhaustion. Oncotarget. 2017;8(70):114554-67.

141. Sun L, Clavijo PE, Robbins Y, Patel P, Friedman J, Greene S, et al. Inhibiting myeloid-derived suppressor cell trafficking enhances T cell immunotherapy. JCI Insight. 2019;4(7).

142. Elliott LA, Doherty GA, Sheahan K, Ryan EJ. Human Tumor-Infiltrating Myeloid Cells: Phenotypic and Functional Diversity. Front Immunol. 2017;8:86.

143. Sinha P, Clements VK, Fulton AM, Ostrand-Rosenberg S. Prostaglandin E2 promotes tumor progression by inducing myeloid-derived suppressor cells. Cancer Res. 2007;67(9):4507-13.

144. Ochoa AC, Zea AH, Hernandez C, Rodriguez PC. Arginase, prostaglandins, and myeloid-derived suppressor cells in renal cell carcinoma. Clin Cancer Res. 2007;13(2 Pt 2):721s-6s.

145. Eruslanov E, Daurkin I, Ortiz J, Vieweg J, Kusmartsev S. Pivotal Advance: Tumor-mediated induction of myeloid-derived suppressor cells and M2-polarized macrophages by altering intracellular PGE_2 catabolism in myeloid cells. J Leukoc Biol. 2010;88(5):839-48.

146. Liu Y, Kosaka A, Ikeura M, Kohanbash G, Fellows-Mayle W, Snyder LA, et al. Premetastatic soil and prevention of breast cancer brain metastasis. Neuro Oncol. 2013;15(7):891-903.

147. Peak TC, Richman A, Gur S, Yafi FA, Hellstrom WJ. The Role of PDE5 Inhibitors and the NO/cGMP Pathway in Cancer. Sex Med Rev. 2016;4(1):74-84.

148. Tai LH, Alkayyal AA, Leslie AL, Sahi S, Bennett S, Tanese de Souza C, et al. Phosphodiesterase-5 inhibition reduces postoperative metastatic disease by targeting surgery-induced myeloid derived suppressor cell-dependent inhibition of Natural Killer cell cytotoxicity. Oncoimmunology. 2018;7(6):e1431082.

149. Serafini P, Meckel K, Kelso M, Noonan K, Califano J, Koch W, et al. Phosphodiesterase-5 inhibition augments endogenous antitumor immunity by reducing myeloid-derived suppressor cell function. J Exp Med. 2006;203(12):2691-702.

150. Glozak MA, Seto E. Histone deacetylases and cancer. Oncogene. 2007;26(37):5420-32.

151. Syndax P, Roche Pharma AG. Randomized Phase 2 Study of Atezolizumab and Entinostat in Patients With aTN Breast Cancer With Phase 1b Lead In. 2021.

152. National Cancer I. Entinostat in Patients With Recurrent Advanced Hormone Receptor-Positive Breast Cancer. 2020.

153. National Cancer I. Entinostat, Nivolumab, and Ipilimumab in Treating Patients With Solid Tumors That Are Metastatic or Cannot Be Removed by Surgery or Locally Advanced or Metastatic HER2-Negative Breast Cancer. 2022.

154. Cassetta L, Pollard JW. Targeting macrophages: therapeutic approaches in cancer. Nat Rev Drug Discov. 2018;17(12):887-904.

155. Martini M, De Santis MC, Braccini L, Gulluni F, Hirsch E. PI3K/AKT signaling pathway and cancer: an updated review. Ann Med. 2014;46(6):372-83.

156. Schmid MC, Franco I, Kang SW, Hirsch E, Quilliam LA, Varner JA. PI3-kinase γ promotes Rap1a-mediated activation of myeloid cell integrin α4β1, leading to tumor inflammation and growth. PLoS One. 2013;8(4):e60226.

157. Infinity Pharmaceuticals I, Roche Pharma AG. Evaluation of IPI-549 Combined With Front-line Treatments in Pts. With Triple-Negative Breast Cancer or Renal Cell Carcinoma (MARIO-3). 2022.

158. Evans CA, Liu T, Lescarbeau A, Nair SJ, Grenier L, Pradeilles JA, et al. Discovery of a Selective Phosphoinositide-3-Kinase (PI3K)-γ Inhibitor (IPI-549) as an Immuno-Oncology Clinical Candidate. ACS Med Chem Lett. 2016;7(9):862-7.

159. Kaneda MM, Messer KS, Ralainirina N, Li H, Leem CJ, Gorjestani S, et al. PI3Kγ is a molecular switch that controls immune suppression. Nature. 2016;539(7629):437-42.

160. Trinchera M, Aronica A, Dall'Olio F. Selectin Ligands Sialyl-Lewis a and Sialyl-Lewis x in Gastrointestinal Cancers. Biology (Basel). 2017;6(1).

161. Zheng M, Fang H, Hakomori S. Functional role of N-glycosylation in alpha 5 beta 1 integrin receptor. De-N-glycosylation induces dissociation or altered association of alpha 5 and beta 1 subunits and concomitant loss of fibronectin binding activity. J Biol Chem. 1994;269(16):12325-31.

162. Zhang Y, Jiao J, Yang P, Lu H. Mass spectrometry-based N-glycoproteomics for cancer biomarker discovery. Clin Proteomics. 2014;11(1):18.

163. Su Y, Bakker T, Harris J, Tsang C, Brown GD, Wormald MR, et al. Glycosylation influences the lectin activities of the macrophage mannose receptor. J Biol Chem. 2005;280(38):32811-20.

164. Jha AK, Huang SC, Sergushichev A, Lampropoulou V, Ivanova Y, Loginicheva E, et al. Network integration of parallel metabolic and transcriptional data reveals metabolic modules that regulate macrophage polarization. Immunity. 2015;42(3):419-30.

165. Yang RY, Rabinovich GA, Liu FT. Galectins: structure, function and therapeutic potential. Expert Rev Mol Med. 2008;10:e17.

166. Smith DF, Cummings RD. Application of microarrays for deciphering the structure and function of the human glycome. Mol Cell Proteomics. 2013;12(4):902-12.

167. Elola MT, Wolfenstein-Todel C, Troncoso MF, Vasta GR, Rabinovich GA. Galectins: matricellular glycan-binding proteins linking cell adhesion, migration, and survival. Cell Mol Life Sci. 2007;64(13):1679-700.

168. Chen J, Tang D, Wang S, Li QG, Zhang JR, Li P, et al. High expressions of galectin-1 and VEGF are associated with poor prognosis in gastric cancer patients. Tumour Biol. 2014;35(3):2513-9.

169. Carlsson MC, Cederfur C, Schaar V, Balog CI, Lepur A, Touret F, et al. Galectin-1-binding glycoforms of haptoglobin with altered intracellular trafficking, and increase in metastatic breast cancer patients. PLoS One. 2011;6(10):e26560.

170. Cooper DN. Galectinomics: finding themes in complexity. Biochim Biophys Acta. 2002;1572(2-3):209-31.

171. Hughes RC. Secretion of the galectin family of mammalian carbohydrate-binding proteins. Biochim Biophys Acta. 1999;1473(1):172-85.

172. Seelenmeyer C, Wegehingel S, Tews I, Künzler M, Aebi M, Nickel W. Cell surface counter receptors are essential components of the unconventional export machinery of galectin-1. J Cell Biol. 2005;171(2):373-81.

173. Cerliani JP, Blidner AG, Toscano MA, Croci DO, Rabinovich GA. Translating the 'Sugar Code' into Immune and Vascular Signaling Programs. Trends Biochem Sci. 2017;42(4):255-73.

174. Thijssen VL, Heusschen R, Caers J, Griffioen AW. Galectin expression in cancer diagnosis and prognosis: A systematic review. Biochim Biophys Acta. 2015;1855(2):235-47.

175. Barrow H, Guo X, Wandall HH, Pedersen JW, Fu B, Zhao Q, et al. Serum galectin-2, -4, and -8 are greatly increased in colon and breast cancer patients and promote cancer cell adhesion to blood vascular endothelium. Clin Cancer Res. 2011;17(22):7035-46.

176. Iurisci I, Tinari N, Natoli C, Angelucci D, Cianchetti E, Iacobelli S. Concentrations of galectin-3 in the sera of normal controls and cancer patients. Clin Cancer Res. 2000;6(4):1389-93.

177. Gurel Cayir E, Demir L, Varol U, Atahan MK, Salman T, Oflazoglu U, et al. Preliminary study of serum Galectin-1 in breast cancer carcinogenesis [Izmir Oncology Group (IZOG) study]. J buon. 2020;25(2):675-80.

178. Ahmed R, Anam K, Ahmed H. Development of Galectin-3 Targeting Drugs for Therapeutic Applications in Various Diseases. Int J Mol Sci. 2023;24(9).

179. Cheng DE, Hung JY, Huang MS, Hsu YL, Lu CY, Tsai EM, et al. Myosin IIa activation is crucial in breast cancer derived galectin-1 mediated tolerogenic dendritic cell differentiation. Biochim Biophys Acta. 2014;1840(6):1965-76.

180. Dalotto-Moreno T, Croci DO, Cerliani JP, Martinez-Allo VC, Dergan-Dylon S, Méndez-Huergo SP, et al. Targeting galectin-1 overcomes breast cancer-associated immunosuppression and prevents metastatic disease. Cancer Res. 2013;73(3):1107-17.

181. Ito K, Scott SA, Cutler S, Dong LF, Neuzil J, Blanchard H, et al. Thiodigalactoside inhibits murine cancers by concurrently blocking effects of galectin-1 on immune dysregulation, angiogenesis and protection against oxidative stress. Angiogenesis. 2011;14(3):293-307.

182. Ito K, Ralph SJ. Inhibiting galectin-1 reduces murine lung metastasis with increased CD4(+) and CD8 (+) T cells and reduced cancer cell adherence. Clin Exp Metastasis. 2012;29(6):561-72.

183. He J, Baum LG. Endothelial cell expression of galectin-1 induced by prostate cancer cells inhibits T-cell transendothelial migration. Lab Invest. 2006;86(6):578-90.

184. Qian D, Lu Z, Xu Q, Wu P, Tian L, Zhao L, et al. Galectin-1-driven upregulation of SDF-1 in pancreatic stellate cells promotes pancreatic cancer metastasis. Cancer Lett. 2017;397:43-51.

185. Orozco CA, Martinez-Bosch N, Guerrero PE, Vinaixa J, Dalotto-Moreno T, Iglesias M, et al. Targeting galectin-1 inhibits pancreatic cancer progression by modulating tumor-stroma crosstalk. Proc Natl Acad Sci U S A. 2018;115(16):E3769-e78.

186. Martínez-Bosch N, Fernández-Barrena MG, Moreno M, Ortiz-Zapater E, Munné-Collado J, Iglesias M, et al. Galectin-1 drives pancreatic carcinogenesis through stroma remodeling and Hedgehog signaling activation. Cancer Res. 2014;74(13):3512-24.

187. Tang D, Gao J, Wang S, Yuan Z, Ye N, Chong Y, et al. Apoptosis and anergy of T cell induced by pancreatic stellate cells-derived galectin-1 in pancreatic cancer. Tumour Biol. 2015;36(7):5617-26.

188. Büchel G, Schulte JH, Harrison L, Batzke K, Schüller U, Hansen W, et al. Immune response modulation by Galectin-1 in a transgenic model of neuroblastoma. Oncoimmunology. 2016;5(5):e1131378.

189. Rubinstein N, Alvarez M, Zwirner NW, Toscano MA, Ilarregui JM, Bravo A, et al. Targeted inhibition of galectin-1 gene expression in tumor cells results in heightened T cell-mediated rejection; A potential mechanism of tumor-immune privilege. Cancer Cell. 2004;5(3):241-51.

190. Juszczynski P, Ouyang J, Monti S, Rodig SJ, Takeyama K, Abramson J, et al. The AP1-dependent secretion of galectin-1 by Reed Sternberg cells fosters immune privilege in classical Hodgkin lymphoma. Proc Natl Acad Sci U S A. 2007;104(32):13134-9.

191. Kuo PL, Hung JY, Huang SK, Chou SH, Cheng DE, Jong YJ, et al. Lung cancer-derived galectin-1 mediates dendritic cell anergy through inhibitor of DNA binding 3/IL-10 signaling pathway. J Immunol. 2011;186(3):1521-30.

192. Banh A, Zhang J, Cao H, Bouley DM, Kwok S, Kong C, et al. Tumor galectin-1 mediates tumor growth and metastasis through regulation of T-cell apoptosis. Cancer Res. 2011;71(13):4423-31.

193. Kuo PL, Huang MS, Cheng DE, Hung JY, Yang CJ, Chou SH. Lung cancer-derived galectin-1 enhances tumorigenic potentiation of tumor-associated dendritic cells by expressing heparin-binding EGF-like growth factor. J Biol Chem. 2012;287(13):9753-64.

194. Chung LY, Tang SJ, Sun GH, Chou TY, Yeh TS, Yu SL, et al. Galectin-1 promotes lung cancer progression and chemoresistance by upregulating p38 MAPK, ERK, and cyclooxygenase-2. Clin Cancer Res. 2012;18(15):4037-47.

195. Nambiar DK, Aguilera T, Cao H, Kwok S, Kong C, Bloomstein J, et al. Galectin-1-driven T cell exclusion in the tumor endothelium promotes immunotherapy resistance. J Clin Invest. 2019;129(12):5553-67.

196. Baker GJ, Chockley P, Yadav VN, Doherty R, Ritt M, Sivaramakrishnan S, et al. Natural killer cells eradicate galectin-1-deficient glioma in the absence of adaptive immunity. Cancer Res. 2014;74(18):5079-90.

197. Verschuere T, Toelen J, Maes W, Poirier F, Boon L, Tousseyn T, et al. Glioma-derived galectin-1 regulates innate and adaptive antitumor immunity. Int J Cancer. 2014;134(4):873-84.

198. Zhao XY, Chen TT, Xia L, Guo M, Xu Y, Yue F, et al. Hypoxia inducible factor-1 mediates expression of galectin-1: the potential role in migration/invasion of colorectal cancer cells. Carcinogenesis. 2010;31(8):1367-75.

199. Baldini A, Gress T, Patel K, Muresu R, Chiariotti L, Williamson P, et al. Mapping on human and mouse chromosomes of the gene for the beta-galactoside-binding protein, an autocrine-negative growth factor. Genomics. 1993;15(1):216-8.

200. Bourne Y, Bolgiano B, Nésa MP, Penfold P, Johnson D, Feizi T, et al. Crystallization and preliminary X-ray diffraction studies of the soluble 14 kDa beta-galactoside-binding lectin from bovine heart. J Mol Biol. 1994;235(2):787-9.

201. Schwarz FP, Ahmed H, Bianchet MA, Amzel LM, Vasta GR. Thermodynamics of bovine spleen galectin-1 binding to disaccharides: correlation with structure and its effect on oligomerization at the denaturation temperature. Biochemistry. 1998;37(17):5867-77.

202. Liao DI, Kapadia G, Ahmed H, Vasta GR, Herzberg O. Structure of S-lectin, a developmentally regulated vertebrate beta-galactoside-binding protein. Proc Natl Acad Sci U S A. 1994;91(4):1428-32.

203. López-Lucendo MF, Solís D, André S, Hirabayashi J, Kasai K, Kaltner H, et al. Growth-regulatory human galectin-1: crystallographic characterisation of the structural changes induced by single-site mutations and their impact on the thermodynamics of ligand binding. J Mol Biol. 2004;343(4):957-70.

204. Zhou D. Why are glycoproteins modified by poly-N-acetyllactosamine glyco-conjugates? Curr Protein Pept Sci. 2003;4(1):1-9.

205. Sundblad V, Morosi LG, Geffner JR, Rabinovich GA. Galectin-1: A Jack-of-All-Trades in the Resolution of Acute and Chronic Inflammation. J Immunol. 2017;199(11):3721-30.

206. Salomonsson E, Larumbe A, Tejler J, Tullberg E, Rydberg H, Sundin A, et al. Monovalent interactions of galectin-1. Biochemistry. 2010;49(44):9518-32.

207. Cho M, Cummings RD. Galectin-1, a beta-galactoside-binding lectin in Chinese hamster ovary cells. I. Physical and chemical characterization. J Biol Chem. 1995;270(10):5198-206.

208. Cho M, Cummings RD. Galectin-1, a beta-galactoside-binding lectin in Chinese hamster ovary cells. II. Localization and biosynthesis. J Biol Chem. 1995;270(10):5207-12.

209. Fulcher JA, Chang MH, Wang S, Almazan T, Hashimi ST, Eriksson AU, et al. Galectin-1 co-clusters CD43/CD45 on dendritic cells and induces cell activation and migration through Syk and protein kinase C signaling. J Biol Chem. 2009;284(39):26860-70.

210. Camby I, Le Mercier M, Lefranc F, Kiss R. Galectin-1: a small protein with major functions. Glycobiology. 2006;16(11):137r-57r.

211. Bertleff-Zieschang N, Bechold J, Grimm C, Reutlinger M, Schneider P, Schneider G, et al. Exploring the Structural Space of the Galectin-1-Ligand Interaction. Chembiochem. 2017;18(15):1477-81.

212. Huang YJ, Shiau AL, Chen SY, Chen YL, Wang CR, Tsai CY, et al. Multivalent structure of galectin-1-nanogold complex serves as potential therapeutics for rheumatoid arthritis by enhancing receptor clustering. Eur Cell Mater. 2012;23:170-81; discussion 81.

213. Nio-Kobayashi J. Tissue- and cell-specific localization of galectins, β-galactose-binding animal lectins, and their potential functions in health and disease. Anat Sci Int. 2017;92(1):25-36.

214. Rabinovich GA. Galectin-1 as a potential cancer target. Br J Cancer. 2005;92(7):1188-92.

215. Kadoya T, Horie H. Structural and functional studies of galectin-1: a novel axonal regeneration-promoting activity for oxidized galectin-1. Curr Drug Targets. 2005;6(4):375-83.

216. Scott SA, Bugarcic A, Blanchard H. Characterisation of oxidized recombinant human galectin-1. Protein Pept Lett. 2009;16(10):1249-55.

217. Horie H, Kadoya T, Hikawa N, Sango K, Inoue H, Takeshita K, et al. Oxidized galectin-1 stimulates macrophages to promote axonal regeneration in peripheral nerves after axotomy. J Neurosci. 2004;24(8):1873-80.

218. Liu FT, Yang RY, Hsu DK. Galectins in acute and chronic inflammation. Ann N Y Acad Sci. 2012;1253:80-91.

219. Perillo NL, Pace KE, Seilhamer JJ, Baum LG. Apoptosis of T cells mediated by galectin-1. Nature. 1995;378(6558):736-9.

220. Grigorian A, Torossian S, Demetriou M. T-cell growth, cell surface organization, and the galectin-glycoprotein lattice. Immunol Rev. 2009;230(1):232-46.

221. Pace KE, Hahn HP, Pang M, Nguyen JT, Baum LG. CD7 delivers a pro-apoptotic signal during galectin-1-induced T cell death. J Immunol. 2000;165(5):2331-4.

222. Kovács-Sólyom F, Blaskó A, Fajka-Boja R, Katona RL, Végh L, Novák J, et al. Mechanism of tumor cell-induced T-cell apoptosis mediated by galectin-1. Immunol Lett. 2010;127(2):108-18.

223. Lange F, Brandt B, Tiedge M, Jonas L, Jeschke U, Pöhland R, et al. Galectin-1 induced activation of the mitochondrial apoptotic pathway: evidence for a connection between death-receptor and mitochondrial pathways in human Jurkat T lymphocytes. Histochem Cell Biol. 2009;132(2):211-23.

224. Vespa GN, Lewis LA, Kozak KR, Moran M, Nguyen JT, Baum LG, et al. Galectin-1 specifically modulates TCR signals to enhance TCR apoptosis but inhibit IL-2 production and proliferation. J Immunol. 1999;162(2):799-806.

225. Chung CD, Patel VP, Moran M, Lewis LA, Miceli MC. Galectin-1 induces partial TCR zeta-chain phosphorylation and antagonizes processive TCR signal transduction. J Immunol. 2000;165(7):3722-9.

226. Matarrese P, Tinari A, Mormone E, Bianco GA, Toscano MA, Ascione B, et al. Galectin-1 sensitizes resting human T lymphocytes to Fas (CD95)-mediated cell death via mitochondrial hyperpolarization, budding, and fission. J Biol Chem. 2005;280(8):6969-85.

227. Amano M, Galvan M, He J, Baum LG. The ST6Gal I sialyltransferase selectively modifies N-glycans on CD45 to negatively regulate galectin-1-induced CD45 clustering, phosphatase modulation, and T cell death. J Biol Chem. 2003;278(9):7469-75.

228. Lau KS, Partridge EA, Grigorian A, Silvescu CI, Reinhold VN, Demetriou M, et al. Complex N-glycan number and degree of branching cooperate to regulate cell proliferation and differentiation. Cell. 2007;129(1):123-34.

229. Toscano MA, Bianco GA, Ilarregui JM, Croci DO, Correale J, Hernandez JD, et al. Differential glycosylation of TH1, TH2 and TH-17 effector cells selectively regulates susceptibility to cell death. Nat Immunol. 2007;8(8):825-34.

230. Espeli M, Mancini SJ, Breton C, Poirier F, Schiff C. Impaired B-cell development at the pre-BII-cell stage in galectin-1-deficient mice due to inefficient pre-BII/stromal cell interactions. Blood. 2009;113(23):5878-86.

231. Mourcin F, Breton C, Tellier J, Narang P, Chasson L, Jorquera A, et al. Galectin-1-expressing stromal cells constitute a specific niche for pre-BII cell development in mouse bone marrow. Blood. 2011;117(24):6552-61.

232. Alhabbab R, Blair P, Smyth LA, Ratnasothy K, Peng Q, Moreau A, et al. Galectin-1 is required for the regulatory function of B cells. Sci Rep. 2018;8(1):2725.

233. Bonzi J, Bornet O, Betzi S, Kasper BT, Mahal LK, Mancini SJ, et al. Pre-B cell receptor binding to galectin-1 modifies galectin-1/carbohydrate affinity to modulate specific galectin-1/glycan lattice interactions. Nat Commun. 2015;6:6194.

234. Tsai CM, Chiu YK, Hsu TL, Lin IY, Hsieh SL, Lin KI. Galectin-1 promotes immunoglobulin production during plasma cell differentiation. J Immunol. 2008;181(7):4570-9.

235. Tabrizi SJ, Niiro H, Masui M, Yoshimoto G, Iino T, Kikushige Y, et al. T cell leukemia/lymphoma 1 and galectin-1 regulate survival/cell death pathways in human naive and IgM+ memory B cells through altering balances in Bcl-2 family proteins. J Immunol. 2009;182(3):1490-9.

236. Anginot A, Espeli M, Chasson L, Mancini SJ, Schiff C. Galectin 1 modulates plasma cell homeostasis and regulates the humoral immune response. J Immunol. 2013;190(11):5526-33.

237. Zhang Y, Ge XH, Guo XJ, Guan SB, Li XM, Gu W, et al. Bone Marrow Mesenchymal Stem Cells Inhibit the Function of Dendritic Cells by Secreting Galectin-1. Biomed Res Int. 2017;2017:3248605.

238. Gao J, Wang X, Wang Y, Han F, Cai W, Zhao B, et al. Murine Sertoli cells promote the development of tolerogenic dendritic cells: a pivotal role of galectin-1. Immunology. 2016;148(3):253-65.

239. Ilarregui JM, Croci DO, Bianco GA, Toscano MA, Salatino M, Vermeulen ME, et al. Tolerogenic signals delivered by dendritic cells to T cells through a galectin-1-driven immunoregulatory circuit involving interleukin 27 and interleukin 10. Nat Immunol. 2009;10(9):981-91.

240. Poncini CV, Ilarregui JM, Batalla EI, Engels S, Cerliani JP, Cucher MA, et al. Trypanosoma cruzi Infection Imparts a Regulatory Program in Dendritic Cells and T Cells via Galectin-1-Dependent Mechanisms. J Immunol. 2015;195(7):3311-24.

241. Fulcher JA, Hashimi ST, Levroney EL, Pang M, Gurney KB, Baum LG, et al. Galectin-1-matured human monocyte-derived dendritic cells have enhanced migration through extracellular matrix. J Immunol. 2006;177(1):216-26.

242. Thiemann S, Man JH, Chang MH, Lee B, Baum LG. Galectin-1 regulates tissue exit of specific dendritic cell populations. J Biol Chem. 2015;290(37):22662-77.

243. Cooper D, Norling LV, Perretti M. Novel insights into the inhibitory effects of Galectin-1 on neutrophil recruitment under flow. J Leukoc Biol. 2008;83(6):1459-66.

244. Iqbal AJ, Sampaio AL, Maione F, Greco KV, Niki T, Hirashima M, et al. Endogenous galectin-1 and acute inflammation: emerging notion of a galectin-9 pro-resolving effect. Am J Pathol. 2011;178(3):1201-9.

245. Auvynet C, Moreno S, Melchy E, Coronado-Martínez I, Montiel JL, Aguilar-Delfin I, et al. Galectin-1 promotes human neutrophil migration. Glycobiology. 2013;23(1):32-42.

246. La M, Cao TV, Cerchiaro G, Chilton K, Hirabayashi J, Kasai K, et al. A novel biological activity for galectin-1: inhibition of leukocyte-endothelial cell interactions in experimental inflammation. Am J Pathol. 2003;163(4):1505-15.

247. Rabinovich GA, Sotomayor CE, Riera CM, Bianco I, Correa SG. Evidence of a role for galectin-1 in acute inflammation. Eur J Immunol. 2000;30(5):1331-9.

248. Stowell SR, Karmakar S, Arthur CM, Ju T, Rodrigues LC, Riul TB, et al. Galectin-1 induces reversible phosphatidylserine exposure at the plasma membrane. Mol Biol Cell. 2009;20(5):1408-18.

249. Karmakar S, Cummings RD, McEver RP. Contributions of Ca2+ to galectin-1-induced exposure of phosphatidylserine on activated neutrophils. J Biol Chem. 2005;280(31):28623-31.

250. Law HL, Wright RD, Iqbal AJ, Norling LV, Cooper D. A Pro-resolving Role for Galectin-1 in Acute Inflammation. Front Pharmacol. 2020;11:274.

251. Rodrigues LC, Kabeya LM, Azzolini A, Cerri DG, Stowell SR, Cummings RD, et al. Galectin-1 modulation of neutrophil reactive oxygen species production depends on the cell activation state. Mol Immunol. 2019;116:80-9.

252. Abebayehu D, Spence A, Boyan BD, Schwartz Z, Ryan JJ, McClure MJ. Galectin-1 promotes an M2 macrophage response to polydioxanone scaffolds. J Biomed Mater Res A. 2017;105(9):2562-71.

253. Barrionuevo P, Beigier-Bompadre M, Ilarregui JM, Toscano MA, Bianco GA, Isturiz MA, et al. A novel function for galectin-1 at the crossroad of innate and adaptive immunity: galectin-1 regulates monocyte/macrophage physiology through a nonapoptotic ERK-dependent pathway. J Immunol. 2007;178(1):436-45.

254. Rostoker R, Yaseen H, Schif-Zuck S, Lichtenstein RG, Rabinovich GA, Ariel A. Galectin-1 induces 12/15-lipoxygenase expression in murine macrophages and favors their conversion toward a pro-resolving phenotype. Prostaglandins Other Lipid Mediat. 2013;107:85-94.

255. Lüth HJ, Arendt T. Co-expression of APP with cNOS but not iNOS after cortical injury in rat. Neuroreport. 1997;8(9-10):2321-4.

256. Levy B, Valtier M, de Chillou C, Bollaert PE, Cane D, Mallie JP. Beneficial effects of L-canavanine, a selective inhibitor of inducible nitric oxide synthase, on lactate metabolism and muscle high energy phosphates during endotoxic shock in rats. Shock. 1999;11(2):98-103.

257. Gahm C, Holmin S, Mathiesen T. Temporal profiles and cellular sources of three nitric oxide synthase isoforms in the brain after experimental contusion. Neurosurgery. 2000;46(1):169-77.

258. Correa SG, Sotomayor CE, Aoki MP, Maldonado CA, Rabinovich GA. Opposite effects of galectin-1 on alternative metabolic pathways of L-arginine in resident, inflammatory, and activated macrophages. Glycobiology. 2003;13(2):119-28.

259. Malik RK, Ghurye RR, Lawrence-Watt DJ, Stewart HJ. Galectin-1 stimulates monocyte chemotaxis via the p44/42 MAP kinase pathway and a pertussis toxin-sensitive pathway. Glycobiology. 2009;19(12):1402-7.

260. Paclik D, Werner L, Guckelberger O, Wiedenmann B, Sturm A. Galectins distinctively regulate central monocyte and macrophage function. Cell Immunol. 2011;271(1):97-103.

261. Echigo Y, Sugiki H, Koizumi Y, Hikitsuchi S, Inoue H. Activation of RAW264.7 macrophages by oxidized galectin-1. Immunol Lett. 2010;131(1):19-23.

262. Kogawa Y, Nakajima K, Sasaguri K, Hamada N, Kawasaki H, Sato S, et al. Oxidized galectin-1 reduces lipopolysaccharide-induced increase of proinflammatory cytokine mRNA in cultured macrophages. Clin Cosmet Investig Dent. 2011;3:1-8.

263. Avni O, Pur Z, Yefenof E, Baniyash M. Complement receptor 3 of macrophages is associated with galectin-1-like protein. J Immunol. 1998;160(12):6151-8.

264. Demetriou M, Granovsky M, Quaggin S, Dennis JW. Negative regulation of T-cell activation and autoimmunity by Mgat5 N-glycosylation. Nature. 2001;409(6821):733-9.

265. Fukuda M, Carlsson SR. Leukosialin, a major sialoglycoprotein on human leukocytes as differentiation antigens. Med Biol. 1986;64(6):335-43.

266. Daniels MA, Hogquist KA, Jameson SC. Sweet 'n' sour: the impact of differential glycosylation on T cell responses. Nat Immunol. 2002;3(10):903-10.

267. Sacchettini JC, Baum LG, Brewer CF. Multivalent protein-carbohydrate interactions. A new paradigm for supermolecular assembly and signal transduction. Biochemistry. 2001;40(10):3009-15.

268. Viallard C, Larrivée B. Tumor angiogenesis and vascular normalization: alternative therapeutic targets. Angiogenesis. 2017;20(4):409-26.

269. Tozer GM, Kanthou C, Baguley BC. Disrupting tumour blood vessels. Nat Rev Cancer. 2005;5(6):423-35.

270. Thijssen VL, Hulsmans S, Griffioen AW. The galectin profile of the endothelium: altered expression and localization in activated and tumor endothelial cells. Am J Pathol. 2008;172(2):545-53.

271. Kawano H, Masuko S. Synaptic inputs of neuropeptide Y-immunoreactive noradrenergic nerve terminals to neurons in the nucleus preopticus medianus which project to the paraventricular nucleus of the hypothalamus of the rat: a combined immunohistochemical and retrograde tracing method. Brain Res. 1993;600(1):74-80.

272. Paz H, Joo EJ, Chou CH, Fei F, Mayo KH, Abdel-Azim H, et al. Treatment of B-cell precursor acute lymphoblastic leukemia with the Galectin-1 inhibitor PTX008. J Exp Clin Cancer Res. 2018;37(1):67.

273. van den Brûle FA, Buicu C, Baldet M, Sobel ME, Cooper DN, Marschal P, et al. Galectin-1 modulates human melanoma cell adhesion to laminin. Biochem Biophys Res Commun. 1995;209(2):760-7.

274. Astorgues-Xerri L, Riveiro ME, Tijeras-Raballand A, Serova M, Neuzillet C, Albert S, et al. Unraveling galectin-1 as a novel therapeutic target for cancer. Cancer Treat Rev. 2014;40(2):307-19.

275. Hsieh SH, Ying NW, Wu MH, Chiang WF, Hsu CL, Wong TY, et al. Galectin-1, a novel ligand of neuropilin-1, activates VEGFR-2 signaling and modulates the migration of vascular endothelial cells. Oncogene. 2008;27(26):3746-53.

276. Gao YH, Li CX, Shen SM, Li H, Chen GQ, Wei Q, et al. Hypoxia-inducible factor 1α mediates the down-regulation of superoxide dismutase 2 in von Hippel-Lindau deficient renal clear cell carcinoma. Biochem Biophys Res Commun. 2013;435(1):46-51.

277. Brown KR, England KM, Goss KL, Snyder JM, Acarregui MJ. VEGF induces airway epithelial cell proliferation in human fetal lung in vitro. Am J Physiol Lung Cell Mol Physiol. 2001;281(4):L1001-10.

278. Matsumoto S, Yasui H, Mitchell JB, Krishna MC. Imaging cycling tumor hypoxia. Cancer Res. 2010;70(24):10019-23.

279. Martinive P, Defresne F, Bouzin C, Saliez J, Lair F, Grégoire V, et al. Preconditioning of the tumor vasculature and tumor cells by intermittent hypoxia: implications for anticancer therapies. Cancer Res. 2006;66(24):11736-44.

280. Dewhirst MW, Cao Y, Moeller B. Cycling hypoxia and free radicals regulate angiogenesis and radiotherapy response. Nat Rev Cancer. 2008;8(6):425-37.

281. Le QT, Shi G, Cao H, Nelson DW, Wang Y, Chen EY, et al. Galectin-1: a link between tumor hypoxia and tumor immune privilege. J Clin Oncol. 2005;23(35):8932-41.

282. Cho HJ, Jeong HG, Lee JS, Woo ER, Hyun JW, Chung MH, et al. Oncogenic H-Ras enhances DNA repair through the Ras/phosphatidylinositol 3-kinase/Rac1 pathway in NIH3T3 cells. Evidence for association with reactive oxygen species. J Biol Chem. 2002;277(22):19358-66.

283. Prior IA, Muncke C, Parton RG, Hancock JF. Direct visualization of Ras proteins in spatially distinct cell surface microdomains. J Cell Biol. 2003;160(2):165-70.

284. Paz A, Haklai R, Elad-Sfadia G, Ballan E, Kloog Y. Galectin-1 binds oncogenic H-Ras to mediate Ras membrane anchorage and cell transformation. Oncogene. 2001;20(51):7486-93.

285. Rotblat B, Niv H, André S, Kaltner H, Gabius HJ, Kloog Y. Galectin-1(L11A) predicted from a computed galectin-1 farnesyl-binding pocket selectively inhibits Ras-GTP. Cancer Res. 2004;64(9):3112-8.

286. Elad-Sfadia G, Haklai R, Ballan E, Gabius HJ, Kloog Y. Galectin-1 augments Ras activation and diverts Ras signals to Raf-1 at the expense of phosphoinositide 3-kinase. J Biol Chem. 2002;277(40):37169-75.

287. Yu X, Scott SA, Pritchard R, Houston TA, Ralph SJ, Blanchard H. Redox state influence on human galectin-1 function. Biochimie. 2015;116:8-16.

288. Jung EJ, Moon HG, Cho BI, Jeong CY, Joo YT, Lee YJ, et al. Galectin-1 expression in cancer-associated stromal cells correlates tumor invasiveness and tumor progression in breast cancer. Int J Cancer. 2007;120(11):2331-8.

289. Grosset AA, Labrie M, Vladoiu MC, Yousef EM, Gaboury L, St-Pierre Y. Galectin signatures contribute to the heterogeneity of breast cancer and provide new prognostic information and therapeutic targets. Oncotarget. 2016;7(14):18183-203.

290. Croci DO, Salatino M, Rubinstein N, Cerliani JP, Cavallin LE, Leung HJ, et al. Disrupting galectin-1 interactions with N-glycans suppresses hypoxia-driven angiogenesis and tumorigenesis in Kaposi's sarcoma. J Exp Med. 2012;209(11):1985-2000.

291. Lai J, Lu D, Zhang C, Zhu H, Gao L, Wang Y, et al. Noninvasive small-animal imaging of galectin-1 upregulation for predicting tumor resistance to radiotherapy. Biomaterials. 2018;158:1-9.

292. Upreti M, Jyoti A, Johnson SE, Swindell EP, Napier D, Sethi P, et al. Radiation-enhanced therapeutic targeting of galectin-1 enriched malignant stroma in triple negative breast cancer. Oncotarget. 2016;7(27):41559-74.

293. Pacienza N, Pozner RG, Bianco GA, D'Atri LP, Croci DO, Negrotto S, et al. The immunoregulatory glycan-binding protein galectin-1 triggers human platelet activation. Faseb j. 2008;22(4):1113-23.

294. Cheng DE, Chang WA, Hung JY, Huang MS, Kuo PL. Involvement of IL-10 and granulocyte colony-stimulating factor in the fate of monocytes controlled by galectin-1. Mol Med Rep. 2014;10(5):2389-94.

295. Zhu X, Wang K, Zhang K, Xu F, Yin Y, Zhu L, et al. Galectin-1 knockdown in carcinoma-associated fibroblasts inhibits migration and invasion of human MDA-MB-231 breast cancer cells by modulating MMP-9 expression. Acta Biochim Biophys Sin (Shanghai). 2016;48(5):462-7.

296. van den Brûle F, Califice S, Garnier F, Fernandez PL, Berchuck A, Castronovo V. Galectin-1 accumulation in the ovary carcinoma peritumoral stroma is induced by ovary carcinoma cells and affects both cancer cell proliferation and adhesion to laminin-1 and fibronectin. Lab Invest. 2003;83(3):377-86.

297. Fischer C, Sanchez-Ruderisch H, Welzel M, Wiedenmann B, Sakai T, André S, et al. Galectin-1 interacts with the {alpha}5{beta}1 fibronectin receptor to restrict carcinoma cell growth via induction of p21 and p27. J Biol Chem. 2005;280(44):37266-77.

298. Nam K, Son SH, Oh S, Jeon D, Kim H, Noh DY, et al. Binding of galectin-1 to integrin β1 potentiates drug resistance by promoting survivin expression in breast cancer cells. Oncotarget. 2017;8(22):35804-23.

299. Watson AP, Evans RL, Egland KA. Multiple functions of sushi domain containing 2 (SUSD2) in breast tumorigenesis. Mol Cancer Res. 2013;11(1):74-85.

300. Lin TW, Chang HT, Chen CH, Chen CH, Lin SW, Hsu TL, et al. Galectin-3 Binding Protein and Galectin-1 Interaction in Breast Cancer Cell Aggregation and Metastasis. J Am Chem Soc. 2015;137(30):9685-93.

301. Gao Y, Li X, Shu Z, Zhang K, Xue X, Li W, et al. Nuclear galectin-1-FOXP3 interaction dampens the tumor-suppressive properties of FOXP3 in breast cancer. Cell Death Dis. 2018;9(4):416.

302. Hultgren EM, Patrick ME, Evans RL, Stoos CT, Egland KA. SUSD2 promotes tumor-associated macrophage recruitment by increasing levels of MCP-1 in breast cancer. PLoS One. 2017;12(5):e0177089.

303. Patrick ME, Egland KA. SUSD2 Proteolytic Cleavage Requires the GDPH Sequence and Inter-Fragment Disulfide Bonds for Surface Presentation of Galectin-1 on Breast Cancer Cells. Int J Mol Sci. 2019;20(15).

304. Tejler J, Salameh B, Leffler H, Nilsson UJ. Fragment-based development of triazole-substituted O-galactosyl aldoximes with fragment-induced affinity and selectivity for galectin-3. Org Biomol Chem. 2009;7(19):3982-90.

305. van Hattum H, Branderhorst HM, Moret EE, Nilsson UJ, Leffler H, Pieters RJ. Tuning the preference of thiodigalactoside- and lactosamine-based ligands to galectin-3 over galectin-1. J Med Chem. 2013;56(3):1350-4.

306. Giguère D, Patnam R, Bellefleur MA, St-Pierre C, Sato S, Roy R. Carbohydrate triazoles and isoxazoles as inhibitors of galectins-1 and -3. Chem Commun (Camb). 2006(22):2379-81.

307. Giguère D, Sato S, St-Pierre C, Sirois S, Roy R. Aryl O- and S-galactosides and lactosides as specific inhibitors of human galectins-1 and -3: role of electrostatic potential at O-3. Bioorg Med Chem Lett. 2006;16(6):1668-72.

308. Cumpstey I, Sundin A, Leffler H, Nilsson UJ. C2-symmetrical thiodigalactoside bis-benzamido derivatives as high-affinity inhibitors of galectin-3: efficient lectin inhibition through double arginine-arene interactions. Angew Chem Int Ed Engl. 2005;44(32):5110-2.

309. Cumpstey I, Salomonsson E, Sundin A, Leffler H, Nilsson UJ. Double affinity amplification of galectin-ligand interactions through arginine-arene interactions: synthetic, thermodynamic, and computational studies with aromatic diamido thiodigalactosides. Chemistry. 2008;14(14):4233-45.

310. Delaine T, Cumpstey I, Ingrassia L, Le Mercier M, Okechukwu P, Leffler H, et al. Galectin-inhibitory thiodigalactoside ester derivatives have antimigratory effects in cultured lung and prostate cancer cells. J Med Chem. 2008;51(24):8109-14.

311. Stowell SR, Cho M, Feasley CL, Arthur CM, Song X, Colucci JK, et al. Ligand reduces galectin-1 sensitivity to oxidative inactivation by enhancing dimer formation. J Biol Chem. 2009;284(8):4989-99.

312. Griffioen AW, van der Schaft DW, Barendsz-Janson AF, Cox A, Struijker Boudier HA, Hillen HF, et al. Anginex, a designed peptide that inhibits angiogenesis. Biochem J. 2001;354(Pt 2):233-42.

313. Salomonsson E, Thijssen VL, Griffioen AW, Nilsson UJ, Leffler H. The anti-angiogenic peptide anginex greatly enhances galectin-1 binding affinity for glycoproteins. J Biol Chem. 2011;286(16):13801-4.

314. Thijssen VL, Postel R, Brandwijk RJ, Dings RP, Nesmelova I, Satijn S, et al. Galectin-1 is essential in tumor angiogenesis and is a target for antiangiogenesis therapy. Proc Natl Acad Sci U S A. 2006;103(43):15975-80.

315. Dings RP, Yokoyama Y, Ramakrishnan S, Griffioen AW, Mayo KH. The designed angiostatic peptide anginex synergistically improves chemotherapy and antiangiogenesis therapy with angiostatin. Cancer Res. 2003;63(2):382-5.

316. Thijssen VL, Barkan B, Shoji H, Aries IM, Mathieu V, Deltour L, et al. Tumor cells secrete galectin-1 to enhance endothelial cell activity. Cancer Res. 2010;70(15):6216-24.

317. Dings RP, Chen X, Hellebrekers DM, van Eijk LI, Zhang Y, Hoye TR, et al. Design of nonpeptidic topomimetics of antiangiogenic proteins with antitumor activities. J Natl Cancer Inst. 2006;98(13):932-6.

318. Dings RP, Van Laar ES, Webber J, Zhang Y, Griffin RJ, Waters SJ, et al. Ovarian tumor growth regression using a combination of vascular targeting agents anginex or topomimetic 0118 and the chemotherapeutic irofulven. Cancer Lett. 2008;265(2):270-80.

319. Zucchetti M, Bonezzi K, Frapolli R, Sala F, Borsotti P, Zangarini M, et al. Pharmacokinetics and antineoplastic activity of galectin-1-targeting OTX008 in combination with sunitinib. Cancer Chemother Pharmacol. 2013;72(4):879-87.

320. Oncoethix Gmb H. A Phase I, First-in-man Study of OTX008 Given Subcutaneously as a Single Agent to Patients With Advanced Solid Tumors. 2013.

321. Balestrieri K, Kew K, McDaniel M, Ramez M, Pittman HK, Murray G, et al. Proteomic identification of tumor- and metastasis-associated galectin-1 in claudin-low breast cancer. Biochim Biophys Acta Gen Subj. 2021;1865(2):129784.

322. Takakura A, Ohnishi Y, Itoh T, Yoshimura M, Urano K, Ueyama Y. Decontamination of human xenotransplantable tumor with mouse hepatitis virus by implantation in nude rat: a case report. Exp Anim. 2000;49(1):39-41.

323. Nakai N, Kawaguchi C, Nawa K, Kobayashi S, Katsuta Y, Watanabe M. Detection and elimination of contaminating microorganisms in transplantable tumors and cell lines. Exp Anim. 2000;49(4):309-13.

324. Zhang Y, Chen Y, Westerhoff P, Crittenden JC. Stability and removal of water soluble CdTe quantum dots in water. Environ Sci Technol. 2008;42(1):321-5.

325. Jongstra-Bilen J, Zhang CX, Wisnicki T, Li MK, White-Alfred S, Ilaalagan R, et al. Oxidized Low-Density Lipoprotein Loading of Macrophages Downregulates TLR-Induced Proinflammatory Responses in a Gene-Specific and Temporal Manner through Transcriptional Control. J Immunol. 2017;199(6):2149-57.

326. Wang D, Wang W, Lin W, Yang W, Zhang P, Chen M, et al. Apoptotic cell induction of miR-10b in macrophages contributes to advanced atherosclerosis progression in ApoE-/- mice. Cardiovasc Res. 2018;114(13):1794-805.

327. Cui K, Podolnikova NP, Bailey W, Szmuc E, Podrez EA, Byzova TV, et al. Inhibition of integrin α(D)β(2)-mediated macrophage adhesion to end product of docosahexaenoic acid (DHA) oxidation prevents macrophage accumulation during inflammation. J Biol Chem. 2019;294(39):14370-82.

328. Liu G, Zhao Y, Angeles A, Hamuro LL, Arnold ME, Shen JX. A novel and cost effective method of removing excess albumin from plasma/serum samples and its impacts on LC-MS/MS bioanalysis of therapeutic proteins. Anal Chem. 2014;86(16):8336-43.

329. Mobley J. UAB Mass Spectrometry/Proteomics Shared Facility Protocols: General In-Solution Digestion2017. Available from: https://www.uab.edu/medicine/msproteomics/images/eduProtPDF/insoldigest.pdf.

330. Thacker JS, Yeung DH, Staines WR, Mielke JG. Total protein or high-abundance protein: Which offers the best loading control for Western blotting? Anal Biochem. 2016;496:76-8.

331. Moritz CP. Tubulin or Not Tubulin: Heading Toward Total Protein Staining as Loading Control in Western Blots. Proteomics. 2017;17(20).

332. Hu X, Du S, Yu J, Yang X, Yang C, Zhou D, et al. Common housekeeping proteins are upregulated in colorectal adenocarcinoma and hepatocellular carcinoma, making the total protein a better "housekeeper". Oncotarget. 2016;7(41):66679-88.

333. Coutelier JP, M AB. Lactate Dehydrogenase-Elevating Virus. The Mouse in Biomedical Research. 2007;6:50036-4.

334. Balestrieri K, Pittman K, Ramez M, Vohra N, Verbanac K. Abstract 948: Characterization of the microenvironment of murine primary triple negative breast cancer. Cancer Research. 2017;77(13_Supplement):948-.

335. Chen Z, Quan L, Huang A, Zhao Q, Yuan Y, Yuan X, et al. seq-ImmuCC: Cell-Centric View of Tissue Transcriptome Measuring Cellular Compositions of Immune Microenvironment From Mouse RNA-Seq Data. Front Immunol. 2018;9:1286.

336. Liu ZY, Lan T, Tang F, He YZ, Liu JS, Yang JZ, et al. ZDHHC15 promotes glioma malignancy and acts as a novel prognostic biomarker for patients with glioma. BMC Cancer. 2023;23(1):420.

337. Zhou B, Hao Q, Liang Y, Kong E. Protein palmitoylation in cancer: molecular functions and therapeutic potential. Mol Oncol. 2023;17(1):3-26.

338. Bell JL, Wächter K, Mühleck B, Pazaitis N, Köhn M, Lederer M, et al. Insulin-like growth factor 2 mRNA-binding proteins (IGF2BPs): post-transcriptional drivers of cancer progression? Cell Mol Life Sci. 2013;70(15):2657-75.

339. Liu X, Chen J, Chen W, Xu Y, Shen Y, Xu X. Targeting IGF2BP3 in Cancer. Int J Mol Sci. 2023;24(11).

340. Jing X, Han C, Li Q, Li F, Zhang J, Jiang Q, et al. IGF2BP3-EGFR-AKT axis promotes breast cancer MDA-MB-231 cell growth. Biochim Biophys Acta Mol Cell Res. 2023:119542.

341. Liu Y, Yu C, Wu Y, Sun X, Su Q, You C, et al. CD44(+) fibroblasts increases breast cancer cell survival and drug resistance via IGF2BP3-CD44-IGF2 signalling. J Cell Mol Med. 2017;21(9):1979-88.

342. Jiang T, He X, Zhao Z, Zhang X, Wang T, Jia L. RNA m6A reader IGF2BP3 promotes metastasis of triple-negative breast cancer via SLIT2 repression. Faseb j. 2022;36(11):e22618.

343. Walter O, Prasad M, Lu S, Quinlan RM, Edmiston KL, Khan A. IMP3 is a novel biomarker for triple negative invasive mammary carcinoma associated with a more aggressive phenotype. Hum Pathol. 2009;40(11):1528-33.

344. Sjekloča N, Tomić S, Mrklić I, Vukmirović F, Vučković L, Lovasić IB, et al. Prognostic value of IMP3 immunohistochemical expression in triple negative breast cancer. Medicine (Baltimore). 2020;99(7):e19091.

345. Wan W, Ao X, Chen Q, Yu Y, Ao L, Xing W, et al. METTL3/IGF2BP3 axis inhibits tumor immune surveillance by upregulating N(6)-methyladenosine modification of PD-L1 mRNA in breast cancer. Mol Cancer. 2022;21(1):60.

346. Zhang M, Liu ZZ, Aoshima K, Cai WL, Sun H, Xu T, et al. CECR2 drives breast cancer metastasis by promoting NF-κB signaling and macrophage-mediated immune suppression. Sci Transl Med. 2022;14(630):eabf5473.

347. Kashyap D, Garg VK, Sandberg EN, Goel N, Bishayee A. Oncogenic and Tumor Suppressive Components of the Cell Cycle in Breast Cancer Progression and Prognosis. Pharmaceutics. 2021;13(4).

348. Sherbet GV, Lakshmi MS. S100A4 (MTS1) calcium binding protein in cancer growth, invasion and metastasis. Anticancer Res. 1998;18(4a):2415-21.

349. Dukhanina EA, Portseva TN, Dukhanin AS, Georgieva SG. Triple-negative and triple-positive breast cancer cells reciprocally control their growth and migration via the S100A4 pathway. Cell Adh Migr. 2022;16(1):65-71.

350. Ismail TM, Crick RG, Du M, Shivkumar U, Carnell A, Barraclough R, et al. Targeted Destruction of S100A4 Inhibits Metastasis of Triple Negative Breast Cancer Cells. Biomolecules. 2023;13(7).

351. Jiao X, Liu R, Huang J, Lu L, Li Z, Xu L, et al. Cellular Retinoic-Acid Binding Protein 2 in Solid Tumor. Curr Protein Pept Sci. 2020;21(5):507-16.

352. Feng X, Zhang M, Wang B, Zhou C, Mu Y, Li J, et al. CRABP2 regulates invasion and metastasis of breast cancer through hippo pathway dependent on ER status. J Exp Clin Cancer Res. 2019;38(1):361.

353. Hanahan D, Weinberg RA. Hallmarks of cancer: the next generation. Cell. 2011;144(5):646-74.

354. Steiner M, Tan AR. The evolving role of immune checkpoint inhibitors in the treatment of triple-negative breast cancer. Clin Adv Hematol Oncol. 2021;19(5):305-15.

355. Keenan TE, Tolaney SM. Role of Immunotherapy in Triple-Negative Breast Cancer. J Natl Compr Canc Netw. 2020;18(4):479-89.

356. Youn JI, Nagaraj S, Collazo M, Gabrilovich DI. Subsets of myeloid-derived suppressor cells in tumor-bearing mice. J Immunol. 2008;181(8):5791-802.

357. Bergenfelz C, Leandersson K. The Generation and Identity of Human Myeloid-Derived Suppressor Cells. Front Oncol. 2020;10:109.

358. Jahchan NS, Mujal AM, Pollack JL, Binnewies M, Sriram V, Reyno L, et al. Tuning the Tumor Myeloid Microenvironment to Fight Cancer. Front Immunol. 2019;10:1611.

359. Cassetta L, Baekkevold ES, Brandau S, Bujko A, Cassatella MA, Dorhoi A, et al. Deciphering myeloid-derived suppressor cells: isolation and markers in humans, mice and non-human primates. Cancer Immunol Immunother. 2019;68(4):687-97.

360. Singh S, Lee N, Pedroza DA, Bado IL, Hamor C, Zhang L, et al. Chemotherapy Coupled to Macrophage Inhibition Induces T-cell and B-cell Infiltration and Durable Regression in Triple-Negative Breast Cancer. Cancer Res. 2022;82(12):2281-97.

361. Ouderkirk JL, Krendel M. Non-muscle myosins in tumor progression, cancer cell invasion, and metastasis. Cytoskeleton (Hoboken). 2014;71(8):447-63.

362. Choi YN, Lee SK, Seo TW, Lee JS, Yoo SJ. C-Terminus of Hsc70-interacting protein regulates profilin1 and breast cancer cell migration. Biochem Biophys Res Commun. 2014;446(4):1060-6.

363. Fabregat A, Jupe S, Matthews L, Sidiropoulos K, Gillespie M, Garapati P, et al. The Reactome Pathway Knowledgebase. Nucleic Acids Res. 2018;46(D1):D649-d55.

364. Szklarczyk D, Morris JH, Cook H, Kuhn M, Wyder S, Simonovic M, et al. The STRING database in 2017: quality-controlled protein-protein association networks, made broadly accessible. Nucleic Acids Res. 2017;45(D1):D362-d8.

365. Ankney JA, Muneer A, Chen X. Relative and Absolute Quantitation in Mass Spectrometry-Based Proteomics. Annu Rev Anal Chem (Palo Alto Calif). 2018;11(1):49-77.

366. Ucal Y, Durer ZA, Atak H, Kadioglu E, Sahin B, Coskun A, et al. Clinical applications of MALDI imaging technologies in cancer and neurodegenerative diseases. Biochim Biophys Acta Proteins Proteom. 2017;1865(7):795-816.

367. Huang Z, Ma L, Huang C, Li Q, Nice EC. Proteomic profiling of human plasma for cancer biomarker discovery. Proteomics. 2017;17(6).

368. Juraschek R, Dülcks T, Karas M. Nanoelectrospray--more than just a minimized-flow electrospray ionization source. J Am Soc Mass Spectrom. 1999;10(4):300-8.

369. Schmidt A, Karas M, Dülcks T. Effect of different solution flow rates on analyte ion signals in nano-ESI MS, or: when does ESI turn into nano-ESI? J Am Soc Mass Spectrom. 2003;14(5):492-500.

370. Andrews GL, Simons BL, Young JB, Hawkridge AM, Muddiman DC. Performance characteristics of a new hybrid quadrupole time-of-flight tandem mass spectrometer (TripleTOF 5600). Anal Chem. 2011;83(13):5442-6.

371. Caprioli RM. Imaging mass spectrometry: enabling a new age of discovery in biology and medicine through molecular microscopy. J Am Soc Mass Spectrom. 2015;26(6):850-2.

372. Jeon YR, Kim SY, Lee EJ, Kim YN, Noh DY, Park SY, et al. Identification of annexin II as a novel secretory biomarker for breast cancer. Proteomics. 2013;13(21):3145-56.

373. Mascini NE, Eijkel GB, ter Brugge P, Jonkers J, Wesseling J, Heeren RM. The use of mass spectrometry imaging to predict treatment response of patient-derived xenograft models of triple-negative breast cancer. J Proteome Res. 2015;14(2):1069-75.

374. Hosokawa Y, Masaki N, Takei S, Horikawa M, Matsushita S, Sugiyama E, et al. Recurrent triple-negative breast cancer (TNBC) tissues contain a higher amount of phosphatidylcholine (32:1) than non-recurrent TNBC tissues. PLoS One. 2017;12(8):e0183724.

375. Basu SS, Agar NYR. Bringing Matrix-Assisted Laser Desorption/Ionization Mass Spectrometry Imaging to the Clinics. Clin Lab Med. 2021;41(2):309-24.

376. Zhu X, Xu T, Peng C, Wu S. Advances in MALDI Mass Spectrometry Imaging Single Cell and Tissues. Front Chem. 2021;9:782432.

377. Teichberg VI, Silman I, Beitsch DD, Resheff G. A beta-D-galactoside binding protein from electric organ tissue of Electrophorus electricus. Proc Natl Acad Sci U S A. 1975;72(4):1383-7.

378. Merkle RK, Cummings RD. Asparagine-linked oligosaccharides containing poly-N-acetyllactosamine chains are preferentially bound by immobilized calf heart agglutinin. J Biol Chem. 1988;263(31):16143-9.

379. Zhou Q, Cummings RD. L-14 lectin recognition of laminin and its promotion of in vitro cell adhesion. Arch Biochem Biophys. 1993;300(1):6-17.

380. Hsieh TJ, Lin HY, Tu Z, Huang BS, Wu SC, Lin CH. Structural Basis Underlying the Binding Preference of Human Galectins-1, -3 and -7 for Galβ1-3/4GlcNAc. PLoS One. 2015;10(5):e0125946.

381. Miller MC, Nesmelova IV, Platt D, Klyosov A, Mayo KH. The carbohydrate-binding domain on galectin-1 is more extensive for a complex glycan than for simple saccharides: implications for galectin-glycan interactions at the cell surface. Biochem J. 2009;421(2):211-21.

382. Leppänen A, Stowell S, Blixt O, Cummings RD. Dimeric galectin-1 binds with high affinity to alpha2,3-sialylated and non-sialylated terminal N-acetyllactosamine units on surface-bound extended glycans. J Biol Chem. 2005;280(7):5549-62.

383. Liu FT, Rabinovich GA. Galectins as modulators of tumour progression. Nat Rev Cancer. 2005;5(1):29-41.

384. Raz A, Lotan R. Lectin-like activities associated with human and murine neoplastic cells. Cancer Res. 1981;41(9 Pt 1):3642-7.

385. Griffin RJ, Koonce NA, Dings RP, Siegel E, Moros EG, Bräuer-Krisch E, et al. Microbeam radiation therapy alters vascular architecture and tumor oxygenation and is enhanced by a galectin-1 targeted anti-angiogenic peptide. Radiat Res. 2012;177(6):804-12.

386. Szebeni GJ, Kriston-Pál É, Blazsó P, Katona RL, Novák J, Szabó E, et al. Identification of galectin-1 as a critical factor in function of mouse mesenchymal stromal cell-mediated tumor promotion. PLoS One. 2012;7(7):e41372.

387. Xu SG, Yan PJ, Shao ZM. Differential proteomic analysis of a highly metastatic variant of human breast cancer cells using two-dimensional differential gel electrophoresis. J Cancer Res Clin Oncol. 2010;136(10):1545-56.

388. Calderón-González KG, Valero Rustarazo ML, Labra-Barrios ML, Bazán-Méndez CI, Tavera-Tapia A, Herrera-Aguirre ME, et al. Determination of the protein expression profiles of breast cancer cell lines by quantitative proteomics using iTRAQ labelling and tandem mass spectrometry. J Proteomics. 2015;124:50-78.

389. Nakayama J, Matsunaga H, Arikawa K, Yoda T, Hosokawa M, Takeyama H, et al. Identification of two cancer stem cell-like populations in triple-negative breast cancer xenografts. Dis Model Mech. 2022;15(6).

390. Lin Y, Xu J, Lan H. Tumor-associated macrophages in tumor metastasis: biological roles and clinical therapeutic applications. J Hematol Oncol. 2019;12(1):76.

391. Genna A, Duran CL, Entenberg D, Condeelis JS, Cox D. Macrophages Promote Tumor Cell Extravasation across an Endothelial Barrier through Thin Membranous Connections. Cancers (Basel). 2023;15(7).

392. Astorgues-Xerri L, Riveiro ME, Tijeras-Raballand A, Serova M, Rabinovich GA, Bieche I, et al. OTX008, a selective small-molecule inhibitor of galectin-1, downregulates cancer cell proliferation, invasion and tumour angiogenesis. Eur J Cancer. 2014;50(14):2463-77.

393. Koonce NA, Griffin RJ, Dings RPM. Galectin-1 Inhibitor OTX008 Induces Tumor Vessel Normalization and Tumor Growth Inhibition in Human Head and Neck Squamous Cell Carcinoma Models. Int J Mol Sci. 2017;18(12).

394. Earl LA, Bi S, Baum LG. Galectin multimerization and lattice formation are regulated by linker region structure. Glycobiology. 2010;21(1):6-12.

395. Dings RP, Miller MC, Nesmelova I, Astorgues-Xerri L, Kumar N, Serova M, et al. Antitumor agent calixarene 0118 targets human galectin-1 as an allosteric inhibitor of carbohydrate binding. J Med Chem. 2012;55(11):5121-9.

396. Radovani B, Gudelj I. N-Glycosylation and Inflammation; the Not-So-Sweet Relation. Front Immunol. 2022;13:893365.

397. Starossom SC, Mascanfroni ID, Imitola J, Cao L, Raddassi K, Hernandez SF, et al. Galectin-1 deactivates classically activated microglia and protects from inflammation-induced neurodegeneration. Immunity. 2012;37(2):249-63.

398. He J, Baum LG. Presentation of galectin-1 by extracellular matrix triggers T cell death. J Biol Chem. 2004;279(6):4705-12.

399. Leung Z, Ko FCF, Tey SK, Kwong EML, Mao X, Liu BHM, et al. Galectin-1 promotes hepatocellular carcinoma and the combined therapeutic effect of OTX008 galectin-1 inhibitor and sorafenib in tumor cells. J Exp Clin Cancer Res. 2019;38(1):423.

400. Brandwijk RJ, Nesmelova I, Dings RP, Mayo KH, Thijssen VL, Griffioen AW. Cloning an artificial gene encoding angiostatic anginex: From designed peptide to functional recombinant protein. Biochem Biophys Res Commun. 2005;333(4):1261-8.

401. Chen Q, Han B, Meng X, Duan C, Yang C, Wu Z, et al. Immunogenomic analysis reveals LGALS1 contributes to the immune heterogeneity and immunosuppression in glioma. Int J Cancer. 2019;145(2):517-30.

402. Fougner C, Bergholtz H, Norum JH, Sørlie T. Re-definition of claudin-low as a breast cancer phenotype. Nat Commun. 2020;11(1):1787.

403. Pan C, Xu A, Ma X, Yao Y, Zhao Y, Wang C, et al. Research progress of Claudin-low breast cancer. Front Oncol. 2023;13:1226118.

404. Prodhomme MK, Péricart S, Pommier RM, Morel AP, Brunac AC, Franchet C, et al. Opposite Roles for ZEB1 and TMEJ in the Regulation of Breast Cancer Genome Stability. Front Cell Dev Biol. 2021;9:727429.

405. Huang Y, Wang HC, Zhao J, Wu MH, Shih TC. Immunosuppressive Roles of Galectin-1 in the Tumor Microenvironment. Biomolecules. 2021;11(10).

406. Tracey BM, Feizi T, Abbott WM, Carruthers RA, Green BN, Lawson AM. Subunit molecular mass assignment of 14,654 Da to the soluble beta-galactoside-binding lectin from bovine heart muscle and demonstration of intramolecular disulfide bonding associated with oxidative inactivation. J Biol Chem. 1992;267(15):10342-7.

407. Fettis MM, Hudalla GA. Engineering Reactive Oxygen Species-Resistant Galectin-1 Dimers with Enhanced Lectin Activity. Bioconjug Chem. 2018;29(7):2489-96.

408. Lim JY, Kim TW, Ryu DB, Park SS, Lee SE, Kim BS, et al. Myeloma-Secreted Galectin-1 Potently Interacts with CD304 on Monocytic Myeloid-Derived Suppressor Cells. Cancer Immunol Res. 2021;9(5):503-13.

409. Ugel S, Bronte V. Galectin-1 Supports a Dangerous Liaison between Monocytes and Multiple Myeloma. Cancer Immunol Res. 2021;9(5):488.

410. Zhang X, Schwartz JC, Guo X, Bhatia S, Cao E, Lorenz M, et al. Structural and functional analysis of the costimulatory receptor programmed death-1. Immunity. 2004;20(3):337-47.

411. Greer PFC, Rich A, Coates DE. Effects of galectin-1 inhibitor OTX008 on oral squamous cell carcinoma cells in vitro and the role of AP-1 and the MAPK/ERK pathway. Arch Oral Biol. 2022;134:105335.

412. Delord J-P, Awada A, Raymond E, Lokiec F, Herait P, Rezai K, et al. Abstract A72: A first-in-man Phase I study of the galectin-1 (gal-1) inhibitor OTX008 given subcutaneously as a single agent to patients with advanced solid tumors. Molecular Cancer Therapeutics. 2013;12(11_Supplement):A72-A.

413. Wu C, Thalhamer T, Franca RF, Xiao S, Wang C, Hotta C, et al. Galectin-9-CD44 interaction enhances stability and function of adaptive regulatory T cells. Immunity. 2014;41(2):270-82.

414. Laderach DJ, Gentilini LD, Giribaldi L, Delgado VC, Nugnes L, Croci DO, et al. A unique galectin signature in human prostate cancer progression suggests galectin-1 as a key target for treatment of advanced disease. Cancer Res. 2013;73(1):86-96.

415. Femel J, van Hooren L, Herre M, Cedervall J, Saupe F, Huijbers EJM, et al. Vaccination against galectin-1 promotes cytotoxic T-cell infiltration in melanoma and reduces tumor burden. Cancer Immunol Immunother. 2022;71(8):2029-40.

416. Dennis JW, Granovsky M, Warren CE. Glycoprotein glycosylation and cancer progression. Biochim Biophys Acta. 1999;1473(1):21-34.

417. Barthel SR, Antonopoulos A, Cedeno-Laurent F, Schaffer L, Hernandez G, Patil SA, et al. Peracetylated 4-fluoro-glucosamine reduces the content and repertoire of N- and O-glycans without direct incorporation. J Biol Chem. 2011;286(24):21717-31.

418. Li D, Li Y, Wu X, Li Q, Yu J, Gen J, et al. Knockdown of Mgat5 inhibits breast cancer cell growth with activation of CD4+ T cells and macrophages. J Immunol. 2008;180(5):3158-65.

419. Cedeno-Laurent F, Opperman MJ, Barthel SR, Hays D, Schatton T, Zhan Q, et al. Metabolic inhibition of galectin-1-binding carbohydrates accentuates antitumor immunity. J Invest Dermatol. 2012;132(2):410-20.

420. Michael JV, Wurtzel JG, Goldfinger LE. Inhibition of Galectin-1 Sensitizes HRAS-driven Tumor Growth to Rapamycin Treatment. Anticancer Res. 2016;36(10):5053-61.

421. Omar FA, Brown TC, Gillanders WE, Fleming TP, Smith MA, Bremner RM, et al. Cytosolic EpCAM cooperates with H-Ras to regulate epithelial to mesenchymal transition through ZEB1. PLoS One. 2023;18(5):e0285707.

APPENDIX A: ANIMAL USE APPROVAL LETTERS

East Carolina University

Animal Care and Use Committee
212 Jo Warren Life Sciences Building
East Carolina University
Greenville, NC 27834
252-744-2436 office
252-744-2355 fax

July 15, 2014

Kathryn Verbanac, Ph.D.
Department of Surgery
Brody 4S-10
ECU Brody School of Medicine

Dear Dr. Verbanac:

The Amendment to your Animal Use Protocol entitled, "Characterization of the Pro-Metastatic Niche in Triple Negative Breast Cancer", (AUP #1255) was reviewed by this institution's Animal Care and Use Committee on 7/15/14. The following action was taken by the Committee:

"Approved as amended"

****Please contact Dale Aycock prior to any hazard use**

A copy of the Amendment is enclosed for your laboratory files. Please be reminded that all animal procedures must be conducted as described in the approved Animal Use Protocol. Modifications of these procedures cannot be performed without prior approval of the ACUC. The Animal Welfare Act and Public Health Service Guidelines require the ACUC to suspend activities not in accordance with approved procedures and report such activities to the responsible University Official (Vice Chancellor for Health Sciences or Vice Chancellor for Academic Affairs) and appropriate federal Agencies. **Please ensure that all personnel associated with this protocol have access to this approved copy of the AUP/Amendment and are familiar with its contents.**

Sincerely yours,

Susan McRae, Ph.D.
Chair, Animal Care and Use Committee

SM/jd

enclosure

East Carolina University

Animal Care and
Use Committee
212 Ed Warren Life
Sciences Building
East Carolina University
Greenville, NC 27834
252-744-2436 office
252-744-2355 fax

June 30, 2016

Kathryn Verbanac, Ph.D.
Department of Surgery
Brody 4S-10
ECU Brody School of Medicine

Dear Dr. Verbanac:

Your Animal Use Protocol entitled, "Characterization of the Pro-Metastatic Niche in Triple Negative Breast Cancer" (AUP #T255a) was reviewed by this institution's Animal Care and Use Committee on June 30, 2016. The following action was taken by the Committee:

"Approved as submitted"

Please contact Aaron Hinkle at 744-2997 prior to hazard use

A copy is enclosed for your laboratory files. Please be reminded that all animal procedures must be conducted as described in the approved Animal Use Protocol. Modifications of these procedures cannot be performed without prior approval of the ACUC. The Animal Welfare Act and Public Health Service Guidelines require the ACUC to suspend activities not in accordance with approved procedures and report such activities to the responsible University Official (Vice Chancellor for Health Sciences or Vice Chancellor for Academic Affairs) and appropriate federal Agencies. **Please ensure that all personnel associated with this protocol have access to this approved copy of the AUP and are familiar with its contents.**

Sincerely yours,

Eddie Johnson/jd

Eddie Johnson
Vice-Chair, Animal Care and Use Committee

EJ/jd

Enclosure

ECU
Animal Care and Use Committee
212 Ed Warren Life Sciences Building | East Carolina University | Greenville, NC 27834-4354
252-744-2436 office | 252-744-2355 fax

May 20, 2019

Kathryn Verbanac, Ph.D.
Department of Surgery
Brody 4S-10
East Carolina University

Dear Dr. Verbanac:

Your Animal Use Protocol entitled, "Characterization of the Pro-Metastatic Niche in Triple Negative Breast Cancer" (AUP #T255b) was reviewed by this institution's Animal Care and Use Committee on May 20, 2019. The following action was taken by the Committee:

"Approved as submitted"

Please contact Aaron Hinkle at 744-2997 prior to hazard use

A copy is enclosed for your laboratory files. Please be reminded that all animal procedures must be conducted as described in the approved Animal Use Protocol. Modifications of these procedures cannot be performed without prior approval of the ACUC. The Animal Welfare Act and Public Health Service Guidelines require the ACUC to suspend activities not in accordance with approved procedures and report such activities to the responsible University Official (Vice Chancellor for Health Sciences or Vice Chancellor for Academic Affairs) and appropriate federal Agencies. **Please ensure that all personnel associated with this protocol have access to this approved copy of the AUP and are familiar with its contents.**

Sincerely yours,

Susan McRae, Ph.D.
Chair, Animal Care and Use Committee

SM/jd

Enclosure

APPENDIX B: HUMAN RESEARCH APPROVAL LETTER

EAST CAROLINA UNIVERSITY
University & Medical Center Institutional Review Board Office
4N-70 Brody Medical Sciences Building· Mail Stop 682
600 Moye Boulevard · Greenville, NC 27834
Office **252-744-2914** · Fax **252-744-2284** · **www.ecu.edu/irb**

Notification of Amendment Approval

From: Biomedical IRB
To: Nasreen Vohra
CC:
Date: 3/9/2016
Re: Ame1 UMCIRB 13-001654
UMCIRB 13-001654
Development of a Breast Cancer Tissue Microarray

Your Amendment has been reviewed and approved using expedited review for the period of 3/8/2016 to 2/9/2017. It was the determination of the UMCIRB Chairperson (or designee) that this revision does not impact the overall risk/benefit ratio of the study and is appropriate for the population and procedures proposed.

Please note that any further changes to this approved research may not be initiated without UMCIRB review except when necessary to eliminate an apparent immediate hazard to the participant. All unanticipated problems involving risks to participants and others must be promptly reported to the UMCIRB. A continuing or final review must be submitted to the UMCIRB prior to the date of study expiration.The investigator must adhere to all reporting requirements for this study.

Approved consent documents with the IRB approval date stamped on the document should be used to consent participants (consent documents with the IRB approval date stamp are found under the Documents tab in the study workspace).

The approval includes the following items:

Document	Description
There are no items to display	

The Chairperson (or designee) does not have a potential for conflict of interest on this study.

EAST CAROLINA UNIVERSITY
University & Medical Center Institutional Review Board Office
4N-70 Brody Medical Sciences Building· Mail Stop 682
600 Moye Boulevard · Greenville, NC 27834
Office **252-744-2914** · Fax **252-744-2284** · **www.ecu.edu/irb**

Notification of Continuing Review Approval: Expedited

From: Biomedical IRB
To: Nasreen Vohra
CC:
Date: 2/11/2016
Re: CR00003989
UMCIRB 13-001654
Development of a Breast Cancer Tissue Microarray

The continuing review of your expedited study was approved. Approval of the study and any consent form(s) is for the period of 2/10/2016 to 2/9/2017. This research study is eligible for review under expedited category #5. The Chairperson (or designee) deemed this study no more than minimal risk.

Changes to this approved research may not be initiated without UMCIRB review except when necessary to eliminate an apparent immediate hazard to the participant. All unanticipated problems involving risks to participants and others must be promptly reported to the UMCIRB. The investigator must submit a continuing review/closure application to the UMCIRB prior to the date of study expiration. The Investigator must adhere to all reporting requirements for this study.

Approved consent documents with the IRB approval date stamped on the document should be used to consent participants (consent documents with the IRB approval date stamp are found under the Documents tab in the study workspace).

The approval includes the following items:

Document	Description
data collection sheet.xlsx(0.01)	Data Collection Sheet
FINAL MTA_35937_exe.pdf(0.01)	Additional Items
Letter to IRB TMA project.pdf(0.01)	COI Management Plan
Letter to IRB TMA project.pdf(0.01)	Additional Items

The Chairperson (or designee) does not have a potential for conflict of interest on this study.

APPENDIX C: PERMISSION LETTER

Re: Permission For Dissertation Use [231116-023900]

Permissions Helpdesk <permissionshelpdesk@elsevier.com>
Fri 11/17/2023 6:30 AM
To:Balestrieri, Kassondra Wright <wrightka14@students.ecu.edu>

You don't often get email from permissionshelpdesk@elsevier.com. Learn why this is important

This email originated from outside ECU.

Dear Kassondra Balestrieri

We hereby grant you permission to reprint the material below at no charge in your thesis subject to the following conditions:

RE: Proteomic identification of tumor- and metastasis-associated galectin-1 in claudin-low breast cancer, Biochimica et Biophysica Acta (BBA) - General Subjects, Volume 1865, Issue 2, 2021, Balestrieri et al.

1. If any part of the material to be used (for example, figures) has appeared in our publication with credit or acknowledgment to another source, permission must also be sought from that source. If such permission is not obtained then that material may not be included in your publication/copies.

2. Suitable acknowledgment to the source must be made, either as a footnote or in a reference list at the end of your publication, as follows:

"This article was published in Publication title, Vol number, Author(s), Title of article, Page Nos, Copyright Elsevier (or appropriate Society name) (Year)."

3. Your thesis may be submitted to your institution in either print or electronic form.

4. Reproduction of this material is confined to the purpose for which permission is hereby given.

5. This permission is granted for non-exclusive world English rights only. For other languages please reapply separately for each one required. Permission excludes use in an electronic form other than submission. Should you have a specific electronic project in mind please reapply for permission.

6. As long as the article is embedded in your thesis, you can post/share your thesis in the University repository.

7. Should your thesis be published commercially, please reapply for permission.

8. Posting of the full article/ chapter online is not permitted. You may post an abstract with a link to the Elsevier website [http://www.elsevier.com,/]www.elsevier.com, or to the article on ScienceDirect if it is available on that platform.

Kind regards,

Roopa Lingayath